Dissertation zur Erlangung des Doktorgrades
der Fakultät für Chemie und Pharmazie
der Ludwig-Maximilians-Universität München

Redox-sensitive and receptor-targeted sequence-defined, cationic carriers for nucleic acid delivery

Philipp Michael Klein
aus Annweiler am Trifels, Deutschland

2017

Erklärung

Diese Dissertation wurde im Sinne von § 7 der Promotionsordnung vom 28. November 2011 von Herrn Prof. Dr. Ernst Wagner betreut.

Eidesstattliche Versicherung

Diese Dissertation wurde eigenständig und ohne unerlaubte Hilfe erarbeitet.

München, 01.06.2017

.....

Philipp Klein

Dissertation eingereicht am 01.06.2017

1. Gutachter: Prof. Dr. Ernst Wagner

2. Gutachter: Prof. Dr. Olivia Merkel

Mündliche Prüfung am 13.07.2017

Meiner Familie

„There are only three problems in gene therapy:

delivery, delivery and delivery“

Inder Verma, 1999

Table of contents

1 Introduction

This chapter should give a brief introduction into the research field of bioreducible polycationic carriers for therapeutic nucleic acids. It was adapted from:

Klein PM, Wagner E. *Bioreducible Polycations as Shuttles for Therapeutic Nucleic Acid and Protein Transfection*. Antioxid Redox Signal. 2014 Aug 10;21(5):804-17

1.1 The requirements for nucleic acid formulations to act as therapeutics

The therapy with bio-derived macromolecules like proteins or nucleic acids such as plasmid DNA (pDNA) [1], small interfering RNA (siRNA) [2, 3], microRNA [4, 5] is a field of major importance and continually growing interest. Live threatening, severe diseases including cancer obtain a new chance for treatment by the use of gene therapy [6, 7]. In order to be used as therapeutics, these macromolecules have to be stabilized against degradation in the bloodstream and clearance, taken up by the target cells and reach the intracellular site of action.

Viral vectors have been the number one carriers for intracellular nucleic acid delivery. However only minor changes in their structures can be made, the size and type of cargo is limited, and they can trigger immune reactions. As such, viral nanoparticles, on the one, hand present excellent natural examples for how to design carriers for intracellular delivery. On the other hand, synthetic carriers that mimic these transfer processes but are not dependent on naturally available nucleotides and amino acids, gain more and more attention.

These synthetic carriers have to handle a lot of challenging tasks. They should offer an optimal extracellular stability and an efficient uptake into the cell. Uptake usually results in delivery into endocytic vesicles which often end in degradative lysosomes. Therefore the same carriers should facilitate an escape from endosomes after uptake and release their nucleic acid cargo to the cytoplasm, optionally followed by transfer to the nucleus (as required in the case of pDNA). In this process the carriers should act like shuttles: while stably associated with their cargo in a covalent or noncovalent

manner in the early extracellular delivery steps, they must not disturb the nucleic acid cargo in functionality inside the cell and should dissociate or disintegrate after delivery.

The demands on delivery differ at the different extracellular and intracellular sites, and also the microenvironments provide uniquely different properties. Carriers can be designed to sense these environmental differences and utilize them to undergo changes beneficial for the delivery process [8]. The molecular programming of such dynamic carriers may include sensors that react to changes in enzyme activities, in pH, or the redox microenvironment (**Fig. 1**). Among the different sensors, bioreducible elements are important tools to distinguish between extra- and intracellular sites, where the redox potential displays big differences. As reviewed in the next sections, the use of disulfide bonds as sensors for reductive environments have a growing impact on the development of oligocation-based delivery systems [9-11].

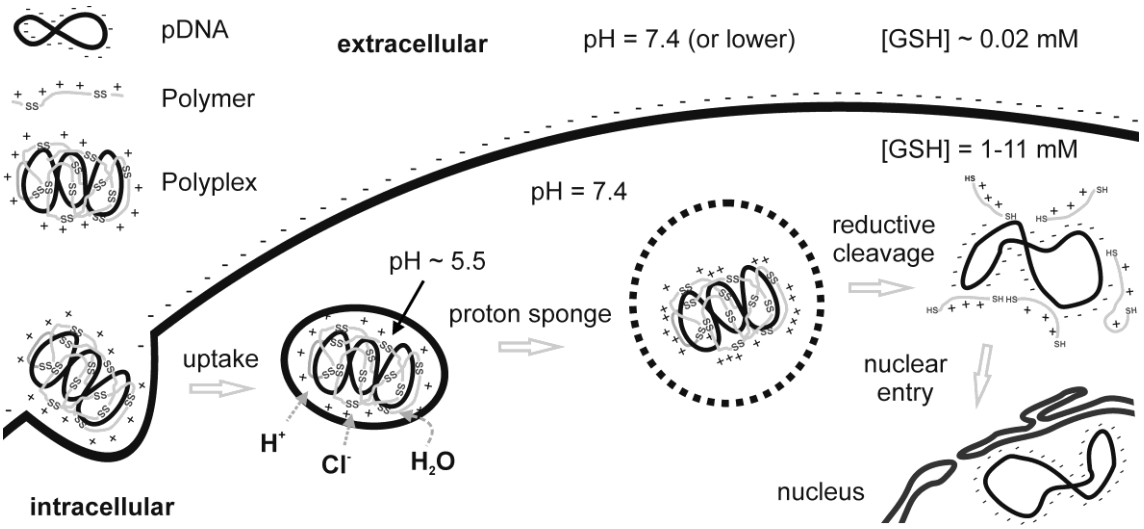

Fig. 1 Dynamic nanocarriers utilizing different cellular microenvironments. Differences in pH (lower in endocytic vesicles and also in special extracellular tumor situations) and redox situation (higher intracellular GSH concentration) can be utilized in the delivery process. Polyplexes stabilized by disulfide formation get internalized by electrostatic interaction with the cell membrane. Protonation of polymers in the acidifying vesicle triggers destabilizing membrane interactions necessary to induce endosomal escape into the cytosol. In the reductive environment of the cytosol, disulfide bonds are cleaved and the cargo is released. pDNA has to enter the nucleus to get transcribed.

1.2 Outside cells stable, inside labile – the delivery paradox

Polyplexes are nanoscaled, interelectrolyte complexes of cationic polymers and negatively charged nucleic acids [12]. The extracellular stability is of the highest importance. In the bloodstream, these particles are exposed to nucleases, which can degrade the cargo, and other serum proteins, that can destabilize the complex by electrostatic exchange actions. Additionally, nucleic acids are compacted to convenient polyplex sizes of virus-like dimensions (around 100 nm). In the case of larger pDNA, this results in favorable compaction and protection. In the case of small nucleic acids such as siRNA or oligonucleotides, this results in increased nanoparticle sizes due to packaging as multimers, which prevents the particles from being cleared too rapidly by the kidney [13]. High molecular weight (HMW) polymeric carriers, usually show better transfection efficiency than low molecular weight (LMW) carriers largely because of insufficient polyplex stability of the latter ones [14-18]. LMW carriers, however, have significant advantages regarding reduced cytotoxicity [19] and better biocompatibility, for example, a reduced complement activation [20] relevant for *in vivo* applications. Moreover, too tight binding by HMW polymers can hinder intracellular vector unpacking [21, 22] and therefore reduce transfection efficiency. pDNA has to be accessible to the transcriptional machinery in the nucleus. siRNA has to be accessible to the RNA-induced silencing complex (RISC) [23] after delivery to the cytosol. Often the window between sufficient large polymer size for effectivity and sufficiently small for high biocompatibility was small or non-existent [24]. To achieve a better carrier profile with stability on demand, strategies using biodegradable polymers have been explored. The concept often included bioreversible cross-linkage of nontoxic LMW oligomers into HMW carriers via hydrolysable ester, acetal bonds or reducible disulfide bonds [25-32]. Thus, extracellular polyplex stability and transfection efficiency are partnered with intracellular disassembly and polymer degradation into nontoxic fragments.

Within physiological proteins, the presence of disulfide bonds dominates outside the cell, both for secreted proteins, matrix proteins, or proteins at cell surfaces [33]. Inside the cell, the combination of high glutathione (GSH) concentrations and enzymes from the thioredoxin family [34] form a reductive environment of the cytosol. With a concentration of 1 - 11 mM GSH [35], the intracellular concentration of GSH is approximately 100 - 1000 times higher than outside the cell. This attribute can also be

used by artificial reducible systems to be intracellularly cleaved and change their properties. Although extracellular stability is expected to be significantly improved by disulfides, the situation is not so clear-cut. Disulfide cleavages may also occur in the *in vivo* situation outside the cell [36]. This was already observed in early *in vivo* work using immunotoxins [37, 38]. The liver as the major organ for GSH production [39, 40] has been considered as responsible for this extracellular degradation of disulfide bonds. Protein disulfide isomerases (PDI) widely known to be localized in the endoplasmatic reticulum (ER) can also occur on the cell surface of hepatocytes and may cleave disulfide bonds [41]. Low concentrations of cysteine (~8 µM) and glutathione (~2 µM) present in human plasma [42] are not considered to significantly contribute to extracellular bioreduction. The extracellular stability of disulfides can be tuned by their structural environment [38, 43]; see also Section 1.6. Thus, appropriate redox chemistry is considered as an excellent approach to solve the conflicting carrier requirements between extracellular stability and intracellular instability.

For example, in early work Rice and coworkers [44] introduced defined oligolysine structures containing one to five cysteine residues (***CWK$_{18}$, II, III, IV, V*** - **Fig. 2**). The oligomers became very reactive at pH 7.5, e. g. oligomer ***V*** oxidized completely within 25 minutes. For this reason, the mercapto forms of oligomers were stored at low pH in the absence of oxygen until use. During the incubation with pDNA at physiological pH, the cysteines formed disulfide bonds. Polyplexes of oligolysines with more than three cysteines, which were able to crosslink in three dimensions, showed the best stability in a shear stress stability test and could outperform polylysine tremendously. Still, the structure with two cysteines that has only the possibility to polymerize in a linear way revealed the best results in transfection with stability properties comparable to polylysine polyplexes. The stability of the resulting particles was higher if the thiols of the cysteines were kept in the reduced form until they were incubated with the DNA. It seems that these bioreducible oligocations created a cage after complexing with the DNA template. This outcome was very promising, especially when considering that these oligolysine structures were not expected to have high transfection efficiency. Endosomal buffer capacity and endosomal escape activity of polylysines were known to be very modest.

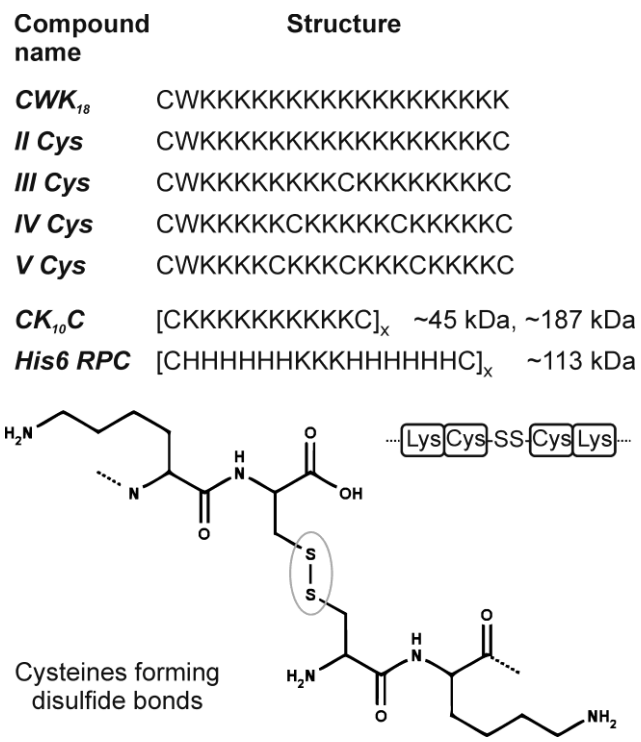

Fig. 2 Polymers based on natural amino acids with cysteine for linking. Structures of oligomers (sequences from N → C-terminus) that are able to form bioreducible linkages by dimerization (***CWK18*** [44]), in a linear (***II Cys*** [44]***, CK10C*** [45]***, His 6*** [46]) or crosslinking (***III-V Cys*** [44]) way. C, cysteine; W, tryptophane; K, lysine; H, histidine.

Based on analogous pre-oxidized polymers, containing Cys-Lys$_{10}$-Cys monomers (***CK$_{10}$C*** - **Fig. 2**), lipopolyplexes were generated [45] by combination with a liposomal transfection agent for enhanced endosomal escape. This lipopolyplex system achieved 187-fold higher gene expression levels for pDNA compared to the analogous non-reducible lipopolylysine formulation. The effect of reducing agents to these polymers was demonstrated by adding 25 mM dithiothreitol (DTT) for 5 minutes to polyplexes in an ethidium bromide pDNA binding assay. In this assay the pDNA polyplexes with non-reducible polylysine showed no significant changes. The pDNA polyplexes with reducible polymers, however, showed a more than two times higher fluorescence intensity than before the addition of DTT. The higher fluorescence intensity represents better accessibility of the DNA to the intercalator ethidium bromide. Importantly, in more general terms the better accessibility based on bioreductive carrier cleavage improves pDNA delivery by facilitating the release of the nucleic acid in a form accessible for transcription into mRNA.

1.3 Bioreducible pDNA carriers with endosomal escape function

For successful gene transfer, several delivery barriers have to be overcome (see **Fig. 1**). Release from endosomes after cellular uptake presents a major bottleneck. Polyethylenimine (PEI), a polymer often used for pDNA transfections, combines optimized DNA binding ability and endosomal buffer capacity within one structure [47, 48]. Its diaminoethane motif [49] offers a remarkable pH-reversible protonation and buffer capacity over a wide pH range, which turns it into an almost perfect “proton sponge” [50-53]. Endosomal protonation of PEI was discovered as an excellent way for triggering lipid membrane disruption and release into the cytosol. In sum, PEI has been established as being a very effective, but also significantly cytotoxic [54, 55] gene carrier. In order to create a less toxic, bioreducible branched PEI, LMW (<4.6 kDa) linear PEI (***LPEI***) was crosslinked with dithiodipropionic acid di(N-succinimidyl ester) (DSP) or N,N‘-bis-(tert-butoxycarbonyl)cystine linkages (**Fig. 3**) [25]. Impressively, this bioreducible PEI version did not only display far lower cytotoxicity at higher PEI doses, but also significantly outperformed the transfection efficiency of standard branched PEI 25kDa, ***LPEI*** 22kDa and several other commercially available reagents in seven cell lines (CHO-K1, COS-7, NIH/3T3, HepG2, HCT116, HeLa, and HEK-293 cells). For the maximum efficiency for these bioreducible polymers, N/P ratios (ratio between protonatable nitrogens in polymer and phosphates in nucleic acid) between 18 and 30 were required, which were much higher than for non-bioreducible polymers.

A related effort to produce a biodegradable PEI was taken by Park and coworkers [56]. They synthesized a bioreducible linear PEI with a diaminoethane motif that was separated by a disulfide bond after every six protonatable amines (***PEIS***). An agarose gel shift showed a less than 2 hours stability in a 5mM GSH solution. As additional development these linear bioreducible PEIS were crosslinked to larger structures with different amounts of bisepoxide. This resulted in branched structures (***bPEIS*** - **Fig. 3**) with increased stability of more than 4 hours in GSH containing buffer. The transfection for the larger branched ***PEIS*** was better than for smaller linear ***PEIS*** and could reach the same level as branched PEI 25kDa at their own optimal N/P ratio. The addition of 5 % bisepoxide showed best effects in general (results of five cell lines – C2C12, HEK 293, HeLa, HUVEC, NIH3T3). By adding 10 % serum the transfection of bioreducible PEIS was reduced by approximately one log scale, which was more than for ***bPEI*** (approximately half a log scale). Due to the bioreducibility and the small, calculable

degradation products, the cell viability tested with MTT assay was significantly improved. On the other hand, serum stability was an issue that still needed improvement.

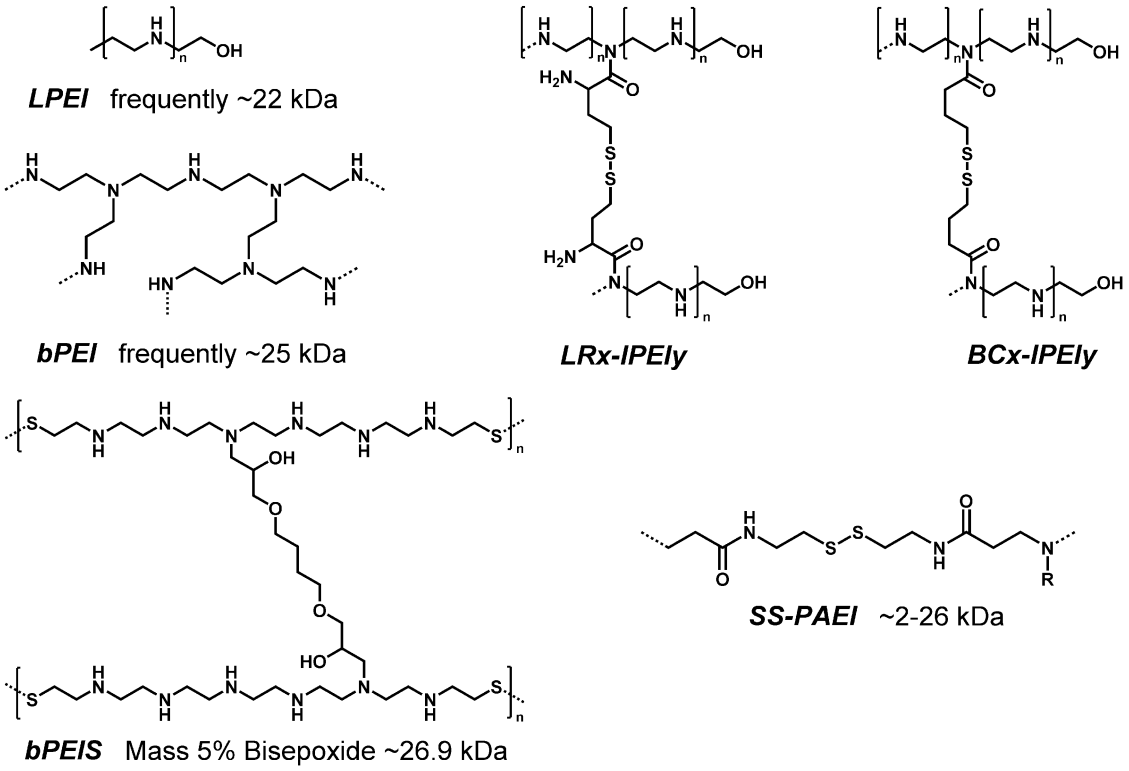

Fig. 3 Structures of PEI and bioreducible polymers. Non-degradable linear ***LPEI*** and branched ***bPEI*** (left top). Bioreducible ***bPEI*** derivates (***LRx-lPEIy*** and ***BCx-lPEIy***) [25] based on ***LPEI*** and crosslinker (x denotes the molar ratio cross-linker/LPEI, and y denotes the MW (kDa) of the LPEI. For ***LRx-lPEIy*** the molar ratio between the linker and ***LPEI*** monomers was 0.5 % - 3 %, for ***BCx-lPEIy*** the molar ratio between the linker and ***LPEI*** monomers was 3 % - 8 %). ***bPEIS*** [56] contains a bioreducible diaminoethane system and a non-degradable crosslinker. ***SS-PAEI*** [57-59] consists of poly(amido ethylenimine) with bioreducible disulfide bonds and variable residues for functionalization (right bottom).

Disulfide-containing poly(amido ethylenimine)s (***SS-PAEIs*** - **Fig. 3**) are another class of bioreducible polymers [57-59]. Agents containing at least two reactive amines like ethylendiamine (EDA), diethylentriamine (DETA) or triethylentetramine (TETA) [57] were reacted by a Michael-type polyaddition with disulfide-containing bisacrylamides to form branched structures. The resulting polymers show very good transfection results. Especially in 10 % serum, they have great advantages compared to branched PEI 25kDa. ***SS-PAEIs*** only had slightly lower transfection efficiency in serum (1.2 × difference for EDA polymers, 1.3 × difference for DETA polymers, 11 × difference for

TETA polymers) in BAEC cells, whereas ***bPEI*** had a dramatic loss with 500 × difference compared to the serum-free group. ***SS-PAEIs*** also offer another topology; comb-like structures can be achieved by introducing side chains into the bioreducible backbone [59]. Additionally, with these side chains, a variety of functional elements can be incorporated. These elements can be tertiary amines for nucleic acid binding, imidazoles for endosomal buffering or protected secondary amines like diaminoethane structures or spermine [58], which can be unprotected after the polyaddition. Beside these cationic structures, other functional groups like hydrophobic elements can be introduced [59]. Polymers resulting from such reactions do not have a precise structure, but due to their bioreducibility the cleavage products are small. These bioreducible poly(amido amine)s as well as related polyaspartamide-based disulfide-containing brushed polyethylenimine derivatives (128) showed lower cytotoxicity and often more efficient gene delivery than branched PEI 25kDa.

A modification that strongly improved the efficacy of polylysine and oligolysine shuttles was the introduction of histidines [46, 60-62]. The second imidazole nitrogen exhibits ideal basicity (pKa 6.0) for an increase of endosomal buffer capacity (lower protonation at physiological than at more acidic endosomal pH) and therefore facilitating endosomal release by the “proton sponge effect” previously hypothesized for polyethylenimine. Hereby it was possible to mediate efficient delivery not only for pDNA but also for mRNA and much smaller siRNA (more information on siRNA delivery in section 1.5) with one single vector [46]. A histidine/lysine ratio of 4:1 in a Cys-His_6-Lys_3-His_6-Cys monomer (***His6 RPC*** - **Fig. 2**) provided the best results.

1.4 Design of precise oligomers for pDNA transfection

To combine the beneficial transfection properties of bioreducible PEI and related oligoethyleneimine polymers with precise chemical structure, solid phase supported polymer synthesis [63-65] was introduced. In particular, artificial amino acids containing short, defined repeats of the diaminoethane motif were prepared in boc/fmoc-protected form, appropriate for standard automated or manual peptide synthesis [66]. These building blocks, optionally in combination with natural amino acids like cysteine and other units were incorporated into peptide-like oligomers. The

artificial amino acids provide the oligomers with proton sponge capacity. For example, Stp (succinoyl tetraethylene pentamine) within a polyamide chain provides three protonatable amines, the building block Sph (succinoyl pentaethylene hexamine) provides four protonatable amines (**Fig. 4**). By solid-phase synthesis technologies, such defined oligomers can be generated with high precision in libraries of various sequences and defined lengths. Initial screenings of such a small library based on the Stp building block were performed for pDNA transfer activity [67]. Compared with standard polymers, the oligomers present LMW carriers. Consistent with their incomplete protonation at physiological pH, oligomers did not display significant cytotoxicity and were well biocompatible. Not unexpectedly, their limited size provides also limited polyplex stability. Compound ***23*** (**Fig. 4**) with 5 Stp units (representing 15 protonatable nitrogens) provided only very low polyplex stability in agarose gel electrophoresis assays and had no transfection efficiency at all. Incorporation of two cysteines, which after pDNA complexation form disulfide bonds by air oxidation strongly improve polyplex stability and gene transfer activity. Compound ***74*** with two cysteines and only two Stps did not transfect, compound ***51*** with 3 Stps showed low but significant gene transfer for N/Ps > 6, and compounds ***78*** and ***82*** with 6 or 8 Stp units and the two terminal cysteines revealed much better transfection results for N/Ps ≥ 15 [67]. These results indicate that even for oligocations that are able to interact with each other by disulfides a certain minimum of cationic binding units in each oligomer is required for activity. An additional measure for optimizing these LMW carriers was the attachment of hydrophobic fatty acids. These have stabilizing effect and mediate pH dependent endosomolytic activity. In optimized form such carriers outperformed the gold standard ***LPEI*** 22 kDa [67].

Standard ***LPEI*** 22 kDa contains approximately 500 protonatable nitrogens. Synthesis of such large linear structures by solid-phase assisted synthesis is not feasible. An approach to circumvent this limitation of length was the design of four-arm structures. These structures contain two consecutive lysines as branching points via both alpha- and epsilon amine modification followed by simultaneous elongation of each arm with two to five units of Stp, Sph or other artificial amino acids. Optionally terminal cysteines were integrated [68]. By this procedure in a few coupling steps easily carriers with up to more than hundred nitrogens (up to 68 protonatable nitrogens) were generated.

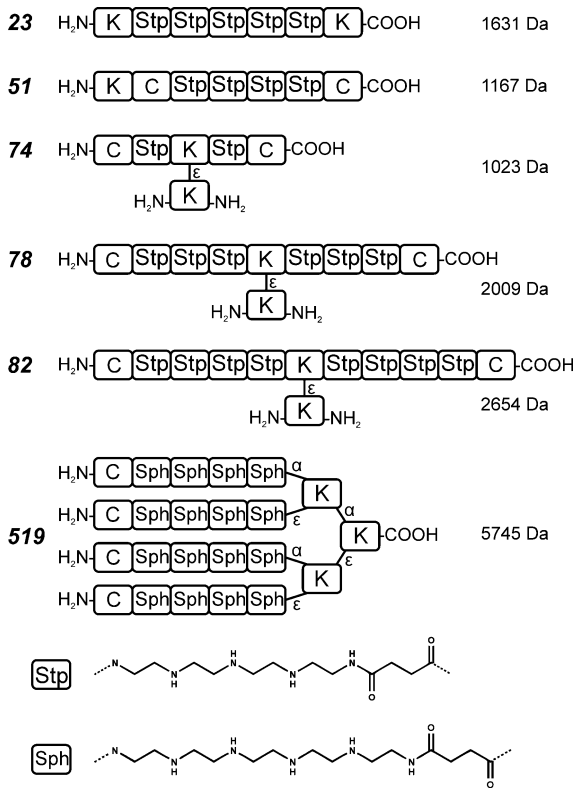

Fig. 4 pDNA carrier polymers based on artificial amino acids. There is no gene transfer activity for small structures without cysteines like compound ***23*** [67]. Structures ***51,74,78,82*** with two cysteines [67] for linear linking profit from the longer cationic binding region. ***519*** [68] presents crosslinking ability in a four-arm structure with the longer diaminoethane motif (Sph).

Screening for pDNA transfection showed the following: the number of nitrogens per building block (Sph containing 6N > Stp with 5N > Gtt with 4N) was more important for pDNA polyplex condensation and transfection than the total number of nitrogens per oligomer. Sph-based four-arm structures with three repeating units per arm (Sph_3, 72 ethylenimine nitrogens in total) displayed comparable transfection activity as ***LPEI*** already in the absence of cysteines, whereas Gtt-based four arms with four repeating units (Gtt_4, 64 ethylenimine nitrogens in total) were inactive. In all cases the presence of terminal cysteines further enhanced transfection activity [68]. Apparently, this bioreversible option for disulfide-based stabilization was beneficial. The transfection activity of the most potent cysteine-containing Sph four-arm compound ***519*** (**Fig. 4**) exceeded the gold standard ***LPEI*** by up to 50-fold for the N/P ratio 12.

1.5 Cargo matters: reversible disulfide bonds stabilizing siRNA polyplexes

The delivery of siRNA with cationic systems poses different challenges than pDNA [13, 69, 70]. Although both nucleic acids contain a negatively charged backbone (phosphodiester for physiological or phosphorothioate in the case for some stabilized nucleic acids), the number of base pairs (bp) per molecule and their topology are different. With a 7 nm rod-shaped size, 21 - 23 bp and 42 - 46 anionic charges per molecule [71, 72], siRNA is comparatively small and cannot offer thousands of negative charges a long cyclic pDNA provides for binding. This results in a lower electrostatic stabilization, less gain in entropy by complex formation, and therefore less stable siRNA polyplexes. Most of the previously described systems for the transport of pDNA, including polylysine [73], and PEI [69] show much less efficiency in siRNA transfection unless appropriate modifications are introduced. One of the encouraging options presents the incorporation of bioreducible stabilizing disulfide bonds; either by crosslinking of siRNA into more 'DNA-like' oligomers [74-76], by linking siRNA with the cationic carrier [77-79], or by crosslinking the cationic carrier molecules.

Based on the knowledge of pDNA delivery systems new carriers have been invented to accomplish the delivery of siRNA. The approximately 4kDa pseudodendritic degradable oligomer ***HDO***, consisting of 800 Da oligoethylenimine (OEI) and 1,6-hexandiol diacrylate was evaluated for siRNA delivery [80]. This LMW polymer previously had been proven as an effective pDNA carrier [81], but it did not mediate siRNA delivery. Modification of siRNA/***HDO*** polyplexes with DSP provided bioreversible stabilization (**Fig. 5**, top), as demonstrated by improved siRNA binding ability in an agarose gel electrophoresis assay. The change in the structures of polyplexes could be monitored by the measurement of size and zeta potential. For example, the size of particles formed at N/P 4 increased from 113 ± 3 nm to 197 ± 3 nm and the zeta potential decreased from 27.6 ± 0.4 mV to 20.1 ± 0.7 mV. Only the disulfide-stabilized siRNA/***HDO*** polyplexes were taken up by cells and resulted in efficient gene silencing.

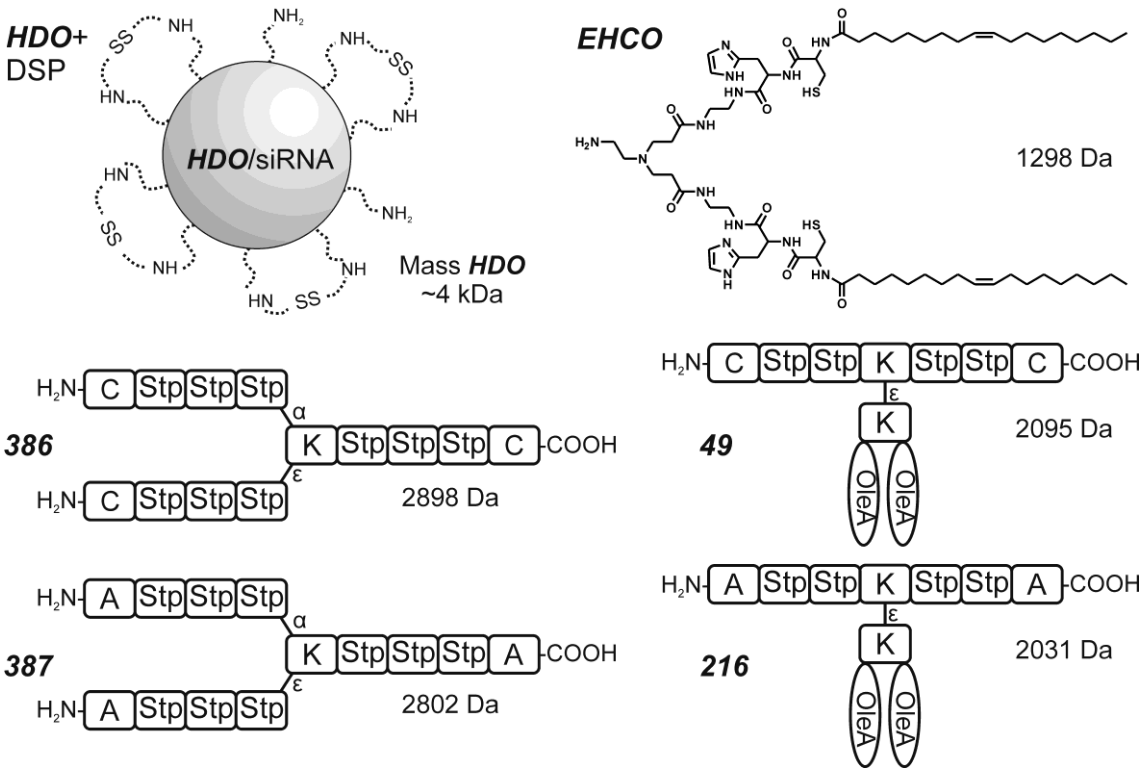

Fig. 5 Carriers optimized for siRNA delivery. DSP (dithiodipropionic acid di(N-succinimidyl ester)) linked with free amines on the surface of ***HDO***/siRNA polyplex [80]. Active three-arm structure ***386*** and its inactive analog ***387*** [82, 83]. Lipo-oligomer ***EHCO*** (122) with histidine, cysteine and oleic acid (OleA). Active t-shape polymer ***49*** and its inactive analog ***216*** [82]***.***

The importance of disulfide-based crosslinking for siRNA can be observed when using precise sequence-defined oligomers built by solid phase synthesis as described earlier. Three-arm structures like ***386*** (**Fig. 5**) [82, 83] that contain Stp units for nucleic acid complexation were able to bind and transfect siRNA only when containing cysteines for crosslinking at the end of each arm. The structure ***386*** showed perfect binding in electrophoresis gel shifts for low N/P ratios from 3 on, whereas control structure ***387*** was inactive. Analogously, four-arm structures [68], which can transfect pDNA even without cysteine incorporations, were inactive for siRNA delivery. Cysteine at the end of each arm (***519*** - **Fig. 4**) resulted in enhanced transfection efficiency for pDNA and was absolutely required for siRNA-based gene silencing.

T-shaped lipo-oligomers such as ***49*** (**Fig. 5**) also were dependent on the two stabilizing cysteines. Both the alanine analog (***216***), as well as compound ***49*** reacted with N-ethylmaleimide (NEM) irreversibly blocking the thiol groups against disulfide based stabilization, had lost the gene silencing activity [82]. FCS measurements in 90 %

serum revealed that the size of ***49*** polyplexes for N/P 12 increased from 49 nm within 30 minutes to 68 nm at room temperature. At 37°C the polyplex was stable after 10 minutes, but some dissociation was observed already after 30 minutes [84]. Disulfide stabilization was also required for gene silencing using the lipo-oligomer ***EHCO*** (**Fig. 5**) [85]. This solid-phase synthesis derived siRNA carrier contains pH-sensitive ethylenediamine, and histidine units, stabilizing cysteine and oleic acid units.

In order to improve polylysine properties, Kataoka and coworkers used a polyethylene glycol (PEG) -polylysine block polymer, which was reacted with iminothiolane [86]. Thereby a few thiols were incorporated onto lysines without losing cationic charges, because the primary amines are converted into positively charged amidines. With siRNA so-called polyion complex (PIC) micelles are formed. The presence of the iminothiolane modification results in disulfide-based crosslinked polymers stabilizing the siRNA containing PIC micelles. These micelles were able to achieve 100-fold higher transfection efficiencies than the analogous micelle without crosslinking. Stability tests with increasing concentrations of sodium chloride revealed that the stability of crosslinked polyplexes was significantly increased and could be abolished with reducing agents. Polyplexes with unmodified PEGylated polylysine were not even stable at physiological ionic strength.

Many multifunctional carriers for siRNA-based on the same principle but including shielding and targeting domains also rely on disulfide bonds [87]. For example, the folate receptor-targeted oligomer ***356*** (**Fig. 6**) formed stable nanosized siRNA complexes of only 6 nm hydrodynamic diameter. Replacing cysteines by serines (compound ***420***) resulted in dramatic loss of siRNA binding as well as gene silencing activity. An additional use of bioreducible disulfides in this polyplex was the reversible covalent linkage of the siRNA with an endosomolytic influenza virus-derived peptide INF7 (**Fig. 6**), which was important for an efficient endosomal escape and cytosolic delivery.

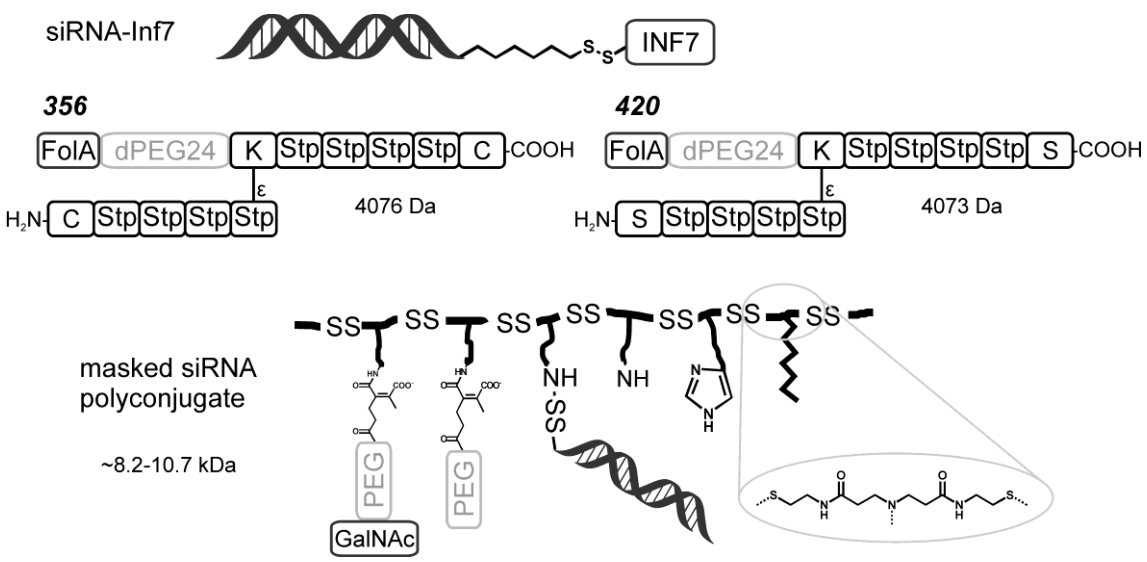

Fig. 6 Multifunctional siRNA polyplexes containing pH-and redox-sensitive components. Active ***356*** forms an efficient carrier with siRNA-INF7, whereas control ***420*** with serine instead of cysteine shows low binding and transfection efficiency [87]. The masked siRNA polyconjugate presents a shuttle with pH reversible PEGylation with and without targeting ligand, covalently bound siRNA, imidazole residues and fatty acids based on a bioreducible poly(amido amine) backbone [79].

This reversible linking can also be used for attaching siRNA directly to a carrier. Using click chemistry, a PEG-folate was covalently attached to siRNA via a disulfide containing linkage [77]. Also polycations were attached in this manner. Disulfides have been used to connect siRNA covalently to a pH-responsive masked endosomolytic polylysine carrier [78]. Wang and coworkers used it for coupling to a bioreducible poly(amido amine) backbone (**Fig. 6**, bottom) [79]. The side chains of the backbone in this carrier were functionalized with hydrophobic modifications, imidazoles, and pH reversible targeting ligands. These multifunctional systems with bioreducible properties demonstrated efficient, targeted gene silencing *in vivo*. The best performing polymer with a mixture of 40/30/30 molar ratio of 2-(2-aminoethoxy)ethyl/ 2-(1H-imidazol-4-yl)ethyl/ dodecyl and a molar weight of ~8.64 kDa showed 80 % mRNA knockdown in mice.

1.6 Tuning the timing and extent of bioreduction of dynamic carriers

The various approaches for dynamic stabilization of bioconjugates and nanoparticulate carriers reviewed in the earlier sections build on the favorable difference between extracellular/intracellular redox conditions and GSH concentration. However, the frequently claimed notions that a) “disulfide bonds are generally stable outside the cell” or b) that “they are easily cleaved in endosomes” should be questioned as already stated earlier in literature [88], and might be even, in part, misconceptions, or, at least, not generally valid.

Several disulfide-bonded protein conjugates and immunotoxins have been found to be cleaved *in vivo* after intravenous application [36, 37]. The questions about the exact site of bioreduction might be less important for some nanocarrier designs but critical for others. The majority of the previously mentioned strategies build on cytosolic cleavage of multiple disulfide bonds of oligocationic carriers that had caged their cargo during the extracellular delivery. In those cases, it might be less important whether bioreduction of some fewer bonds starts at the cell surface, significantly takes place in the endosomal vesicle system, or largely happens in the cytosol. When cleavages of large numbers (approximately hundreds) of disulfide bonds per nanoparticles are required, the majority of cleavage processes can be assumed for the cytosolic location because of its larger reduction capacity.

Bioreducible disulfide linkages, however, have also been considered dynamic elements in earlier steps of the delivery process: For example, in the process of nanocarrier deshielding, which might be beneficial to occur at the cell surface or within endosomes, or for activation of endosomolytic domains within endosomal vesicles. The so-called “PEG dilemma” comprises the experiences that surface shielding of nanocarriers with PEG is very beneficial for extended blood circulation and (passive or active) tissue targeting, however, negatively affects intracellular uptake across endosomal membranes. Endosomal pH-sensitive cleavable PEGs are able to overcome this dilemma [89-93]. Thus, bioreductive cleavage of disulfide-bound PEG at the cell surface would be a very useful process [94-97]. In our own research group, productive deshielding of PEGylated pDNA/PEI polyplexes was far more successful in utilizing pH-labile bonded hydrazone [93] instead of disulfide-bonded [98] PEG chains.

Some approaches such as those reported by Lee and coworkers [99] successfully build on reductive liberation of endosomolytic agents within the endosome for subsequent cytosolic transport of the cargo. Such strategies are rationally supported by natural examples, including toxins and viral translocation that include a disulfide cleavage as a part of the translocation process [100-107]. For example, several toxins of the AB_5 family (A toxic subunit, B receptor-binding carrier units), including cholera toxin, shiga toxin, or pertussis toxin, enter cells by endocytosis. This is followed by retrograde transport into the ER lumen, where repair chaperone PDIs recognize single disulfide bonds as “misfolded protein domains”. Then, a physiological repair process named ER-associated degradation (ERAD) retro-translocates the A unit through a pore to the cytosol for proteasome-mediated degradation (**Fig. 7**) [106].

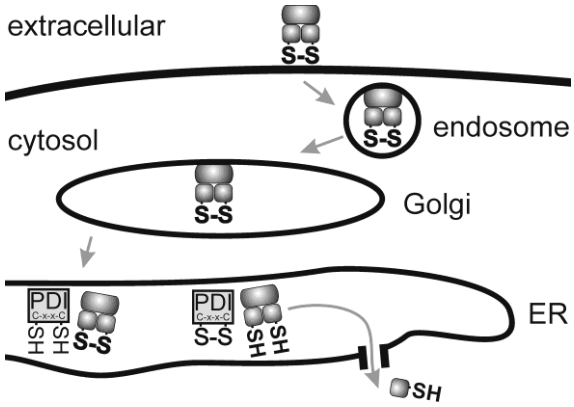

Fig. 7 Retrograde transport followed by reductive translocation to the cytosol. Several protein toxins (*e.g*. Cholera toxin, Shiga toxin, Pertussis toxin, ricin, or Pseudomonas exotoxin A) attach to receptors on the surface of the cell and are transported via Golgi to the Endoplasmic Reticulum (ER) by retrograde transport. A key disulfide is recognized as a “misfolded ER substrate” and reduced in the presence of a protein disulfide isomerase (PDI) followed by translocation of a toxin fragment to the cytosol.

AB-type toxins such as ricin or Pseudomonas exotoxin, or some viruses such as SV40 [104], also contain disulfide linkages, which require cleavage for cytosolic translocation, presumably mediated by PDIs. For translocation, diphtheria toxin requires an analogous cleavage by PDI in the endosomal compartment [103]. It, however, should be kept in mind that bioreductive potential in standard acidifying endosomes might be more limited [88] and applicable for special cases only.

In sum, many bioreductive approaches are built merely on educated guesses that are supported by facts from nature and empirical findings and imagination (hopefully not too far from reality). A more quantitative understanding of the bioreductive behavior of cellular processes, however, would provide enormous help for improved designs and, thus, present important opportunities for the future.

In this direction, Leroux and coworkers [108] developed a well-characterized, defined dendrimeric oligomer probe for analysis of bioreductive disulfide cleavage in cellular systems. The probe consists of generation 3 dendrimer PAMAM-G3 with disulfide-linked dye $(BODIPY)_2$, which provides the ability to distinguish between reduction of internal (dendrimer core) and surface disulfide bonds. Applying this system to four cell lines with different reductive potency (HeLa, A549>PC3>Caco-2 cells), both interesting expected findings and surprising findings were made. For example, data based on pulsed thiol depletion and endocytosis inhibitor studies revealed the rather surprising finding that probe disulfide cleavage occurred exclusively at the extracellular cell surface, possibly triggered by cell surface oxidoreductases such as PDIs or chaperones (also belonging to the PDI family), with secreted thiols such as GSH acting as cofactors. Incubation with a cell membrane-impermeable oxidant completely suppressed bioreduction.

The same study evaluated bioreduction of the PAMAM probe after pDNA complex formation. Incorporation into such DNA polyplexes reduced the cell surface bioreduction, which is consistent with sterically restricted access of the probe to cell surface oxidoreductases. For the most reducing HeLa cell line, the logical distinction between cleavable disulfides in surface and core states became apparent. Moreover, the expected subsequent bioreduction after delivery into the acidic endosomal environment was incomplete. Intentionally, the authors had selected G3 PAMAM, which in contrast to higher-generation PAMAM or PEI does not have “proton sponge” based endosomal escape properties. The addition of chloroquine as an endosomolytic agent strongly enhanced bioreduction, which was consistent with endosomal escape and efficient reduction in the cytosol. As the authors note, “efficient bioreduction in the endosomes, while sometimes reported, is not a universal phenomenon and should be verified for each new system and its corresponding target cell line” [108].

How may we utilize an increased knowledge about reductive characteristics of different biological microenvironments? Not only the biological surrounding influences the fate of disulfide bonds, but also the molecular chemical environment of disulfide bonds within a dynamic carrier can be tuned. For example, by stabilizing disulfide bonds by bulky groups providing sterical hindrance [38, 109], different exposure (core or surface) within a nanoparticle system (as illustrated in the PAMAM polymer example discussed earlier), the electrostatic environment facilitating or restricting electrostatic interaction with a reducing agent [108, 110], or the number and positioning of multiple disulfide bonds [43].

The influence of bulky groups on disulfide stability was shown *in vitro* with structures with methyl, benzene, and cationic residues localized next to disulfide bonds [38]. When treated with 0.03 mM DTT at pH 7.4, the stability was as follows: The most stable derivate was the one with methyl and benzene residue at the α-C next to the disulfide bond, followed by the same derivate without methyl group, followed by a structure with an alkyl chain next to the disulfide group. The presence of a cationic charge in δ-C position next to the disulfide resulted in a faster reduction than with all uncharged linkers mentioned earlier. Based on this information, the most stable and the most labile structure were incorporated in a linker to connect an antibody (OX7) with a Ricin A toxin subunit to form immunotoxins. These immunotoxins were tested in mice for stability *in vivo*. From the more stable disulfide-linked immunotoxin with methyl and benzene residue, 50 % in active form and 50 % in free antibody form were present in blood 48 h after an intravenous injection. In contrast, the bioreducible linkage with the cationic element in its environment reached the same cleavage stage (50/50 ratio immunotoxin/free antibody) after only 8 h [38]. More recently [109], a systematic study of disulfide-linked antibody-maytansinoid immunotoxins was reported while evaluating the disulfide-linker stability and antitumoral activity *in vivo* in mice. Sterical hindrance (by methyl group substitutions flanking the disulfide bonds) enhanced stability to reductive cleavage by DTT and plasma stability in mice. In *in vivo* efficacy testing, a conjugate with intermediate disulfide bond stability (having two methyl groups on the maytansinoid side of the disulfide linkage but no methyl substitution on the antibody linker side) displayed the highest antitumoral efficacy.

Not only the sterical and electrostatic environment of disulfides, but also the reducing agents and the pH have a crucial influence on the stability of a disulfide bond. It has

been shown that positively charged amino acids next to a cysteine in a peptide destabilized the disulfide bond between oxidized dimers in a 10 mM GSH solution at pH 4.9 (mimics late endosomal/lysosomal environment) [110]. The influence was higher for amino acids with higher pKa values (highest for arginine with pKa 12.1) and if more positively charged amino acids were incorporated. The distance (α- or β- amino acid next to cysteine) played a minor role. Analogous negatively charged amino acids with low pKa values (glutamic acid with pKa 4.3 has the strongest influence) stabilized the disulfide bond. Consequently, the half-life of structures with α- and β-arginine was only 0.17 h compared with 8.7 h for structures with α- and β-glutamic acid. If GSH, which is also present in its deprotonated GS^--form, was exchanged by cysteine as a reducing agent, which also can be deprotonated, the same tendency could be observed. If cysteamine, which does not have a negatively charged form, was used, the half-life for all tested peptides was comparable. For higher pH values, such as pH 7.4 in the cytosol, the cleavage kinetics in GSH redox buffer accelerated profoundly (from 8.7 h for pH 4.9 to 0.1 h in half life for the structure with α- and β-glutamic acid). The higher amounts of charged GS^-at higher pH seem to be responsible for this faster cleavage. Special formations of cysteines embedded in a peptidic environment can influence not only the kinetics but also the formation of disulfides in structures. A motif consisting of cysteine – any amino acid – cysteine (C-X-C) was evaluated for different flanking and central natural amino acids and revealed the best properties for the cationic amino acid arginine combined with the flanking amino acids glutamic acid (G-C-R-C-G) [43]. The motif not only offered a prolonged resistance against a reducing solution with 0.02 mM GSH redox buffer (more than 60 % remaining, compared with less than 10 % for single cysteines after 6 h), but also formed orthogonal twin disulfide dimers in the presence of single cysteines selectively. The arginine was shown to strongly direct the equilibrium toward the twin disulfide dimers. Responsible for this effect seems to be the positive charge that promotes the reactivity of thiolates, which are intermediately required to form a disulfide bond. The surrounding glutamic acids seem to stabilize the disulfide bond by reducing the rates of disulfides exchange in GSH redox buffer.

1.7 Aim of the thesis

The bioreducible structure of disulfide bonds offers a very beneficial tool for oligocationic gene delivery carriers. Importantly, it provides a straightforward option for the design of dynamic carriers and shuttles discriminating between intracellular and extracellular cytosolic locations.

The recent development of a solid-phase synthesis platform for the assembly of sequence-defined oligo(ethanamino)amides enables quick and easy synthesis of cationic oligomers for complexing nucleic acids. Beside specialized cationic building blocks, all natural amino acids, and further units can be incorporated to customize those delivery systems. The synthesis of precise gene delivery vehicles is an effective way to establish structure–activity relationships and optimize existing carriers. In this thesis, two strategies were tested to enrich the library of oligocationic carriers by new redox-sensitive structures.

As a first aim of the thesis, cationic oligomers with different topologies had to be modified with twin disulfide-forming cysteine – arginine – cysteine (CRC) motifs. Recently Wu et al. introduced this new bioreducible dynamic covalent bond, called the twin disulfide, which has orthogonal disulfide pairing characteristics to the standard single disulfide [43]. Peptides containing the CRC motifs were found to selectively form stable twin disulfide dimers with other CRC peptides, which are more stable against reducing agents. The influence of this motif versus single disulfide on the biophysical properties and biological performance of polyplexes were to be investigated with pDNA and siRNA as nucleic acid cargoes. Properties of the structures like nucleic acid binding, serum stability, response to reducing agents, and gene transfer/silencing should be analyzed. The main focus was to be put on the effect of the CRC motif on polyplex stability. Beside non-targeted structures, shielded and folate-targeted structures had to be included in this study.

The second aim was the evaluation of the bioactivity of redox-sensitive siRNA lipopolyplexes. Although high stability of siRNA polyplexes is desirable in the extracellular space and for cellular uptake, intracellular disassembly is important for the cytosolic release of siRNA and RNA-induced silencing complex formation. To improve the release of siRNA, bioreducible lipo-oligomers should be synthesized by solid-phase assisted synthesis using the building block Fmoc-succinoyl-cystamine for

precise positioning of a disulfide unit between a lipophilic diacyl (bis-myristyl, bis-stearyl or bis-cholestanyl) domain and an ionizable oligocationic siRNA binding unit. Especially the effect on transfection efficiency and toxicity had to be analyzed.

As a third aim, the most potent lipo-oligomers from the last section were to be extended by azide functions to form siRNA polyplexes that could further be modified with DBCO-bearing shielding and targeting agents. The new peptidic agent poly(sarcosine) should be tested for its shielding ability *in vitro* and *in vivo*. The folate ligand was to be used for targeting specific cells.

The last aim was the optimization of DBCO click reagents. A solid phase approach should be used for synthesizing folate-targeted DBCO poly(ethylene glycol) agents. Hereby the surface covering part of the gene delivery system can be designed in a precise way. Correlations of PEG length and DBCO moieties with biological activity should be analyzed.

2 Materials and Methods

2.1 Materials

The solvents, reagents and buffers used for the experiments are presented in **Table 1**, **Table 2** and **Table 3**.

Table 1 Solvents used for experimental procedures

Solvent	CAS-No.	Supplier
Acetonitrile[1]	75-05-8	VWR Int. (Darmstadt, Germany)
Chloroform[2]	67-66-3	VWR Int. (Darmstadt, Germany)
Chloroform-d[3]	865-49-6	Euriso-Top (Saint-Aubin Cedex, France)
Deuterium oxide[3]	7789-20-0	Euriso-Top (Saint-Aubin Cedex, France)
Dichloromethane[4]	75-09-2	Bernd Kraft (Duisburg, Germany)
*N,N-D*imethylformamide[5]	68-12-2	Iris Biotech (Marktredewitz, Germany)
Dimethyl sulfoxide[6]	67-68-5	Sigma-Aldrich (Munich, Germany)
Ethanol absolute[4]	64-17-5	VWR Int. (Darmstadt, Germany)
Ethyl acetate[7]	141-78-6	Staub & Co. (Nürnberg, Germany)
n-Heptane[8]	142-82-5	Grüssing (Filsum, Germany)
n-Hexane[8]	110-54-3	Brenntag (Mülheim/Ruhr, Germany)
Methanol[4]	67-56-1	Fisher Scientific (Schwerte, Germany)
Methanol-d4[3]	811-98-3	Euriso-Top (Saint-Aubin Cedex, France)
Methyl-*tert*-butyl ether[9]	1634-04-4	Brenntag (Mülheim/Ruhr, Germany)
N-Methyl-2-pyrrolidone[5]	872-50-4	Iris Biotech (Marktredewitz, Germany)
Tetrahydrofuran[4]	109-99-9	Fisher Scientific (Schwerte, Germany)
Water[10]	7732-18-5	In-house purification

[1] HPLC grade; [2] DAB grade, distilled before use; [3] NMR grade (> 99.9 %); [4] analytical grade; [5] peptide grade; [6] BioReagent grade (> 99.9 %); [7] purum, distilled before use; [8] purissimum; [9] synthesis grade; [10] purified, deionized;

Table 2 Reagents used for experimental procedures

Reagent	CAS-No.	Supplier
1-Hydroxybenzotriazole hydrate	123333-53-9	Sigma-Aldrich (Munich, Germany)
2-Chlorotritylchloride resin	42074-68-0	Iris Biotech (Marktredewitz, Germany)
5,5′-Dithiobis(2-nitrobenzoic acid)	69-78-3	Sigma-Aldrich (Munich, Germany)
5β-Cholanic acid	546-18-9	Sigma-Aldrich (Munich, Germany)
Acetic acid	64-19-7	Sigma-Aldrich (Munich, Germany)
Acetic anhydride	108-24-7	Sigma-Aldrich (Munich, Germany)
Agarose NEEO Ultra	9012-36-6	Carl Roth (Karlsruhe, Germany)
Ammonia solution 25 %	1336-21-6	Carl Roth (Karlsruhe, Germany)
Boc-L-Cys(Trt)-OH	21947-98-8	Iris Biotech (Marktredewitz, Germany)
Bromophenol blue	115-39-9	Sigma-Aldrich (Munich, Germany)
Chloroquine diphosphate	50-63-5	Sigma-Aldrich (Munich, Germany)
Cystamine · 2HCl	56-17-7	Sigma-Aldrich (Munich, Germany)

D-(+)-Glucose monohydrate	14431-43-7	Merck Millipore (Darmstadt, Germany)
DBU	6674-22-2	Sigma-Aldrich (Munich, Germany)
Dde-L-Lys(Fmoc)-OH	156648-40-7	Iris Biotech (Marktredewitz, Germany)
Dibenzocyclooctyne-acid	1353016-70-2	Sigma-Aldrich (Munich, Germany)
EDTA disodium salt dihydrate	6381-92-6	Sigma-Aldrich (Munich, Germany)
Fmoc-L-Arg(Pbf)-OH	154445-77-9	Iris Biotech (Marktredewitz, Germany)
Fmoc-L-Cys(Trt)-OH	103213-32-7	Iris Biotech (Marktredewitz, Germany)
Fmoc-L-Glu-OtBu	84793-07-7	Merck Millipore (Darmstadt, Germany)
Fmoc-L-Gly-OH	29022-11-5	Iris Biotech (Marktredewitz, Germany)
Fmoc-L-His(Trt)-OH	109425-51-6	Iris Biotech (Marktredewitz, Germany)
Fmoc-L-Leu-OH	35661-60-0	Iris Biotech (Marktredewitz, Germany)
Fmoc-L-Lys(Boc)-OH	71989-26-9	Iris Biotech (Marktredewitz, Germany)
Fmoc-L-Lys(Fmoc)-OH	78081-87-5	Iris Biotech (Marktredewitz, Germany)
Fmoc-L-Lys(ivDde)-OH	204777-78-6	Iris Biotech (Marktredewitz, Germany)
Fmoc-L-Lys(N_3)-OH	159610-89-6	Iris Biotech (Marktredewitz, Germany)
Fmoc-L-Trp(Boc)-OH	43824-78-6	Iris Biotech (Marktredewitz, Germany)
Fmoc-L-Tyr(tBu)-OH	71989-38-3	Iris Biotech (Marktredewitz, Germany)
Fmoc-L-Val-OH	68858-20-8	Iris Biotech (Marktredewitz, Germany)
Fmoc-*N*-amido-dPEG$_{24}$-acid	756526-01-9	Quanta Biodesign (Powell, Ohio, USA)
Fmoc-OSu	82911-69-1	Iris Biotech (Marktredewitz, Germany)
Fmoc-Stp(Boc$_3$)-OH	-	In-house synthesis [66]
Folic acid	59-30-3	Sigma-Aldrich (Munich, Germany)
GelRed	-	Biotium Inc. (Hayward, CA, USA)
Glutathione reduced	70-18-8	Sigma-Aldrich (Munich, Germany)
HBTU	94790-37-1	Multisyntech (Witten, Germany)
Heparin sodium 5000 I.E/mL	9041-08-1	ratiopharm GmbH (Ulm,.Germany)
HEPES	7365-45-9	Biomol (Hamburg, Germany)
Hydrazine monohydrate	7803-57-8	Sigma-Aldrich (Munich, Germany)
Hydrochloric acid solution (1 M)	7647-01-0	Sigma-Aldrich (Munich, Germany)
Iminodiacetic acid	142-73-4	Sigma-Aldrich (Munich, Germany)
LPEI	9002-98-6	In-house synthesis [111]
MTT	298-93-1	Sigma-Aldrich (Munich, Germany)
Myristic acid	544-63-8	Sigma-Aldrich (Munich, Germany)
N,N-Diisopropylethylamine	7087-68-5	Iris Biotech (Marktredewitz, Germany)
N10-(Trifluoroacetyl)pteroic acid	37793-53-6	Clauson-Kass A/S (Farum, Denmark)
Ninhydrin	485-47-2	Sigma-Aldrich (Munich, Germany)
Oleic acid	112-80-1	Sigma-Aldrich (Munich, Germany)
PEI-Suc 10 %	-	In-house synthesis [112]
Phenol	108-95-2	Sigma-Aldrich (Munich, Germany)
Piperidine	110-89-4	Iris Biotech (Marktredewitz, Germany)
Potassium cyanide	151-50-8	Sigma-Aldrich (Munich, Germany)
Pybop®	128625-52-5	Multisyntech GmbH (Witten, Germany)
Sephadex® G-10	9050-68-4	GE Healthcare (Freiburg, Germany)
Sodium hydroxide (anhydrous)	1310-73-2	Sigma-Aldrich (Munich, Germany)
Sodium hydroxide solution (0.05 M)	1310-73-2	Sigma-Aldrich (Munich, Germany)
Stearic acid	57-11-4	Sigma-Aldrich (Munich, Germany)
Succinic anhydride	108-30-5	Sigma-Aldrich (Munich, Germany)
Tetraethylene pentamine · 5HCl	4961-41-5	Sigma-Aldrich (Munich, Germany)
Triethylamine	121-44-8	Sigma-Aldrich (Munich, Germany)

Trifluoroacetic acid	76-05-1	Iris Biotech (Marktredewitz, Germany)
Triisopropylsilane	6485-79-6	Sigma-Aldrich (Munich, Germany)
Triton™ X-100	9002-93-1	Sigma-Aldrich (Munich, Germany)
Trizma® base	77-86-1	Sigma-Aldrich (Munich, Germany)

Table 3 Buffers used for experimental procedures

Buffer	Composition
10 mM HCl SEC solvent	693 mL water, 300 mL acetonitrile, 7 mL 1M HCl solution
Electrophoresis loading buffer	6 mL glycerine, 1.2 mL 0.5 M EDTA solution (pH 8.0), 2.8 mL H_2O, 20 mg bromophenol blue
Ellman buffer	0.1 M sodium phosphate buffer (pH 8.0), 1mM EDTA
HBG	20 mM HEPES, 5 % glucose, pH 7.4
TBE buffer	89 mM Trizma® base, 89 mM boric acid, 2 mM EDTA-Na_2

Citrate-buffered human blood for erythrocyte leakage assays was kindly supplied by Klinikum der Universität München (Munich, Germany).

2.1.1 Equipment for solid-phase synthesis

Automated parallel synthesis or synthesis with microwave irradiation was carried out using a Biotage Syro Wave (Biotage AB, Uppsala, Sweden) peptide synthesizer. Disposable polypropylene (PP) syringe microreactors with the volume sizes 2 mL, 5 mL, and 10 mL were purchased from Multisyntech (Witten, Germany). It was conducted with polytetrafluoroethylene (PTFE) filters. The recommended size of the reactors was chosen according to the resin amount. For manual solid-phase synthesis microreactors with polyethylene filters were used. Reactors were mixed with an overhead shaker during reactions.

2.1.2 Nucleic acids

2.1.2.1 pDNA

The plasmid pCMVLuc (encoding for firefly luciferase under control of the CMV promoter) was purchased from Plasmid Factory (Bielefeld, Germany) or amplified in *E. coli* DH5α and purified from the bacterial lysate using a Qiagen Plasmid Giga Kit (Qiagen, Hilden, Germany). The concentration of nucleic acid solutions was determined photometrically using an Eppendorf BioPhotometer (Eppendorf, Hamburg,

Germany). Cy5-labeled nucleic acids were produced with a Cy5-labelling kit obtained from Mirus Bio (Madison, WI, USA).

2.1.2.2 siRNA

All siRNAs and modified siRNA compounds used are presented in **Table 4**. They were synthesized by Roche Kulmbach GmbH (now Axolabs GmbH, Kulmbach, Germany). The INF7 peptide (sequence: H_2N-GLFEAIEGFIENGWEGMIDGWYGC-amide) was purchased from Biosyntan (Berlin, Germany) and conjugated to HS-C_6-siRNA according to [87].

Table 4 siRNA strands

siRNA	Target	Sequence
INF7-siCtrl	-	5'-(INF7)(SSC_6)AuGuAuuGGccuGuAuuAGdTsdT-3' (sense) 5'-CuAAuAcAGGCcAAuAcAUdTsdT-3' (antisense)
INF7-siGFP	eGFP-Luc	5'-(INF7)(SSC_6)AuAucAuGGccGAcAAGcAdTsdT-3' (sense) 5'-UGCUUGUCGGCcAUGAuAUdTsdT-3' (antisense)
Cy5-siAHA1	AHA1	5'-(Cy5)(NHC_6)GGAuGAAGuGGAGAuuAGudTsdT-3' (sense) 5'-ACuAAUCUCcACUUcAUCCdTsdT-3' (antisense)
Cy7-siAHA1	AHA1	5'-(Cy7)(NHC_6)GGAuGAAGuGGAGAuuAGudTsdT-3' (sense) 5'-ACuAAUCUCcACUUcAUCCdTsdT-3' (antisense)
siCtrl	-	5'-AuGuAuuGGccuGuAuuAGdTsdT-3' (sense) 5'-CuAAuAcAGGCcAAuAcAUdTsdT-3' (antisense)
siEG5	EG5 / KSP	5'-ucGAGAAucuAAAcuAAcudTsdT-3' (sense) 5'-AGUuAGUUuAGAUUCUCGAdTsdT-3' (antisense)
siGFP	eGFP-Luc	5'-AuAucAuGGccGAcAAGcAdTsdT-3' (sense) 5'-UGCUUGUCGGCcAUGAuAUdTsdT-3' (antisense)

Small letters: 2'-methoxy-RNA, s: phosphorothioate. All nucleic acids were synthesized by the Roche Kulmbach GmbH (now Axolabs GmbH, Kulmbach, Germany). INF7 modified siRNAs were synthesized according to [87].

2.1.3 Cell culture

Cell culture work was carried out by Dr. Petra Kos, Ana Krhac Levacic, Dr. Daniel Edinger, Dr. Katharina Müller, Dr. Dian-Jang Lee and Dr. Wei Zhang (Pharmaceutical Biotechnology, LMU). All cell culture media, antibiotics and fetal bovine serum (FBS) were purchased from Invitrogen (Karlsruhe, Germany). The individual media used for the different cell cultures are summarized in **Table 5**. All media were supplemented with 10 % FBS, 4 mM stable glutamine, 100 U/mL penicillin and 100 µg/mL

streptomycin. Exponentially growing cells were detached from the culture flasks using trypsin-EDTA solution (Invitrogen, Karlsruhe, Germany) and cell suspensions were seeded at the desired density for each experiment. Luciferase cell culture lysis buffer and D-luciferin sodium salt were purchased from Promega (Mannheim, Germany).

Table 5 Overview of the used cell lines and culture media

Cell line	Description	Medium
DU145/eGFPLuc	Human prostate cancer cells expressing the eGFP-Luciferase fusion gene	RPMI-1640
KB	Human cervix carcinoma cells	RPMI-1640, folate-free
KB/eGFPLuc	Human cervix carcinoma cells expressing the eGFP-Luciferase fusion gene	RPMI-1640, folate-free
L1210	Mouse lymphocytic leukemia cells	RPMI-1640, folate-free
Neuro2A	Mouse neuroblastoma cells	DMEM
Neuro2A/eGFPLuc	Mouse neuroblastoma cells expressing the eGFP-Luciferase fusion gene	DMEM

2.2 Methods

2.2.1 Synthesis of disulfide-linker building block (ssbb):

Fmoc-succinoyl-cystamine

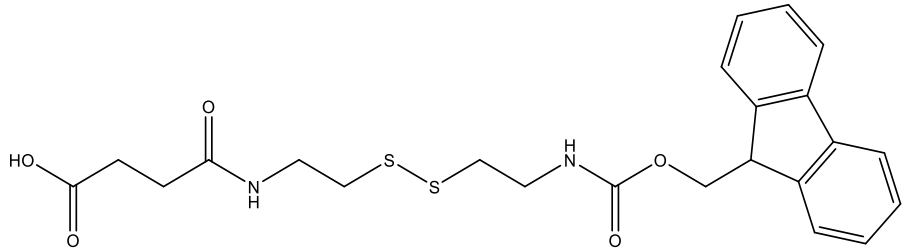

15.0 g of cystamine dihydrochloride (66.6 mmol, 1 eq.) were suspended in 150 mL of THF with 23.2 ml of DIPEA (133.2 mmol, 2 eq.) and cooled down to -80 °C. 18.0 g (53.3 mmol, 0.8 eq.) of Fmoc-OSu were dissolved in 200 mL of THF and added dropwise over the course of 3 h. The reaction was stirred for additional 1 h at -80 °C and then for 1 h at RT. DIPEA (23.2 mL, 133.2 mmol, 2 eq.) was added and the reaction mixture was cooled to 0 °C. Succinic anhydride (12.0 g, 119.9 mmol, 1.8 eq.) was dissolved in 150 mL of THF. This solution was added dropwise to the reaction mixture at 0 °C and stirred over-night. The reaction mixture was concentrated to approximately 200 mL, mixed with 200 mL of DCM and was washed 5 × with 0.1 M sodium citrate buffer (pH 5.2). The organic phase was dried over sodium bicarbonate, concentrated and purified by dry column vacuum chromatography (DCVC) using a n-heptane/EtOAc gradient (starting from 1 : 1) to elute Fmoc-byproducts, followed by a EtOAc/MeOH gradient to isolate the product. The solvent was removed under reduced pressure to give 6.2 g of a white solid (13.1 mmol, 24.5 %).

2.2.2 Loading of a 2-chlorotrityl chloride resin with an Fmoc protected amino acid

After swelling of 750 mg of a 2-chlorotrityl chloride resin (1.2 mmol chloride, 1 eq) in water-free DCM for 10 min, the first Fmoc protected amino acid (T-shape: 0.3 eq. Fmoc-Tyr(tBu)-OH, Fmoc-Cys(Trt)-OH or Fmoc-L-Lys(N_3)-OH; 3-arm: 0.3 eq. Fmoc-Cys(Trt)-OH; PEGylated 2-arm: 0.3 eq. Fmoc-Lys(ivDde)-OH; i-shape: 0.3 eq. Fmoc-Stp(Boc_3)-OH; U-shape: 0.3 eq. Fmoc-Lys(fmoc)-OH; DBCO PEG agents: 0.3 eq. Fmoc-Lys(Dde)-OH and DIPEA (0.6 eq.) were added to the resin for 1 h. The reaction

solvent was drained and a mixture of DCM/MeOH/DIPEA (80/15/5) was added twice for 10 min. After the removal of the reaction mixture, the resin was washed 5 times with DCM.

About 30 mg of the resin were removed and dried to determine the loading of the resin. Therefore, an exact amount of resin was treated with 1 mL deprotection solution (20 % piperidine in DMF) for 1 h. Afterwards, the solution was diluted and absorption was measured at 301 nm. The loading was then calculated according to the equation: resin load [mmol/g] = (A*1000)/(m [mg]*7800*df) with df as dilution factor.

The resin was treated twice with 20 % piperidine in DMF and twice with 20 % piperidine DMF with 2 % DBU to remove the Fmoc protection group. Reaction progress was monitored by Kaiser test. Afterwards, the resin was washed with DMF, DCM and n-hexane and dried in vacuo.

2.2.3 Oligomer and DBCO agent synthesis

Oligomers were synthesized using a 2-chlorotrityl resin preloaded with the first C-terminal amino acid of the respective topology (see **2.2.2**) as solid support. All sequences and topologies of oligomers can be found in **Table 18**, all sequences of DBCO agents can be found in **Table 19**. Unless otherwise stated, coupling steps were carried out using 4 eq. Fmoc-amino acid, 4 eq. HOBt, 4 eq. PyBOP or HBTU and 8 eq. DIPEA (10 mL g^{-1} resin) for 90 min. General steps of a manual and automated synthesis are shown in **Table 6** and **Table 7**.

Table 6 General steps of a manual synthesis cycle

Step	Description	Solvent	Volume	Time
1	Coupling	DCM/DMF 50/50	5 mL/g resin	90 min
2	Wash	DMF, DCM	10 mL/g resin	3 × 1 min DMF 3 × 1 min DCM
3	Kaiser test	-	-	-
4	Fmoc deprotection	20 % piperidine/DMF	10 mL/g resin	4 × 10 min
5	Wash	DMF, DCM	10 mL/g resin	3 × 1 min DMF 3 × 1 min DCM
6	Kaiser test	-	-	-

Table 7 General steps of an automatic synthesis cycle with microwave

Step	Description	Solvent	Volume	Time
1	Coupling	NMP/DMF	5 mL/g resin	12 min at 50°C
2	Double-coupling	NMP/DMF	5 mL/g resin	12 min at 50°C
2	Wash	DMF	8 mL/g resin	5 × 1 min
3	Fmoc deprotection	20 % piperidine/DMF	7 mL/g resin	5 × 10 min
4	Wash	DMF	8 mL/g resin	5 × 1 min

2.2.3.1 Synthesis of T-shapes

After swelling the preloaded resin, backbones were synthesized with an automated synthesizer with microwave support like described in **Table 7**. Before deprotection of the central Dde or ivDde group with 2 % hydrazine solution, the N-terminal NH_2-group was protected with 10 eq Boc anhydride and 10 eq DIPEA in DCM/DMF. In case of an N-terminal cysteine, Boc-Cys(Trt)-OH was used to prevent that step. (iv)Dde-deprotection was performed 30 times with a Syro Wave™ synthesizer (Biotage, Uppsala, Sweden). Hydrazine–DMF solution 1 : 50 was added and vortexed for 2 min. The reaction solvent was drained and fresh solution was added again. Afterwards, the resin was washed with 5 × 1 min DMF 5 × 1 min 10 % DIPEA/DMF and 3 × 1 min DCM (10 mL g^{-1} resin). The following coupling steps were carried out using the manual protocol in **Table 6**. In case of a positive result of the Kaiser test after coupling, the last coupling step was repeated. In case of a negative result after deprotection, the last deprotection step was repeated (optionally with 2 % DBU added to the 20 % piperidine solution). In case of coupling Fmoc-succinoyl-cystamine, no HOBt was used and only DMF was used as solvent (Kaiser tests are not always correct after the deprotection; deprotection steps were not performed with additional DBU). All couplings after Fmoc-succinoyl-cystamine were carried out without HOBt. Symmetrical branching points were introduced using Fmoc-Lys(Fmoc)-OH, asymmetric branching in T-shape structures was introduced using Fmoc-Lys(Dde)-OH.

2.2.3.2 Synthesis of 3-arms

After swelling the preloaded resin, the structures were synthesized manually like described in **Table 6**. Symmetrical branching points were introduced using Fmoc-Lys(Fmoc)-OH. For the N-terminal cysteine, Boc-Cys(Trt)-OH was used. In case of a positive result of the Kaiser test after coupling, the last coupling step was repeated. In case of a negative result after deprotection, the last deprotection step was redone with 2 % DBU added to the 20 % piperidine solution.

2.2.3.3 Synthesis of PEGylated 2-arms (736-739)

After swelling of 0.080 mmol of Fmoc-Lys(ivDde)-chlorotrityl resin in DMF for 30 min, the backbone (Stp(Boc)$_3$-Stp(Boc)$_3$-Stp(Boc)$_3$-Stp(Boc)$_3$-Lys(Stp(Boc)$_3$-Stp(Boc)$_3$-Stp(Boc)$_3$-Stp(Boc)$_3$)-Lys(ivDde) was synthesized with a Syro WaveTM synthesizer (Biotage, Uppsala, Sweden). For the automated coupling three equivalents of Fmoc-Lys(Fmoc)-OH, DIPEA (6 eq) and HBTU/HOBt (3 eq) in DMF were added and occasionally vortexed for 60 min. The reaction solvent was drained and the resin was washed one time with DMF. Double coupling was performed under the same conditions. The reaction solvent was drained and the resin was washed six times with DMF. To remove the Fmoc protection group, the resin was treated five times with 20 % piperidine in DMF. The resin was washed with DMF (6x). To complete the backbone, 3 equivalents of Fmoc-Stp(boc)$_3$-OH per free primary amine (6 eq because of 2 free amines after branching lysine) were coupled the same way. After the automated synthesis of the backbone, the resin was split in 2 equal parts (0.040 mmol each). The following couplings were performed manually with 4 eq amino acid, 8 eq DIPEA and 4 eq PyBOP®/HOBt per free primary amine in DCM/DMF. After 60 min reaction time, the reaction solvent was drained and the resin was washed three times with DMF and DCM each. Reaction progress was monitored with Kaiser test. After successful reaction, the resin was treated twice with 20 % piperidine in DMF (for 10 and 15 min) and twice with 20 % piperidine in DMF with 2 % DBU (for 5 min). The reaction solvent was drained and the resin was washed three times with DMF and DCM. For structures with single cysteines (***736, 737***) Boc-Cys(Trt)-OH was coupled. For CRC-structures (***738, 739***) Fmoc-Cys(Trt)-OH, Fmoc-Arg(Pbf)-OH and Boc-Cys(Trt)-OH were coupled. The ivDde-deprotection was performed with then Syro WaveTM synthesizer (Biotage, Uppsala, Sweden). Hydrazine/DMF solution (4/96; vol/vol) was added and vortexed for 2 min. The reaction solvent was drained and Hydrazine/DMF solution (4/96; vol/vol) was added again. After 10 cycles the supernatant's absorption was measured at 290 nm to monitor the progression of the reaction. After 50 cycles absorption was less than 0.1 in all approaches.

The PEGylation was performed with 4 eq of Fmoc-dPEG$_{24}$-OH the same way the other manual couplings were done. After Fmoc-deprotection the resin of the 2 reactors was split again resulting in 4 batches. To get negative control structures (***736, 738***) 8 eq succinic anhydride and 16 eq DIPEA in DCM were added to the resin. To produce

structures with folic acid ligand (***737, 739***) Fmoc-Glu-OtBu followed by N^{10}-(trifluoroacetyl)pteroic acid were coupled manually like the other amino acids. For the deprotection of the trifluoroacetyl-group of pteroic acid, the resin was treated with 25 % aqueous ammonia solution/DMF (1 : 1) 4 times for 30 min. After each deprotection cycle, the resin was washed with DMF.

2.2.3.4 Synthesis of i-shapes

After swelling the preloaded resin, the structures were synthesized manually like described in **Table 6**. Symmetrical branching points were introduced using Fmoc-Lys(Fmoc)-OH. In case of coupling Fmoc-succinoyl-cystamine, no HOBt was used and only DMF was used as the solvent (Kaiser tests are not always correct after the deprotection). All couplings after Fmoc-succinoyl-cystamine were carried out without HOBt.

2.2.3.5 Synthesis of U-shapes

After swelling the preloaded resin, the structures were synthesized manually like described in **Table 6**. Symmetrical branching points were introduced using Fmoc-Lys(Fmoc)-OH. In case of coupling Fmoc-succinoyl-cystamine, no HOBt was used and only DMF was used as solvent (Kaiser tests are not always correct after the deprotection). All couplings after Fmoc-succinoyl-cystamine were carried out without HOBt.

2.2.3.6 Synthesis of DBCO PEG shielding agents

After swelling the preloaded resin, the structures were synthesized manually like described in **Table 6**. In case of folate targeted structures, folic acid was first synthesized by coupling of Fmoc-Glu-OtBu at a Lys(Dde)-loaded resin followed by N^{10}-(trifluoroacetyl)pteroic acid. Dde-deprotection was then performed 20 times with a Syro Wave™ synthesizer (Biotage, Uppsala, Sweden). Hydrazine/DMF solution (1 : 50) was added and vortexed for 2 min. The reaction solvent was drained and fresh solution was added again. Afterwards, the resin was washed with 5 × 1 min DMF 5 × 1 min 10 % DIPEA/DMF and 3 × 1 min DCM (10 mL g^{-1} resin). For the deprotection of the trifluoroacetyl-group of pteroic acid the resin was treated with 25 % aqueous ammonia solution/DMF (1 : 1) 4 times for 30 min. After each deprotection cycle the resin was washed with DMF. Then, Fmoc-$dPEG_{24}$-OH was coupled. In case of Bis-DBCO structures, the branching points was introduced using Fmoc-Lys(Fmoc)-OH. In case of

coupling Fmoc-succinoyl-cystamine, no HOBt was used and only DMF was used as solvent (Kaiser tests are not always correct after the deprotection). The coupling after Fmoc-succinoyl-cystamine was carried out without HOBt. Finally 3 eq DBCO acid were coupled using 3 eq DIPEA and 3 eq PyBOP® in DCM/DMF.

After completion of the reaction, the resin was washed with DMF, DCM and n-hexane and dried in vacuo.

2.2.4 Kaiser test

Free amines of deprotected amino acids on the resin were determined qualitatively by the Kaiser test [67]. A small sample of DCM washed resin was transferred into an Eppendorf reaction tube. One drop of each 80 % phenol in EtOH (w/v), 5 % ninhydrin in EtOH (w/v) and 20 µM potassium cyanide (KCN) in pyridine (mixture of 1 mL aqueous 0.001 M KCN solution and 49 mL pyridine) were added. The tube was incubated at 99 °C for 4 min under shaking. The presence of free amines was indicated by a deep blue color.

2.2.5 Cleavage conditions

2.2.5.1 General cleavage conditions

All oligomers were cleaved off the resin by incubation with TFA–TIS–H_2O (95 : 2.5 : 2.5) (10 mL g^{-1} resin) for 90 min. The cleavage solution was concentrated by flushing nitrogen and oligomers were precipitated in 40 mL of pre-cooled MTBE – n-hexane (1 : 1). All oligomers were purified by size exclusion chromatography using a Äkta purifier system (GE Healthcare Bio-Sciences AB, Uppsala, Sweden), a Sephadex G-10 column and 10 mM hydrochloric acid solution–acetonitrile (7 : 3) as solvent. All oligomers were lyophilized.

2.2.5.2 Cleavage of oligomers containing oleic acid

The cleavage of the structures off the resin was performed according to an optimized protocol (Sören Reinhard, PhD study, LMU Pharmaceutical Biotechnology) by incubation with TFA–TIS–H_2O 95 : 2.5 : 2.5 (10 mL g^{-1} resin cooled to 4 °C prior to addition) for 30 min followed by immediate precipitation in 40 mL of pre-cooled MTBE

– n-hexane (1 : 1). The oleic acid containing oligomers were then purified by size exclusion chromatography using a Äkta purifier system (GE Healthcare Bio-Sciences AB, Uppsala, Sweden), a Sephadex G-10 column and 10 mM hydrochloric acid solution–acetonitrile (7 : 3) as solvent. The oligomers were lyophilized.

2.2.5.3 Cleavage of DBCO containing reagents

The cleavage of the structures off the resin was performed by incubating the dried resin with DCM–TFA–TIS (92.2 : 5 : 2.5) for 60 min followed by immediate precipitation in 40 mL of pre-cooled MTBE–n-hexane (1 : 4). The precipitate was then dissolved in 0.05 M NaOH solution. The pH was adjusted to 7 and the structure was purified by dialysis with a 1000 Da cut-off membrane against deionized water. The obtained DBCO reagents were lyophilized.

2.2.6 pDNA polyplex formation

Nucleic acid and oligomers were dissolved at concentrated stock solutions in water, and diluted with 20 mM HEPES buffered 5 % glucose pH 7.4 (HBG). pDNA and oligomer were prepared in separate tubes. Unless otherwise stated, pDNA at a concentration of 20 ng/µL was used. According to the indicated nitrogen/phosphate (N/P) ratio, oligomer solutions were prepared and the same volume of pDNA was added to the oligomer. Only protonatable nitrogens were considered in the N/P calculations (see **Table 18**). The mixture was rapidly pipetted at least 5 × and incubated for 40 min at RT.

2.2.7 siRNA polyplex formation

Nucleic acid and oligomers were dissolved at concentrated stock solutions in water, and diluted with 20 mM HEPES buffered 5 % glucose pH 7.4 (HBG). siRNA and oligomer were prepared in separate tubes. For most cases, siRNA at a concentration of 50 ng/µL was used. In some experiments higher concentrations of siRNA were prepared. Especially for experiments related to *in vivo* work, siRNA concentrations of 500 ng/µL. According to the indicated nitrogen/phosphate (N/P) ratio, oligomer solutions were prepared and the same volume of siRNA was added to the oligomer.

Only protonatable nitrogens were considered in the N/P calculations (see **Table 18**). The mixture was rapidly pipetted at least 5 × and incubated for 40 min at RT.

2.2.7.1 Modification with DBCO reagents

For modifying siRNA polyplexes with DBCO click agents, solutions with reagents were prepared in ¼ of the volume of polyplex solutions prepared before. The concentration of the solution was calculated according to the respective equivalents (eq). Equivalents represent the molar ratio of shielding agents to oligomers in the polyplex solution. Unless otherwise stated, the reaction time was 4 h.

2.2.8 pDNA binding assays

A 1 % agarose gel for pDNA analyses was prepared by dissolving agarose in TBE buffer (Trizma base 10.8 g, boric acid 5.5 g, disodium EDTA 0.75 g, and 1 L of water) and boiling everything up to 100 °C. After cooling down to about 50 °C and addition of GelRed™ (Biotum, Hayward, U.S.A.), the agarose gel was casted in the electrophoresis unit. Polyplexes with 200 ng pDNA were formed as described and placed into the sample pockets after 4 µL of loading buffer (prepared from 6 mL of glycerine, 1.2 mL of 0.5 M EDTA, 2.8 mL of H_2O, 0.02 g of bromophenol blue) was added. Electrophoresis was performed at 120 V for 80 min.

2.2.9 siRNA binding assays

Unless otherwise stated, a 2.5 % agarose gel was prepared by dissolving agarose in TBE buffer (10.8 g of trizma base, 5.5 g of boric acid, 0.75 g of disodium EDTA, and 1 L of water) and subsequent boiling. After cooling down to about 50 °C, GelRed™ was added. Polyplexes with 500 ng siRNA were formed using the stated N/P ratios. In case of concentrated formulations, polyplexes were diluted with HBG to a final volume of 20 µL. Samples were placed into the pockets after 4 µl of loading buffer (prepared from 6 mL of glycerine, 1.2 mL of 0.5 M EDTA, 2.8 mL of H_2O, 0.02 g of bromophenol blue) was added. Unless otherwise stated, electrophoresis was performed at 100 V for 40 min.

2.2.10 pDNA and siRNA polyplexes under reducing conditions

pDNA polyplexes were formed at N/P ratio 12 and 200 ng pDNA in 20µL. siRNA polyplexes were formed at N/P ratio 20 and 500 ng siRNA in 20µL. After polyplex incubation, 5 µL of a GSH solution were added to 20 µL of the polyplex solution. The GSH stock solution had a concentration of 50 mM and pH was adjusted to 7.4. It was diluted to concentrations of 5 mM and 0.5 mM. Consequently, the resulting solutions had the final concentrations 0.1 mM, 1 mM and 10 mM, respectively. HBG was used as negative control (0 mM GSH). The solutions were incubated at 37 °C for 90 min. 5 µL loading buffer was added and a binding assay (see 2.2.8 and 2.2.9) was performed.

2.2.11 pDNA and siRNA polyplex stability in 90 % serum

Polyplexes were formed using 1.0 µg of pDNA or 2.5 µg siRNA in 6.25 µL HBG mixed with the oligomer at N/P 12 resulting in a total volume of 12.5 µL. Afterwards, the incubation 112.5 µl fetal bovine serum (FBS) was added to the samples. All samples had a final concentration of 90 % FBS. The samples were incubated at 37 °C for 2 h. 20 µL of the samples and 4 µL loading buffer were carefully mixed and a binding assay (see 2.2.8 and 2.2.9) was performed.

2.2.12 Particle size and zeta potential

For dynamic light scattering (DLS) measurements the polyplex solution was measured in a folded capillary cell (DTS 1070) using a Zetasizer Nano ZS with backscatter detection (Malvern Instruments, Worcestershire, UK). Polyplexes were formed using 1.5 µg siRNA and the oligomer at indicated N/P ratio. In case of concentrated polyplex solutions, samples were diluted with HBG resulting in a total volume of 60 µL. For size measurements, the equilibration time was 0 min, the temperature was 25 °C and an automatic attenuator was used. The refractive index of the solvent was 1.330 and the viscosity was 0.8872 mPa•s. Each sample was measured 3 times. For zeta potential measurements with at least 6 runs. The sample was diluted to 800 µL with 20 mM HEPES buffer or 10 mM NaCl to measure zeta potential. Zeta potentials were

calculated by the Smoluchowski equation. Ten to fifteen sub runs lasting 10 s each at 25 °C (n = 3) were measured.

2.2.13 Ellman´s assay

The oligomers containing ssbb elements were diluted to a concentration of 1.67 mg/mL. 30 µL of the solution was mixed with 170 µL working solution (2.44 mL Ellman´s buffer (0.2 M Na_2HPO_4, 1 mM EDTA, pH 8.0) and 60 µL DTNB solution in methanol (c = 4 mg/mL)). After 15 min incubation at 37 °C absorption was measured at 412 nm using a GENESYS™ UV-VIS spectrophotometer (Thermo Scientific). The percentage of free mercapto groups is based on the theoretical amount (100 %) of thiols in case of complete cleavage.

2.2.14 Buffer capacity of oligomers

The oligomer sample, containing 15 µmol protonatable amines, was diluted in a total volume of 3.5 mL NaCl solution (50 mM) and the pH was adjusted to 2 by addition of hydrochloric acid. Afterwards, a back titration with 0.05 M NaOH was performed with an automatic titration system (Titrando 905 from Metrohm, Germany) equipped with a Biotrode pH electrode (METROHM GmbH & Co. KG, Filderstadt, Germany), until a pH of 11 was reached. To distinguish oligomer and solvent effects, a control titration of 50 mM sodium chloride solution without oligomer was performed. Volume differences (ΔV) between defined pH values were determined. Total endolysosomal buffer capacity C in the pH range between 5 and 7.4 was calculated according to the following formula:

$$C_{\mathrm{pH\,5-pH\,7.4}} = \frac{[\Delta V(\mathrm{Sample})_{\mathrm{pH\,5-pH\,7.4}} - \Delta V(\mathrm{NaCl})_{\mathrm{pH\,5-pH\,7.4}}] \cdot 50\ \mathrm{mM}}{15\ \mu\,\mathrm{moles}} \cdot 100\ \%$$

2.2.15 Erythrocyte leakage assay with or without previous reductive treatment

Fresh, citrate-buffered human blood was washed with phosphate-buffered saline (PBS). The washed human erythrocyte suspension was centrifuged and the pellet was diluted to 5×10^7 erythrocytes per mL with PBS (pH 7.4, 6.5 and 5.5). In case of GSH treatment, oligomers were incubated in 10 mM GSH in HEPES (pH adjusted to 7.4) at

a concentration of 1 mg/mL at 37 °C for 90 min. A volume of 75 µl of erythrocyte suspension and 75 µL of oligomer solution (previously diluted with PBS of the respective pH) were added to each well of a V-bottom 96-well plate (NUNC, Denmark), resulting in a final concentration of 7.5 µM oligomer per well. The plates were incubated at 37 °C under constant shaking for 1 h. After centrifugation, 100 µL of the supernatant was analyzed for hemoglobin release at 405 nm wavelength using a microplate reader (Spectrafluor Plus, Tecan Austria GmbH, Grödig, Austria).

2.2.16 Ethidium bromide compaction assay with incubated polyplexes

A Cary Eclipse spectrophotometer (Varian, Germany) was used for the quantification of ethidium bromide (EtBr) fluorescence at the excitation wavelength λex = 510 nm and emission wavelength λem = 590 nm. pDNA polyplexes were incubated with 2 µg pDNA and the oligomer at N/P 12 in 200 µL HBG for 40 minutes. siRNA polyplexes were incubated with 5 µg siRNA and the oligomer at N/P 20 in 200 µL HBG for 40 minutes. Before the measurement 800µL of EtBr solution (c = 0.4 µg/mL) was added. 200 µL HBG buffer + 800 µL of EtBr solution (c = 0.4 µg/mL) was used as blank. 200µL of nucleic acid solution (2 µg pDNA or 5 µg siRNA) + 800 µL of EtBr solution (c = 0.4 µg/mL) was assigned to 100 %. The fluorescence intensity of EtBr measured after 3 minutes of incubation was determined in relation to the 100 % value. Triplicates were measured.

2.2.17 Confocal fluorescence microscopy

KB cells or Neuro2A cells were seeded into an 8-well Labtek chamber slide coated with collagen at a density of 3×10^4 cells/well in 300 µL of growth medium 24 h prior to treatment. Polyplexes were formed as described using a mixture of 80 % unlabeled and 20 % Cy5 labeled nucleic acid (in total 0.6 µg DNA, 1.2 µg siRNA for PEGylated polyplexes and 1.5 µg siRNA for non-PEGylated polyplexes) and oligomer at N/P 12 (pDNA) or oligomer at N/P 20 (siRNA) in 60 µL of HBG. The medium was replaced with 240 µL of fresh growth medium, and the polyplex solution was added. For PEGylated polyplexes, the chamber slide was incubated at 37°C for 45 min. Afterwards, the medium was changed and cells were incubated again for 4h. Then

cells were washed twice with 500 µl PBS and fixed with 4 % PFA solution for 30 min at room temperature. For non-PEGylated polyplexes, cells were incubated for 24 h and washed and fixed as described before. Cell nuclei were stained with DAPI and actin was stained with rhodium phalloidin (Life Technologies). A Leica TCS SP8 confocal microscope was used for image acquisition.

2.2.18 Cellular internalization of pDNA polyplexes

KB or KB/eGFPLuc cells were seeded into 24-well plates coated with collagen at a density of 5×10^4 cells/well. After 24 h, the culture medium was replaced with 400 µL fresh growth medium. pDNA polyplexes (N/P 12) in 100 µL HBG, containing 1 µg pDNA (20 % of the nucleic acid was Cy5-labeled) were added to each well and incubated at 37 °C for 45 min. All experiments were performed in triplicates. Subsequently, cells were washed with 500 µL PBS containing 500 IU of heparin for 15 min to remove any polyplexes sticking to the cell surface. After an additional PBS washing step, cells were detached with trypsin/EDTA and taken up in growth medium, centrifuged to receive a cell pellet, and taken up in PBS with 10 % FBS. Cellular internalization was assayed by excitation of Cy5 at 635 nm and detection of emission at 665 nm. Cells were appropriately gated by forward/sideward scatter and pulse width for the exclusion of doublets. DAPI (4′,6-diamidino-2-phenylindole) was used to discriminate between viable and dead cells. Data were recorded by Cyan™ ADP flow cytometer (Dako, Hamburg, Germany) using Summit™ acquisition software (Summit, Jamesville, NY, USA) and analyzed by FlowJo® 7.6.5 flow cytometric analysis software.

2.2.19 Cell association and cellular internalization of siRNA polyplexes

Neuro2A cells or KB cells were seeded in 24-well plates with 5×10^4 cells/well at 24 h before the experiment, and fresh media were provided before the experiment. Polyplexes containing 1.5 µg siRNA (including 20 % Cy5 labeled siRNA) per well were added into each well incubated 30 min on ice or 45 min at 37 ^{o}C in 5 % CO_2 for cell association or cellular internalization respectively. Cells were washed with PBS for 3 times to remove free polyplexes. For cellular internalization, cells were then incubated with 500 I.U. heparin to remove polyplexes non-specifically associated to

the cell surface. Finally, cells were collected and resuspended in PBS buffer with 10 % FBS. For folate competition experiment, cells were incubated with folate acid (1 mM) for 30 min on ice to block FA receptor before polyplexes added. All samples were measured by flow cytometry with CyanTM ADP (Dako, Hamburg, Germany) through excitation at 635 nm, and detection of emission at 665 nm. Dead cells were detected by DAPI fluorescence and removed by gating in order to analyze polyplex uptake into living cells. Data were analyzed by FlowJo® 7.6.5 flow cytometric analysis software.

2.2.20 Luciferase gene transfer

Neuro2A cells or KB cells were seeded 24 h prior to pDNA delivery using 1×10^4 Neuro2A cells/well or 8000 KB cells/well in 96-well plates. In vitro transfection efficiencies of the oligomers were evaluated using 200 ng pCMVLuc per well. All experiments were performed in quintuplicate. Before transfection medium was replaced with 80 µL fresh medium containing 10 % FBS. Transfection complexes formed at different protonatable nitrogen/phosphate (N/P) ratios in 20 µL HBG were added to each well and incubated at 37 °C. For targeted oligomers medium was replaced 45 min after transfection by fresh medium or chloroquine (0.1 mM) containing medium. After 4 h incubation at 37 °C, the medium was replaced again with fresh medium. For both, targeted and untargeted oligomers, 24 h after initial transfection, the medium was removed and cells were treated with 100 µL cell lysis buffer (25 mM Tris, pH 7.8, 2 mM EDTA, 2 mM DTT, 10 % glycerol, 1 % Triton X-100). Luciferase activity in the cell lysate was measured using a luciferase assay kit (100 mL Luciferase Assay Buffer, Promega, Mannheim, Germany) and a Centro LB 960 plate reader luminometer (Berthold Technologies, Bad Wildbad, Germany). Transfection efficiency was evaluated as relative light units (RLU) per well.

2.2.21 Gene silencing with siRNA

Gene silencing experiments were performed in Neuro2A/eGFPLuc, KB/eGFPLuc cells or DU145/eGFPLuc cells. Applied siRNAs were either the unmodified siRNA against eGFP for silencing the eGFPLuc fusion protein, its control sequence siCtrl, or the lytic peptide modified INF7-siGFP, with its control sequence INF7-siCtrl. Silencing

experiments were performed in triplicates in 96-well plates with 5000 cells for Neuro2A/eGFPLuc cell line and DU145/eGFPLuc cell line or 4000 cells for KB/eGFPLuc cell line and 500 ng siRNA for untargeted oligomers or 200 ng siRNA for targeted oligomers per well. In case of concentrated formulations, polyplexes were diluted with cell culture medium to facilitate handling. Cells were seeded 24 h prior to transfection and then medium was replaced with 80 µL fresh growth medium containing 10 % FBS. Transfection complexes for siRNA delivery (20 µL in HBG, prepared as described above) at different N/P ratios were added to each well and incubated at 37 °C. At 45 min, medium was replaced by fresh medium in case of targeted oligomers. In both cases 48 h after initial transfection. Luciferase activity in the cell lysate was measured using a luciferase assay kit (Promega, Mannheim, Germany) and a Centro LB 960 plate reader luminometer (Berthold Technologies, Bad Wildbad, Germany). The experiments were performed in triplicates, and the relative light units (RLU) were presented as percentage of the luciferase gene expression obtained with HBG-treated control cells.

2.2.22 Cell cycle analysis after EG5 siRNA transfection

L1210 cells transfected with EG5 siRNA (1.5 µg/well) were collected by centrifugation at 24 h after transfection and washed with PBS, then incubated with 100 µL propidium iodide staining solution (0.1 % sodium citrate, 0.1 % Triton-X100, 50 µg/mL propidium iodide in Millipore water) for 3 h on ice in dark. Cells were centrifuged after adding 1 mL PBS buffer and resuspended in 500 µL PBS and measured with the Cyan™ ADP flow cytometer. Data were analyzed by FlowJo® 7.6.5 flow cytometric analysis software.

2.2.23 Cell viability assay (MTT)

Neuro2A or KB cells were seeded into 96-well plates at a density of 1×10^4 Neuro2A cells/well or 8000 KB cells/well. After 24 h, the culture medium was replaced with 80 µL fresh growth medium containing 10 % FBS and transfection complexes (20 µL in HBG) at different N/P ratios were added according to transfections. All studies were performed in quintuplicates. For targeted oligomers, the medium was replaced 45 min after transfection by fresh medium or medium containing chloroquine (0.1 mM). After

4 h incubation at 37 °C, the medium was replaced again with fresh medium. For both, targeted and untargeted oligomers, 24 h post transfection, 10 µl 3-(4,5-Dimethylthiazol-2-yl)-2,5-diphenyltetrazolium bromide (MTT, 5 mg/mL) were added to each well reaching a final concentration of 0.5 mg MTT/mL. After an incubation time of 2 h at 37 °C, unreacted dye and medium were removed and cells were lysed by freezing at -80 °C. 100 µl of DMSO were added and plates were incubated at 37 °C for 30 min under shaking. The purple formazan product was quantified by a microplate reader (Tecan, Switzerland) at 530 nm with background correction at 630 nm. The relative cell viability (in %) related to control wells containing cell culture medium with 20 µL HBG was calculated by [A] test/[A] control × 100.

2.2.24 Mouse tumor model

Female 8-week-old nude mice, Rj: NMRI-nu (nu/nu) (Janvier, Le Genest-Saint-Isle, France), were housed in isolated ventilated cages under specific pathogen-free condition with a 12 h light/dark interval and were acclimated for at least 7 days prior to experiments. Food and water were provided *ad libitum*. Animals were injected with 1×10^6 L1210 cells or 5×10^6 Neuro2A cells subcutaneously. The body weight was recorded, and the tumor volume was measured by caliper and calculated as [0.5 × (longest diameter) × (shortest diameter)^2]. All animal experiments were performed according to guidelines of the German law for the protection of animal life and were approved by the local animal ethics committee.

2.2.25 Biodistribution study

For near infrared (NIR) *in vivo* imaging, unlabeled control siRNA (siCtrl) was spiked with 50 % of Cy7-labeled siRNA (Cy7-siAHA1) in HBG. When tumors reached the size of 500 - 1000 mm^3, the mice (n = 2-3/per group) were anesthetized with 3 % isoflurane in oxygen. siRNA polyplexes containing 50 µg of Cy7-labeled siRNA (N/P 10) in 250 µL (100 µL siRNA solution, 100 µL oligomer solution, 50 µL agent solution or buffer) of HBG were injected intravenously (i.v.), and fluorescence was measured with a CCD camera at different time points. For evaluation of images, the efficiency of fluorescence

signals was analyzed after color bar scales were equalized using the IVIS Lumina system with Living Image software 3.2 (Caliper Life Sciences, Hopkinton, MA, USA).

2.2.26 Gene silencing mediated by EG5-siRNA *in vivo*

When tumors reached 500 mm^3, mice (n = 5) were injected i.v. with siRNA polyplexes containing 50 µg of siEG5 or siCtrl (N/P 10) 48 h and 24 h before euthanasia. As a part of the terminal procedure, blood samples were obtained by cardiac puncture for blood biochemistry examinations. After tumors had been harvested and homogenized, total RNA was extracted using Trifast (Peqlab, Erlangen, Germany) according to the manufacturer's protocol.

2.2.27 qRT-PCR

Quantitative real-time polymerase chain reaction (qRT-PCR) was performed to determine the mRNA level of EG5 gene in the tumor samples. 1 µg of total RNA was used to generate cDNA using qScript cDNA Synthesis Kit (Quanta Biosciences, Beverly, MA, USA). Quantitative RT-PCR was performed on a LightCycler 480 system (Roche, Mannheim, Germany) using UPL Probes (Roche, Mannheim, Germany) and Probes Master (Roche, Mannheim, Germany) with GADPH as housekeeping gene. The following probes and primer sequences were used: murine GAPDH (ready-to-use in UPL), and EG5 (UPL Probe #100) forward: TTCCCCTGCATCTTTCAATC, reverse: TTCAGGCTTATTCATTATGTTCTTTG). Results were analyzed by the ΔC_T method. C_T values of GAPDH were subtracted from C_T values of EG5. ΔC_T values of treated animals were calculated as percentage of untreated control animals.

2.2.28 Blood biochemistry examinations

To isolate plasma, blood samples were collected in EDTA-coated tubes (Multivette 600, Sarstedt, Nümbrecht, Germany) and centrifuged at 3000 rpm for 7 minutes. The supernatant was analyzed for clinical biochemistry parameters: alanine aminotransferase (ALT), aspartate aminotransferase (AST), blood urea nitrogen (BUN)

and creatinine in the Clinic of Small Animal Medicine, Faculty of Veterinary Medicine, Ludwig-Maximilians-Universität München.

2.2.29 HPLC analysis

The redox-sensitivity of oligomer ***740*** was analyzed by RP-HPLC using a Waters HPLC system equipped with a Waters 600E multisolvent delivery system and a Waters 996 PDA detector. The compounds were analyzed using a Xbridge C18 column (5 µm, 4.6 × 150 mm) and a water/acetonitrile gradient (95:5 – 0:100) containing 0.1 % TFA. For detection, the extinction at 280 nm was monitored.

2.2.30 Proton ^{1}H NMR spectroscopy

^{1}H NMR spectra were recorded using a Jeol JNMR-GX 400 (400 MHz) by Jeol or an AVANCE III HD 500 (500 MHz) by Bruker with a 5 mm CPPBBO probe. All spectra were recorded without TMS as internal standard and therefore all signals were calibrated to the residual proton signal of the deuterium oxide (D_2O) solvent, or methanol-d4 (MeOD). Chemical shifts are reported in ppm and refer to the solvent as internal standard (D_2O at 4.79, MeOH at 3.31). Integration was performed manually. The spectra were analyzed using MestreNova (Ver. 5.2.5, Ver. 8.1.1, Ver. 9.0 and Ver. 10.0 by MestReLab Research).

2.2.31 MALDI mass spectrometry

One µL matrix droplet consisting of a saturated solution of Super-DHB (sum of 2,5-dihydroxybenzoic acid and 2-hydroxy-5-methoxybenzoic acid) in acetonitrile / water (1 : 1) containing 0.1 % (v/v) TFA was spotted on an MTP AnchorChip (Bruker Daltonics, Bremen, Germany). After the Super-DHB matrix had crystallized, one µL of the sample solution (10 mg/mL in water) was added to the matrix spot. Samples were analyzed using an Autoflex II mass spectrometer (Bruker Daltonics, Bremen, Germany). All spectra were recorded in positive mode.

2.2.32 Statistical analysis

The results are presented as mean values of experiments performed in at least triplicates. Unless otherwise stated error bars show standard deviation (SD). In case of *in vivo* data statistical analysis of the results are presented as mean ± SEM. was evaluated by unpaired t test: *p<0.05; **p<0.01; ***p<0.001. Two-tailed Student's t-test, calculations and graphical presentation were performed with Prism 5 & 6 (GraphPad Software Inc.) and Microsoft Excel 2007 & 2010 (Microsoft Corp.).

3 Results

3.1 Twin disulfides as opportunity for improving stability and transfection efficiency

This chapter has been adapted from:

Klein PM, Müller K, Gutmann C, Kos P, Krhac Levacic A, Edinger D, Höhn M, Leroux JC, Gauthier MA, Wagner E. *Twin disulfides as opportunity for improving stability and transfection efficiency of oligoaminoethane polyplexes.* J Control Release. 2015 May 10;205:109-19

Recently Wu et al. introduced a new bioreducible dynamic covalent bond, called the twin disulfide, which has orthogonal disulfide pairing characteristics to the standard single disulfide [43]. Peptides containing CXC (cysteine – any amino acid – cysteine) motifs were found to selectively form stable twin disulfide dimers with other CXC peptides. The process was particularly enhanced when the central amino acid is arginine (i.e., CRC or cysteine – arginine – cysteine).

Based on the discovery of this new type of bioreducible bond, this chapter describes the influence of replacing single cysteine residues with a CRC motif in oligoaminoethane carriers on the stability and transfection efficiency of pDNA and siRNA polyplexes. Oligomer structures were selected based on their ability to efficiently transfect as established in our previous work [67, 68, 72, 82, 83, 113]. These were chosen to demonstrate structure-activity relations, also in the presence of other polyplex stabilizing motifs or nanoparticle destabilizing polyethylene glycol (PEG) chains [114].

3.1.1 Influence of stabilizing CRC motifs on pDNA and siRNA polyplex stability

In previous studies, our laboratory has established a library of polycationic structures, prepared by solid-supported synthesis, as precise carriers for gene delivery [66, 67, 83]. These structures consist of natural amino acids combined with artificial building blocks. For example, succinoyl-tetraethylene-pentamine (Stp) has been used as artificial polyamino acid for nucleic acid complexation and for endosomal buffering.

Lysine residues are exploited as branching units within the structures, and cysteine residues as disulfide forming units [68, 82, 83]. In addition, hydrophobic domains containing fatty acids [82, 83] and hydrophilic domains containing PEG shielding units or targeting peptides [62, 113, 114] can be incorporated.

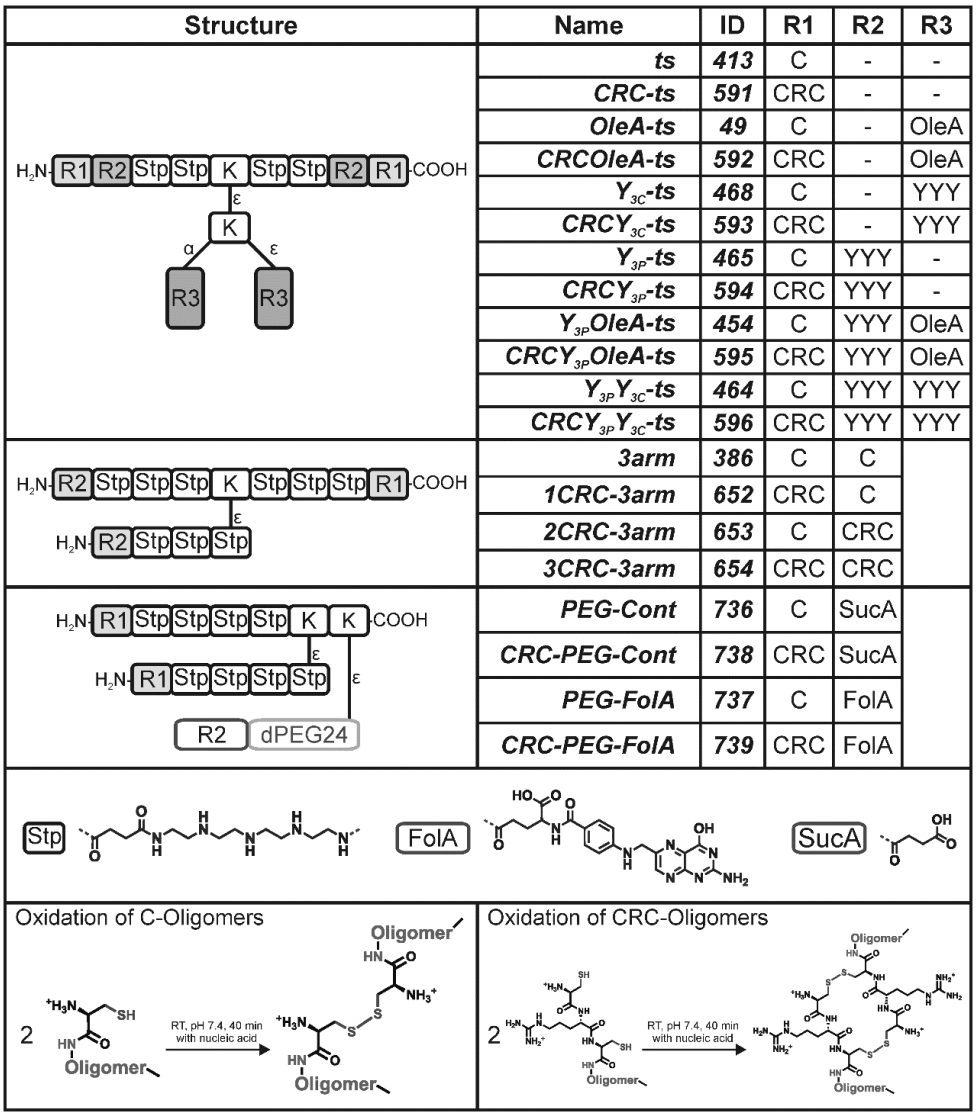

Fig. 8 Sequence-defined oligomers with T-shape (ts), 3-arm (3arm) and PEGylated 2-arm (PEG) topology. Schematic overview of the structures with different modifications (C: cysteine, CRC: cysteine-arginine-cysteine, OleA: oleic acid, YYY: tyrosine-tyrosine-tyrosine, SucA: succinic acid, FolA: folic acid, Stp: succinoyl-tetraethylene-pentamine, K: lysine). Each structure has a short name used for identification in this study and an internal database identification number. The formation of disulfide bonds, respectively twin disulfide bonds (bottom of figure), occurs during the incubation with nucleic acid. T-shape oligomers were synthesized by Christina Gutmann (PhD study C. Troiber, Pharmaceutical Biotechnology, LMU).

Due to the rather low molecular weight (usually below 5 kDa) of the sequence-defined cationic oligomers, cytotoxicity is very low. However, nucleic acid polyplex stability becomes a critical issue [13]. This is of great concern for polyplexes of siRNA because the size of this nucleic acid is significantly smaller than pDNA, resulting in less inter-electrolyte interactions. This known polyplex stability problem has been solved by us and others in several ways [13, 69, 115-118]. For example, the size of the cationic oligomer can be increased by branching into three or four arms. Incorporation of cysteine residues at the end of each arm was found to be crucial for the formation of bioactive siRNA polyplexes stabilized by disulfide crosslinks [68, 82]. Alternatively, T-shape oligomers with two terminal cysteine residues and two central fatty acids [82, 83] were prepared given that the fatty acids stabilize the polyplex via hydrophobic interactions and additionally improve its endosomal escape (by pH-dependant lysis of the endosomal membrane). Recently, tyrosine trimers were shown to improve the transfection properties of siRNA polyplexes by stabilizing them via aromatic interactions [119, 120].

In the present study, six T-shape structures with increasing integration of oleic acid and tyrosine units in the periphery or the center were chosen to analyze the effect of replacing the two single terminal cysteine residues with CRC motifs (**Fig. 8**). Cysteines of oligomers were kept in reduced state until oligomers were incubated with nucleic acid. The stabilizing formation of disulfide bonds, respectively twin disulfide bonds, occurs during the subsequent polyplex incubation. At first, to compare nucleic acid binding ability, pDNA and siRNA agarose gel shift assays were performed at different N/P ratios (ratio between protonatable nitrogen atoms within the oligomer and phosphate atoms of the nucleic acid).

Free nucleic acid migrates in the gel due to its negative charge, whereas polyplexes are retained and can even remain in the loading pockets of the agarose gel (**Fig. 9**). For all of the tested oligomers, an improvement in binding ability and stability was observed for the twin versus the single disulfide.

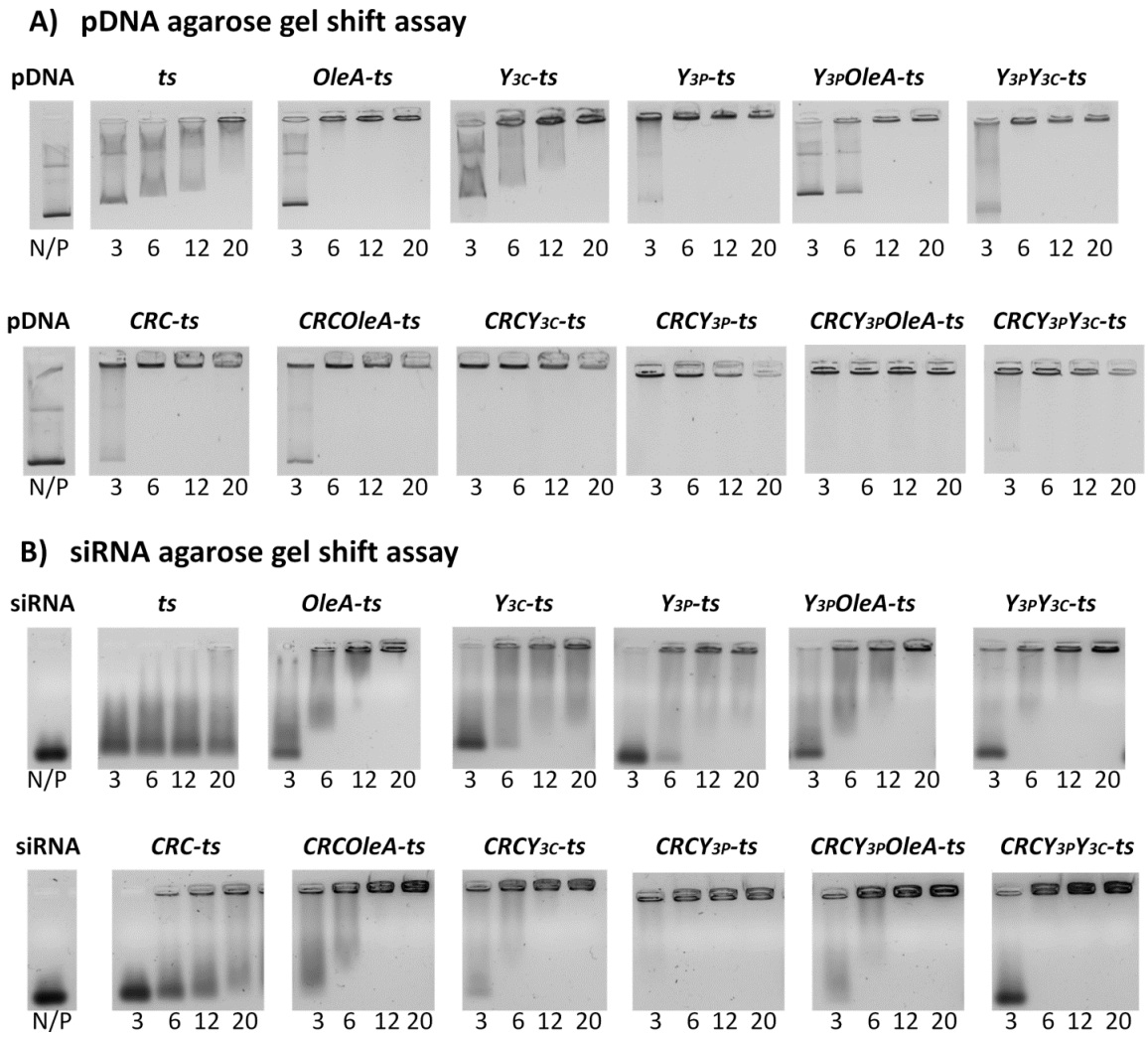

Fig. 9 Stability of polyplexes with T-shape (***ts***) oligomers determined in agarose gel shift assays. A) pDNA binding of single disulfide forming oligomers (top) and corresponding twin disulfide forming analogs (bottom). Left lane: free pDNA. B) siRNA binding of single disulfide forming oligomers (top) and corresponding twin disulfide forming analogs (bottom). Left lane: free siRNA. Gel shift assays were performed by Christina Gutmann (PhD study C. Troiber, Pharmaceutical Biotechnology, LMU).

The basic structure ***ts***, bearing terminal cysteine residues for stabilization, shows low pDNA binding. Insertion of the CRC motif led to complete binding from N/P ratios of 6 and up. In contrast, despite a strong enhancement in the siRNA binding ability of oligomer ***ts*** containing CRC motifs (***CRC-ts***), it remained insufficient. Nevertheless, T-shape structures with central oleic acid displayed good binding properties for both the single and twin disulfide analogs (***CRCOleA-ts*** and ***OleA-ts***). Tyrosine trimers in the central position (***Y3C-ts***) positively influenced nucleic acid binding, which in conjunction with the CRC motif became complete for pDNA and very good for siRNA

(***CRCY$_{3C}$-ts***). The addition of tyrosine trimers to the periphery (***Y$_{3P}$-ts***, ***Y$_{3P}$OleA-ts***, ***Y$_{3P}$Y$_{3C}$-ts*)** led to very good pDNA complexation and could be further improved using twin disulfides. The twin disulfide structure ***CRCY$_{3P}$-ts*** without central modification outperformed the other T-shapes. It could even bind siRNA completely. The addition of oleic acid or tyrosine residues in the central position to ***Y$_{3P}$-ts*** further improved siRNA complexation, but diminished binding ability of the CRC analog.

Size measurements revealed smaller, more compact sizes and higher zeta potentials for all structures without hydrophobic stabilization (**Table 8**). For example, the incorporation of twin disulfides in siRNA polyplexes with sizes above 1500 nm (***Y$_{3P}$-ts***) or that could not be detected (***Y$_{3C}$-ts***) led to the formation of particles smaller than 200 nm (analyzed for N/P 12). The small size of siRNA particles with oleic acid (<100 nm) increased with the replacement of single cysteine residues by CRC motifs. For the pDNA polyplexes, the same tendency was observed, although less distinct (**Table 8**).

Table 8 Particle size (Z-average) and zeta potential of pDNA and siRNA polyplexes formed in HEPES buffer determined with DLS. Polyplexes were diluted 1:20 before measurement. Variations refer to the median of three measurements of the same sample. DLS measurements were performed by Christina Gutmann (PhD study C. Troiber, Pharmaceutical Biotechnology, LMU).

DNA polyplex	Z-average [nm]	Zeta potential [mV]	DNA polyplex	Z-average [nm]	Zeta potential [mV]
CRC-ts	285 ± 22	23.9 ± 0.5	***ts***	358 ± 8	16.2 ± 1.3
CRC-OleA-ts	121 ± 1	38.2 ± 1.2	***OleA-ts***	114 ± 1	43.6 ± 1.3
Y$_{3C}$-ts	105 ± 2	35.8 ± 0.4	***Y$_{3C}$-ts***	542 ± 22	12.7 ± 1.8
CRCY$_{3P}$-ts	188 ± 3	27.4 ± 1.3	***Y$_{3P}$-ts***	244 ± 18	14.0 ± 2.5
CRCY$_{3P}$OleA-ts	100 ± 1	41.3 ± 1.2	***Y$_{3P}$OleA-ts***	99 ± 1	53.2 ± 2.8
CRCY$_{3P}$Y$_{3C}$-ts	115 ± 2	33.3 ± 0.8	***Y$_{3P}$Y$_{3C}$-ts***	180 ± 5	21.5 ± 1.8
siRNA polyplex			**siRNA polyplex**		
CRC-ts	n. d.*	n. d.*	***ts***	n. d.*	n. d.*
CRC-OleA-ts	672 ± 76	33.5 ± 0.9	***OleA-ts***	23 ± 4	24.9 ± 1.0
Y$_{3C}$-ts	160 ± 6	24.7 ± 0.9	***Y$_{3C}$-ts***	n. d.*	n. d.*
CRCY$_{3P}$-ts	197 ± 1	20.0 ± 1.2	***Y$_{3P}$-ts***	1570 ± 194	11.8 ± 0.7
CRCY$_{3P}$OleA-ts	162 ± 5	37.4 ± 1.4	***Y$_{3P}$OleA-ts***	99 ± 2	50.7 ± 0.8
CRCY$_{3P}$Y$_{3C}$-ts	192 ± 2	17.5 ± 0.6	***Y$_{3P}$Y$_{3C}$-ts***	243 ± 12	13.3 ± 0.4

* n.d. = not detectable by DLS;

Three-armed oligomers containing one terminal cysteine residue on each arm were also evaluated. Oxidation of the cysteine residues is expected to provide a 3-dimensional disulfide-cross-linked network that stabilizes polyplexes. This approach has been previously demonstrated to lead to efficient nucleic acid binding and efficient pDNA and siRNA delivery [33]. In the current study, the single cysteine residues in each arm of ***3arm*** were sequentially replaced by CRC motifs, resulting in three novel oligomers with the potential to form one, two or three twin disulfides (**Fig. 8**). Since the standard ***3arm*** forms stable pDNA polyplexes and shows complete binding and good transfection efficiency, no further improvements could be observed in the gel retardation assay (**Fig. 10A**).

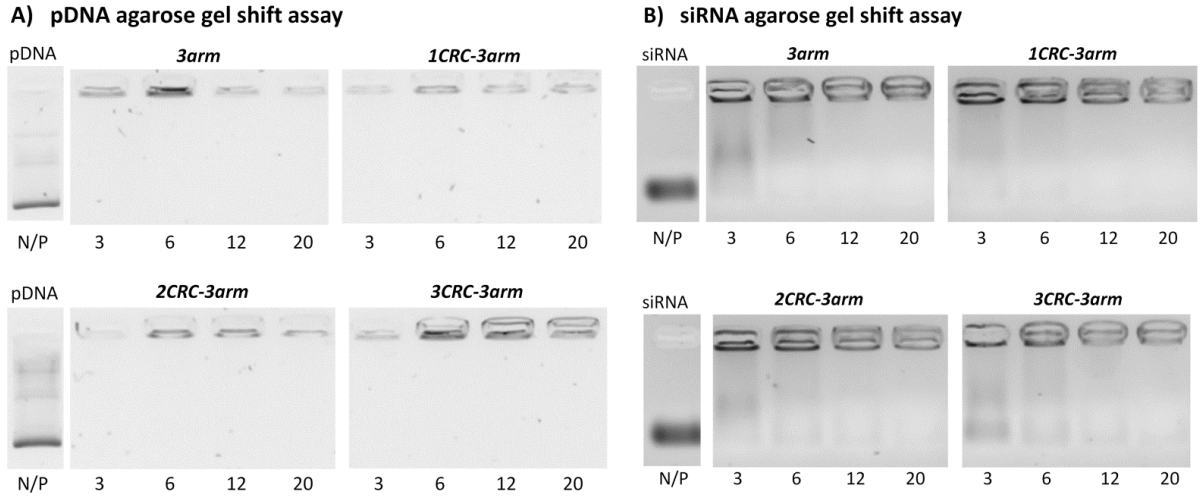

Fig. 10 Stability of polyplexes with three-armed oligomers in agarose gel shift assay. A) pDNA binding and B) siRNA binding. Left lanes: free pDNA or free siRNA, respectively.

In addition, the compaction of nucleic acid into a condensed polyplex form was evaluated by ethidium bromide exclusion assays (**Fig. 20A**). Such a compaction is mainly influenced by the cationic backbone and not necessarily linked to polyplex stability. As the binding region within the 3-arm topology consists of the same cationic backbone made of Stp, only minor differences were found. A slight tendency towards more compact pDNA polyplexes with increasing numbers of CRC-motifs was observed. Polyplex stabilization is more critical for siRNA and complete binding of siRNA by ***3arm*** was only observed for N/P ratios higher than 6. Moreover, rather large (almost micrometer) particles were formed [83]. In this case, the introduction of CRC motifs led to better binding (**Fig. 10B**). Particle size and zeta potential of these siRNA

polyplexes were analyzed by dynamic light scattering (DLS). A successive decrease of the particle size from more than 800 nm (***3arm***) to less than 200 nm (***3CRC-3arm***) was observed for the structures with twin disulfides (**Table 9**). An enhanced compaction ability in the ethidium bromide exclusion assay was observed only for the 3-arm structure with 3 CRC-motifs incorporated (***3CRC-3arm* – Fig. 20B**).

Table 9 Particle size (Z-average) and zeta potential of siRNA polyplexes formed in HEPES buffer determined with DLS. Polyplexes were diluted 1:20 before measurement. Variations refer to the median of three measurements of the same sample.

siRNA polyplex	N/P	Z-average [nm]	Mean PDI	Mean Zeta Potential [mV]
3arm*	12	951± 26	0.34 ± 0.03	17.7 ± 0.4
3arm*	20	806 ± 21	0.36 ± 0.04	20.0 ± 0.6
1CRC-3arm	16	450 ± 8	0.26 ± 0.01	22.8 ± 0.5
2CRC-3arm	16	358 ± 1	0.19 ± 0.01	23.4 ± 0.4
3CRC-3arm	16	191 ± 2	0.09 ± 0.01	28.3 ± 0.3

*Data from published work [83]; PDI: Polydispersity index.

Thus, the number of CRC motifs correlated inversely to the size of the resulting polyplexes. The zeta potential increased and the polydispersity decreased. This implies that ***3arm*** polyplexes rich in CRC motifs are smaller, more defined and provide a higher positive charge on the surface.

3.1.2 pDNA and siRNA transfection efficiency

Regarding pDNA transfection activity, all tested T-shape oligomer polyplexes were efficient at N/P 12 (**Fig. 11A**). Oligomers with low stability (***ts***, ***Y_{3C}-ts***) demonstrated a slight improvement with the CRC motif. In contrast, gene transfer efficiency of all other pDNA polyplexes, especially the ones with oleic acid, was lower than for the structural analogs with single cysteine residues. Cell viability assays did not reveal any cytotoxicity for tested pDNA–oligomer complexes (**Fig. 12**).

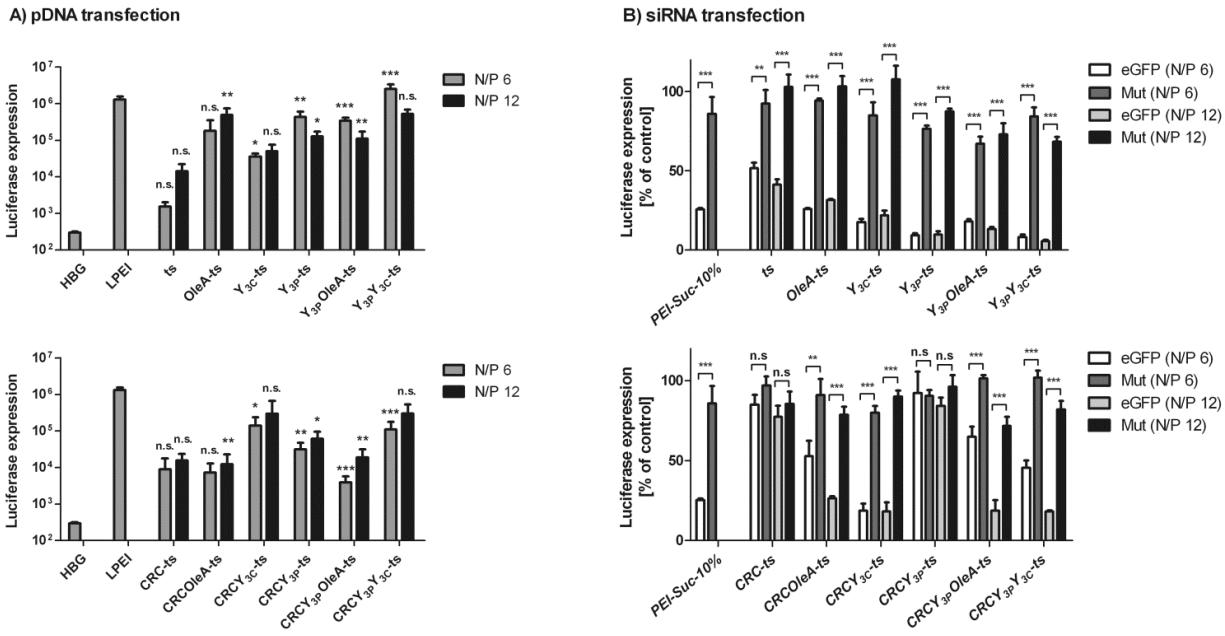

Fig. 11 Gene transfer (A) and gene silencing (B) of T-shape oligomers in neuroblastoma cells. Luciferase pDNA polyplexes were tested for luciferase expression in Neuro2A cells, eGFP-targeted siRNA (eGFP) or control siRNA (Mut) polyplexes for eGFPLuc gene silencing in Neuro2A-eGFPLuc cells, both at N/P 6 and 12. Top: polyplexes of previously published oligomers [34] with single disulfides. Bottom: polyplexes of analogous oligomers with twin disulfides. Linear PEI (LPEI) and succinylated branched PEI (PEI-Suc-10 %) served as positive controls for pDNA or siRNA transfections, respectively. HBG, buffer negative control. Data are presented as mean value (±SD) out of quintuplicate for pDNA and triplicates for siRNA; notes on top of pDNA transfections (A) indicate if there is statistical significance between single cysteine structure and its corresponding CRC analogous for same N/P ratio (n. s. = $p>0.05$; *$p<0.05$; **$p<0.01$; ***$p<0.001$, student's t-test, two-tailed). Transfections were performed by Daniel Edinger (PhD study, Pharmaceutical Biotechnology, LMU).

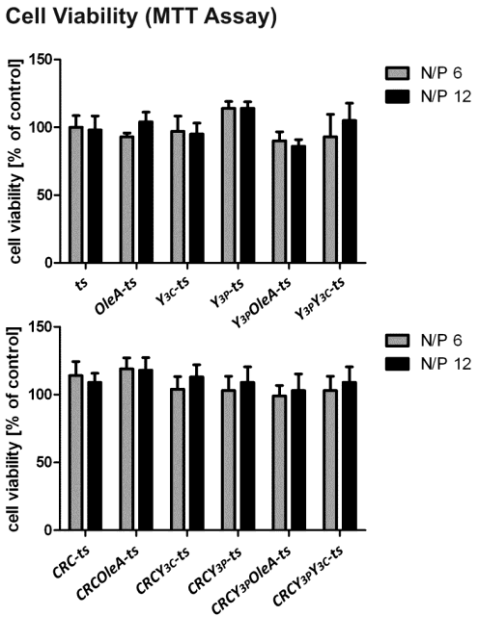

Fig. 12 Cell viability tested with MTT Assay for T-Shape structures with pDNA. Top: polyplexes of previously published oligomers [119] with single disulfides. Bottom: polyplexes of analogous oligomers with twin disulfides. The assay was performed by Daniel Edinger (PhD study, Pharmaceutical Biotechnology, LMU).

For siRNA delivery, standard polyplexes with peripheral tyrosine residues and single cysteine residues were very good at gene knockdown. Interestingly, for the majority of the T-shape oligomers, the addition of twin disulfides reduced siRNA transfection efficiency (**Fig. 11B**). In fact, silencing for the two polyplexes formed with ***CRC-ts*** and ***CRCY$_{3P}$-ts*** was abolished.

Consistent transfection results were obtained with three-armed oligomers (**Fig. 13**).

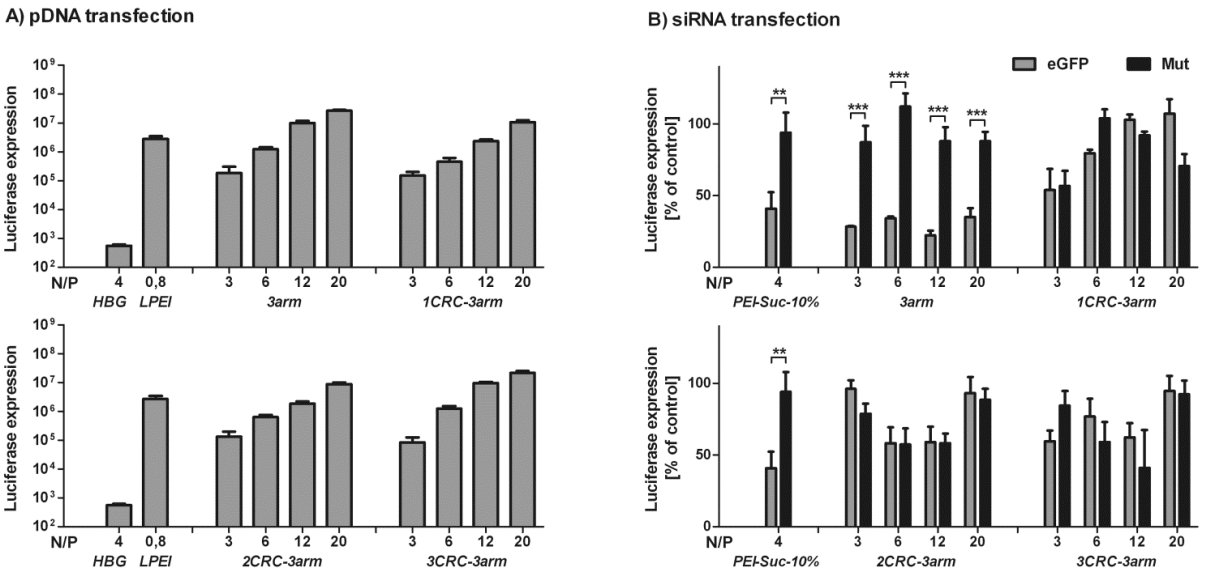

Fig. 13 Gene transfer (A) and gene silencing (B) of 3-arm structures. Luciferase pDNA polyplexes were tested for luciferase expression in Neuro2A cells, eGFP-targeted siRNA (eGFP) or control siRNA (Mut) polyplexes were tested for eGFPLuc gene silencing in Neuro2A-eGFPLuc cells, polyplexes were tested at N/P 3, 6, 12 and 20. Linear PEI (LPEI) and succinylated branched PEI (PEI-Suc-10 %) served as positive controls for pDNA or siRNA transfections, respectively. Data are presented as mean value (±SD) out of quintuplicate for pDNA and triplicates for siRNA. All pDNA transfections significantly (at least $p<0.05$) differ from HGB control; (**$p<0.01$; ***$p<0.001$, student's t-test, two-tailed). Transfections were performed by Petra Kos and Katharina Müller (PhD studies, Pharmaceutical Biotechnology, LMU).

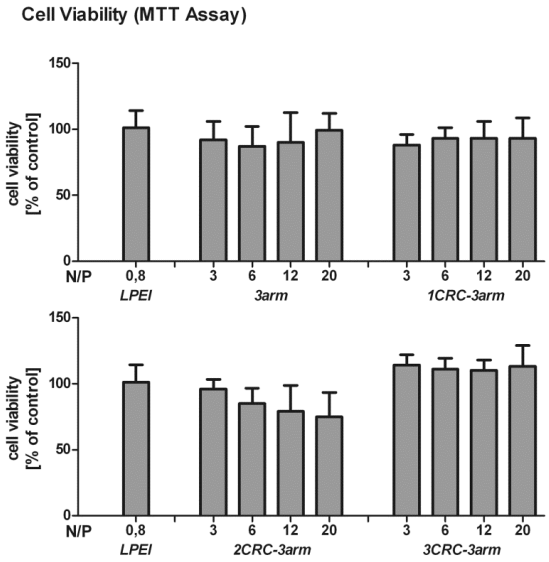

Fig. 14 Cell viability tested with MTT Assay for 3-arm structures with pDNA. Assay was performed by Petra Kos (PhD study, Pharmaceutical Biotechnology, LMU).

For pDNA delivery, incorporation of one to three CRC motifs did not significantly alter the efficient transfection levels or toxicity (**Fig. 13A, Fig. 14**). Confocal microscopy data indicate intracellular uptake of polyplexes, with less particle aggregation for the polyplexes including the CRC-motif (**Fig. 15**).

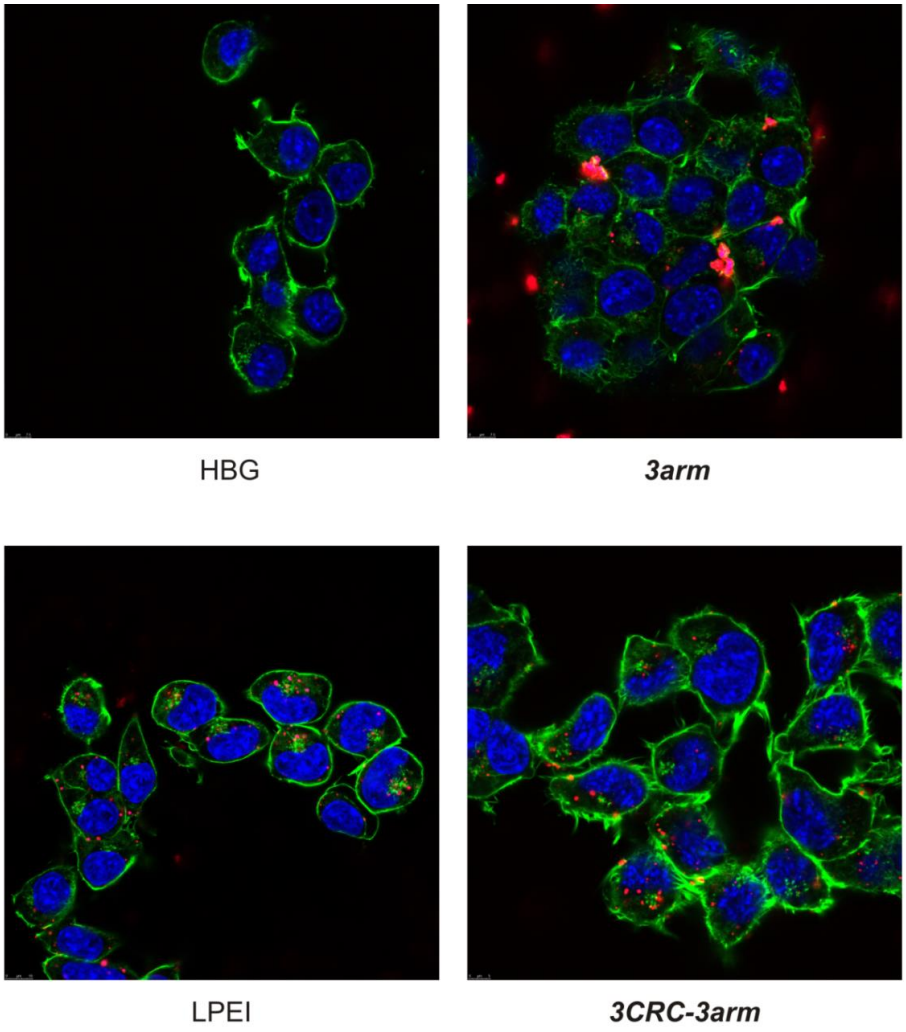

Fig. 15 Intracellular distribution of 3-arm pDNA polyplexes in Neuro2A cells acquired by confocal laser scanning microscopy. Nuclei were stained with Hoechst 33342 (blue), actin cytoskeleton was stained with rhodamine phalloidin (green) and pDNA was spiked with 20 % Cy5-labeled pDNA (red). The images show the overlay of the different channels. Transfections were performed by Ana Krhac Levacic (PhD study, Pharmaceutical Biotechnology, LMU), confocal microscopy was performed by Miriam Höhn (Pharmaceutical Biotechnology, LMU).

For siRNA delivery, incorporation of CRC resulted in loss of gene silencing activity (**Fig. 13B**). The reasons for the reduced silencing activity of CRC T-shape and 3-arm

oligomers, despite the more compact and stable nature of the formed polyplexes, are not completely clear. Reduced cell uptake, reduced endosomal escape into the cytosol, or reduced release of siRNA from polyplexes are possible reasons. Changes in cellular uptake are unlikely since confocal microscopy data (**Fig. 16**) for 3-arm structures showed similar nucleic acid uptake.

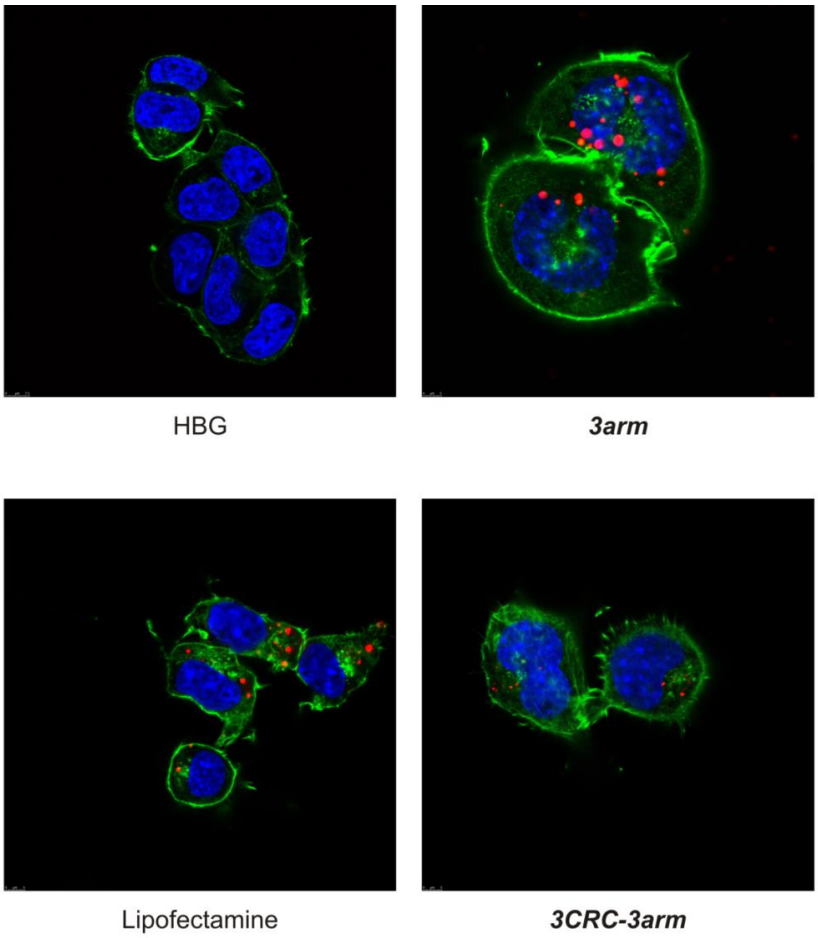

Fig. 16 Intracellular distribution of 3-arm siRNA polyplexes in Neuro2A cells acquired by confocal laser scanning microscopy. Nuclei were stained with Hoechst 33342 (blue), actin was stained with rhodamine phalloidin (green) and siRNA was spiked with 20 % Cy5-labeled siRNA (red). The images show the overlay of the different channels. Transfections were performed by Katharina Müller (PhD study Pharmaceutical Biotechnology, LMU), confocal microscopy was performed by Miriam Höhn (Pharmaceutical Biotechnology, LMU).

We can rule out an unfavorable change in endosomal buffer capacity between the endosomal pH ≈ 5.5 and the physiological pH 7.4, which for all oligomers are in the same range of 16 % – 17 % (**Table 10**).

Table 10 Buffer capacity of T-shape and 3-arm oligomers between pH 5.0 and 7.4 determined by acidification to pH 2 and back titration with NaOH. Measurements for T-shape structures were performed by Christina Gutmann (PhD study C. Troiber, Pharmaceutical Biotechnology, LMU).

Oligomer	Buffer capacity [%]	**Oligomer**	Buffer capacity [%]
CRC-ts	14.9	***ts***	-
CRC-OleA-ts	19.9	***OleA-ts***	19.0
Y_{3C}-ts	22.4	***Y_{3C}-ts***	21.1
$CRCY_{3P}$-ts	19.2	***Y_{3P}-ts***	19.0
$CRCY_{3P}$OleA-ts	21.2	***Y_{3P}OleA-ts***	22.2
$CRCY_{3P}Y_{3C}$-ts	21.5	***$Y_{3P}Y_{3C}$-ts***	21.4
3arm	17.0		
1CRC-3arm	15.8		
2CRC-3arm	16.1		
3CRC-3arm	16.3		
LPEI 22kDa	20.9		

A striking difference was the observation of larger aggregated polyplexes in cellular vesicles for the standard 3-arm polyplexes but not the stabilized CRC polyplexes (**Fig. 16**). It is known from the study of PEI polyplexes that larger particle size may favorably promote endosomal escape in cell culture transfections [121]. In fact, performing transfections of CRC T-shapes in the presence of the endolysosomotropic agent chloroquine [122, 123] recovers the siRNA transfection activity (**Fig. 17**), suggesting endosomal escape as the main bottleneck. Chloroquine can also facilitate polyplex dissociation [124, 125]. Cytosolic release from the oligomers might also be beneficial especially for siRNA.

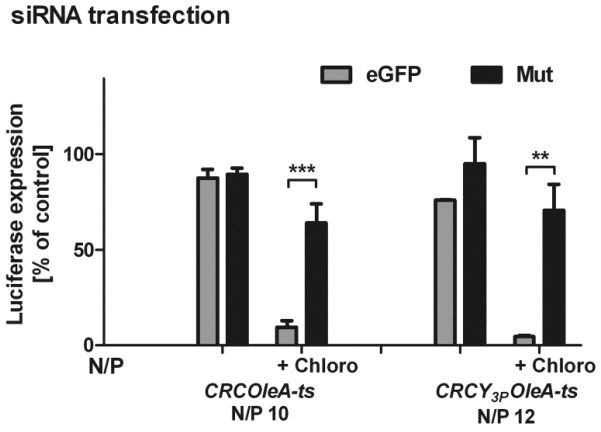

Fig. 17 Gene silencing of T-shape oligomers in KB/eGFPLuc cells. eGFP-targeted siRNA (eGFP) or control siRNA (Mut) polyplexes for eGFPLuc gene silencing in KB/eGFPLuc cells, polyplexes were tested at N/P 10 or 12 with and without chloroquine. Data are presented as mean value (±SD) out of triplicates; (**p<0.01; ***p<0.001, student's t-test, two-tailed). Transfections were performed by Katharina Müller (PhD study, Pharmaceutical Biotechnology, LMU).

3.1.3 Stability of CRC-containing oligomer polyplexes in serum

Since some T-shape oligomers (e.g., ***CRCY$_{3C}$-ts***) possessed improved stability (versus single disulfide analogs), suitable sizes and good transfection efficiency, which are all important criteria for future *in vivo* application, serum gel shift assays were performed in the presence of 90 % fetal bovine serum (FBS) (see **Fig. 18**). For this experiment, polyplexes were first formed in HEPES buffer, and then FBS was added. Samples were incubated at room temperature or 37 °C for up to 90 minutes and gel electrophoresis was performed to investigate the stability of polyplexes. This showed that siRNA migration was only observable for the labile polyplex ***CRC-ts***. In contrast, all other CRC-polyplexes were stable in 90 % FBS. These data show that the twin disulfides may promote favorable stabilization and improved resistance to serum protein-mediated disassembly. This is particularly important for labile structures without hydrophobic modifications, as the stabilizing effect of twin disulfides influences the properties of polyplexes in a positive way and may make it possible to use them in *in vivo* conditions.

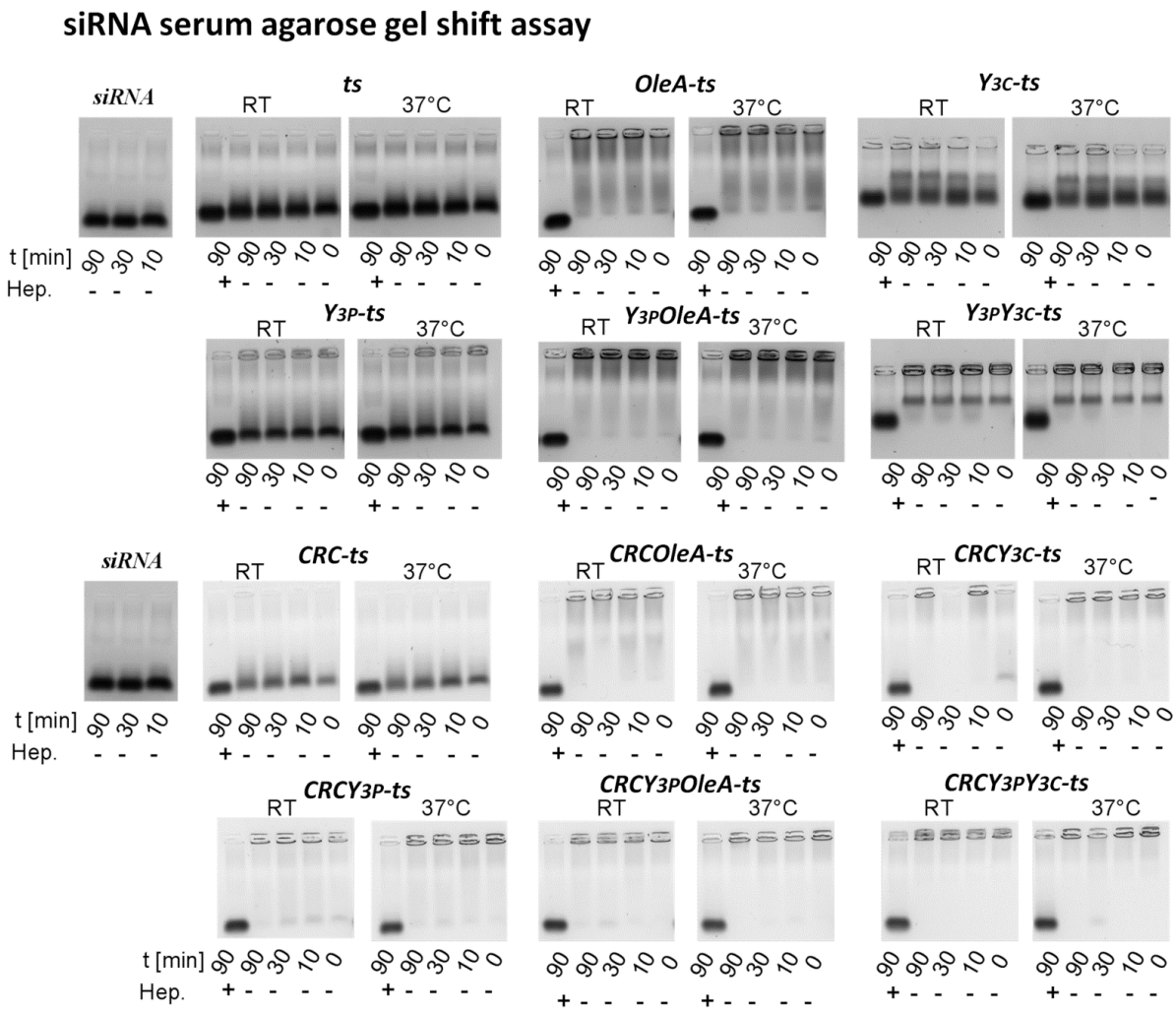

Fig. 18 Stability of siRNA polyplexes with T-shape oligomers (at N/P 12) in agarose gel shift assay after up to 90 min incubation at room temperature or 37°C in 90 % FBS. Top: single cysteine oligomers. Bottom: corresponding twin disulfide-forming analogs. Polyplexes were incubated at room temperature for 40 min before FBS was added. Heparin (50 I.U.) was added to dissociate polyplexes. Left lanes: free pDNA or free siRNA, respectively. Gel shifts were performed by Christina Gutmann (PhD study C. Troiber, Pharmaceutical Biotechnology, LMU).

3.1.4 Twin disulfides in PEG-shielded and targeted structures

One feature of gene carriers important for *in vivo* applications is targeting to specific cell populations. To minimize unspecific interactions, shielding agents like PEG are coupled to cationic systems (so-called “PEGylation”). A ligand is conjugated to the PEG-chain to achieve specific uptake into cells. PEGylation, however, may influence polyplex stability [24, 114, 126, 127] depending on the types and molecular weights of polycation – PEG blocks. For smaller oligomers as investigated in the current study, the PEG units within a polyplex can reduce the binding and compaction ability of

ethylenimine units [113, 114]. The findings reported above suggest that introduction of CRC motifs might improve the biophysical properties of polyplexes. For this reason, PEGylated structures with either targeting ligands or negative control ligands were analyzed next. Based on effective targeting in previous studies [87], we chose folic acid (FolA) as targeting ligand and succinic acid (SucA) as control ligand connected to a PEG_{24} unit. Folic acid has a high affinity for folate receptors, which are commonly over-expressed on the surface of many human cancers [128, 129]. The succinic acid control has the same negative charge as folic acid, but should not mediate receptor-promoted cellular uptake. Oligomeric structures consisting of a cationic backbone with 2 arms (each with 4 Stp units and either a single terminal cysteine residue or CRC motif) were used to bind nucleic acid (**Fig. 8**). Agarose gel shifts were performed for both, pDNA and siRNA. In both cases, improved binding was observed for the CRC motif containing polyplexes (**Fig. 19**).

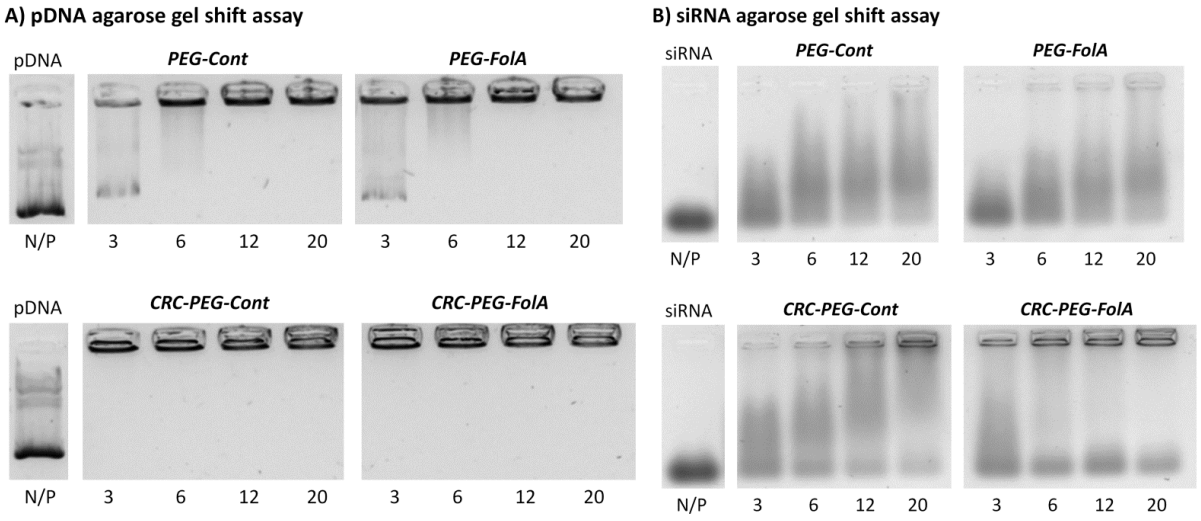

Fig. 19 Stability of polyplexes with PEGylated oligomers in agarose gel shift assay. A) pDNA binding and B) siRNA binding of single cysteine oligomers (top) and corresponding twin disulfide-forming analogs (bottom). Left lanes: free pDNA or free siRNA, respectively.

The retention of siRNA was particularly increased by incorporation of the CRC motif. Ethidium bromide exclusion assay showed a tendency towards more compact pDNA polyplexes including twin disulfides, whereas compaction of siRNA polyplexes was not influenced (**Fig. 20**).

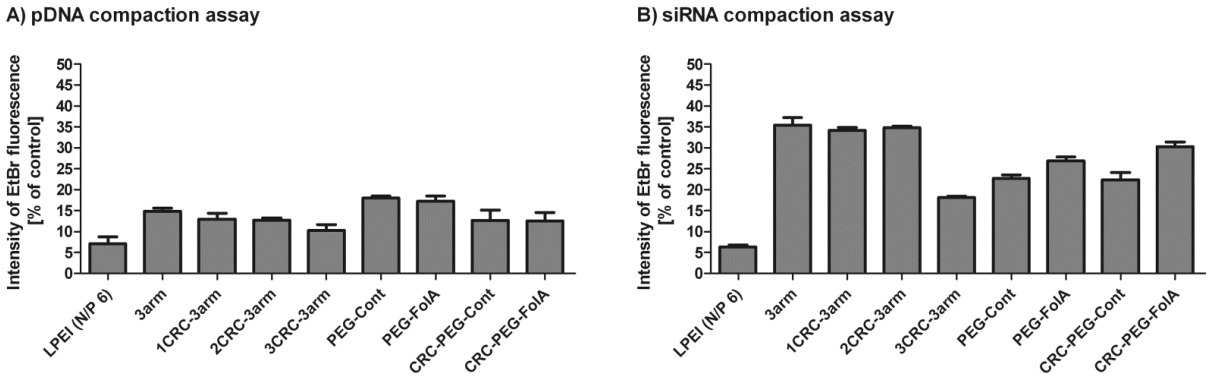

Fig. 20 Nucleic acid compaction within polyplexes as determined in an ethidium bromide exclusion assay. At 40 min after formation, polyplexes were incubated with EtBr for 3 min. Lower intensity of EtBr fluorescence indicates better compaction of the nucleic acid with the cationic oligomer and less nucleic acid intercalation of EtBr. 100 % would represent pDNA or siRNA, respectively, without cationic oligomers. A) pDNA compaction at oligomer N/P 12 and LPEI (N/P 6) as control; B) siRNA compaction at oligomer N/P 20 and LPEI (N/P 6) as a control.

Polyplex surface charge is an important property of PEGylated particles since it allows drawing inferences about the degree of shielding. Zeta potential measurements of pDNA and siRNA polyplexes revealed near neutral values, between -0.1 and 0.2 mV, indicating excellent shielding (**Table 11**). With regards to size, siRNA particles were smaller than pDNA particles.

Table 11 Particle size (Z-average) and zeta potential of pDNA and siRNA polyplexes formed in HEPES buffer determined with DLS. Polyplexes were diluted 1:20 before measurement. Variations refer to the median of three measurements of the same sample.

pDNA polyplex	N/P	Z-average [nm]	Mean PDI	Mean Zeta Potential [mV]
PEG-Cont	12	277 ± 49	0.97 ± 0.03	0.00 ± 0.16
PEG-FolA	12	354 ± 36	0.26 ± 0.04	-0.03 ± 0.14
CRC-PEG-Cont	12	292 ± 47	0.73 ± 0.09	0.04 ± 0.1
CRC-PEG-FolA	12	350 ± 22	0.25 ± 0.03	-0.02 ± 0.03
siRNA polyplex				
PEG-Cont	20	65 ± 23	0.42 ± 0.12	0.17 ± 0.27
PEG-FolA	20	105 ± 7	0.08 ± 0.02	0.06 ± 0.07
CRC-PEG-Cont	20	95 ± 9	0.18 ± 0.02	-0.11 ± 0.34
CRC-PEG-FolA	20	171 ± 24	0.12 ± 0.03	-0.10 ± 0.06

PDI: Polydispersity index.

The insertion of the CRC motif did not cause any changes for pDNA polyplexes, whereas the size of siRNA polyplexes increased. For folate-targeted structures, there was a clear tendency towards the formation of bigger particles in comparison to untargeted controls.

Transfection of pDNA polyplexes into folate receptor-expressing KB cells in the presence of chloroquine showed high efficiency for the targeted oligomers ***PEG-FolA*** and ***CRC-PEG-FolA***, whereas the negative control complexes did not show any effect (**Fig. 21A**). The highest efficiency was achieved for ***CRC-PEG-FolA*** at a low N/P ratio of 6, whereas higher ratios led to a reduction. Once again, no significant cytotoxicity was observed (**Fig. 22**).

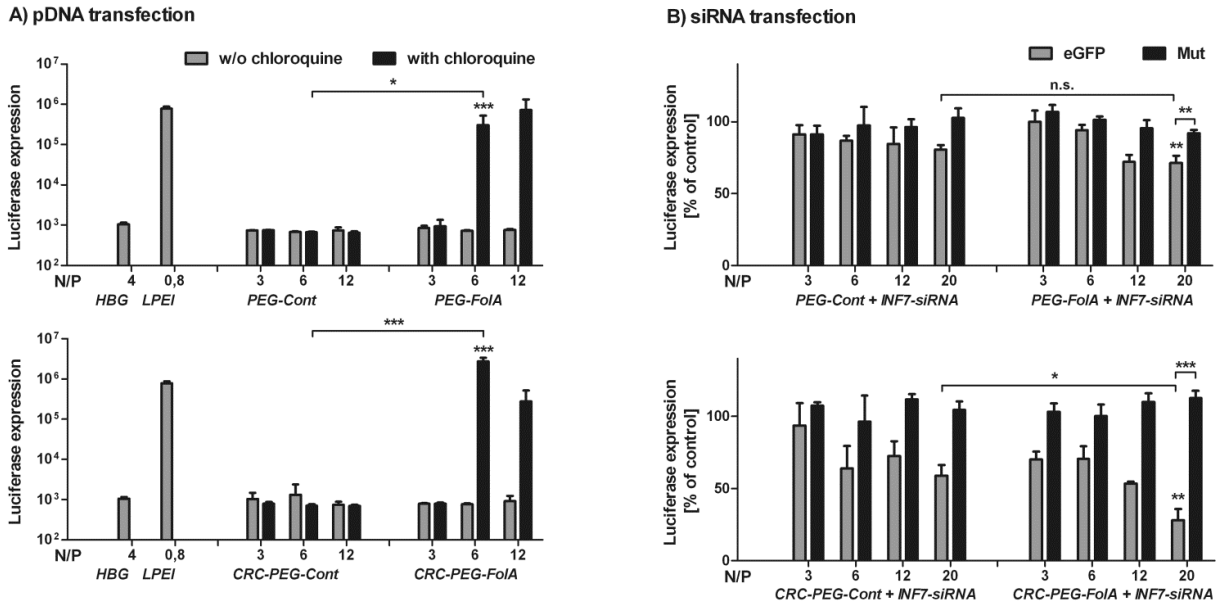

Fig. 21 A) Luciferase pDNA polyplexes were tested for luciferase expression in KB cells. Grey bars show transfection efficiency without chloroquine, black bars with chloroquine. Linear PEI (LPEI) served as positive control for pDNA transfection. B) eGFP-targeted INF7-siRNA (eGFP) or control INF7-siRNA polyplexes (Mut) were analyzed for eGFPLuc gene silencing in KB/eGFPLuc cells. Positive control siRNA (eGFP) transfections with Lipofectamine in these cells were reported in our recent paper Dohmen et al. [87]. Polyplexes were formed at indicated N/P ratios. Top: polyplexes with single cysteine oligomers. Bottom: polyplexes with twin disulfide-forming oligomers. Data are presented as mean value (±SD) out of quintuplicate for pDNA and triplicates for siRNA; notes on top of transfections bars without arrow indicate if there is statistical significance between single cysteine structure and its corresponding CRC analogous for same N/P (n. s. = p>0.05; *p<0.05; **p<0.01; ***p<0.001, student's t-test, two-tailed). Transfections were performed by Ana Krhac Levacic and Katharina Müller (PhD studies, Pharmaceutical Biotechnology, LMU).

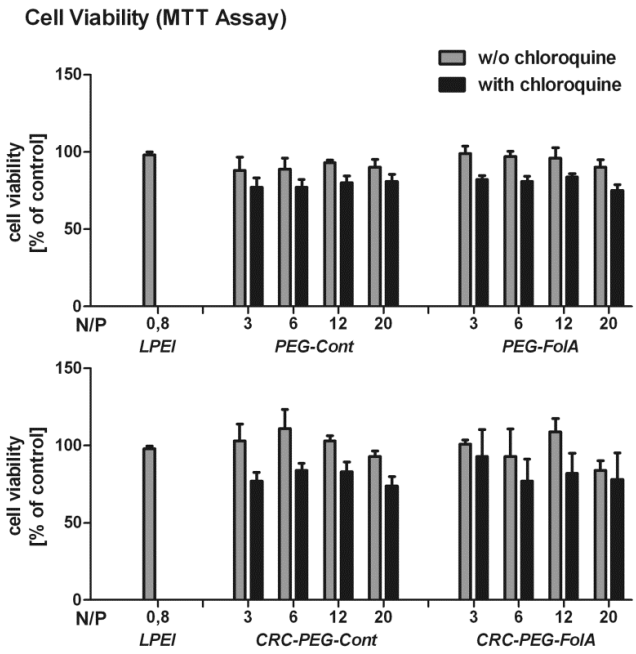

Fig. 22 Cell viability tested with MTT Assay for PEGylated structures with pDNA. The experiment was performed with and without chloroquine. Assay was performed by Ana Krhac Levacic (PhD study, Pharmaceutical Biotechnology, LMU).

In the absence of chloroquine, well consistent with previous findings [116], no gene transfer could be observed, which indicates that polyplexes could not escape endosomes. This limitation can be overcome by various means [62, 87]. For this reason, siRNA transfections were performed with a lytic peptide INF7 covalently coupled to siRNA via a disulfide bond [87]. This led to improved transfection efficiency and thus to gene knockdown. Gene silencing with the targeted oligomers could be improved up to 70 % for N/P 20 by the insertion of twin disulfides (***CRC-PEG-FolA***; **Fig. 21B**). The non-targeted control structures mediated only moderate gene knockdown which proved target-specific transfection. Polyplexes with siRNA lacking INF7 also did not mediate any gene silencing (**Fig. 23**).

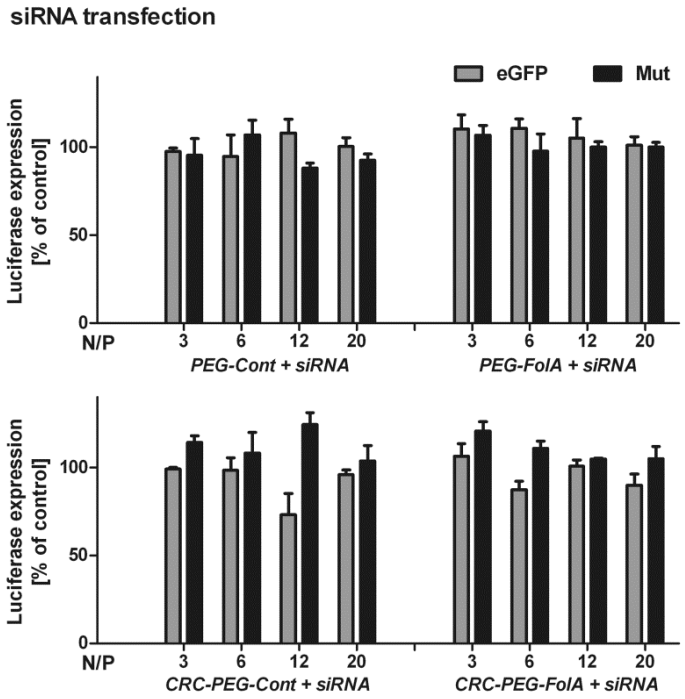

Fig. 23 eGFP-targeted siRNA (eGFP) or control siRNA polyplexes (Mut) were tested for eGFPLuc gene silencing in Neuro2A-eGFPLuc cells at indicated N/P ratios. Top: polyplexes with single cysteine oligomers. Bottom: polyplexes with twin disulfide-forming oligomers. Data are presented as mean value (±SD) out of triplicates for siRNA. Transfections were performed by Katharina Müller (PhD study, Pharmaceutical Biotechnology, LMU).

Cellular internalization studies of PEGylated polyplexes formed with Cy5-labeled pDNA and siRNA were performed using folate receptor-rich KB cells (**Fig. 24**).

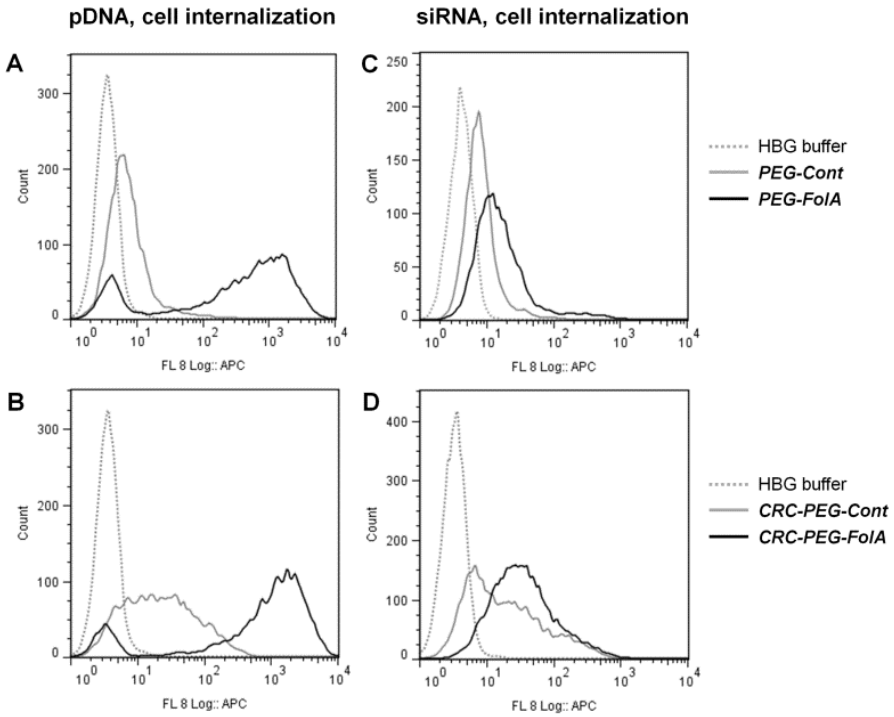

Fig. 24 Cellular internalization of Cy5-labeled pDNA (N/P 12) or Cy5-labeled siRNA (N/P 20) polyplexes after 45 min determined by flow cytometry. The intensity of the Cy5 signal indicates the amount of polyplexes being internalized by KB cells (pDNA) or KB/eGFPLuc (siRNA). A) pDNA, ***PEG-Cont*** (gMFI = 7.2) in solid gray, ***PEG-FolA*** (gMFI = 222.0) in solid black and HBG buffer only treated cells in dotted gray. B) pDNA, ***CRC-PEG-Cont*** (gMFI = 21.1) in solid gray, ***CRC-PEG-FolA*** (gMFI = 468.0) in solid black and HBG buffer only treated cells in dotted gray. C) siRNA, **PEG-Cont** (gMFI = 8.1) in solid gray, ***PEG-FolA*** (gMFI = 15.9) in solid black and HBG buffer only treated cells in dotted gray. D) siRNA, ***CRC-PEG-Cont*** (gMFI = 18.3) in solid gray, ***CRC-PEG-FolA*** (gMFI = 31.4) in solid black and HBG buffer (gMFI = 4.5) only treated cells in dotted gray. gMFI indicates the geometric mean fluorescence intensity. Experiments were performed by Ana Krhac Levacic and Katharina Müller (PhD studies, Pharmaceutical Biotechnology, LMU).

In all cases folate-targeted structures showed a higher cellular internalization than non-targeted control structures.

Beneficial uptake of targeted versus nontargeted PEGylated structures into cells could also be observed by confocal microscopy (**Fig. 25, Fig. 26**). The results are consistent

with the transfection data and confirm that the targeting effect is the reason for superiority in transfection.

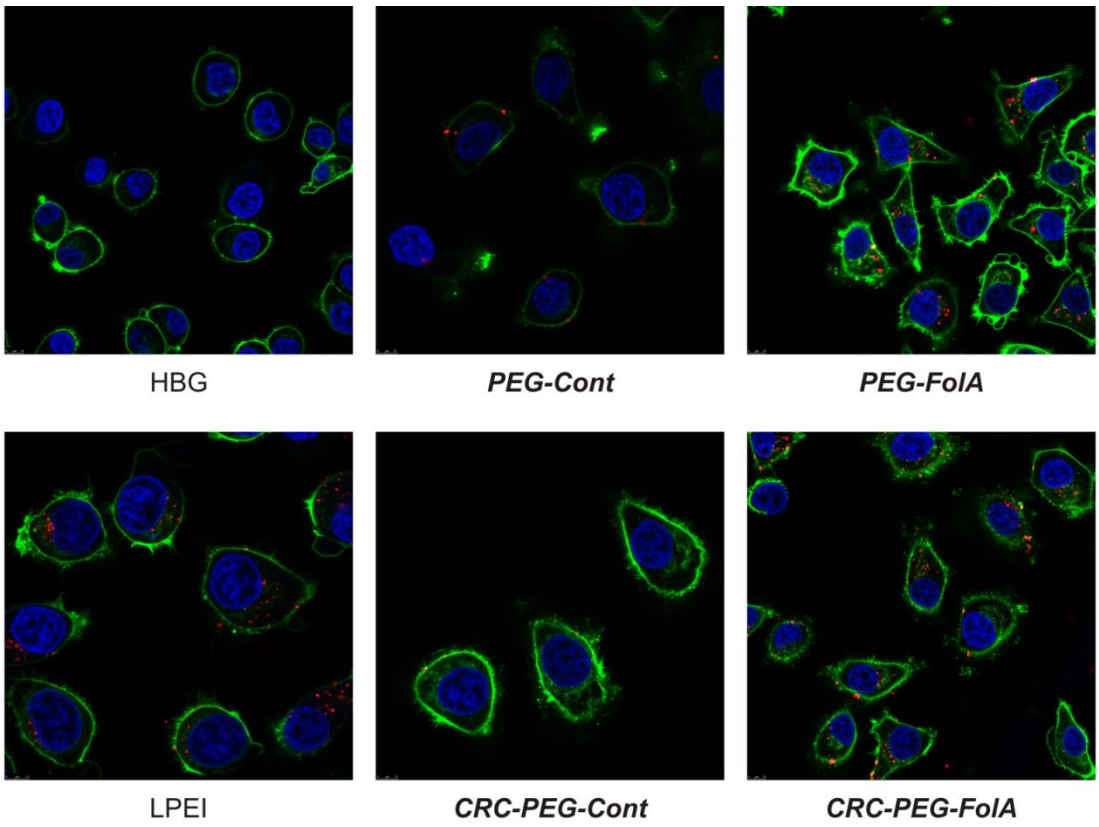

Fig. 25 Intracellular distribution of PEGylated pDNA polyplexes in KB cells acquired by confocal laser scanning microscopy. Nuclei were stained with Hoechst 33342 (blue), actin was stained with rhodamine phalloidin (green) and pDNA was spiked with 20 % Cy5-labeled pDNA (red). The images show the overlay of the different channels. Transfections were performed by Ana Krhac Levacic (PhD study, Pharmaceutical Biotechnology, LMU), confocal microscopy was performed by Miriam Höhn (Pharmaceutical Biotechnology, LMU).

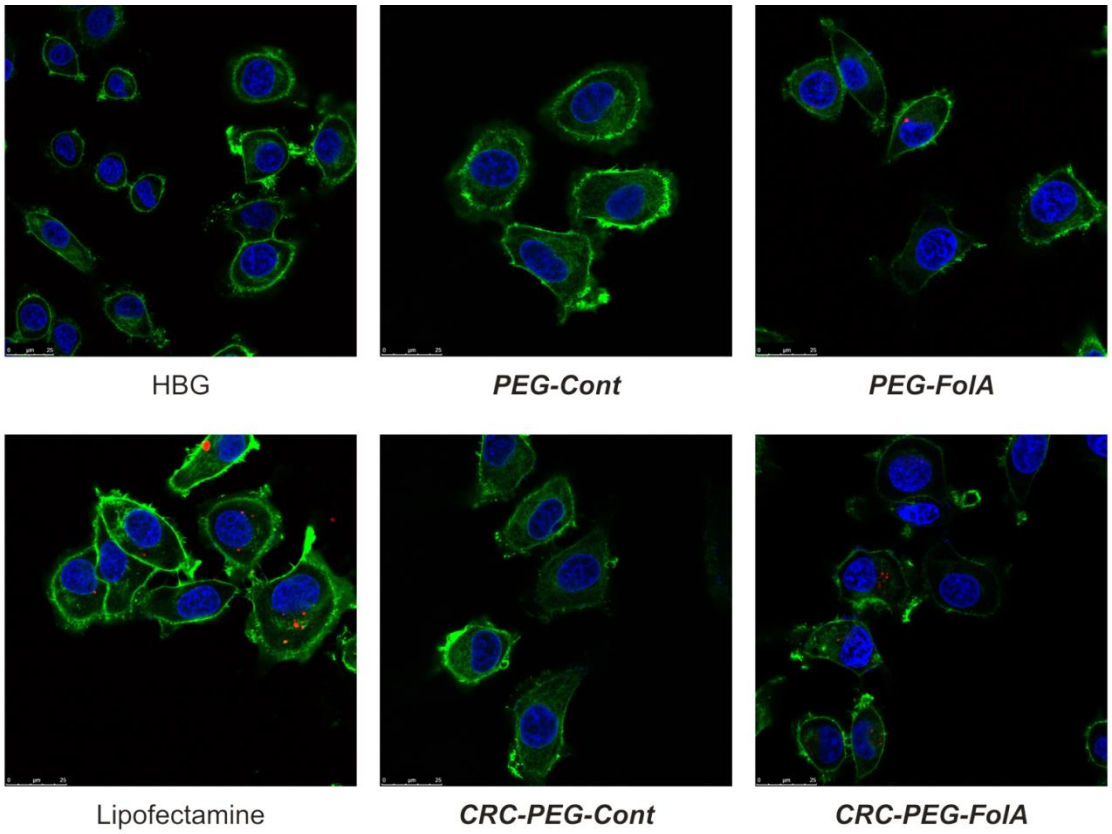

Fig. 26 Intracellular distribution of PEGylated siRNA polyplexes in KB cells acquired by confocal laser scanning microscopy. Nuclei were stained with Hoechst 33342 (blue), actin was stained with rhodamine phalloidin (green) and siRNA was spiked with 20 % Cy5-labeled siRNA (red). The images show the overlay of the different channels. Transfections were performed by Katharina Müller (PhD study, Pharmaceutical Biotechnology, LMU), confocal microscopy was performed by Miriam Höhn (Pharmaceutical Biotechnology, LMU).

Gel-shift assays in the presence of serum at 37 °C did not reveal any major differences between single cysteine structures and the ones with CRC motifs (**Fig. 27**). The pDNA complexes with and without CRC motifs were stable in serum at N/P 12. The siRNA structures were less stable and incorporation of CRC only slightly improved this though, even at 90 min, the majority of siRNA remained complexed (see 90 min time point plus/minus heparin treatment).

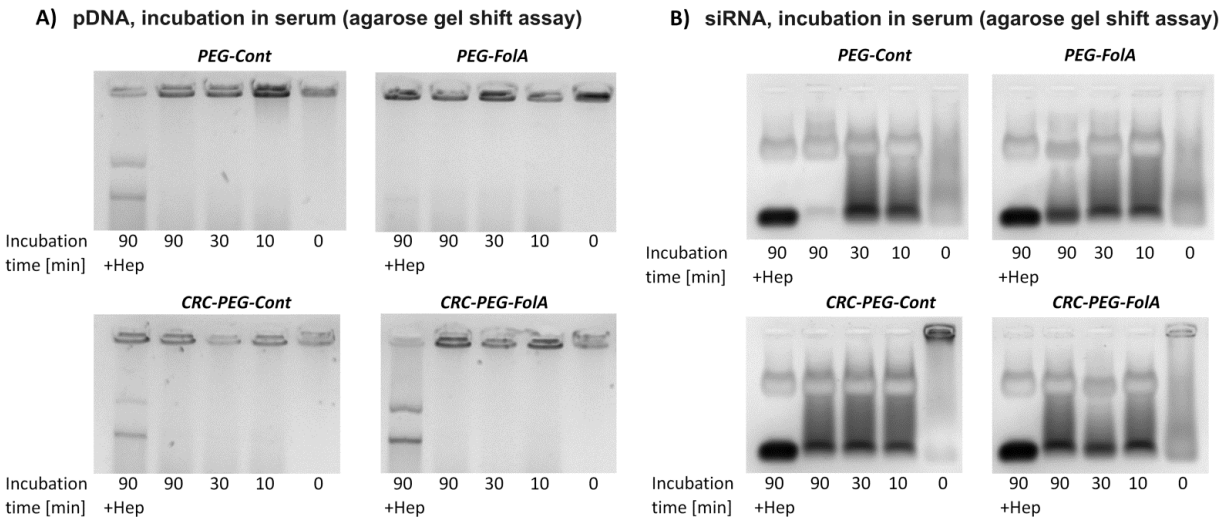

Fig. 27 Stability of polyplexes with PEGylated oligomers in agarose gel shift assay after up to 90 min incubation at 37°C in 90 % FBS. A) pDNA binding at N/P 12 and B) siRNA binding at N/P 20 of single cysteine oligomers (top) and corresponding twin disulfide-forming analogs (bottom). Polyplexes were incubated at room temperature for 40 min before FBS was added. Heparin (50 I.U.) was added to dissociate polyplexes.

To better understand polyplex response towards physiological reducing agents, a reducing gel-shift with different concentrations of glutathione (GSH) at 37 °C was performed. Polyplexes should be stable at lower GSH concentrations that occur outside a cell (0.02 mM GSH) and disulfide should degrade at higher concentrations inside the cell (1 – 11 mM GSH) [37]. For pDNA polyplexes with single cysteine residues, disassembly could be observed at N/P 12 with 10 mM GSH (**Fig. 28A** – ***PEG-Cont***, ***PEG-FolA***). The analogs with CRC motifs (***CRC-PEG-Cont***, ***CRC-PEG-FolA***) did not show any sensitivity towards the analyzed GSH concentrations. The siRNA binding ability for N/P 20 for single cysteine polyplexes was weak for all GSH concentrations (**Fig. 28B**; ***PEG-Cont***, ***PEG-FolA***).

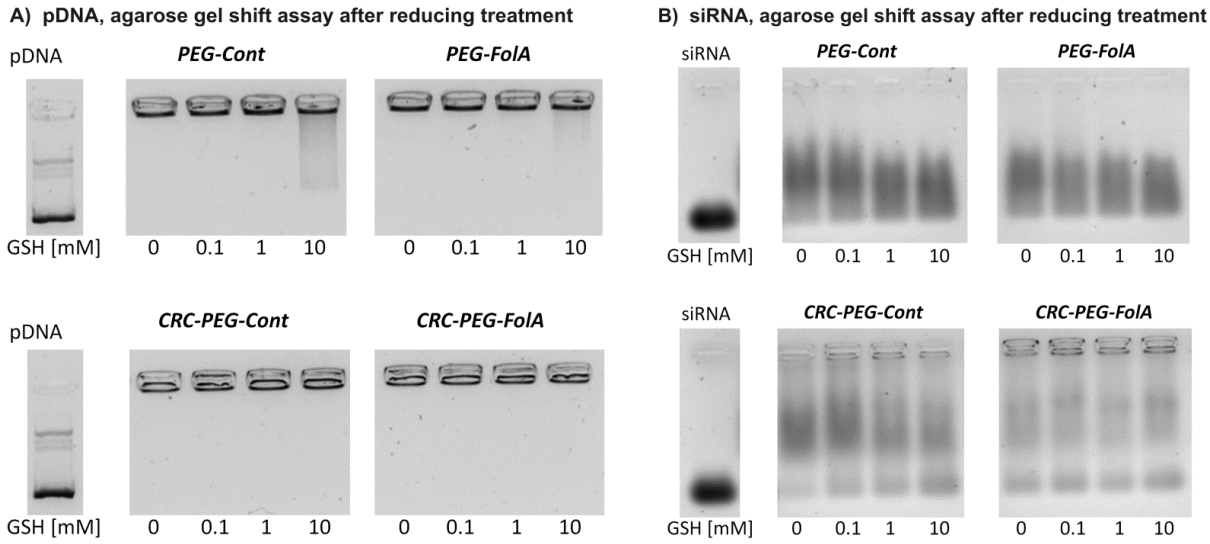

Fig. 28 Stability of polyplexes with PEGylated oligomers in agarose gel shift assay after 2 h incubation at 37 °C at different concentrations of glutathione (GSH). A) pDNA binding at N/P 12 and B) siRNA binding at N/P 20 of single cysteine oligomers (top) and corresponding twin disulfide-forming analogs (bottom). Left lanes: free pDNA or free siRNA, respectively.

Nevertheless, with increasing GSH concentrations a tendency towards weaker binding could be observed. Incorporation of the CRC motif increased the stability of the siRNA polyplexes significantly and did not decrease in the presence of GSH. All data indicate that the introduction of the CRC motif leads to a significant increase in stability. For oligomer structures with sufficient stability in the absence of CRC, this increase of stability did not improve but often decreased transfection efficiency. Labile siRNA polyplexes with PEGylated oligomers, like ***PEG-FolA***, however, may benefit from twin disulfides.

3.2 Precise redox-sensitive cleavage sites for improved bioactivity of siRNA lipopolyplexes

This chapter has been adapted from:

Klein PM*, Reinhard S*, Lee DJ, Müller K, Ponader D, Hartmann L, Wagner E. *Precise redox-sensitive cleavage sites for improved bioactivity of siRNA lipopolyplexes*. Nanoscale. 2016 Oct 27;8(42):18098-18104

**contributed equally*

Cysteine-based disulfide formation during polyplex formation by air oxygen is a poorly controllable, incomplete process [83, 130]. Alternatively, integration of bioreducible bonds into carriers can be achieved before nanoparticle formation [115, 131, 132]. Disulfide bonds can be accurately integrated during SPS of polymers, as already demonstrated by Hartmann et al. [63]. Cleavable cationic domains, as well as disassembly of stabilizing domains, have been demonstrated to improve delivery systems [133].

In this chapter, we designed novel bioreducible cationic lipo-oligomers. By precisely positioning the disulfide bond between the fatty acid and polycationic domain (and not into the polycationic domain) via a Fmoc-succinoyl-cystamine building block, we intended to obtain a most drastic molecular change upon bioreduction. The amphiphilic, detergent-like character, which is considered favorable for endosomolysis but might also be associated with cytotoxicity, should be abolished upon entry into the reductive cytosol by the split into separate pure lipidic and cationic fragments; the latter have insufficient ability to bind siRNA.

We evaluate three lipo-oligomer topologies (T-shape, i-shape and U-shape) and different representatives of fatty acids as variables, which previously were found [82] to affect polyplex characteristics such as siRNA binding and lytic potential of oligomers, gene silencing efficacy and toxicity of polyplexes. Compared with their nonreducible lipo-oligomer analogs, the favorable polyplex characteristics should remain indifferent until intracellular release into the cytosol, where improved siRNA release and biocompatibility would be expected.

3.2.1 Synthesis of the bioreducible Fmoc-succinoyl-cystamine building block and evaluation of its sensitivity towards reducing conditions

A building block applicable for standard Fmoc solid-phase peptide synthesis requires a protected amino group and a free carboxylic acid function. The synthesis of the disulfide building block (ssbb) was carried out starting from cystamine by selective protection of one terminal amine with Fmoc in the first step avoiding change of protecting groups as was previously presented [134]. To achieve reaction selectivity towards mono-functionalization, 0.8 eq. Fmoc-succinimide (Fmoc-OSu) was added dropwise to a cooled solution (-80 C) of cystamine dihydrochloride in THF with DIPEA as a base. The carboxylic acid function was introduced in the second step by addition of 1.8 eq. succinic anhydride (Succ anhydride) solved in THF with DIPEA (**Fig. 29A**). The ssbb structure was purified via column chromatography and the identity confirmed by ^{1}H-NMR.

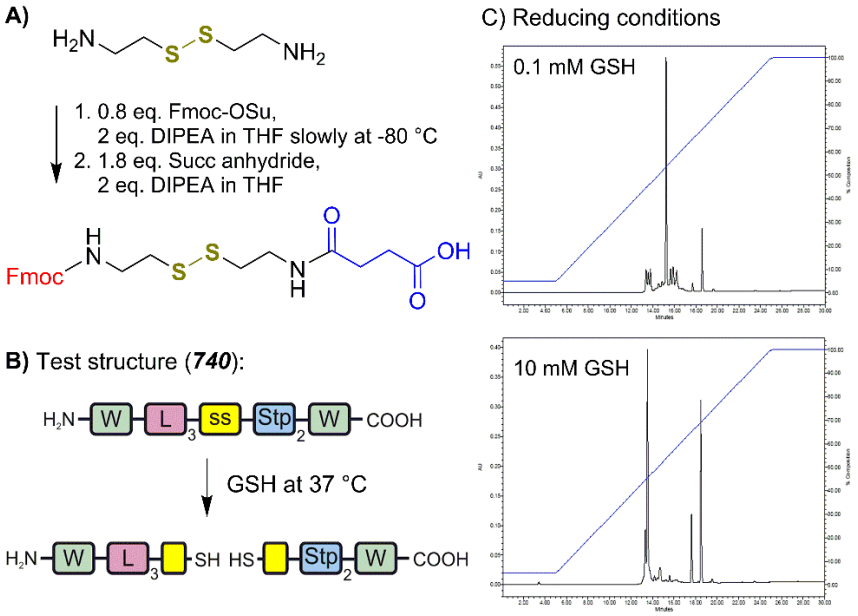

Fig. 29 A) Synthesis of the disulfide building block Fmoc-succinoyl-cystamine (Fmoc-ssbb). B) Glutathione (GSH) triggered cleavage of the test structure (***740***) with a hydrophilic (Stp_2) and a hydrophobic (L_3) part connected by ssbb. C) Test structure monitored by HPLC (280 nm wavelength) after incubation for 90 min at 37 °C in 0.1 mM GSH- (top) and 10 mM GSH- (bottom) containing HEPES buffer pH 7.4.

A test structure (***740***) was synthesized on solid phase to prove the applicability for SPS. Here the ssbb connects a lipophilic peptide sequence containing three leucines (L_3) to a hydrophilic sequence with two succinoyl-tetraethylene pentamine (Stp) units (**Fig. 29B**). Tryptophane (W) was incorporated into both parts to facilitate photometric analysis. The product structure was confirmed by mass spectrometry and ^{1}H-NMR. The product was incubated with increasing concentrations of the physiological antioxidant glutathione (GSH) at 37 °C to simulate the behavior of the ssbb at different extra- and intracellular milieus. A GSH concentration of 0.1 mM mimics the barely reducing extracellular environment. As expected, the test oligomer mostly retained its structural integrity. Increasing the GSH concentration to 10 mM resembling the cytosolic reducing conditions resulted in cleavage of the test structure without detectable fractions of the intact oligomer (**Fig. 29C**).

3.2.2 Design and synthesis of cationic lipo-oligomers to form siRNA polyplexes

The ssbb unit was applied in SPS of lipo-oligomers supposed to form siRNA polyplexes that are stable in the extracellular and labile in the intracellular environment. Lipo-oligomers with three different topologies, T-shape, i-shape, and U-shape, were synthesized (**Fig. 30** top and **Fig. 31**). As shown in our previous work, topologies, as well as specific moieties of structures, may influence the biophysical and biological properties of the resulting polyplexes [82, 83, 119, 135]. For bioreducible crosslinking between oligocations, previous oligomers were designed with cysteines terminating the cationic backbone [82, 83, 119]. Differently, in the current work, the ssbb unit was positioned between the ionizable oligocationic part of the molecule and a bis (fatty acid) unit.

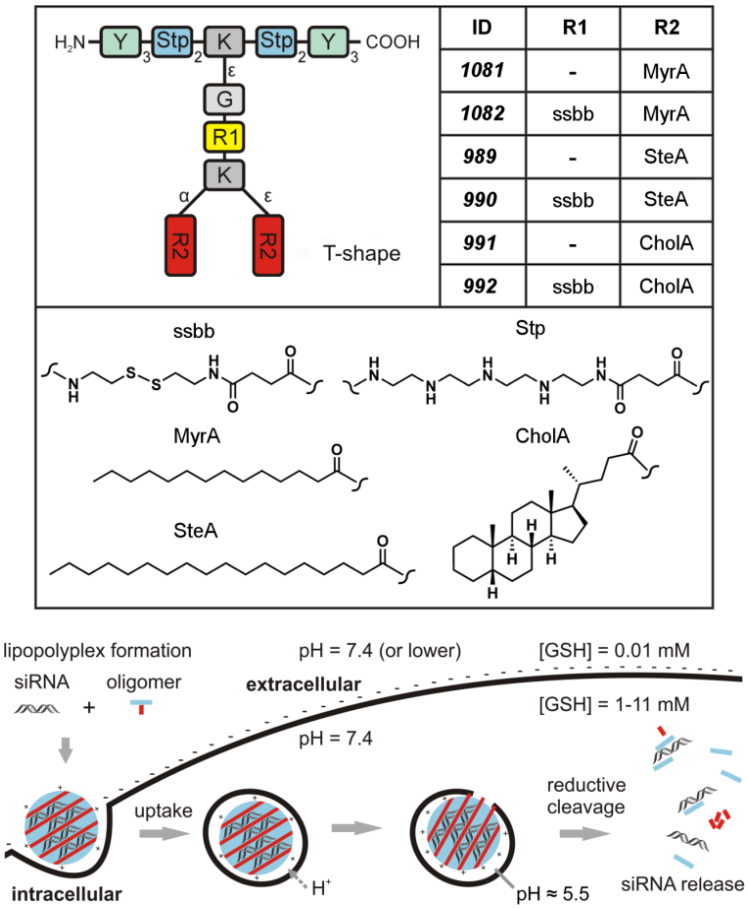

ID	R1	R2
1081	-	MyrA
1082	ssbb	MyrA
989	-	SteA
990	ssbb	SteA
991	-	CholA
992	ssbb	CholA

Fig. 30 Sequence-defined oligomers with T-shape topology. Top: schematic overview of the structures with different modifications (Y: tyrosine, K: lysine, G: glycine, Stp: succinoyl-tetraethylene-pentamine, ssbb: succinoyl-cystamine, MyrA: myristic acid, SteA: stearic acid, CholA: 5β-Cholanic acid). The broken lines represent amide linkages. IDs are unique database identification numbers. Bottom: cellular uptake, acidic pH-triggered endosomal escape, and GSH triggered cytosolic disassembly of siRNA polyplexes. Structures ***1081, 1082, 989*** and ***990*** were synthesized by Sören Reinhard (PhD study, Pharmaceutical Biotechnology, LMU).

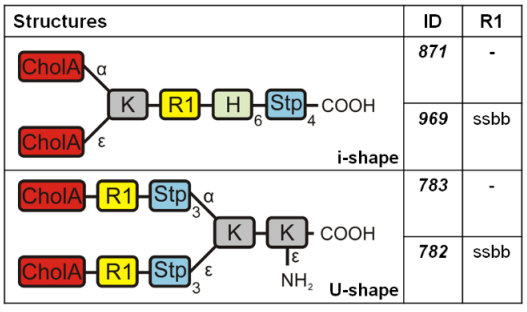

Structures	ID	R1
	871	-
	969	ssbb
	783	-
	782	ssbb

Fig. 31 Sequence-defined oligomers with i-shape and U-shape topology. Schematic overview of the structures with different modifications (K: lysine, H: histidine, Stp: succinoyl-tetraethylene-pentamine, ssbb: succinoyl-cystamine, CholA: 5β-Cholanic acid). IDs are unique database identification numbers. i-shape structures were synthesized by Sören Reinhard (PhD study, Pharmaceutical Biotechnology, LMU).

Thus, upon reductive cleavage maximum destabilization of the polyplex on the one hand, and abolition of the membrane-active amphiphilic character on the other hand, should be achieved. The oligocation part contains several Stp units as artificial oligoamino acids for nucleic acid binding and endosomal protonation [66], and lysines (K) as branching units. Additionally, the cationic part was equipped with tyrosine trimers (Y_3) [119] for further hydrophobic stabilization of the T-shape oligomers (**Fig. 30**), and with histidine blocks (H_6) for increased endosomal buffering of the i-shape oligomers. The saturated C14 short chain myristic acid (MyrA), the stearic acid (SteA) with the longer C18 chain, and the bulky cholanic acid (CholA) were incorporated as fatty acids for hydrophobic polyplex stabilization. For all oligomers, the corresponding non-reducible control structures lacking ssbb were synthesized. The ssbb was incorporated into various different structures to proof the concept independently of shape and other functional domains and to put this work into a broader context. The structures were analyzed with mass spectrometry and ^{1}H-NMR (Appendix 6.4.2). To exclude that lipo-oligomers contain significant amounts of reduced fragments, Ellman´s assay was performed to detect free thiols (**Table 12**). Lack of free thiols (< 3 %) indicate high integrity of the ssbb linkage.

Table 12 Determination of free thiols in reducible T-shape, i-shape and U-shape structures via Ellman´s assay

Oligomer	Ratio of free thiols (in %)
1082 **(MyrA-ss-t)**	2.0
990 **(SteA-ss-t)**	2.3
992 **(CholA-ss-t)**	2.7
969 **(CholA-ss-i)**	1.2
782 **(CholA-ss-u)**	0.6

3.2.3 Formulation of siRNA polyplexes and biophysical characterization

Polyplexes were formed by mixing the cationic oligomers with siRNA, followed by 40 minutes incubation and biophysical characterization (**Fig. 32** shows a summery for stable and reducible CholA T-shapes ***991*** and ***992***). The siRNA binding ability of oligomers was determined by measuring the electrophoretic mobility of siRNA in a

2.5 % agarose gel. Different N/P values depict the ratio of protonatable amines (N) of the oligomer to phosphates (P) of the siRNA.

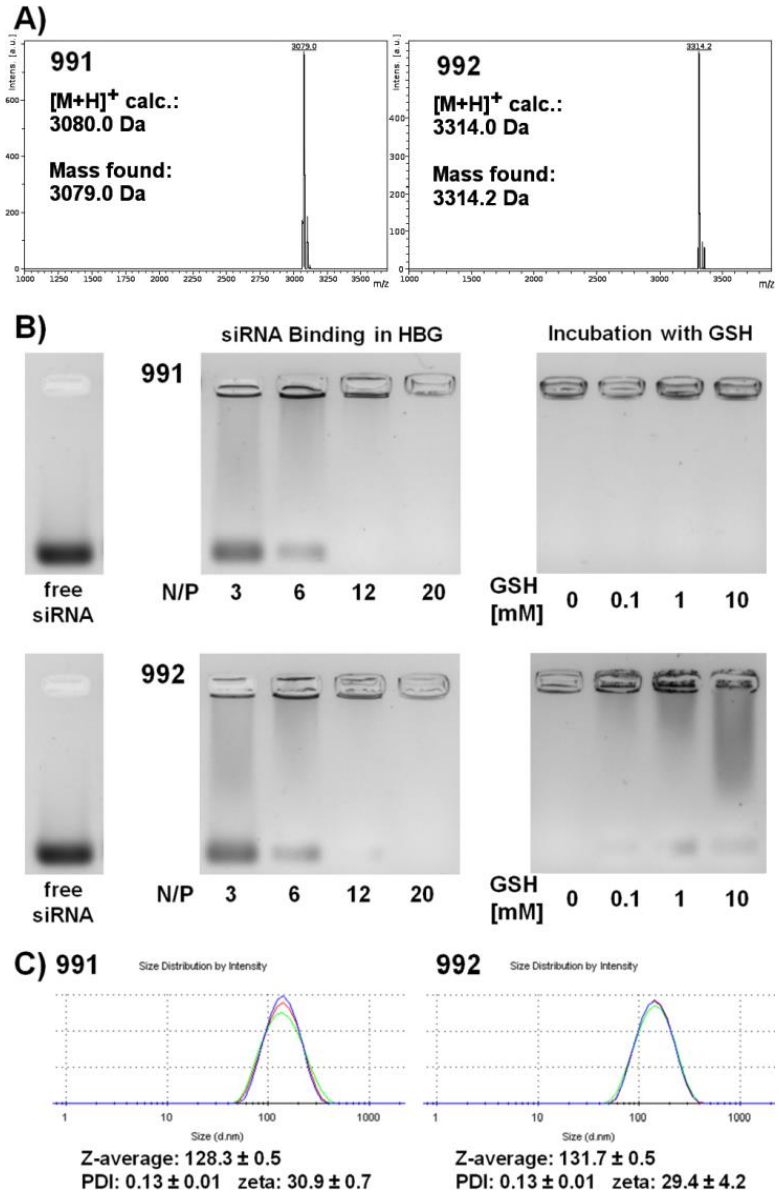

Fig. 32 A) Analytical characterization of stable oligomer ***991*** and bioreducible oligomer ***992*** by mass spectrometry. B) Agarose gel shift assays. Left: siRNA binding at different N/P ratios. Right: Lipopolyplexes formed at N/P 20 and subsequent 90 min treatment at 37 °C with different concentrations of GSH in HEPES buffer pH 7.4. C) Biophysical characterizations of lipopolyplexes formed with oligomers and siRNA at N/P 12 by DLS. Mass spectrometry and gel shifts were performed by Sören Reinhard (PhD study, Pharmaceutical Biotechnology, LMU).

This does not present charge ratios, as only a fraction of the protonatable amines are protonated at physiological pH. All T-shape, i-shape and U-shape structures showed sufficient binding at N/P ≥ 12 (**Fig. 33**, **Fig. 34**).

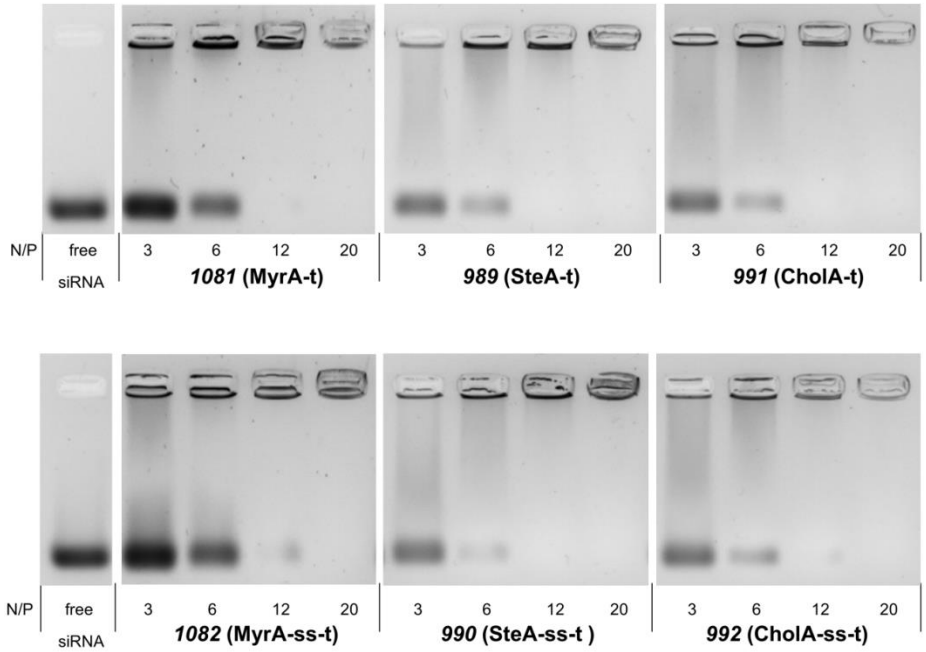

Fig. 33 siRNA binding ability of T-shape structures analyzed with an agarose gel shift assay. The left lane shows the running distance of free siRNA in HBG that is not complexed by lipo-oligomers. Polyplexes were tested for siRNA binding ability at different N/P ratios. Top: stable structures, bottom: reducible structures. Gel shifts were performed by Sören Reinhard (PhD study, Pharmaceutical Biotechnology, LMU).

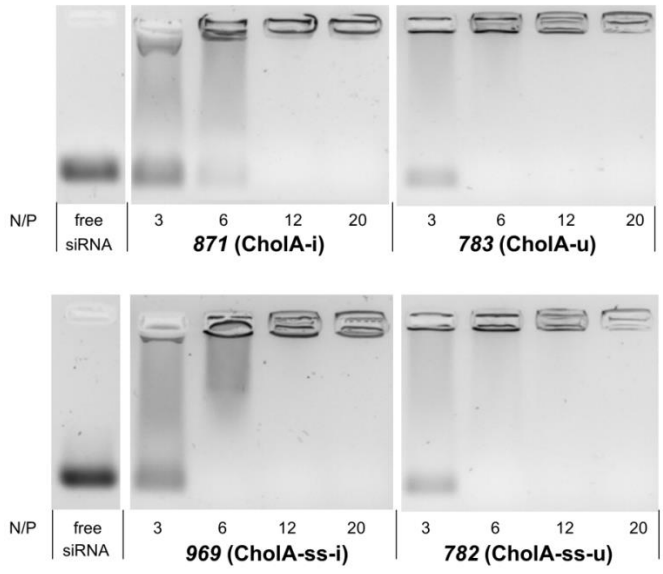

Fig. 34 siRNA binding ability of i-shape and U-shape structures analyzed with an agarose gel shift assay. The left lane shows the running distance of free siRNA in HBG that is not complexed by lipo-oligomers. Polyplexes were tested for siRNA binding ability at different N/P ratios. Top: stable structures, bottom: reducible structures. Gel shifts for i-shape structures were performed by Sören Reinhard (PhD study, Pharmaceutical Biotechnology, LMU).

Neither stable nor reducible polyplexes released free siRNA when exposed to 90 % full serum at 37 °C for two hours, indicating a high extracellular stability (**Fig. 35**).

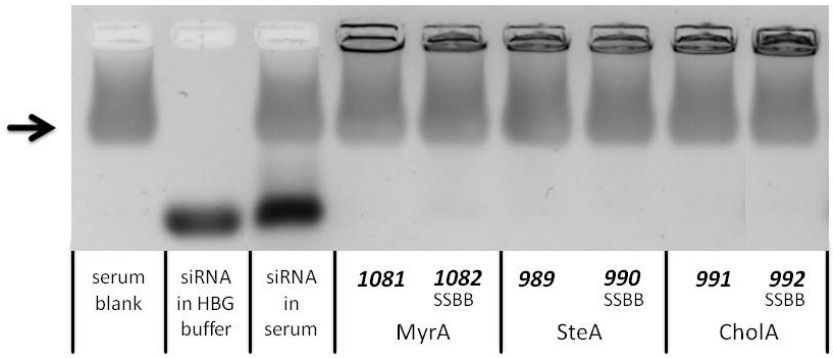

Fig. 35 Gel retardation assay of siRNA polyplexes incubated at N/P 12 for 40 min, followed by treatment with 90 % full serum for two hours at 37 °C. The black arrow points at a band that is caused by serum (see serum blank in band one). Running distance of free siRNA in HBG buffer and in 90 % serum are shown in band two and three.

In contrast, treatment of polyplexes with the physiological reducing agent GSH at 37 °C resulted in a dose-dependent loss of siRNA binding efficacy for the reducible but not the stable oligomers (**Fig. 36**, **Fig. 37**). Due to the particular position of the ssbb unit, reductive cleavage leads to the release of the lipid as the most important stabilization motif, thus keeping only a weak binding ability of the remaining cationic backbone [119]. This destabilization of polyplexes is expected to provide better accessibility of siRNA at intracellular GSH concentrations (~10 mM).

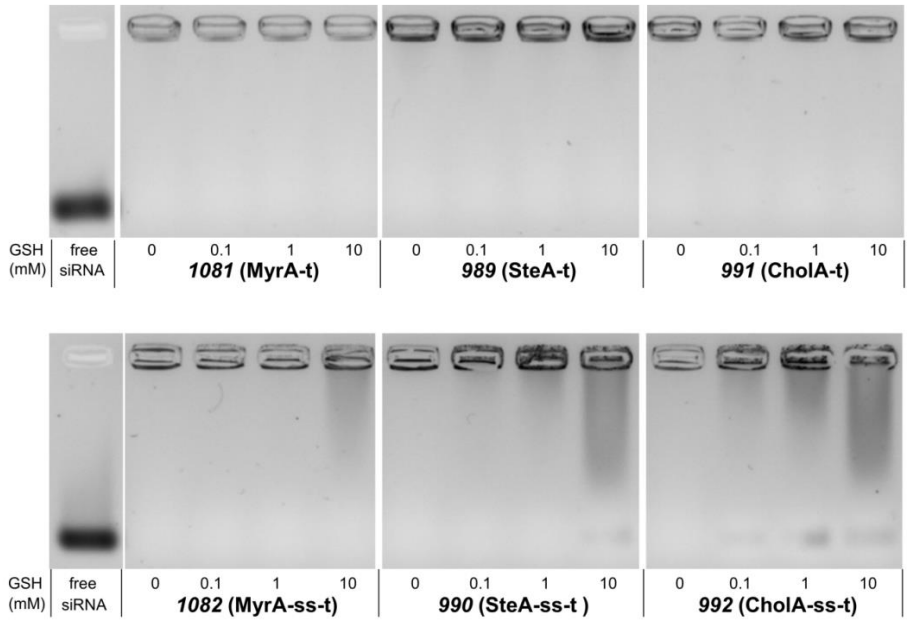

Fig. 36 siRNA binding ability of T-shape structures under reducing conditions analyzed with an agarose gel shift assay. The left lane shows the running distance of free siRNA in HBG that is not complexed by lipo-oligomers. Lipopolyplexes were formed at N/P 20 followed by 90 min treatment at 37 °C with different concentrations of GSH in HEPES buffer pH 7.4. Top: stable structures, bottom: reducible structures. Gel shifts were performed by Sören Reinhard (PhD study, Pharmaceutical Biotechnology, LMU).

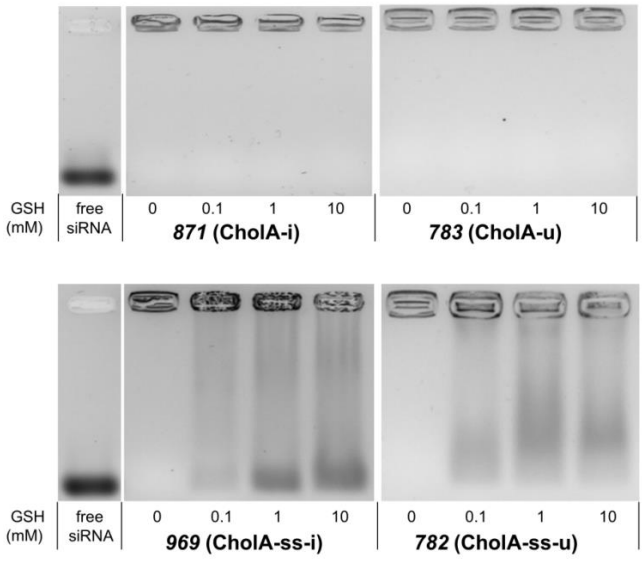

Fig. 37 siRNA binding ability of i-shape and U-shape structures under reducing conditions analyzed with an agarose gel shift assay. The left lane shows the running distance of free siRNA in HBG that is not complexed by lipo-oligomers. Lipopolyplexes were formed at N/P 20 followed by 90 min treatment at 37 °C with different concentrations of GSH in HEPES buffer pH 7.4. Top: stable structures, bottom: reducible structures. Gel shifts for i-shape structures were performed by Sören Reinhard (PhD study, Pharmaceutical Biotechnology, LMU).

The particle sizes of siRNA lipopolyplexes were measured by dynamic light scattering (DLS). All T-shape polyplexes showed uniform sizes between 105 - 138 nm z-average (**Table 13**).

Table 13 Particle size (Z-average) and zeta potential of siRNA polyplexes determined with a DLS zetasizer. Measurements for i-shape structures were performed by Sören Reinhard (PhD study, Pharmaceutical Biotechnology, LMU).

Oligomer	N/P	z-average [nm]	Mean PDI	Mean Zeta Potential [mV]
***1081* (MyrA-t)**	12	105.0 ± 1.8	0.15 ± 0.01	27.0 ± 0.8
***1082* (MyrA-ss-t)**	12	107.7 ± 0.5	0.14 ± 0.02	28.6 ± 0.8
***989* (SteA-t)**	12	125.3 ± 1.0	0.12 ± 0.01	29.3 ± 1.6
***990* (SteA-ss-t)**	12	137.9 ± 1.6	0.13 ± 0.01	26.8 ± 0.9
***991* (CholA-t)**	12	131.7 ± 0.5	0.13 ± 0.01	29.4 ± 4.2
***992* (CholA-ss-t)**	12	128.3 ± 0.5	0.13 ± 0.01	30.9 ± 0.7
***871* (CholA-i)**	12	275.0 ± 7.2	0.24 ± 0.01	23.4 ± 0.7
***969* (CholA-ss-i)**	12	237.8 ± 4.2	0.20 ± 0.01	25.2 ± 0.3
***783* (CholA-u)**	12	122.7 ± 2.0	0.26 ± 0.02	31.5 ± 0.7
***782* (CholA-ss-u)**	12	181.2 ± 4.7	0.27 ± 0.01	29.1 ± 3.3

The sizes of i-shape and U-shape polyplexes showed higher polydispersity. All formulations revealed a positive zeta potential of around 23 – 32 mV due to an excess of cationic oligomer (**Table 13**). T-shape oligomers were found as well-suited for the evaluation of structure-activity relationships, since all of them formed polyplexes with reliable sizes and low polydispersity.

3.2.4 siRNA transfection efficiency

Gene silencing experiments were performed in Neuro2A neuroblastoma cells stably expressing an eGFP-Luciferase fusion protein (**Fig. 38**). Silencing by siGFP (light bars) can be quantified by a standard luciferase assay. In all cases, gene silencing was more effective for the bioreducible T-shape oligomers (**Fig. 38B**) as compared to their stable analogs (**Fig. 38A**). A reduced luciferase expression in control experiments using siCtrl (dark bars) is caused by unspecific cytotoxic effects and not by a specific knockdown of the eGFPLuc gene. Thus, from evaluating the luciferase levels of the siCtrl

polyplexes, an enhanced biocompatibility of the reducible structures (**Fig. 38B**) can be concluded.

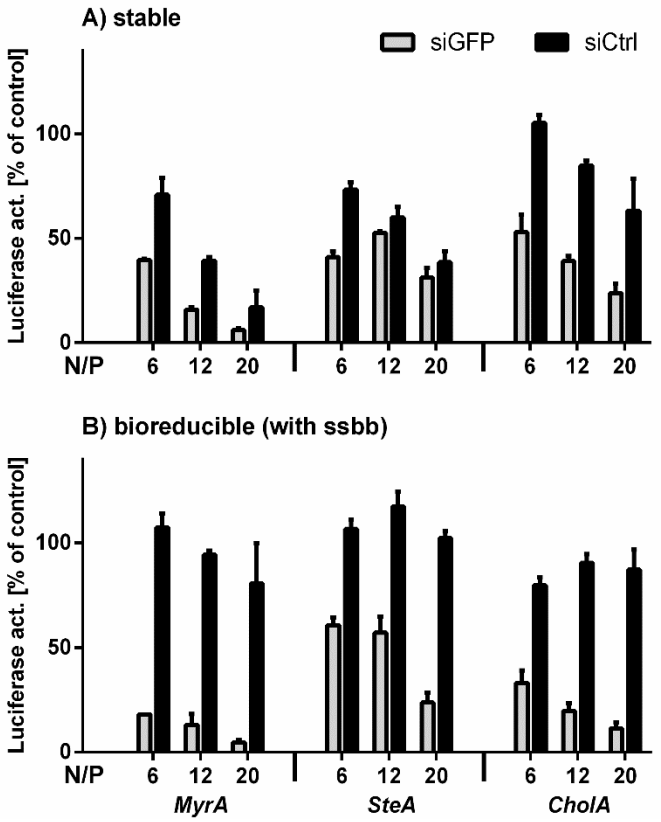

Fig. 38 Gene silencing of T-shape oligomers in neuroblastoma cells. Lipopolyplexes with 500 ng / 37 pmol eGFP-targeted siRNA (siGFP) / well respectively control siRNA (siCtrl) at N/P 6, 12 and 20 were tested for eGFPLuc gene silencing in Neuro2A-eGFPLuc cells. A) Lipopolyplexes made of stable structures ***1081***, ***989*** and ***991*** B) Lipopolyplexes made of bioreducible structures ***1082***, ***990*** and ***992***. The luciferase activity of siRNA-treated cells is presented related to buffer-treated cells. HBG-treated cells were set to 100 %. Data are presented as mean value (± SD) out of triplicates**.** Dose-dependent gene silencing transfections are shown in Fig. S8 and S9. Transfections were performed by Dian-Jang Lee (PhD study, Pharmaceutical Biotechnology, LMU).

Similar findings, an enhanced gene silencing and especially the reduction of cytotoxicity, were also made for bioreducible i-shape and U-shape lipo-oligomers (**Fig. 39**).

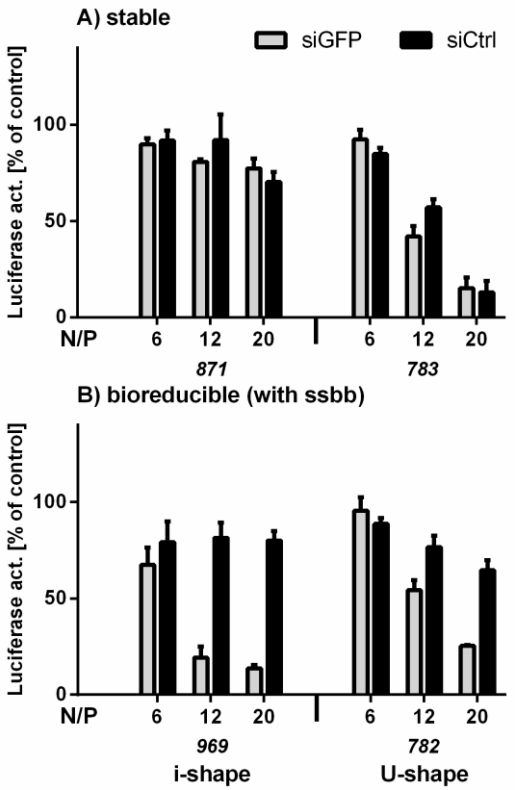

Fig. 39 Gene silencing of i-shape and U-shape oligomers in neuroblastoma cells. Lipopolyplexes with 500 ng / 37 pmol eGFP-targeted siRNA (siGFP) / well respectively control siRNA (siCtrl) at N/P 6, 12 and 20 were tested for eGFPLuc gene silencing in Neuro2A/eGFPLuc cells. A) Lipopolyplexes made of stable structures ***871*** and ***783*** B) Lipopolyplexes made of bioreducible structures ***969*** and ***782***. The luciferase activity of siRNA-treated cells is presented related to buffer-treated cells. HBG-treated cells were set to 100 %. Data are presented as mean value (± SD) out of triplicates**.** Transfections for i-shapes were performed by Dian-Jang Lee, transfections for u-shapes were performed by Katharina Müller (PhD studies, Pharmaceutical Biotechnology, LMU).

For the best-performing T-shape structures with MyrA and CholA, dose-dependent gene silencing experiments were carried out. Based on the starting formulation of 37 pmol siRNA (370 nM) with 1.44 nmol oligomer (N/P 12), the dose of siRNA was reduced either at a constant N/P 12 (**Fig. 40**) or a constant dose of 1.44 nmol oligomer (**Fig. 41**). In the latter case, significant gene silencing was still observed for reducible MyrA polyplexes at 1.2 pmol / 12 nM siRNA.

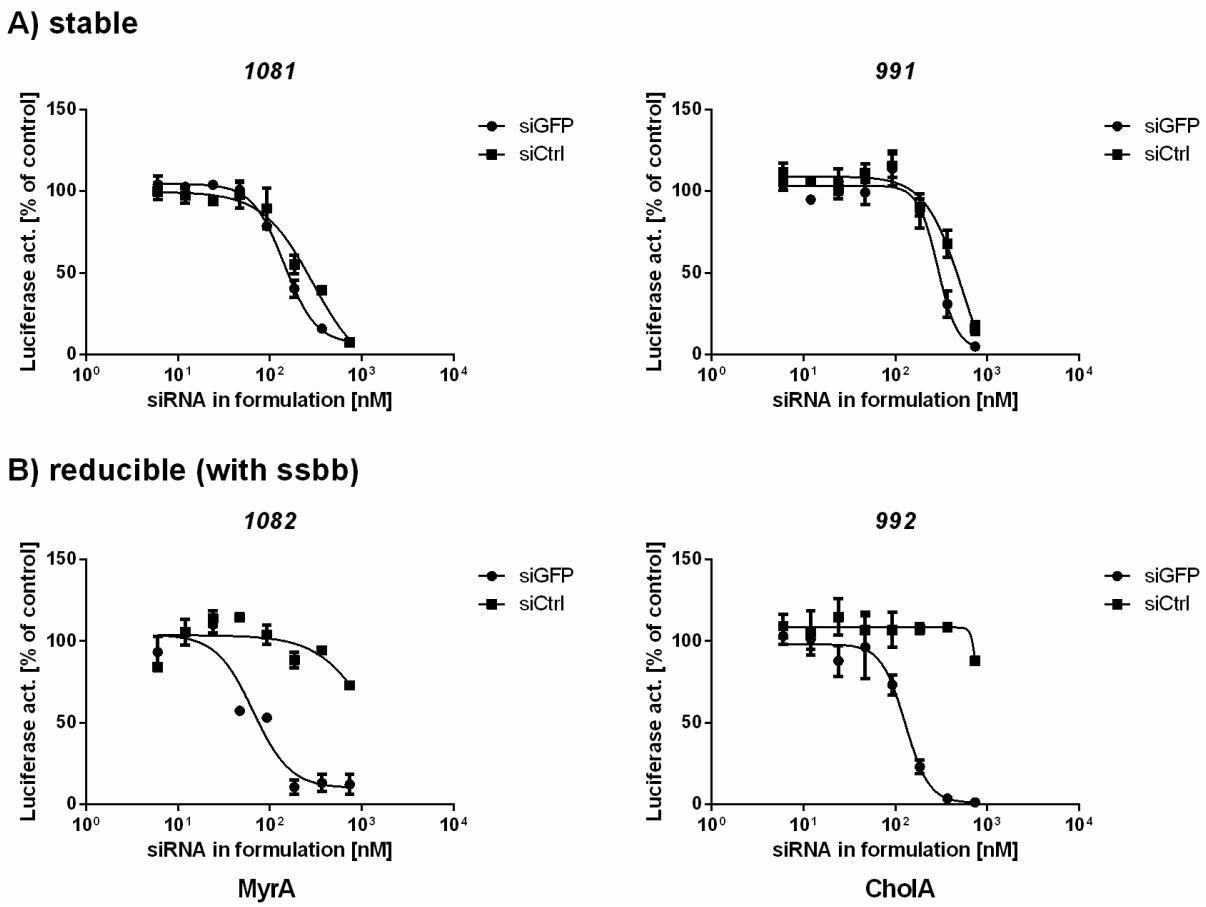

Fig. 40 Dose-dependent gene silencing of T-shape oligomers at N/P 12 in neuroblastoma cells. Lipopolyplexes with eGFP-targeted siRNA (siGFP) respectively control siRNA (siCtrl) were examined for eGFPLuc gene silencing in Neuro2A/eGFPLuc cells. The oligomer amount was adjusted for each formulation to keep it constant at N/P 12. Formulations including siRNA from 6, 12, 27, 47, 93, 185, 370 up to 740 nM were tested. A) Lipopolyplexes made of stable structures ***1081*** and ***991*** B) Lipopolyplexes made of bioreducible structures ***1082*** and ***992***. The luciferase activity of siRNA-treated cells is presented related to buffer-treated cells. HBG-treated cells were set to 100 %. Data are presented as mean value (± SD) out of triplicates. Transfections were performed by Dian-Jang Lee (PhD study, Pharmaceutical Biotechnology, LMU).

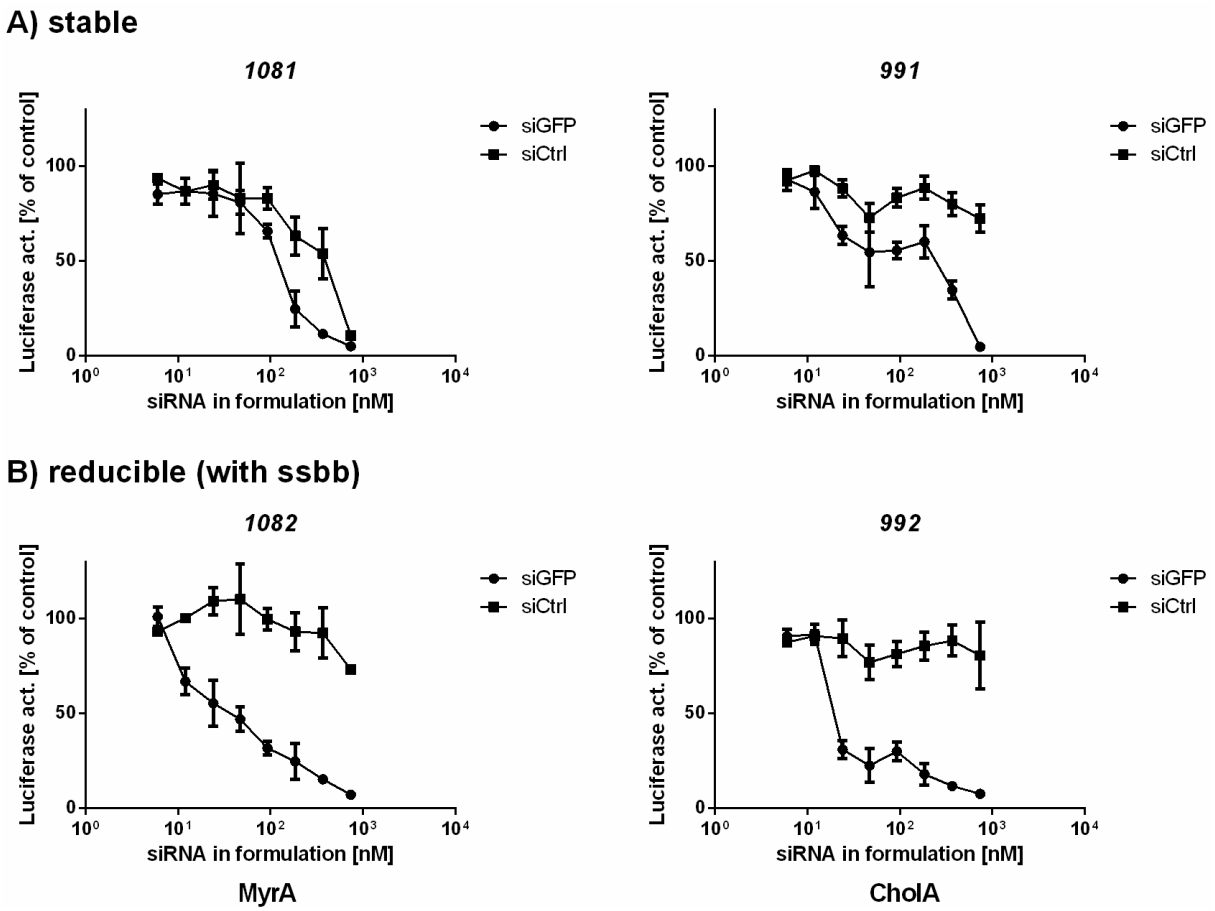

Fig. 41 Dose-dependent gene silencing of T-shape oligomers in neuroblastoma cells. Lipopolyplexes with eGFP-targeted siRNA (siGFP) respectively control siRNA (siCtrl) at constant oligomer amount of 1.44 nmol (N/P 12 at 500 ng siRNA) were examined for eGFPLuc gene silencing in Neuro2A/eGFPLuc cells. Formulations including siRNA from 6, 12, 27, 47, 93, 185, 370 up to 740 nM were tested. A) Lipopolyplexes made of stable structures ***1081*** and ***991*** B) Lipopolyplexes made of bioreducible structures ***1082*** and ***992***. The luciferase activity of siRNA-treated cells is presented related to buffer-treated cells. HBG-treated cells were set to 100 %. Data are presented as mean value (± SD) out of triplicates. Transfections were performed by Dian-Jang Lee (PhD study, Pharmaceutical Biotechnology, LMU).

The beneficial effects of reducible polyplexes are also confirmed in DU145/eGFPLuc prostate cancer cells (**Fig. 42**).

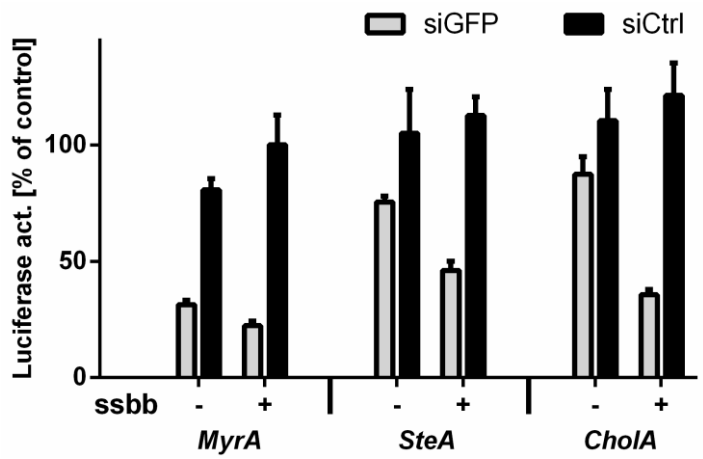

Fig. 42 Gene silencing of T-shape oligomers in prostate cancer cells. Lipopolyplexes with 500 ng eGFP-targeted siRNA (siGFP) respectively control siRNA (siCtrl) at N/P 12 were tested for eGFPLuc gene silencing in DU145/eGFPLuc cells. Lipopolyplexes made of stable structures (***1081***, ***989*** and ***991***) and bioreducible structures (***1082***, ***990*** and ***992***) are shown. The luciferase activity of siRNA treated cells is presented related to buffer-treated cells. HBG-treated cells were set to 100 %. Data are presented as mean value (± SD) out of triplicates. Transfections were performed by Dian-Jang Lee (PhD study, Pharmaceutical Biotechnology, LMU).

Nevertheless, not all cell lines profit from the bioreducible character of oligomers. Testing the structures on KB/eGFPLuc cells (derived from the cervical cancer cell line HeLa) revealed that the bioreducible character can even have a negative influence on gene silencing. In contrast to the stable structures that mediate gene silencing, the efficiency for all bioreducible structures was strongly decreased (**Fig. 43**). One explanation for this finding is disulfide cleavage occurring at the extracellular cell surface. High extracellular disulfide cleavage was actually previously reported for HeLa cells [108].

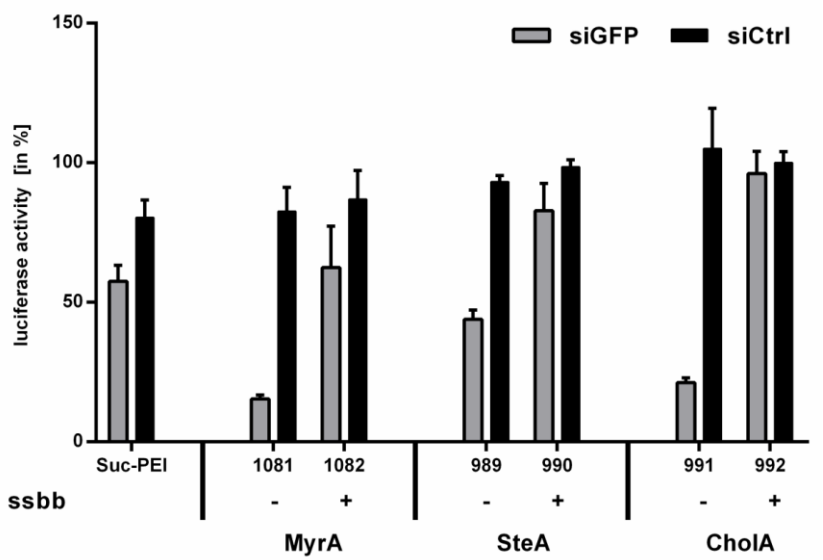

Fig. 43 Gene silencing of T-shape oligomers in KB cells**.** Lipopolyplexes with 500 ng/37 pmol eGFP-targeted siRNA (siGFP) per well respectively control siRNA (siCtrl) at N/P 12 were tested for eGFPLuc gene silencing in KB-eGFPLuc cells. Lipopolyplexes made of stable structures ***1081***, ***989*** and ***991*** (- ssbb) and lipopolyplexes made of bioreducible structures ***1082***, ***990*** and ***992*** (+ ssbb) were tested. The luciferase activity of siRNA-treated cells is presented related to buffer-treated cells. HBG-treated cells were set to 100 %. Data are presented as mean value (± SD) out of triplicates. Transfections were performed by Dr. Dian-Jang Lee (Pharmaceutical Biotechnology, LMU).

When focusing on the comparison of the three different fatty acids, SteA and CholA lipo-oligomers (no or only moderate silencing for the stable versions) strongly benefited from the incorporation of the ssbb with regard to gene silencing in Neuro2A and DU145 cell lines. In contrast, the stable MyrA lipo-oligomer displayed gene silencing activity combined with significant cytotoxicity (**Fig. 38A**); here the reducible ssbb unit eliminated the cytotoxicity without reducing the gene silencing activity (**Fig. 38B**). The findings for non-reducible lipo-oligomers are consistent with our earlier observations [82], where SteA derivatives showed poor gene silencing activity and MyrA derivatives exhibited not only gene silencing activity but cytotoxicity. For non-reducible structures, the unsaturated C18 fatty acids oleic acid and linoleic acid were the optimum lipid units with regard to transfection efficacy and cell tolerability [82, 83, 119]. Still, due to the higher stability during synthesis and storage, in the current work saturated fatty acids were the preferred option for integration into solid phase synthesized lipo-oligomers.

Nevertheless, incorporation of the bioreducible linker into oleic acid containing oligomers was also found to further enhance transfection efficacy and cell tolerability (**Fig. 44**).

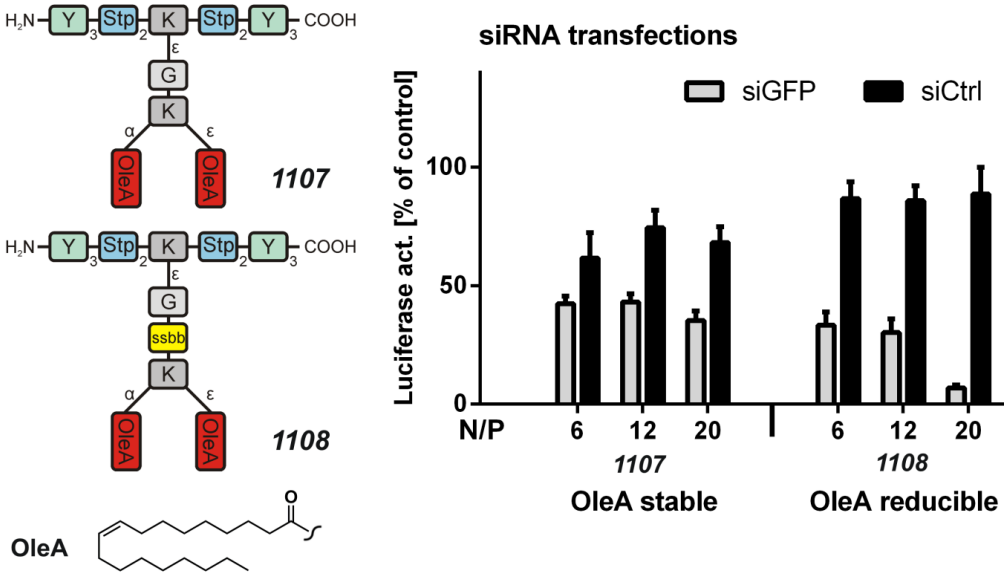

Fig. 44 Gene silencing of oleic acid containing T-shape oligomers in neuroblastoma cells. Lipopolyplexes with 500 ng / 37 pmol eGFP-targeted siRNA (siGFP) / well respectively control siRNA (siCtrl) at N/P 6, 12 and 20 were tested for eGFPLuc gene silencing in Neuro2A/eGFPLuc cells. The luciferase activity of siRNA-treated cells is presented related to buffer-treated cells. HBG-treated cells were set to 100 %. Data are presented as mean value (± SD) out of triplicates**.** Transfections were performed by Dian-Jang Lee (PhD study, Pharmaceutical Biotechnology, LMU).

The different fatty acids may influence the extent of hydrophobic stabilization of siRNA polyplexes, but do also strongly affect the lytic properties of the lipo-oligomers, both in the stable and reducible setting. At endosomal pH, the cationic parts receive increased cationization, which in combination with the hydrophobic domain facilitates endosomal membrane destabilization and escape into the cytosol. An erythrocyte leakage assay compared the different fatty acid versions of stable (**Fig. 45A**) and the ssbb containing reducible (**Fig. 45B**) lipo-oligomers. MyrA structures displayed a far higher leakage activity (highest at pH 5.5) than the SteA structures, whereas oligomers with the bulky CholA did not display lytic effects.

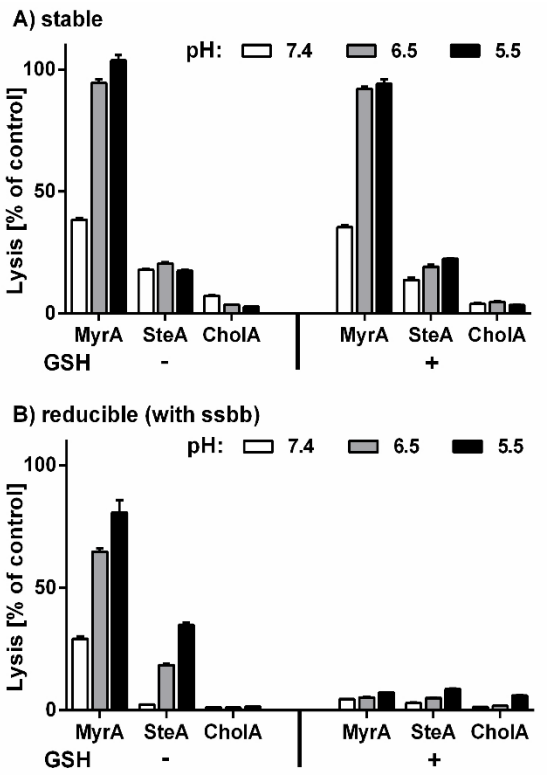

Fig. 45 Erythrocyte leakage of oligomers at different pH and under reducing conditions. A) Stable lipo-oligomers ***1081***, ***989*** and ***991***. B) bioreducible lipo-oligomers ***1082***, ***990*** and ***992***. The final concentration of oligomers was 7.5 µM. GSH treated lipo-oligomers were incubated with 10 mM GSH in PBS adjusted to pH 7.4 at 37 °C for 90 min (right-hand side). PBS-treated erythrocytes were set to 0 %. Triton X served as positive control and was set to 100 %. Data are presented as mean value (± SD) out of quadruplicates. Erythrocyte leakage assay performed by Sören Reinhard (PhD study, Pharmaceutical Biotechnology, LMU).

This finding is in agreement with literature, showing that cationic dimyristyl lipids strongly promote membrane fusion events. Deviations of hydrophobic volume and hydrophilic-lipophilic ratio from an optimum hampered membrane interactions [136]. Treatment with GSH did not affect the stable analogs but extinguished the lytic activity of the reducible lipo-oligomers, consistent with their lower cytotoxicity. This observation can be attributed to the integration of the ssbb as a linker between the cationic and the lipophilic part, as reductive cleavage results in an uncharged fatty acid structure and an oligocationic part with significantly reduced amphiphilic character. Both compounds alone were not able to lyse membranes anymore.

3.3 Functionalized poly(sarcosine) as shielding agent for lipopolyplexes

In this chapter, optimized redox-sensitive lipo-oligomers (presented in 3.2) were extended by azido functionalities to serve as reactants for click chemistry. After formation of siRNA lipopolyplexes, the azido groups were used to covalently modify the nanoparticle surface with DBCO-modified poly(sarcosine) (PSar). Polymerized sarcosine (N-methylglycine) is hydrophilic and biodegradable. These PSar-modified lipopolyplexes were tested for shielding properties in terms of reduction of zeta potential and cellular uptake. Folic acid functionalized PSar agents were tested for their *in vitro* targeting ability. *In vivo* bioimaging studies were performed in mice to assess the distribution of intravenously injected siRNA lipopolyplexes with 8 kDa poly(sarcosine) or 5 kDa poly(ethylene glycol) shields.

3.3.1 Design and synthesis of a lipo-oligomer for click chemistry

In previous work, we have established a new class of redox-sensitive lipo-oligomers prepared by solid-phase supported synthesis (SPSS) to serve as carriers for siRNA delivery [137]. The T-shape structure ***992*** introduced in this work, was chosen as starting point for further modifications because it forms stable siRNA polyplexes with sizes below 200 nm hydrodynamic diameter that have high transfection efficiency. This structure combines natural amino acids and artificial building blocks (**Fig. 46** - top). It consists of four repeats of the cationic polyamino acid succinoyl-tetraethylene-pentamine (Stp) used for complexation of nucleic acid and for endosomal buffering. Two tyrosine trimer units flanking the cationic domain stabilize the polyplex due to their hydrophobicity and π–π stacking ability. In the center of the cationic Stp units two hydrophobic cholanic acids branch off the cationic backbone (T-shape) for lipopolyplex stabilization. The lipid and cationic domains are connected via a bioreducible linking unit (ssbb) [137]. In the new approach, the structure was extended by azidolysines placed at the N- and/or C-terminal end of the backbone (structures ***1073*** and ***1076,*** **Fig. 46** - top). This enables the structure to be subsequently further conjugated with an alkyne via click chemistry. Strain promoted copper-free click reaction of a cyclooctyne derivate, instead of a standard alkyne, with an azide [138-140] has several advantages towards other reactions. No catalyst is needed, no side reactions with

other functional domains of the oligomer can occur, and no toxic by-products are generated.

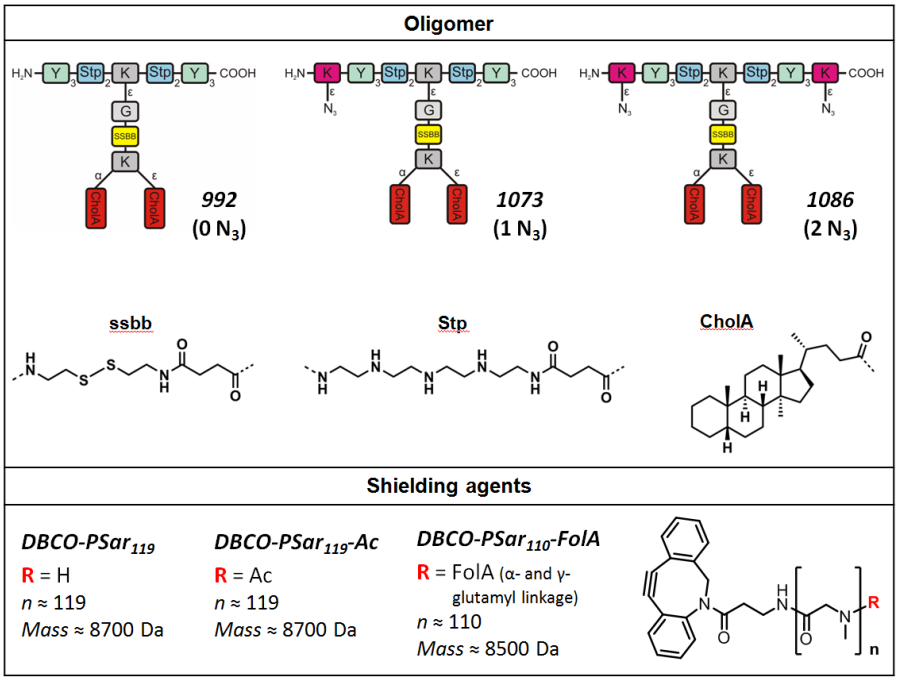

Fig. 46 Overview of chemical compounds. Top: schematic illustration of sequence-defined oligomers with T-shape topology; ***992***, ***1073*** and ***1086*** with no, one or two terminal azidolysines K(N3). Other units of the oligomers: Y: tyrosine, K: lysine, G: glycine, Stp: succinoyl-tetraethylene-pentamine, ssbb: succinoyl-cystamine, CholA: 5β-Cholanic acid. The broken lines represent amide linkages. IDs are unique database identification numbers. Bottom: structure of the shielding agents ***DBCO-PSar$_{119}$*** (abbr.: PSar), ***DBCO-PSar$_{119}$-Ac*** (abbr.: PSarAc) and ***DBCO-PSar$_{110}$-FolA*** (abbr.: PSarFolA). All pSar shielding agents were synthesized by Kristina Klinker (PhD study, Institute of Organic Chemistry, JGU Mainz) under supervision of PD Dr. Matthias Barz.

3.3.2 DBCO-modified poly(sarcosine) as a click shielding agent

Polymerized sarcosine (N-methylglycine) is a hydrophilic, nonionic peptidic structure, which is a weak hydrogen bond acceptor. These properties provide a high resistance against protein adsorption [141] and make it an ideal material for shielding electrostatic complexes [142]. Importantly, it has been reported that poly(sarcosine) has a low immunogenicity in various animal models [143, 144]. Poly(sarcosine) can be functionalized at its N- and C-terminal end. It is obtained by ring opening polymerization of α-amino acid N-carboxyanhydrides (NCA) with a low degree of polydispersity [145]. Initiating the reaction with a dibenzocyclooctyne-amine (DBCO-amine) leads to a C-terminal DBCO tail group. A DBCO function can efficiently react with azide-modified

structures in aqueous solutions. Mixing azido modified cationic oligomers with siRNA leads to spontaneous assembly of polyplexes. Due to oligomer excess, several azido functions remain free in solution. Others are located in the core of the nanoparticle or on its surface. Azido functions on the surface of siRNA polyplexes serve as anchors for functionalization with DBCO-modified poly(sarcosine). The N-terminal free amine can further be modified with a nonionic acetyl residue or a targeting ligand like folic acid. All shielding agents are presented in **Fig. 46** on the bottom. The syntheses and analyses of those agents were performed by Kristina Klinker within her PhD study at the laboratory of PD Dr.Matthias Barz, Institute of Organic Chemistry, University of Mainz, Germany.

3.3.3 Biophysical evaluation of poly(sarcosine) shielded lipopolyplexes

The structures (***1073*** and ***1086***) were incubated with siRNA for 40 min with a final concentration of 25 ng siRNA/µL to form polyplexes. The electrophoretic mobility of incorporated siRNA was measured with an agarose gel shift assay to test the new oligomers' ability to bind nucleic acid. Different N/P values depict the ratio of protonatable amines (N) of the oligomers to phosphates (P) of the siRNA. Like its analog ***992*** (**Fig. 33** [137]), the oligomers showed complete retention of siRNA in the pockets of the gel at an N/P ratio of 12 (**Fig. 47**). No changes in binding ability were observed for the incorporation of one or two azidolysines.

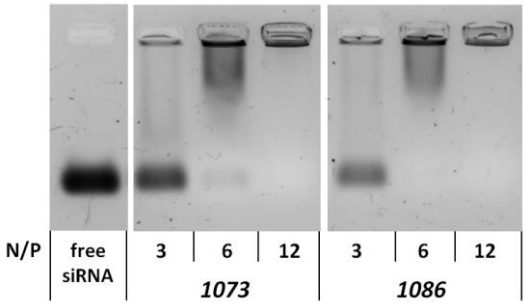

Fig. 47 siRNA binding ability of T-shape structures analyzed with an agarose gel shift assay. The left lane shows the running distance of free siRNA in HBG that is not complexed by lipo-oligomers. Polyplexes were tested for siRNA binding ability at different N/P ratios. 2.5 % agarose gel, 100V, 40 min runtime.

Next, we wanted to evaluate the influence of the DBCO poly(sarcosine) (PSar) shielding agent on electrophoretic mobility of the polyplex. For all formulations modified with PSar, an N/P ratio of 12 was used to ensure complete complexation of siRNA (**Fig. 48**). First, polyplexes formed with the structures differing in the amount of azido functions (N_3 = 0, 1, 2) were incubated with a fixed amount of PSar (**Fig. 48**) for 16 h. The siRNA concentration of the functionalized formulations was 20 ng / µL. The azido-bearing polyplexes migrated in the gel towards the cathode, whereas the polyplex without azido function remained in the pocket. This showed that a covalent bond connecting the shielding agent to the nanoparticle was required to mediate this effect. The migration of the integrated siRNA against its own negative charge demonstrated that it was not accessible to the electric field inside a polyplex covered with shielding agent. When increasing the equivalents of PSar, stronger migration could be observed indicating that this effect can be related to the degree of surface modification of the polyplex (**Fig. 48B**). For the oligomer with one azido function (***1073***), maximum migration was achieved with equimolar amounts of DBCO click agent (1 eq / oligomer). More PSar (2 eq), did not increase the effect. ***1086*** siRNA polyplexes with two azido functions within the carrier also showed the maximum migration for equimolar ratios of azide to DBCO (2 eq PSar).

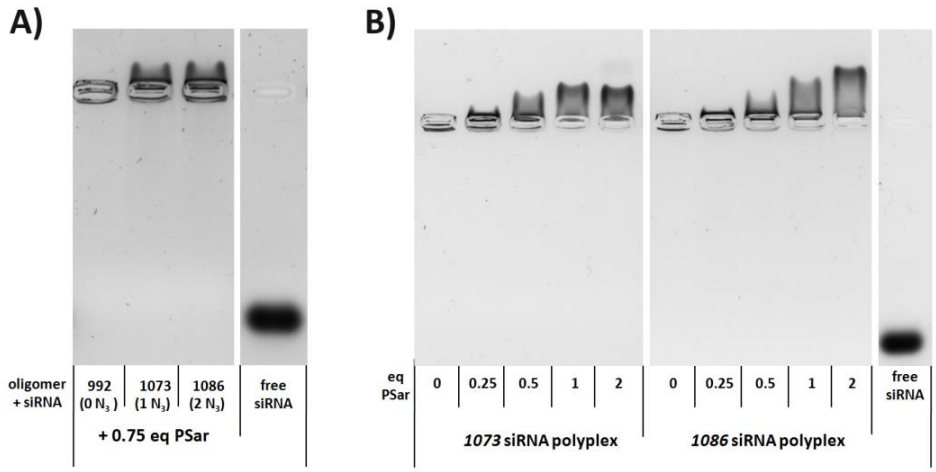

Fig. 48 Electrophoretic mobility of siRNA polyplex formulations analyzed with an agarose gel shift assay A) siRNA polyplexes formed with oligomers bearing no (***992***), one (***1073***) and 2 (***1086***) azide functions incubated with 0.75 equivalents of ***DBCO-PSar$_{119}$*** (PSar) 1 % agarose gel, 70 V, 80 min runtime. B) Formulations with increasing equivalents (eq mol/mol) of ***DBCO-PSar$_{119}$*** (PSar). 0.75 % agarose gel, 100V, 80 min runtime. All polyplexes were incubated for 40 min at N/P 12, followed by PSar addition for 16 h at room temperature. The right lane shows the running distance of free siRNA in HBG that is not complexed by lipo-oligomers.

The degree of surface modification and shielding of a nanoparticle can also be evaluated by determining its zeta potential by measuring its mobility under electric field with light scattering. Hereby, we showed that the positive zeta potential of an unshielded particle could be strongly reduced with poly(sarcosine) (**Table 14**). By using 0.5 eq PSar / oligomer, the zeta potential can already be reduced by 50 %. Due to the N-terminal cationic head group, the zeta potential always remains slightly positive.

Table 14 Particle size (z-average) and zeta potential of poly(sarcosine) siRNA formulations determined with the DLS zetasizer.

siRNA formulation	eq PSar	N/P	z-average [nm]	Mean PDI	Mean Zeta Potential [mV]
1073	0	12	81.0 ± 5.0	0.26 ± 0.02	20.9 ± 0.9
	0.5	12	86.7 ± 2.8	0.24 ± 0.02	9.4 ± 0.5
	1	12	91.8 ± 2.9	0.26 ± 0.02	8.5 ± 0.6
	2	12	96.8 ± 4.0	0.27 ± 0.02	6.0 ± 1.1
1086	0	12	90.6 ± 0.9	0.15 ± 0.03	17.2 ± 0.8
	0.5	12	98.7 ± 1.3	0.15 ± 0.01	7.7 ± 0.6
	1	12	102.3 ± 2.1	0.19 ± 0.01	6.3 ± 1.0
	2	12	105.1 ± 1.9	0.17 ± 0.01	2.5 ± 0.3

The hydrodynamic diameters of the polyplexes, determined by dynamic light scattering (DLS), are in the area of 100 nm. With increasing amounts of PSar, the nanoparticle size increases by up to 16 nm in diameter. A layer of PSar covering the particle surface seems to be the most plausible explanation for the increase in size.

3.3.4 Evaluation of poly(sarcosine) shielding agents *in vitro*

A reduced interaction of nanoparticles with cell membranes is an important indication of shielding. Therefore, we performed uptake studies with the poly(sarcosine) shielded polyplexes. Polyplex formulations were prepared with Cy5-labled siRNA for this assay. We incubated Neuroblastoma Neuro2A cells with the formulations for 4 h at standard culture conditions and analyzed them by flow cytometry. The signal intensity of cells labeled with fluorescent dye correlates with the amount of polyplexes being internalized (**Fig. 49** and **Table 15**). Unshielded material and material shielded with low equivalents of PSar showed significant uptake into cells after 4 h incubation time for both polyplex formulations prepared with one and two azido bearing backbones (***1073*** and ***1086***).

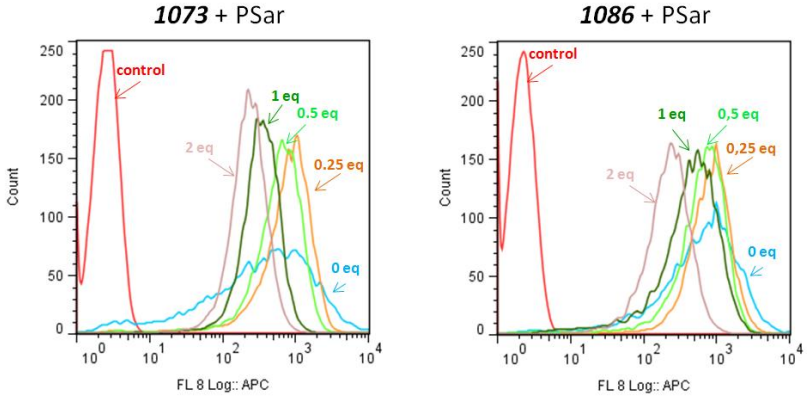

Fig. 49 Cellular internalization of siRNA formulations (left: ***1073***; right: ***1086***) shielded with increasing equivalents (eq mol/mol) of ***DBCO-PSar$_{119}$*** (PSar) determined by flow cytometry. All polyplexes were incubated for 40 min at N/P 12 with siRNA (20 % Cy5-labeled), followed by PSar for 16 h at room temperature. Cells were incubated with the formulations for 4 h at 37°C and washed with PBS buffer and heparin solution. The intensity of the Cy5 signal indicates the amount of polyplexes being internalized by Neuro2A-eGFP-Luc cells. Control: HBG buffer treated cells. Experiments were performed by Dr. Wei Zhang (Pharmaceutical Biotechnology, LMU).

For ***1073*** formulations a significant reduction in fluorescence intensity was observed for 1 eq of PSar per oligomer, whereas 2 eq of PSar were needed for ***1086*** formulations to reach similar levels (**Table 15**). The increase of azido functions in the ***1086*** backbone did not mediate a better surface modification of the polyplexes. Apart from that, more PSar is required to achieve the same shielding effect.

Table 15 Mean fluorescence intensity (MFI) data for cellular internalization of Cy5-labeled siRNA formulations (left: ***1073***; right: ***1086***) shielded with increasing equivalents (eq mol/mol) of ***DBCO-PSar$_{119}$*** (PSar) determined by flow cytometry. Performed by Dr. Wei Zhang (Pharmaceutical Biotechnology, LMU).

siRNA formulation	eq PSar	MFI	siRNA formulation	eq PSar	MFI
1073	0	780.5 ± 2.5	***1086***	0	883.0 ± 86.0
	0.25	881.5 ± 25.5		0.25	870.5 ± 62.5
	0.5	715.0 ± 24.0		0.5	785.5 ± 38.5
	1	359.0 ± 14.0		1	602.5 ± 37.5
	2	245.5 ± 8.0		2	263.5 ± 4.5

This is most probably because more azides are free in solution scavenging the DBCO click agents.

Next, the cells were incubated with ***1073*** formulations in a similar way and confocal laser scanning microscopy was performed. Again, the Cy5-labeled siRNA (red) represents the polyplexes internalized into the cells (**Fig. 50**). Compared to the unshielded material, which was avidly taken up by cells, 0.5 eq of PSar showed a reduction in cellular internalization. For 1 eq of PSar, only a few polyplexes were taken up by cells, indicating a strong shielding ability. This experiment confirmed the observations made in the previously described flow cytometry studies.

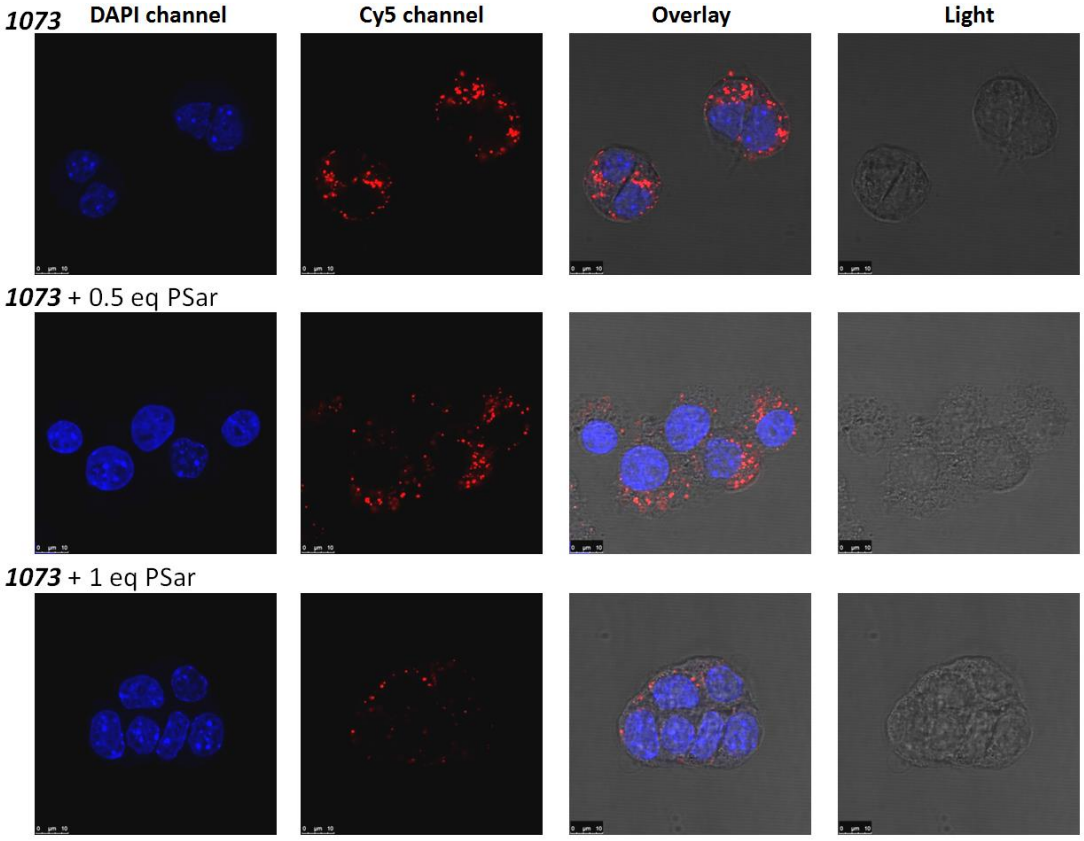

Fig. 50 Intracellular distribution of siRNA formulations in Neuro2A-eGFP-Luc cells with increasing equivalents (eq mol/mol) of ***DBCO-PSar$_{119}$*** (PSar) acquired by confocal laser scanning microscopy. Cells were incubated with the formulations for 4 h and washed with PBS buffer. Nuclei were stained with DAPI (blue) and siRNA was spiked with 20 % Cy5-labeled siRNA (red). The overlay image shows the merged channels and the light microscope image. Transfections were performed by Dr. Wei Zhang (Pharmaceutical Biotechnology, LMU), confocal microscopy was performed by Miriam Höhn (Pharmaceutical Biotechnology, LMU).

3.3.5 Distribution of poly(sarcosine) functionalized polyplexes *in vivo*

The evaluation of poly(sarcosine) functionalized polyplexes in biophysical and *in vitro* assays highlights their shielding ability. For *in vivo* distribution, a siRNA polyplex

formulation prepared with ***DBCO-PEG5k*** (abbr. PEG), with acetylated poly(sarcosine) (***DBCO-PSar$_{119}$-Ac***; abbr. PSarAc, **Fig. 46**, bottom) and an unshielded siRNA polyplex were compared. In terms of surface charge, the uncharged terminal head group of PsarAc is more similar to the commercial PEG agent, which has a terminal methoxy head group (for detailed biophysical analytics see chapter 3.3.6). ***1073*** siRNA polyplexes were prepared with 50 % Cy7-labeled siRNA and incubated with 1 eq of the respective shielding agent per oligomer for 4 h. A concentration of 200 ng siRNA / µL was used for this experiment. 50 µg of siRNA and oligomers at an N/P ratio of 10 were used.

The formulations were injected into Neuro2A tumor-bearing mice via *i. v.* tail-vain injection and the distribution of the NIR (near infrared) fluorescent dye was monitored at various time points for one day by bioimaging in living mice (**Fig. 51**). The unshielded polyplex started accumulating in the liver after 15 min. Such finding was also observed for other unmodified T-shape backbone structures in previous work [119, 146]. In contrast to the unshielded lipopolyplexes, both shielded formulations showed a much-expanded *in vivo* distribution. At 60 minutes after injection of the material, the shielded formulations were still detectable in all areas of the body including the tumor site. A strong signal was detected in the exposed periphery, such as the paws of mice injected with shielded polyplexes after more than 4 hours. In comparison, formulations with the 8 kDa poly(sarcosine) and the 5 kDa poly(ethylene glycol) displayed only minor differences. The PSarAc formulation showed a slightly better distribution in ears, flanks and abdomen. After 4 h the intensity of the signals decreased. The strongest signals remained in liver and bladder. An enhanced permeability and retention (EPR) effect at the tumor site was not observed. This effect was reported for nanoparticles that circulate for a prolonged period and thereby have a higher probability to extravasate through leaky vasculature at the tumor site [147]. Since the size of particles was in a suitable range for the EPR effect, the short half-life of shielded polyplexes, as well as the lack of active targeting ligands, might be the limiting factors.

Summing up, poly(sarcosine) represents a suitable shielding agent and an at least adequate alternative for PEG that extends the circulation of lipopolyplexes in mice and reduces unspecific cellular interactions.

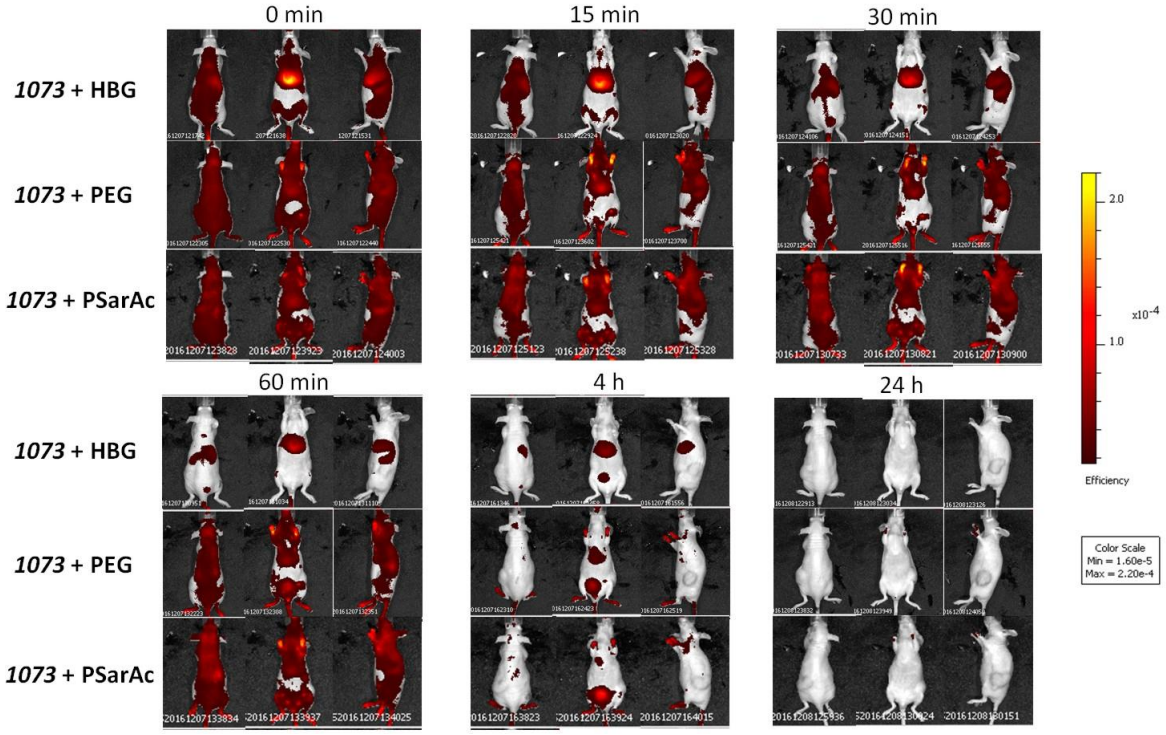

Fig. 51 Biodistribution of ***1073*** formulations at N/P 10 in NMRI-nude mice bearing Neuro2A tumors via *i.v.* administration. Biodistribution determined by NIR fluorescence bioimaging of 50 µg siRNA (50 % Cy7-labeled) with ***1073*** with 1 eq ***DBCO-PEG5k*** (PEG), 1 eq acetylated ***DBCO-PSar$_{119}$Ac*** (PSarAc) or hepes buffered glucose (HBG). Experiments were performed with two animals per group for time points until 60 min and one animal per group for later time points; a representative animal of each group is shown. Animals are presented in the dorsal, ventral and lateral view. Experiment was performed by Sarah Kern and Eva Kessel (veterinary MD studies, Pharmaceutical Biotechnology, LMU).

3.3.6 Functionalization of the poly(sarcosine) head group with folic acid for receptor targeting

A shielding agent should prevent unspecific interaction with proteins and biological surfaces such as cell membranes. This inhibition of unspecific cell binding is an important requirement for specific cell targeting. A targeting ligand needs to be attached to its surface to enable the nanoparticle to only target specific receptors on cell membranes. PSar offers the possibility to be further functionalized at its free secondary amino function. The targeting ligand folic acid (FolA) was chosen to be conjugated to the N-terminal amino head group of ***DBCO-PSar$_{110}$*** (Kristina Klinker /Dr.Matthias Barz, University of Mainz). The conjugation was performed with folic acid and HBTU/HOBt/DIPEA in DMSO and the product was purified via size exclusion

chromatography. This reaction results in α- and γ-glutamyl conjugated agents (***DBCO-PSar$_{110}$-FolA*** (abbr. PSarFolA), **Fig. 46**, bottom). As a negative control, PSar acetylated with acetic anhydride and TEA in DMF (***DBCO-PSar$_{119}$-Ac*** (abbr. PSarAc), **Fig. 46**, bottom) was used. Beside the untargeted shielding agents PSar and PSarAc, the commercially available ***DBCO-PEG5k*** (abbr. PEG) was included for evaluation. The PEG standard we chose has a DBCO tail group, a chain of ~5 kDa of poly(ethylene glycol) and a methoxy head group.

For further experiments, the formulations were prepared at the same conditions used for the *in vivo* experiment in the last chapter (200 ng siRNA per µL in the final formulation, N/P 10). The electrophoretic mobility of incorporate siRNA was measured with an agarose gel assay. All formulations form stable polyplexes at increased *in vivo* concentrations at N/P 10. siRNA lipopolyplexes shielded with ***DBCO-PEG5k*** showed migration in the gel towards the cathode similar to PSar shielded formulations. The acetyl-PSar control formulation (PSarAc) revealed a shorter migration distance than its uncapped analog with a positively charged head group (**Fig. 52**).

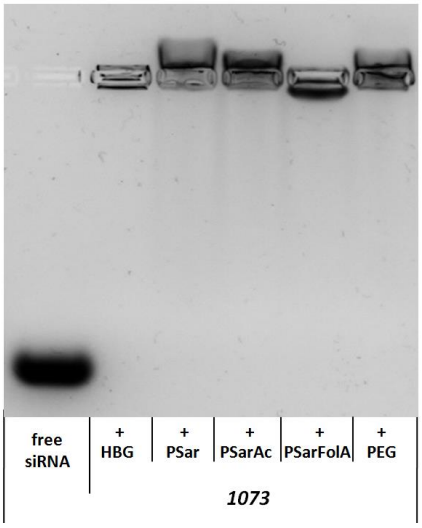

Fig. 52 Electrophoretic mobility of formulations with 1 eq ***DBCO-PSar$_{119}$*** (PSar), 1 eq ***DBCO-PSar$_{119}$-Ac*** (PSarAc), 1 eq ***DBCO-PSar$_{110}$-FolA*** (PSarFolA), 1 eq ***DBCO-PEG5k*** (PEG) or hepes buffered glucose (HBG) analyzed with an agarose gel shift assay. All polyplexes were incubated at *in vivo* concentrations (200µg/µl) at N/P 10 for 40 min, followed by HBG, PEG or PSar incubation for 4 h at room temperature. The solutions were diluted 1 : 8 with HBG and loaded onto the gel. The left lane shows the running distance of free siRNA in HBG that is not complexed by lipo-oligomers. 1 % agarose gel, 70 V, 80 min runtime.

In contrast to the other formulations, the siRNA within the targeted PSarFolA polyplex migrated in the gel towards the anode. This can be explained by the negatively charged folic acid head group of the PSarFolA shielding agent.

Due to acetylation of the N-terminal PSar head group (**Table 16**), the zeta potential of formulations reduced from ~10 mV to ~0 mV. This reduction in surface charge is most probably responsible for the weaker migration in the gel. For the PEG shielded formulation, a low zeta potential of ~4 mV was measured. Compared to lower concentrations used in the first section, the incubation at high *in vivo* concentrations led to much higher zeta potential of the unshielded material (~33 mV). The zeta potential of the targeted PSarFolA formulation was reduced with increasing equivalents. For one equivalent, a neutral surface charge of ~1 mV was measured.

Table 16 Particle size (z-average) and zeta potential of siRNA formulations determined with a DLS zetasizer. Formulations were prepared at 200 ng siRNA/µL concentration with ***DBCO-PSar$_{119}$*** (PSar), acetylated ***DBCO-PSar$_{119}$Ac*** (PSarAc), ***DBCO-PEG5k*** (PEG), targeted ***DBCO-PSar$_{110}$FolA*** (PSarFolA), or hepes buffered glucose (HBG) and diluted 1 : 8 with HGB before size measurements

***1073* siRNA formulation**	**N/P**	**z-average [nm]**	**Mean PDI**	**Mean Zeta Potentianl [mV]**
+ HBG buffer	10	161.2 ± 5.3	0.15 ± 0.01	33.3 ± 0.3
+ 1 eq Psar	10	173.8 ± 1.1	0.13 ± 0.02	9.9 ± 0.2
+ 1 eq PSarAc	10	188.6 ± 3.8	0.17 ± 0.01	0.1 ± 0.5
+ 1 eq PEG	10	169.9 ± 1.4	0.15 ± 0.01	3.9 ± 0.2
+ 0.25 eq PSarFolA	10	171.2 ± 3.9	0.22 ± 0.01	7.7 ± 0.3
+ 0.5 eq PSarFolA	10	1013.8 ± 195.1	0.79 ± 0.09	5.8 ± 0.2
+ 0.75 eq PSarFolA	10	4092.3 ± 384.4	0.66 ± 0.30	3.4 ± 0.1
+ 1 eq PSarFolA	10	25.4 ± 0.7	0.20 ± 0.01	1.5 ± 0.4

The sizes of all untargeted formulations are in the same range (~160 – 190 nm) and increased by ~70 % due to increasing concentrations to 200 ng siRNA/µL (**Table 16**). For the targeted PSarFolA formulation apparently, a rearrangement of polyplexes with increasing equivalents was observed, affecting their sizes measured by DLS. With 0.25 eq of folic acid agent, the particles keep their original size. For increasing equivalents, aggregates were measured (high polydispersity). Similar findings were observed for PEG-shielded folic acid targeted lipo-polyplexes before [148] Surprisingly, with one equivalent of PSarFolA, nanoparticles became very small with a hydrodynamic diameter of ~25 nm and a small polydispersity was small again. This can only be

explained with PSarFolA induced instability following a complete rearrangement of particles into a uniform nano-sized population.

The KB/eGFPLuc cell line was used for evaluating the folic acid receptor binding ability of formulations. This human cervix carcinoma cell line overexpresses the folic acid receptor and can therefore be targeted using the vitamin folic acid. KB cells were incubated with ***1073*** formulations spiked with 20 % Cy5-labled siRNA for 30 min on ice. The short incubation on ice prevented the active uptake of the polyplexes into the cells. After washing the cells with PBS, cells were analyzed by flow cytometry. The fluorescent dye intensity signal is assumed to correlate with the amount of polyplexes bound to the cell membrane (**Fig. 53A**). For the formulations further modified with acetylated PSar (PSarAc), only a very weak binding was found. The PSar functionalized with folic acid (PSarFolA) showed a high binding to KB cells. Unshielded ***1073*** polyplexes were also able to bind to the membranes. This can be explained by the high positive charge of the particles.

To further evaluate the binding specificity of PSarFolA formulations, the cellular folate receptors were blocked by using 1 mM free folate in the cell culture medium. Hereby, the binding of the folate-targeted formulations could be inhibited, indicating that the binding is receptor mediated. For receptor-mediated endocytosis, binding of a ligand is one requirement but not necessarily sufficient. Cells were incubated with the formulations for 45 min at 37 °C and washed with PBS and heparin to analyze if cellular internalization works with the folate-targeted polyplexes. The negatively charged heparin dissociates material from the cell membranes. Afterwards, cells were analyzed by flow cytometry and Cy5 intensity was quantified (**Fig. 53B**). In contrast to the strong binding of folic acid targeted nanoparticles (PSarFolA), the receptor-mediated uptake was found as very weak (MFI = 93.4 ± 3.1). It is even weaker than the acetylated PSarAc (MFI = 157.0 ± 13.1).

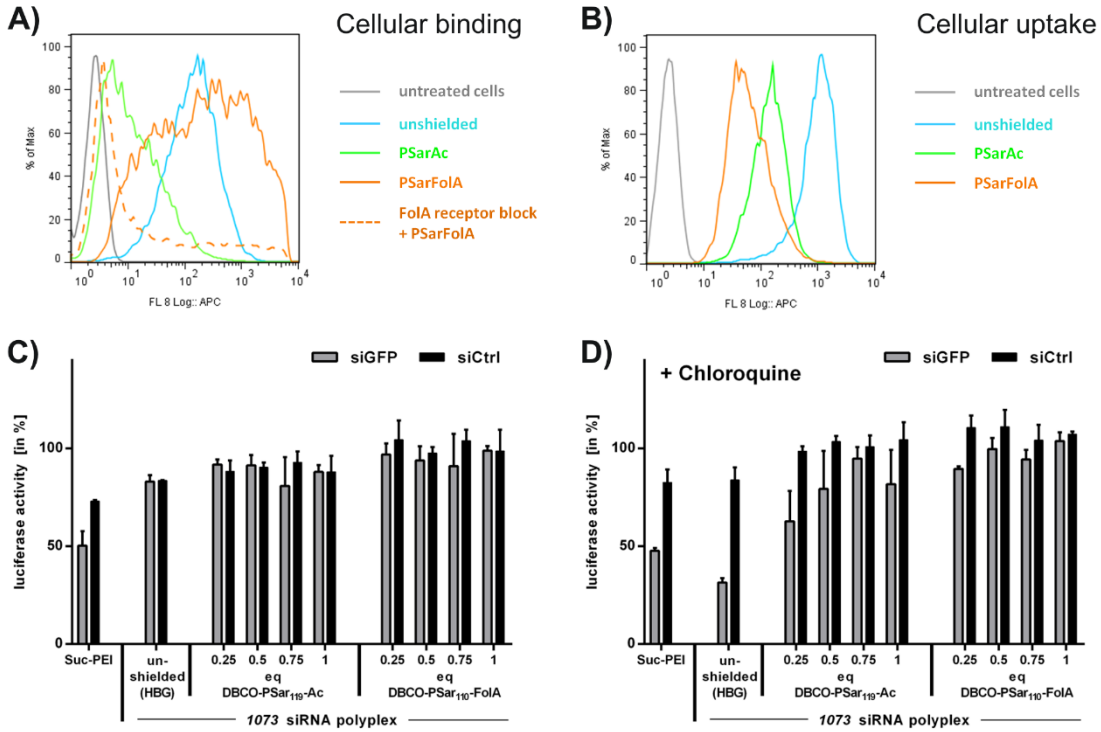

Fig. 53 A) Cellular binding of Cy5-labled (20 %) unshielded siRNA formulations with HBG buffer instead of agent or shielded with 1 eq (mol/mol) of ***DBCO-PSar$_{119}$-Ac*** (PSarAc), ***DBCO-PSar$_{110}$-FolA*** (PSarFolA) determined by flow cytometry. KB cells were incubated with the formulations for 30 min on ice and washed with PBS buffer. For the FolA receptor block cell culture medium with 1 mM free folate was used. B) Cellular internalization of Cy5-labled (20 %) unshielded siRNA formulations or shielded with 1 eq (mol/mol) of ***DBCO-PSar$_{119}$-Ac*** (PSarAc), ***DBCO-PSar$_{110}$-FolA*** (PSarFolA) determined by flow cytometry. KB cells were incubated with the formulations for 45 min and washed with PBS buffer and heparin solution. C) Lipopolyplex formulations with eGFP-targeted siRNA (siGFP) or control siRNA (siCtrl) were tested for eGFPLuc gene silencing in KB-eGFPLuc cells. Formulations with ***1073*** siRNA polyplex modified with increasing equivalents (eq mol/mol) of ***DBCO-PSar$_{119}$-Ac***, ***DBCO-PSar$_{110}$-FolA*** or unshielded ***1073*** siRNA polyplex (addition of HBG buffer instead of agent). Cells were incubated with formulations for 45 min and washed; the luciferase readout was after 48 h. D) Experiment performed like in C), but after incubation of the cells with formulations for 45 min, chloroquine was added and cells were washed after 4 h, the luciferase readout was after 48 h. The luciferase activity of siRNA-treated cells is presented related to HBG-treated cells. Data are presented as mean value (±SD) out of triplicates. All polyplexes were incubated for 40 min at N/P 10 with siRNA, followed by shielding agent for 4 h at room temperature. Formulations were prepared at a concentration of 200 ng siRNA/µL and diluted 1 : 8 with cell culture medium before incubation with the cells. Experiments were performed by Dr. Wei Zhang (Pharmaceutical Biotechnology, LMU).

This finding shows that binding does not always lead to internalization. The vitamin folate that usually binds the folic acid receptor is a small molecule with less than 500 Da

weight. It is likely that the mechanism for the uptake of much bigger nanoparticles is different. It has often been reported that folic acid targeted cationic delivery systems can get internalized into cells [87, 148, 149]. The trafficking of folate via the folate receptors is thought to occur by independent of clathrin or caveolae (CLIC/GEEC endocytosis pathway) [150, 151]. For folate-targeted nanoparticles uptake pathways like caveolae- and clathrin-mediated endocytosis were found [152-154]. The size of the nanoparticle and the ligand density on their surface were reported to influence the cellular uptake pathway. The reasons for ~8 kDa poly(sarcosine) to prevent the internalization despite the presence of a folate ligand are not yet understood. Unshielded ***1073*** siRNA polyplexes again showed considerable uptake (MFI = 1041.7 ± 104.4). The cationic surface charge of the unshielded material can interact with cell membranes and promotes internalization.

Finally, the siRNA delivery efficiency of formulations was tested by performing gene silencing experiments in KB/eGFPLuc cells stably expressing an eGFP-Luciferase fusion protein (**Fig. 53C + D**). As in several related experiments [148], incubation of cells with siRNA lipopolyplexes was restricted to a short period of only 45 min before removal of the nanoparticles, to emphasize receptor-mediated uptake processes. After further incubation for 48 hours, silencing of the eGFP-Luciferase fusion protein mediated by siRNA against eGFP (siGFP - gray bars) was quantified by a luciferase assay. After this 45 min short-time contact, neither the unshielded negative control nor the formulations modified with the negative control shield PSarAc and the targeted PSarFolA mediated gene silencing in KB cells (**Fig. 53C**). This finding can be explained by insufficient cellular uptake of the formulations. The unshielded siRNA lipopolyplexes showed no silencing activity despite notable uptake. The same finding was previously made for ***454*** siRNA nanoparticles which trigger efficient gene silencing only upon 48 h long-term incubation with cells [148]. For endosomal escape [62, 72, 120], a critical minimum amount of pH sensitive carriers needs to be internalized into endosomes to mediate the rupture of endosomal membranes. This threshold apparently was not reached with the 45 min incubations. In cell culture, however, this limitation of endosomal escape can be overcome by coincubation with the lysosomotropic agent chloroquine (**Fig. 53D**) [122-125]. Therefore, we transfected cells with the formulations again and added chloroquine after 45 min for 4 h. (**Fig. 53D**). For unshielded ***1073*** formulations, this treatment led to gene silencing, demonstrated by a ~60 % reduction

of luciferase activity. Weakly shielded formulations (0.25 – 0.5 eq) showed some minor gene silencing efficiency, particles shielded with high equivalents did not mediate any silencing. Well shielded delivery systems are known to have reduced endosomal escape ability [92, 151-154]. Based on the luciferase levels of the analogous siCtrl polyplexes, we can exclude that the tested formulations mediate unspecific cell toxicity. In summary, ***1073*** siRNA nanoparticles functionalized with poly(sarcosine) and folic acid ligands attached to the surface of cells, but cannot be found to be internalized by KB cells. The transfection efficiency is limited because of a lack of internalization and endosomal escape. It also has to be kept in mind that ***1073*** contains the bioreducible disulfide building block (ssbb), which previously was found to delete gene silencing ability in KB cells by premature disulfide cleavage (see section 3.2, **Fig. 43**, compare ***991*** with ***992***). In sum, further work (for example removal of ssbb unit) needs to be performed to combine nice *in vivo* shielding with functional receptor-targeted gene silencing.

3.4 Folate receptor-directed orthogonal click-functionalization of siRNA lipopolyplexes for tumor-targeted gene silencing *in vivo*

3.4.1 Design and synthesis of an azide-bearing lipo-oligomer for click chemistry

During the last years, our laboratory established a library of more than 1000 polycationic structures, prepared by solid-supported synthesis (SPS), to serve as carriers for gene delivery [68, 82, 83, 119]. These structures are combinations of natural amino acids and artificial building blocks. A topological subclass of carriers, so called T-shapes, was found to be very potent for siRNA delivery. Typically, a T-shape structure consists of 4-6 repeats of a cationizable polyamino acid like succinoyl-tetraethylene-pentamine (Stp) for complexation of nucleic acid and for endosomal buffering and a hydrophobic domain branching off the cationic backbone in the oligomer center. Usually two fatty acids [82, 83, 119] or cholanic acids are attached via branching lysines and are supposed to augment siRNA complexes by hydrophobic stabilization and endosomal membrane destabilization. Optionally, other stabilization motifs like tyrosine trimers or cysteines terminate the cationic backbone on both sides. The current work is based on the T-shape structure ***991***, which was published in *Nanoscale* 2016 [137]. Formation of stable siRNA polyplexes with sizes below 150 nm it is an ideal starting position for further modification. Furthermore, ***991*** is a potent oligomer for transfecting the folic acid receptor-positive KB cell line (**Fig. 43**), which was used for screening the efficiency of formulations. To improve the circulation and to equip the delivery system with targeting functionality, copper-free click chemistry was used to modify the surface of the nanoparticles. The high ring strain of a cyclooctyne derivate facilitates click reaction with an azide [138-140]. The reaction is orthogonal to all other functional domains of the oligomer, very efficient, and no byproducts are generated. The azido function was incorporated into the oligomer during standard Fmoc solid-supported synthesis via an azido lysine at the N-terminal end (**Fig. 54**, top). The free amino function at the N-terminus increases hydrophilicity of the microenvironment and can thereby increase the accessibility of the azide on the nanoparticle surface in aqueous solution. In previous work, this position has been shown to be well suitable for systems using other post-modifications [146, 148, 155].

By mixing these azido-oligomers with siRNA, polyplexes will spontaneously assemble. Due to oligomer excess, part of azido carriers remain free in solution. Others are located in the core of the nanoparticle or on its surface. Azido functions on the surface of siRNA polyplexes serve as anchors for functionalization with shielding agents. DBCO was chosen as the azide's reaction partner. It can be incorporated into the shielding agents via SPS by using DBCO acid. The use of SPS allows for changes to each unit of the shielding agent. Thereby we synthesized structures containing PEG of different lengths (24, 48 and 72 ethylene glycol repetitions), the targeting ligand folic acid (FolA), and one or two DBCO units in the final SPS assembly step (structures shown in **Fig. 54**, bottom). For the structures with two DBCO compounds, a bioreducible linker was added next to the final DBCO units. This linker is supposed to *i)* increase the distance of the two units for facilitating a crosslinking reaction with a second oligomer and *ii*) to enable the structures to faster disassemble in the reductive cellular compartments including the cytosol [133, 137]. One critical part of the synthesis of shielding agents is the cleavage of the structures from the resin, because DBCO is labile towards high concentrations of trifluoro acetic acid (TFA) [156]. For this reason only 5 % of TFA had to be used in the cleavage cocktail.

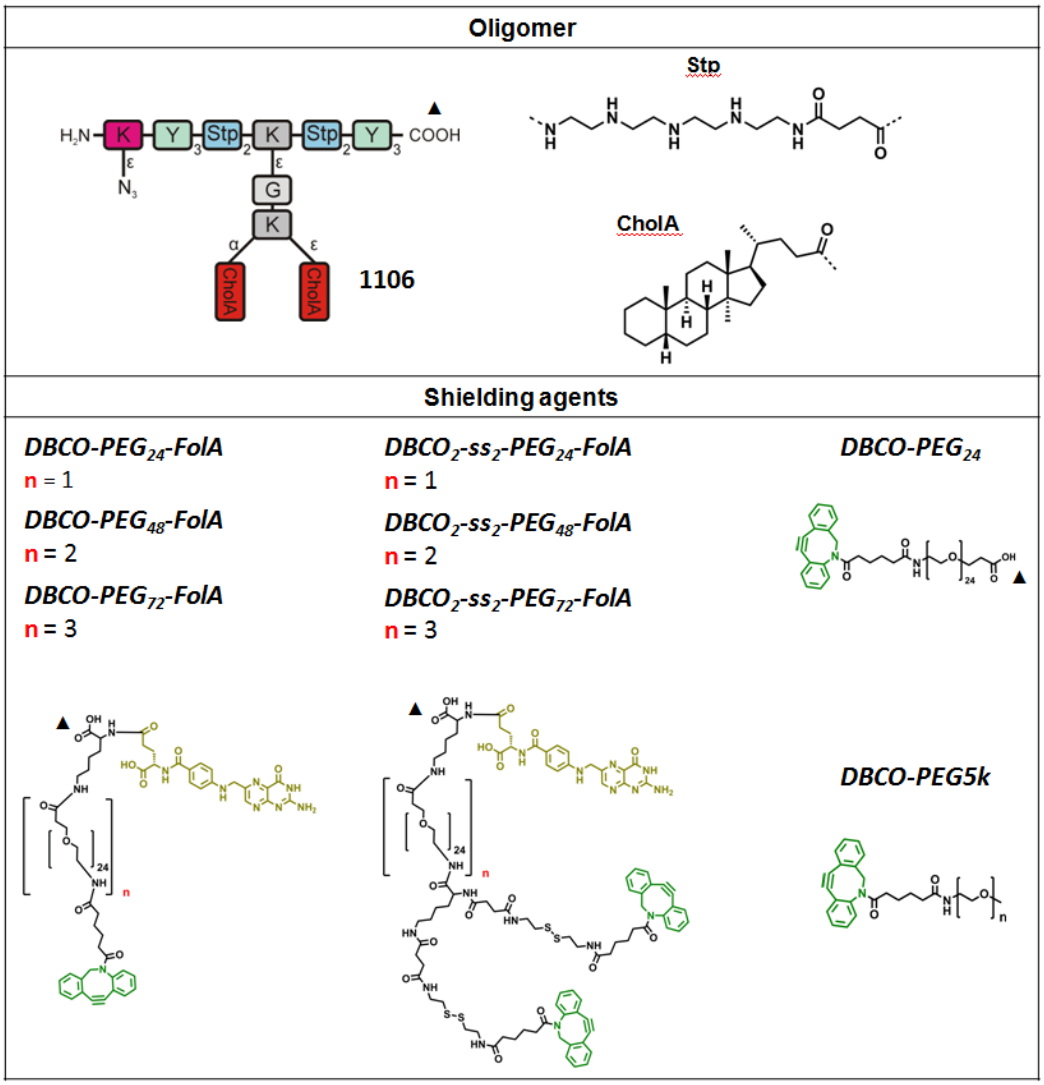

Fig. 54 Overview of chemical compounds. Top: schematic illustration of the sequence-defined oligomer ***1106*** (azidolysine K(N3) bearing analog of the T-shape oligomer ***991***). Other units of the oligomers: Y: tyrosine, K: lysine, G: glycine, Stp: succinoyl-tetraethylene-pentamine, CholA: 5β-cholanic acid. The ID ***1106*** is the database identification number. Bottom: structure of the shielding agents varying in PEG (poly ethylene glycol) length, modification of ss (succinoyl-cystamine) and amount of DBCO (dibenzocyclooctyne). The triangle (▲) indicates the starting point for SPS syntheses: ***1106*** at C-terminal Y; folate-targeted compounds at C-terminal K; ***DBCO-PEG$_{24}$*** at PEG$_{24}$ amino acid. ***DBCO-***PEG5k is commercially available.

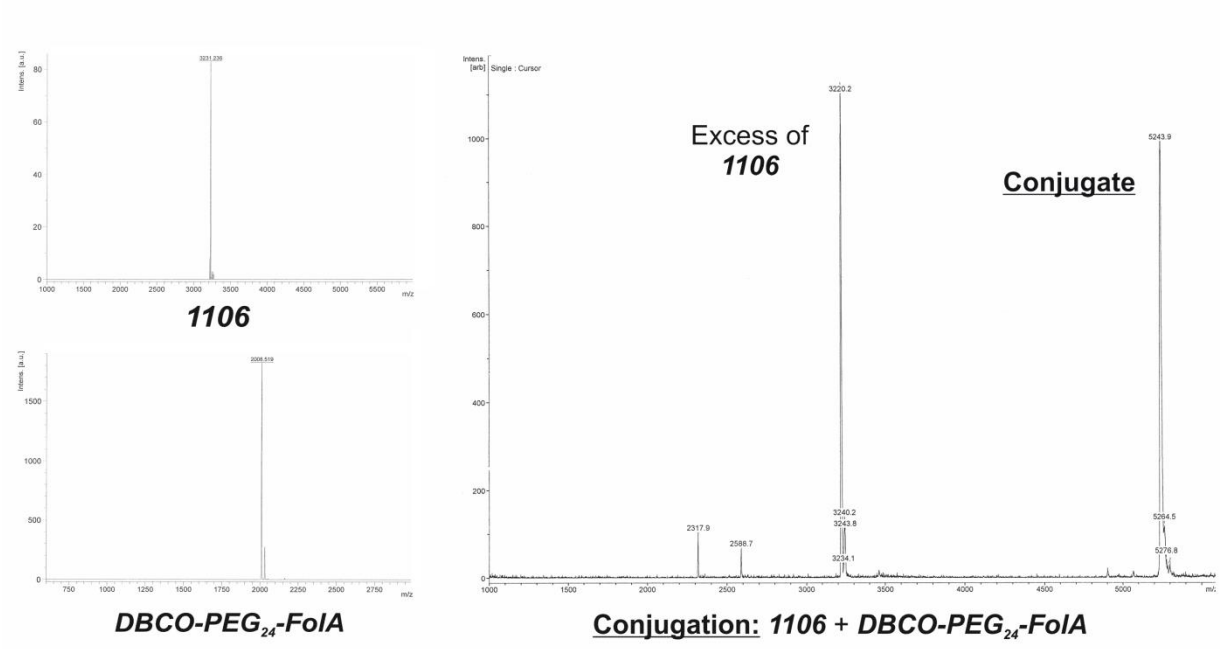

Fig. 55 Reaction of azido-containing oligomer and DBCO-containing post-PEGylation agent. Oligomer ***1106*** and 0.5 eq of ***DBCO-PEG$_{24}$-FolA*** were mixed and incubated for 4 h. MALDI mass spectrometry of the single compounds (left) and the reaction mixture (right) was performed. Mass spectrometry was performed by Stephan Morys (PhD studies, Pharmaceutical Biotechnology, LMU).

To show the integrity and reactivity of the structures, the cationic azido oligomer ***1106*** was mixed with ***DBCO-PEG$_{24}$-FolA***, incubated for 4 h and mass spectrometry was performed. The mass of the conjugate could be detected (**Fig. 55**), which was the proof that both compounds are intact.

3.4.2 Modification of siRNA polyplexes and biophysical characterization

After confirming the successful click reaction of the two compounds in solution, the next step was to perform the reaction on the surface of particles formed with siRNA. For this purpose, the oligomer ***1106*** was incubated with siRNA for 40 min to form lipopolyplexes. The siRNA binding ability of oligomer ***1106*** was determined by measuring the electrophoretic mobility of siRNA in a 1 % agarose gel. Different N/P values depict the ratio of protonatable amines (N) of the oligomer ***1106*** to phosphates (P) of the siRNA. This N/P ratio does not present the charge ratio, as only a fraction of the protonatable amines is protonated at physiological pH. The oligomer showed

complete retention of siRNA in the pockets of the gel at N/P ≥ 6, demonstrating largely electroneutral ***1106*** siRNA complex formation (**Fig. 57**).

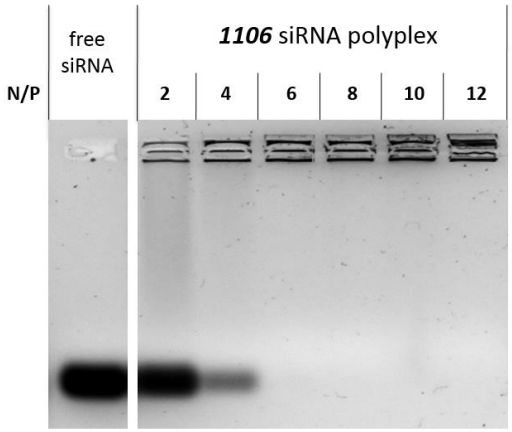

Fig. 56 Electrophoretic mobility of ***1106*** siRNA polyplexes analyzed with an agarose gel shift assay at different N/P ratios. The left lane shows the running distance of free siRNA in HBG that is not complexed by a lipo-oligomer. 1 % agarose gel, 70 V, 60 min running time.

An N/P ratio of 10 was used for all formulations to ensure complete complexation of siRNA. After siRNA complex formation, indicated amounts of click shielding agent were added to the lipopolyplex solution. The amount of added DBCO shielding agent is indicated as molar equivalents (eq) of agent related to the cationic oligomer (mol/mol). Interestingly, all formulations with longer PEG shields show mobility in the gel (**Fig. 57**). Click reaction with the control shielding agent ***DBCO-PEG5k*** resulted in migration of the lipopolyplex in the unusual, opposite direction to the cathode of the gel electrophoresis (**Fig. 57A**). This is consistent with intact nanoparticles sufficiently shielded to migrate within the gel and an overall slightly positive net charge. Higher mobility is observed for higher equivalents of applied shielding agent, indicating a relation to the degree of surface modification of the polyplex. In contrast to all other shielding agents, ***DBCO-PEG5k*** has no negative terminal charge. This explains movement to the opposite direction.

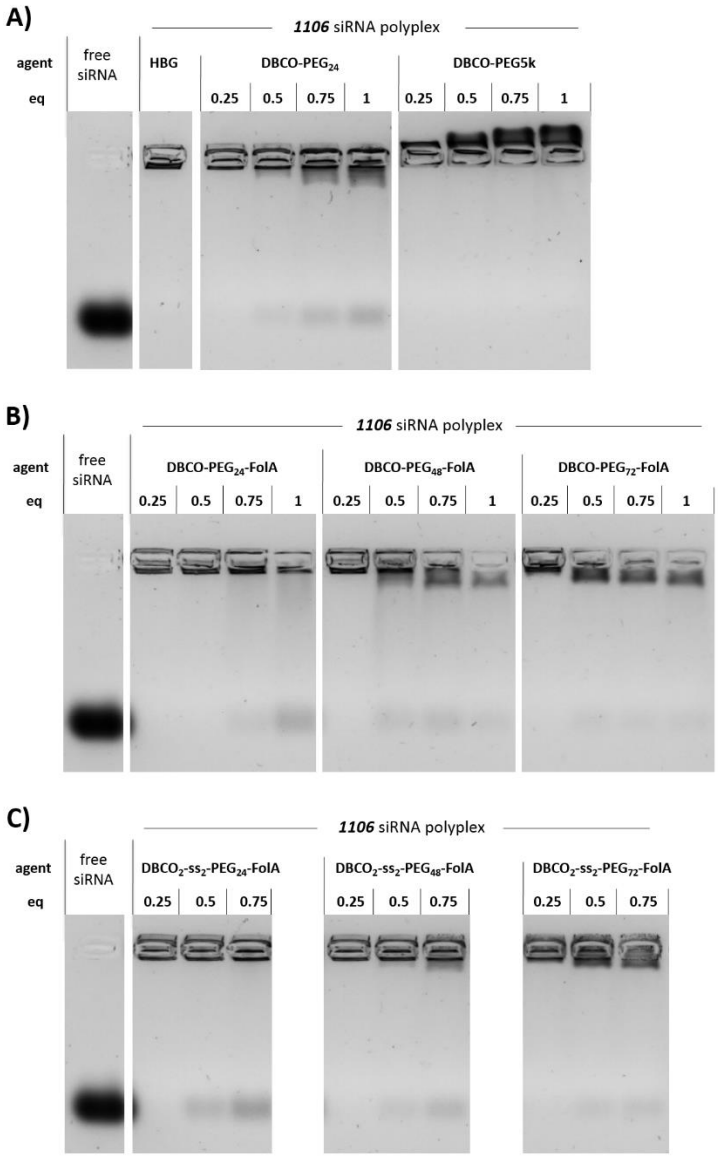

Fig. 57 Electrophoretic mobility of ***1106*** siRNA polyplex formulations analyzed with an agarose gel shift assay. A) Unshielded ***1106*** siRNA polyplex (HBG buffer instead of agents) and modified with increasing equivalents (eq mol/mol) of the control agents ***DBCO-PEG$_{24}$*** or ***DBCO-PEG5k***. B) Formulations with ***1106*** siRNA polyplex modified with increasing equivalents (eq mol/mol) of ***DBCO-PEG$_{24}$-FolA***, ***DBCO-PEG$_{48}$-FolA*** or ***DBCO-PEG$_{72}$-FolA*** C) Formulations with ***1106*** siRNA polyplex modified with increasing equivalents (eq mol/mol) of ***DBCO$_2$-ss$_2$-PEG$_{24}$-FolA***, ***DBCO$_2$-ss$_2$-PEG$_{48}$-FolA*** or ***DBCO$_2$-ss$_2$-PEG$_{72}$-FolA***. All polyplexes were incubated for 40 min at N/P 10, followed by addition of a post-PEGylation agent for 4 h at room temperature. The left lane shows the running distance of free siRNA in HBG that is not complexed by a lipo-oligomer. 1 % agarose gel, 70 V, 60 min running time.

The other click agents show no or slow mobility in the gel towards the anode, but by far not as strong as free siRNA (**Fig. 57B + C**). The mobility observed for nanoparticles with negatively charged folate-containing shielding agents showed an analog effect

observed for ***DBCO-PEG5k*** that the migration correlates with the degree of nanoparticle modification. To further evaluate the *in vivo* relevance of click agent mediated instability, the formulations were incubated in 88 % fetal bovine serum for 24 h before agarose gel electrophoreses were performed (**Fig. 58**).

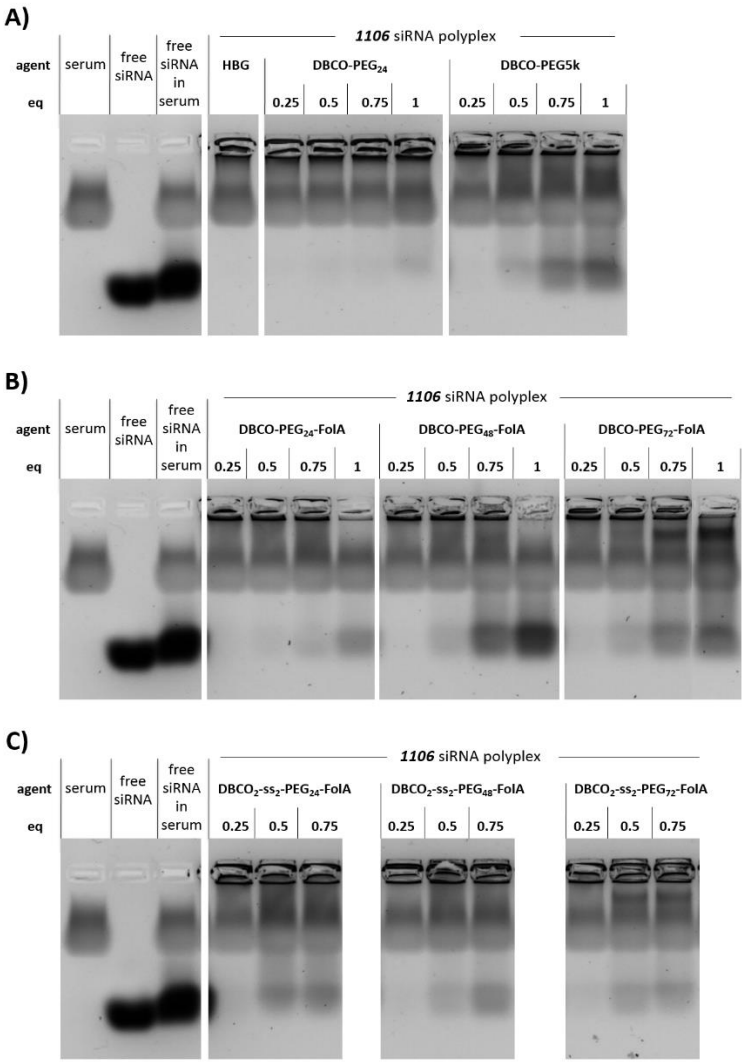

Fig. 58 Electrophoretic mobility of ***1106*** siRNA polyplex formulations after incubation in serum analyzed with an agarose gel shift assay. A) Unshielded ***1106*** siRNA polyplex (**HBG**) and modified with increasing equivalents (eq mol/mol) of the control agents ***DBCO-PEG$_{24}$*** or ***DBCO-PEG5k***. B) Formulations with ***1106*** siRNA polyplex modified with increasing equivalents (eq mol/mol) of ***DBCO-PEG$_{24}$-FolA***, ***DBCO-PEG$_{48}$-FolA*** or ***DBCO-PEG$_{72}$-FolA*** or C) increasing equivalents (eq mol/mol) of ***DBCO$_2$-ss$_2$-PEG$_{24}$-FolA***, ***DBCO$_2$-ss$_2$-PEG$_{48}$-FolA*** or ***DBCO$_2$-ss$_2$-PEG$_{72}$-FolA***. All polyplexes were incubated for 40 min at N/P 10, followed by addition of a post-PEGylation agent for 4 h at room temperature. The formulations were mixed with FBS (fetal bovine serum) to a final concentration of 88 % and incubated for 24 h. The left lanes show the band of serum alone, the running distance of free siRNA in HBG and the running distance of free siRNA in serum. 1 % agarose gel, 70 V, 60 min running time.

Interestingly, the PEG length seems to be the most relevant parameter for stability in serum. Significant siRNA release from polyplexes was observed for 24 h long-term incubations of lipopolyplexes with higher equivalents of shielding agents. Nevertheless, all formulations seem to be quite stable, if less than 0.75 eq of click agents were used.

Table 17 Particle size (z-average) and zeta potential of ***1106*** siRNA formulations determined with a DLS zetasizer. The ***1106*** siRNA polyplexes were prepared at N/P 10 and modified with the indicated agents. Formulations were incubated at *in vivo* conditions and diluted with HBG before the size measurement, followed by 10 mM NaCl for zeta measurement.

***1106* siRNA formulation**	**eq agent**	**z-average [nm]**	**Mean PDI**	**Mean Zeta Potential [mV]**
Unshielded	-	188.3 ± 1.4	0.26 ± 0.01	34.5 ± 0.8
DBCO-PEG$_{24}$-FolA	0.25	246.7 ± 47.0	0.24 ± 0.04	20.2 ± 1.1
	0.5	253.3 ± 2.5	0.24 ± 0.02	23.9 ± 0.4
	0.75	397.4 ± 9.1	0.30 ± 0.02	21.7 ± 0.7
	1	1437.3 ± 34.8	0.43 ± 0.16	15.9 ± 1.0
DBCO-PEG$_{48}$-FolA	0.25	219.0 ± 14.9	0.24 ± 0.03	15.8 ± 0.7
	0.5	919.6 ± 168.4	0.26 ± 0.01	13.3 ± 0.7
	0.75	1598.0 ± 408.9	0.93 ± 0.09	11.9 ± 0.5
	1	345.7 ± 65.8	0.34 ± 0.10	9.5 ± 0.2
DBCO-PEG$_{72}$-FolA	0.25	230.8 ± 6.0	0.36 ± 0.01	11.7 ± 0.8
	0.5	923.1 ± 266.3	0.40 ± 0.13	9.2 ± 0.3
	0.75	835.2 ± 114.2	0.64 ± 0.06	4.8 ± 1.7
	1	512.2 ± 59.9	0.50 ± 0.04	5.4 ± 0.4
DBCO$_2$-SS$_2$-PEG$_{24}$-FolA	0.25	179.8 ± 0.4	0.22 ± 0.02	23.8 ± 0.9
	0.5	191.8 ± 1.3	0.25 ± 0.01	22.8 ± 0.4
	0.75	201.4 ± 2.2	0.24 ± 0.02	22.6 ± 0.5
DBCO$_2$-SS$_2$-PEG$_{48}$-FolA	0.25	219.4 ± 2.4	0.36 ± 0.01	16.4 ± 0.8
	0.5	502.9 ± 97.8	0.30 ± 0.03	12.5 ± 0.6
	0.75	1606.0 ± 334.9	0.64 ± 0.32	10.5 ± 0.7
DBCO$_2$-SS$_2$-PEG$_{72}$-FolA	0.25	218.9 ± 3.6	0.30 ± 0.03	12.2 ± 0.7
	0.5	854.6 ± 185.8	0.59 ± 0.16	10.2 ± 0.9
	0.75	4330.7 ± 1992.3	1.00 ± 0.01	2.9 ± 1.7
DBCO-PEG$_{24}$	0.25	169.2 ± 1.7	0.21 ± 0.02	17.2 ± 2.0
	0.5	367.4 ± 8.0	0.31 ± 0.06	14.6 ± 0.5
	0.75	637.1 ± 25.9	0.34 ± 0.06	12.1 ± 0.6
	1	1048.6 ± 56.0	0.40 ± 0.26	11.5 ± 0.5
DBCO-PEG5k	0.25	170.9 ± 1.3	0.22 ± 0.02	6.9 ± 0.5
	0.5	165.4 ± 0.9	0.16 ± 0.02	4.1 ± 0.9
	0.75	194.0 ± 2.3	0.25 ± 0.01	3.8 ± 0.7
	1	168.5 ± 2.1	0.17 ± 0.02	2.3 ± 0.3

The size and shape of siRNA polyplexes were evaluated by dynamic light scattering (DLS) and transmission electron microscopy (TEM). The sizes of the unshielded, the ***DBCO-PEG5k*** shielded and the ***DBCO$_2$-ss$_2$-PEG$_{24}$-FolA*** modified particles ranged around 200 nm and showed a low polydispersity for all tested equivalents (**Table 17**). The other FolA-containing formulations showed bigger sizes and aggregations for higher equivalents of click agents when measured with DLS. The formation of aggregates could not be confirmed by particle analysis with TEM (**Fig. 59**). Hence, we think that aggregates were rare and/or only loose and may disassemble. Since large particles strongly contribute to scatter light in DLS measurements, such measurements are very sensitive to even small fractions of aggregates. All particles visualized by TEM have a spherical shape and sizes range between 50 and 200 nm independent of the PEG agent they were modified with (**Fig. 59**).

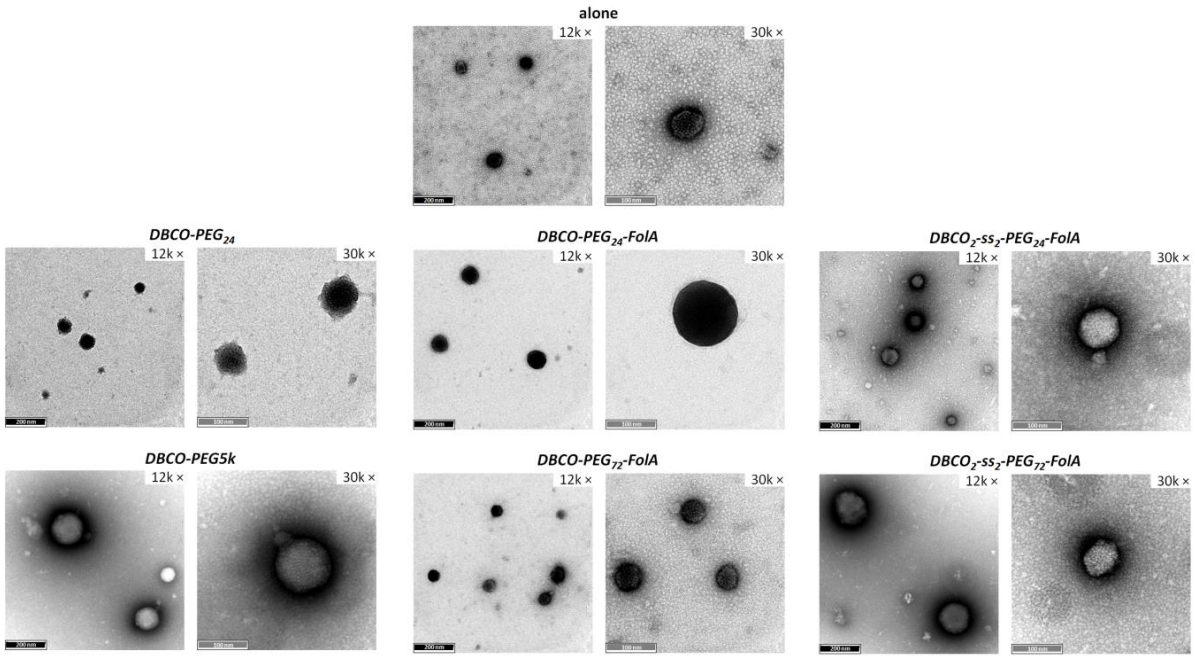

Fig. 59 TEM micrographs of formulations. Top: ***1106*** siRNA polyplex (**alone**); Middle: ***1106*** siRNA polyplex modified with DBCO agents with short PEG (control ***DBCO-PEG$_{24}$***, ***DBCO-PEG$_{24}$-FolA*** and ***DBCO$_2$-ss$_2$-PEG$_{24}$-FolA***); Bottom: ***1106*** siRNA polyplex modified with DBCO agents with longer PEG (control ***DBCO-PEG5k***, ***DBCO-PEG$_{72}$-FolA*** and ***DBCO$_2$-ss$_2$-PEG$_{72}$-FolA***). Black scale bar indicates 200 nm (left image of the set); gray scale bar indicates 100 nm (right image of the set). TEM grids were incubated with the sample solution (polyplexes incubated at N/P 10 as described and diluted with water to 25 ng siRNA/µL) for 2.5 minutes, washed with water and stained with uranyl acetate solution for 5 seconds. TEM was performed by Susanne Kämpter (Faculty of Physics, LMU).

The degree of surface modification and shielding of a nanoparticle can also be evaluated by determining its zeta potential by measuring its mobility under electric field with light scattering. We can show that an unshielded particle's zeta potential is reduced from 34.5 mV by more than 35 % using a PEG_{24} agent (**Table 17**). Longer PEG chains (PEG_{72} and PEG5k) reduced the zeta potential to less than 5 mV, indicating efficient shielding.

3.4.3 Targeted delivery of siRNA formulations and gene silencing *in vitro*

Gene silencing experiments were performed in KB/eGFPLuc cells stably expressing an eGFP-Luciferase fusion protein (**Fig. 60**) to evaluate the targeting and transfection efficiency of formulations. This human cervix carcinoma cell line overexpresses the folic acid receptor and can therefore be targeted using the vitamin folic acid. Silencing of the eGFP-Luciferase fusion protein mediated by siRNA against eGFP (siGFP - light bars) can be quantified by a standard luciferase assay. Well consistent with zeta potential data the untargeted siRNA polyplexes with short PEG_{24} (***DBCO-PEG$_{24}$***) mediate moderate gene silencing, whereas the long 5 kDa PEG (***DBCO-PEG5k***) completely prevented gene silencing (**Fig. 60A**). For the targeted formulations the two main findings with this cell line were: i) folic acid ligands strongly increase the silencing efficiency and ii) longer PEG shields decrease silencing efficiency (**Fig. 60B + C**). Higher equivalents of a shielding and targeting agent enhanced the respective effects. The effects overlap for surface modifying compounds that combine longer PEG and folic acid targeting ligand. Altogether, PEG_{24} structures with folic acid (***DBCO-PEG$_{24}$-FolA*** and ***DBCO$_2$-ss$_2$-PEG$_{24}$-FolA***) provided the highest efficiency. Both structures provided very efficient gene silencing (far better than without targeting) but still do not perfectly shielded the polyplex. We can exclude unspecific cell toxicity of formulations by evaluation of the luciferase levels of the analogous siCtrl polyplexes, which did not significantly change luciferase expression.

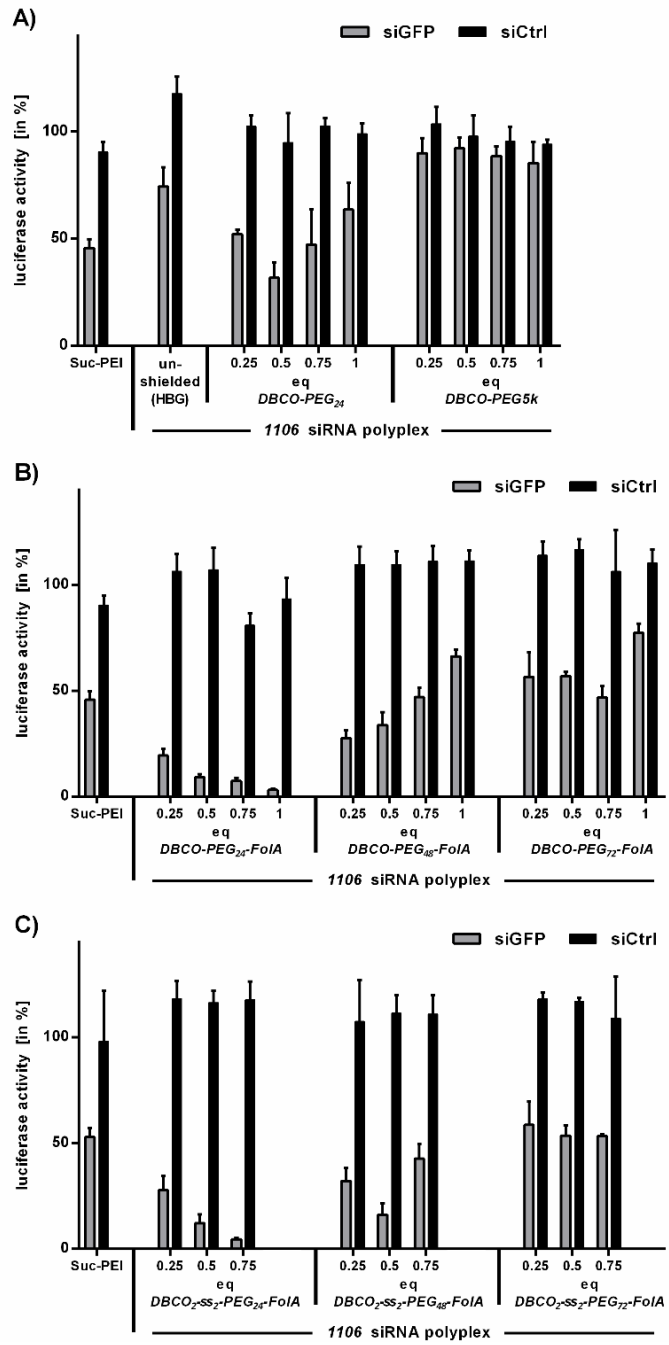

Fig. 60 Gene silencing of targeted formulations in KB cells. Lipopolyplex formulations with eGFP-targeted siRNA (siGFP) or control siRNA (siCtrl) at N/P 10 were tested for eGFPLuc gene silencing in KB-eGFPLuc cells. A) Unshielded ***1106*** siRNA polyplex (addition of HBG buffer only) and modified with increasing equivalents (eq mol/mol) of the control agents ***DBCO-PEG$_{24}$*** and ***DBCO-PEG5k***. Formulations with ***1106*** siRNA polyplex modified with B) increasing equivalents (eq mol/mol) of ***DBCO-PEG$_{24}$-FolA***, ***DBCO-PEG$_{48}$-FolA*** or ***DBCO-PEG$_{72}$-FolA*** C) increasing equivalents (eq mol/mol) of ***DBCO$_2$-ss$_2$-PEG$_{24}$-FolA***, ***DBCO$_2$-ss$_2$-PEG$_{48}$-FolA*** or ***DBCO$_2$-ss$_2$-PEG$_{72}$-FolA***. Cells were incubated for 45 min with formulations and washed. The luciferase activity of siRNA-treated cells was measured after 48 h. It is presented related to HBG-treated cells. Data are presented as mean value (±SD) out of triplicates. Transfections were performed by Dr. Wei Zhang (Pharmaceutical Biotechnology, LMU).

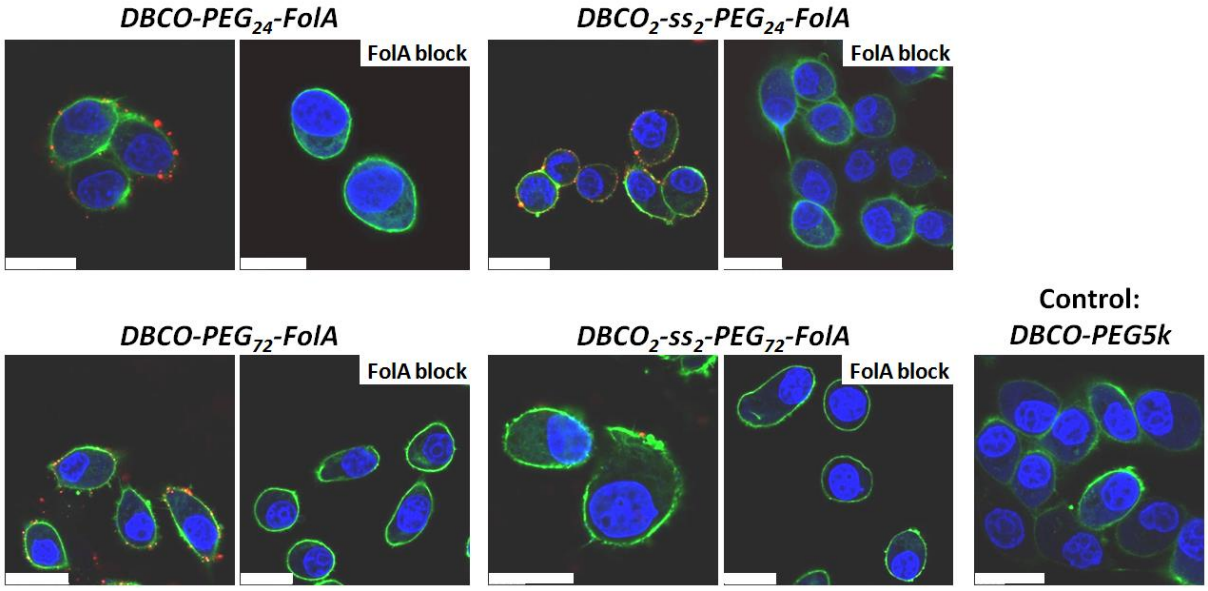

Fig. 61 Cellular association of siRNA formulations in KB cells acquired by confocal laser scanning microscopy. Cells were incubated with the ***1106*** formulations shielded with 0.5 eq (mol/mol) of ***DBCO-PEG$_{24}$-FolA***, ***DBCO-PEG$_{72}$-FolA***, ***DBCO$_2$-ss$_2$-PEG$_{24}$-FolA, DBCO$_2$-ss$_2$-PEG$_{72}$-FolA*** and ***DBCO-PEG5k*** for 30 min on ice and washed with PBS buffer. The FolA block samples were incubated with 100 µM free folic acid solution prior to incubation with the formulation. Nuclei were stained with DAPI (blue) and actin cytoskeleton was stained with rhodamine phalloidin (green). siRNA was spiked with 20 % Cy5-labeled siRNA (red). Scale bars indicate 25 µm. Transfections were performed by Dr. Dian-Jang Lee (Pharmaceutical Biotechnology, LMU), confocal microscopy was performed by Miriam Höhn (Pharmaceutical Biotechnology, LMU).

To analyze if the transfection result is folic acid receptor mediated, microscopy studies were performed with and without folic receptor block by free folate. Polyplexes shielded with short PEG$_{24}$ and long PEG$_{72}$ agents were used. KB cells were incubated with formulations formed with Cy5-labled siRNA for 30 min on ice (**Fig. 61**). The short incubation on ice prevents the active uptake of the polyplexes into the cell. After washing the cells, imaging was performed using confocal laser scanning microscopy. The particles modified with folic acid bearing agents showed strong colocalization with the membrane of the cells, except for ***DBCO$_2$-ss$_2$-PEG$_{72}$-FolA,*** which had a much weaker binding to the cell surface. If the cells were pre-incubated with free folate before incubation with the formulations, no cellular association of the polyplexes was detected. Demonstrating that the binding of formulations could be blocked indicates a receptor-mediated association to the membrane. The negative control (***DBCO-***

PEG5k), lacking the folic acid ligand, did not show any interaction with the cell membrane.

To quantify the results, the cell binding was analyzed by flow cytometry. PEG_{48} agents with medium PEG length ware included this time. The data confirmed the microscopy results. All mono-DBCO agents bound sufficiently to KB cell membranes (**Fig. 62A**). For bis-DBCO structures, the binding ability decreased with increasing PEG length. It cannot be excluded that bioreducible spacer blocks incorporated into the bivalent DBCO structures might be responsible for the weak cell binding. Premature cleavage on the cell surface might cause dissociation from the cell.

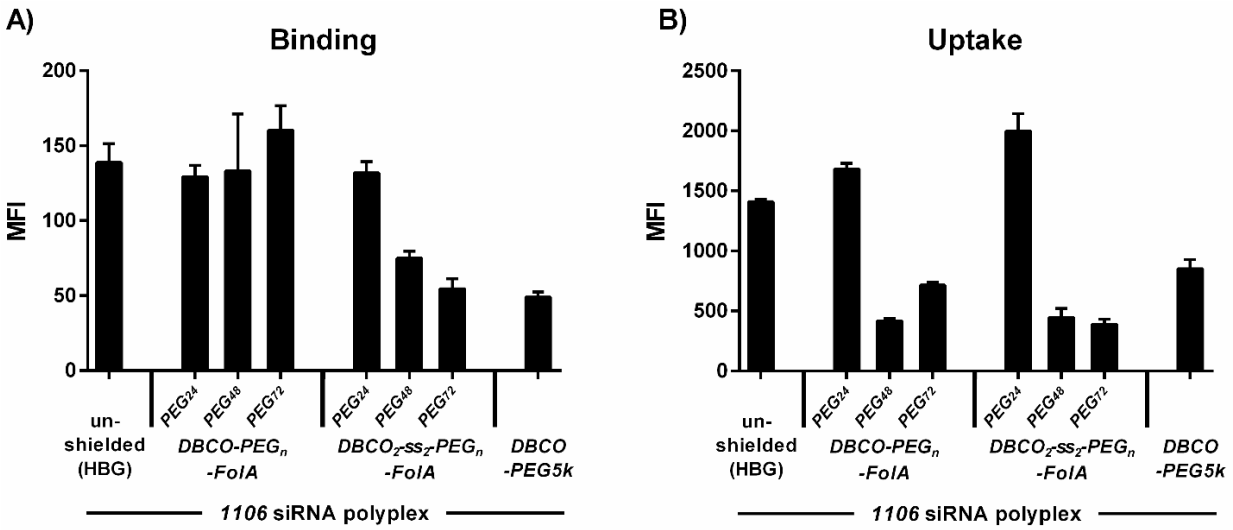

Fig. 62 Binding and uptake of folic acid containing polyplexes. A) Cellular binding of Cy5-labled (20 %) siRNA ***1106*** formulations without (unshielded – HBG buffer instead of agent) or with shielding agents; 0.5 eq (mol/mol) of ***DBCO-PEG$_{24}$-FolA***, ***DBCO-PEG$_{48}$-FolA***, ***DBCO-PEG$_{72}$-FolA***, ***DBCO$_2$-ss$_2$-PEG$_{24}$-FolA, DBCO$_2$-ss$_2$-PEG$_{48}$-FolA, DBCO$_2$-ss$_2$-PEG$_{72}$-FolA*** and ***DBCO-PEG5k*** determined by flow cytometry. KB cells were incubated with the formulations for 30 min on ice and washed with PBS buffer. B) Cellular internalization of the same Cy5-labled (20 %) ***1106*** siRNA formulations determined by flow cytometry. KB cells were incubated with the formulations for 45 min and washed with PBS buffer and heparin solution. Experiments were performed by Dr. Wei Zhang (Pharmaceutical Biotechnology, LMU).

To analyze if cellular internalization is the limiting factor for transfection efficiency, cells were incubated with the formulations for 45 min at 37 °C and washed with PBS and heparin. The negatively charged heparin dissociates material from the cell membranes. Afterwards, cells were analyzed by flow cytometry and Cy5 intensity was

quantified (**Fig. 62B**). In contrast to well cell binding of mono-DBCO functionalized folic acid targeted nanoparticles, the receptor-mediated uptake is strongly decreased for the longer PEG_{48} and PEG_{72} (mono- and bis-DBCO) agents. This finding shows that binding to the folate receptor does not necessarily lead to internalization. The trafficking of the vitamin folate via folate receptors is thought to occur by a nonclathrin, noncaveolar pathway also known as CLIC/GEEC endocytosis pathway [150, 151]. Previously caveolae were thought to be the involved in the uptake pathway [157]. It could be demonstrated that the uptake pathway indeed changes to caveolae-mediated endocytosis when glycosyl-phosphatidylinositol-anchored proteins (GPI-AP), like the folate receptor, were cross-linked on cell surfaces [150, 158]. For folate-targeted nanoparticles, uptake pathways like caveolae- and clathrin-mediated endocytosis were found [152-154]. The size of the nanoparticle and the ligand density on their surface were reported to influence the cellular uptake pathway. Both parameters also changed for longer PEG_{48} and PEG_{72} chains in targeted ***1106*** siRNA polyplexes. The resulting particle properties might be unfavorable for the polyplex internalization.

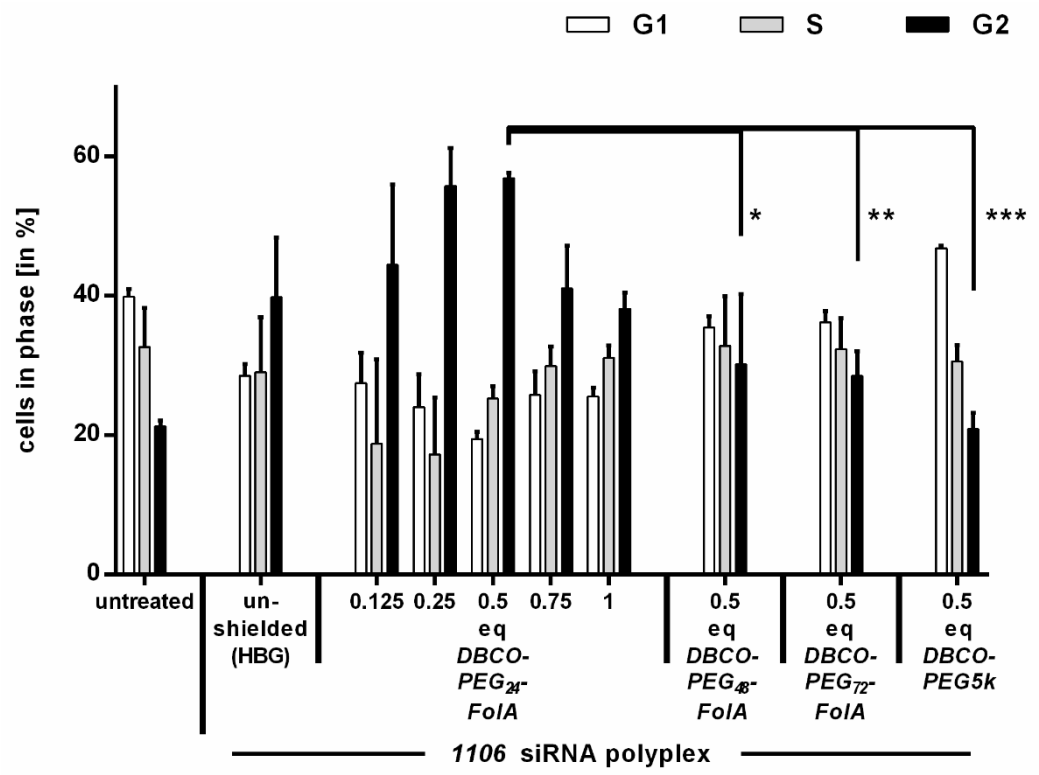

Fig. 63 Cell cycle analysis of siRNA formulations targeting Eg5 in L1210 cells. Folic acid-targeted lipopolyplex formulations with siRNA targeting the mitotic kinesin Eg5 were prepared at N/P 10 and tested on folic acid receptor-positive L1210 cells. The knockout of Eg5 is known to lead to an arrest in G2 phase. The cell cycle status of untreated cells was compared with cells treated with unshielded ***1106*** siRNA polyplex (addition of HBG buffer instead of agent), with ***1106*** siRNA polyplexes modified with increasing equivalents (eq mol/mol) of the ***DBCO-PEG$_{24}$-FolA*** and formulations with 0.5 eq of ***DBCO-PEG$_{48}$-FolA, DBCO-PEG$_{72}$-FolA*** or negative control ***DBCO-PEG5k***. All cells were incubated with the formulations for 24 h. The phase of the cells was determined by propidium iodide staining followed by flow cytometry analysis. Statistics: unpaired t-test with Welch's correction: * $p<0.05$, ** $p<0.005$, *** $p<0.001$. Experiment was performed by Dr. Wei Zhang (Pharmaceutical Biotechnology, LMU).

To test the system with another cell line and another siRNA, we established a cell cycle analysis assay with siRNA targeting the mitotic kinesin Eg5 (siEG5). A knockout of Eg5 leads to an arrest in G2 phase. Afterwards, in case of tumor cells such as L1210, the cell usually undergoes apoptosis. The folic acid receptor overexpressing mouse lymphocytic leukemia suspension cell line L1210 was used for this assay. The analysis of the cell cycle revealed that the formulation with 0.5 eq ***DBCO-PEG$_{24}$-FolA*** promoted the strongest arrest in G2 phase (**Fig. 63**). Analog to the previous silencing study,

longer PEG shields decrease the silencing efficiency. The well-shielded formulation with 0.5 eq ***DBCO-PEG5k*** did not change the cell cycle.

3.4.4 Delivery of siRNA formulations *in vivo*

Systemic delivery of siRNA is a major challenge, since siRNA is readily degraded by serum endonucleases and due to the small size also quickly eliminated by glomerular filtration with plasma half-life of less than ten minutes [159]. For systemic *in vivo* tumor targeting, formulations with 0.5 eq of click agent with short PEG_{24} and folic acid ligand were chosen, because they efficiently transfect folic acid receptor-positive cells (***DBCO-PEG$_{24}$-FolA*** and ***DBCO$_2$-ss$_2$-PEG$_{24}$-FolA***). Those formulations also show high serum stability and suitable sizes [160]. In addition, the folic acid positive formulations with PEG_{72} (***DBCO-PEG$_{72}$-FolA*** and ***DBCO$_2$-ss$_2$-PEG$_{72}$-FolA***) were included, because longer PEG chains might be beneficial for the circulation in mice. The short-chained ***DBCO-PEG$_{24}$*** and the commercially available, long-chained ***DBCO-PEG5k*** served as untargeted control. The formulations were prepared with Cy7-labeled siRNA, injected into tumor-bearing NMRI-nude mice via tail-vein injection and the distribution of the dye was monitored at various time points for 1 day by NIR bioimaging in living mice (**Fig. 64** and **Fig. 65**). The unshielded polyplex accumulated in the liver after 1 h. This finding could be observed for other T-shape structures in previous work as well [119, 146]. No improvement in circulation was determined for the control ***DBCO-PEG$_{24}$***. Interestingly, the folic acid ligand strongly improved blood circulation, with the ***DBCO-PEG$_{24}$-FolA*** formulation displaying an expanded *in vivo* distribution after 3 hours. The bis-DBCO function (***DBCO$_2$-ss$_2$-PEG$_{24}$-FolA***) further improved the residence in circulation. After 4 hours, signals could be detected in most parts of the body including the tumor site. The long-chained PEG control formulation with ***DBCO-PEG5k*** fulfilled our expectations and improved the distribution of the siRNA polyplexes. A strong signal was detected at superficial peripheral sites such as in paws of mice after 4 hours. In contrast to this untargeted formulation, the ***DBCO-PEG$_{72}$-FolA*** formulation with long PEG and folic acid showed a weaker distribution and retention in the mouse's body. When bis-DBCO was attached to the agent (***DBCO$_2$-ss$_2$-PEG$_{72}$-FolA***), the formulation first retained in the lung and then slowly diffused out into the whole body. After 2 hours, this formulation is also widely distributed all over the body, however, in contrast to the other targeted formulations, it did barely reach the subcutaneous tumor site.

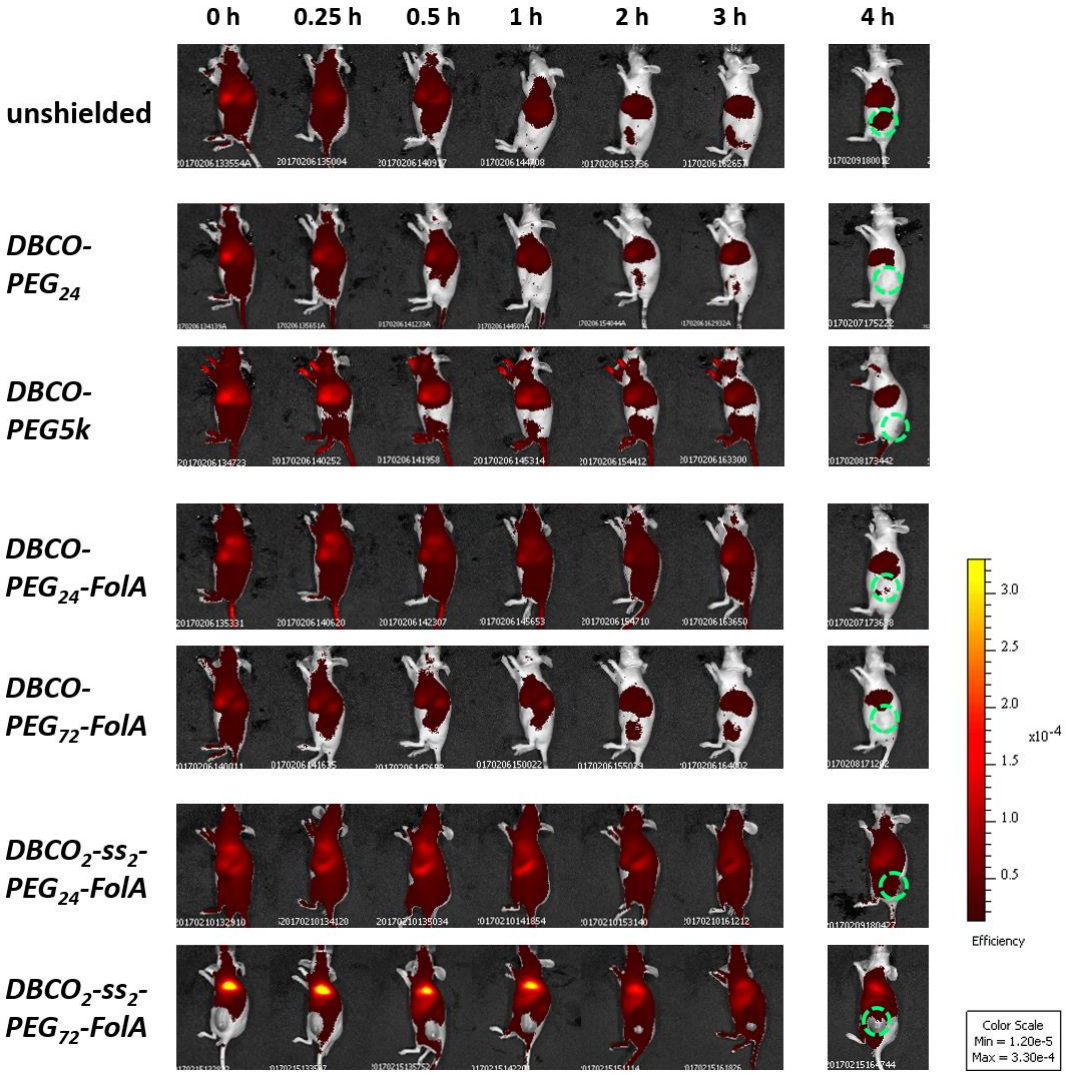

Fig. 64 Biodistribution of ***1106*** siRNA formulations at N/P 10 in L1210 tumor-bearing NMRI nude mice after *i. v.* administration. Biodistribution determined by NIR fluorescence bioimaging of 50 µg siRNA (50 % Cy7-labeled siRNA) with ***1106*** alone (**unshielded** – addition of HBG buffer instead of shielding agent), with 0.5 eq ***DBCO-PEG24***, 0.5 eq ***DBCO-PEG5k***, 0.5 eq ***DBCO-PEG24-FolA***, 0.5 eq ***DBCO-PEG72-FolA***, 0.5 eq ***DBCO2-ss2-PEG24-FolA*** and 0.5 eq ***DBCO2-ss2-PEG72-FolA***. Experiments were performed with three animals per group for time points until 1 h, one animal per group for time points 2 h and 3 h and two animals for the 4 h time point; a representative animal of each group is shown. See **Fig. 65** for all animals. Animals are presented in lateral view to present the tumor sites. Green circles indicate the tumor site. Experiment was performed by Dr. Dian-Jang Lee (Pharmaceutical Biotechnology, LMU) and Sarah Kern (veterinary MD study, Pharmaceutical Biotechnology, LMU).

In sum, the agent combining short PEG_{24}, bis-DBCO and folic acid targeting ligand showed the best circulation *in vivo* and the longest retention at the tumor site.

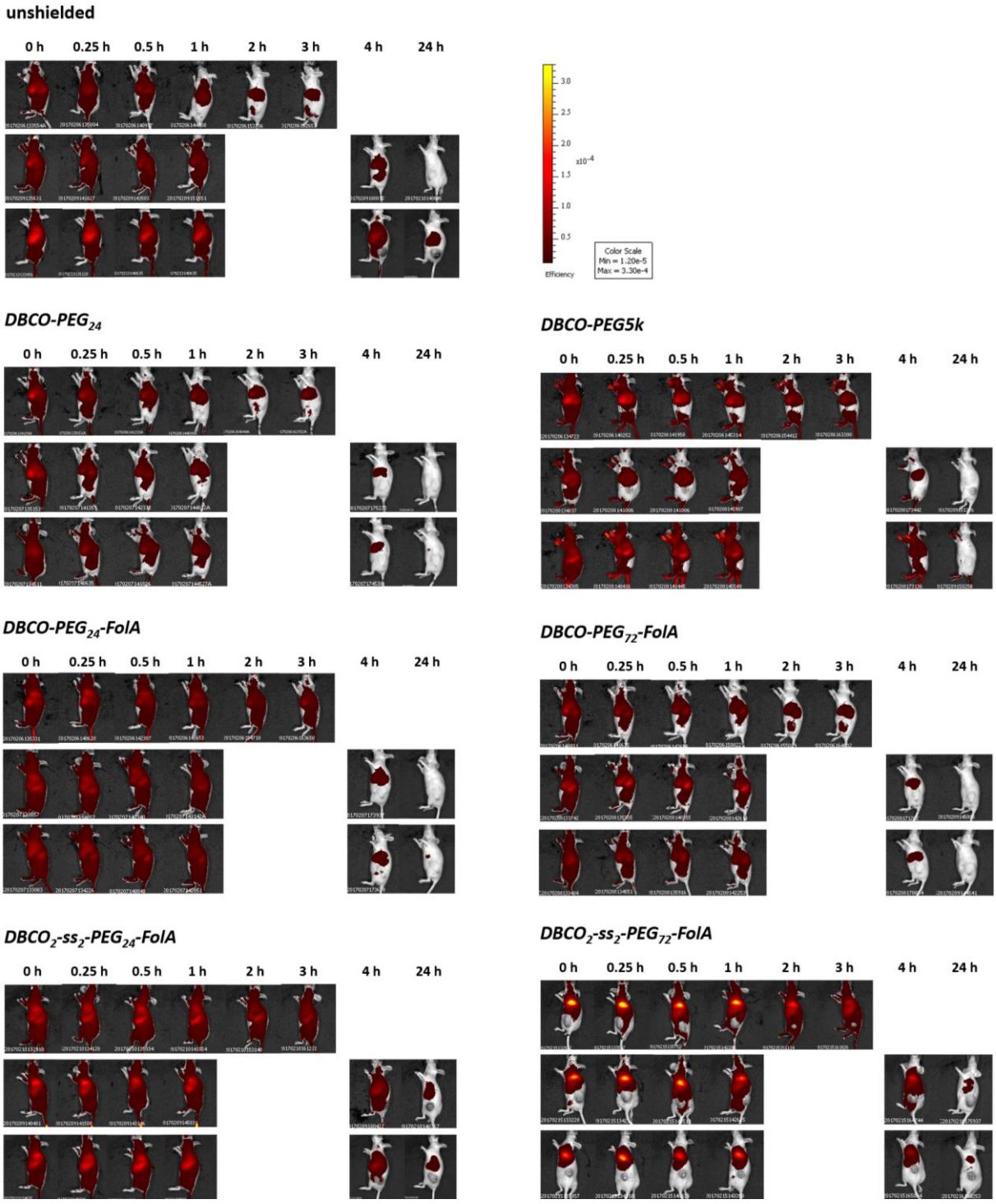

Fig. 65 Overview of biodistribution of all animals injected with ***1106*** siRNA formulations at N/P 10 in L1210 tumor-bearing NMRI nude mice after *i. v.* administration. Biodistribution determined by NIR fluorescence bioimaging of 50 µg siRNA (50 % Cy7-labeled siRNA) Experiments were performed with three animals per group for time points until 1 h, one animal per group for time points 2 h and 3 h and two animals for time points 4 h and 24 h; Animals are presented in lateral view to present the tumor sites. Experiment was performed by Dr. Dian-Jang Lee (Pharmaceutical Biotechnology, LMU) and Sarah Kern (veterinary MD study, Pharmaceutical Biotechnology, LMU).

The influence of folic acid on improved biodistribution for short PEG agents, but decreased distribution for long PEG agents, was an unexpected finding. One explanation for the prolonged retention of targeted polyplexes in other tissues might be targeting of L1210 tumor cells disseminated from subcutaneous to systemic sites; L1210 tumors are known to rapidly metastasize to other parts of the body. In this experiment pathogenic enlargement in size of spleen was frequently noticed in tumor-bearing animals. Bis-DBCO structures might have the ability to crosslink two lipo-oligomers on the surface of polyplexes. Although previous experiments did not indicate an increased stability of formulations with structures with two attached DBCO units (at least in the absence of reducing agents), the bivalent attachment might be a possible explanation of their advantage, for example by reducing the risk of premature disassembly of the coat.

The best performing candidate ***DBCO$_2$-ss$_2$-PEG$_{24}$-FolA*** was then analyzed for gene silencing *in vivo*. ***1106*** polyplexes were prepared with active siEG5 or siCtrl (50 µg of siRNA) and 0.5 eq ***DBCO$_2$-ss$_2$-PEG$_{24}$-FolA***. As the untargeted delivery control, ***1106*** polyplexes were prepared with siEG5 and 0.5 eq ***DBCO-PEG$_{24}$.*** Five mice per group were prepared with L1210 tumor and the weight and the tumor size of the animals were monitored (**Fig. 66**). When tumors reached a size of 500 mm^3, the formulations were administered via tail vain injection twice at daily interval. At 24 h after the second treatment, tumors were harvested, RNA was extracted and the EG5 mRNA levels were quantified by qRT-PCR (**Fig. 67A**).

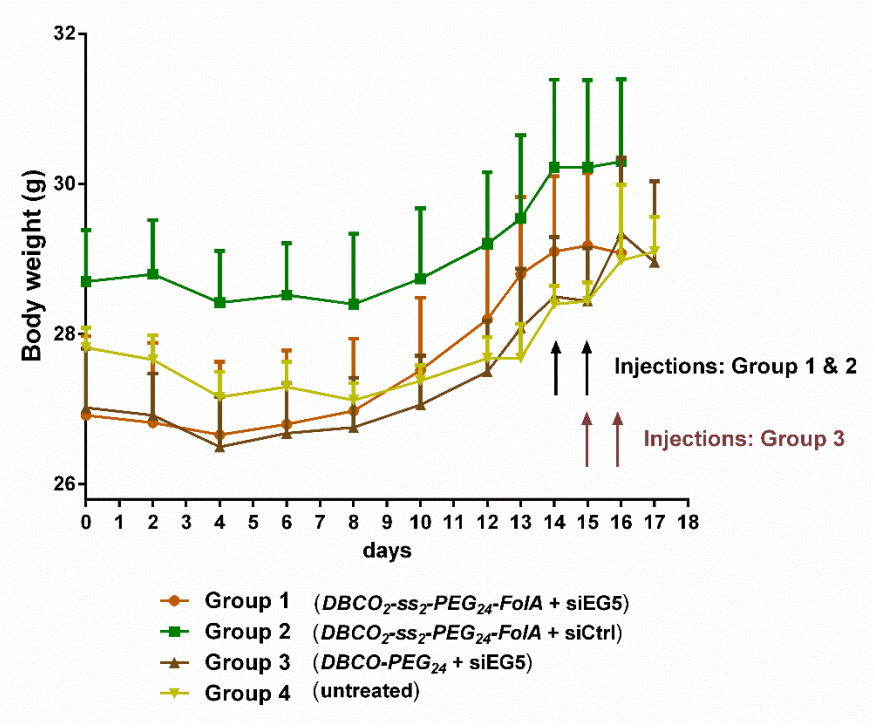

Fig. 66 Body weight of mice after injection of L1210 tumor cells. The arrows indicate the time of the injection of ***1106*** formulations. 50 µg siRNA were injected per mouse twice with a delay of 24 h. 24 h after the second injection the mice were sacrificed and tumors were harvested. Day 0 indicates the day of tumor cell inoculation. Body weight of 5 animals per group is presented as mean ± SEM. Experiment was performed by Dr. Dian-Jang Lee (Pharmaceutical Biotechnology, LMU) and Sarah Kern (veterinary MD study, Pharmaceutical Biotechnology, LMU).

Compared to untreated controls, the ***1106*** siEG5 ***DBCO$_2$-ss$_2$-PEG$_{24}$-FolA*** induced a significant downregulation of EG5 mRNA expression by ~60 %. ***1106*** siCtrl ***DBCO$_2$-ss$_2$-PEG$_{24}$-FolA*** showed a weak, but not significant reduction of EG5 mRNA levels as compared to untreated tumors. Untargeted ***1106 DBCO-PEG$_{24}$*** siEG5 polyplexes revealed negligible effects on EG5 mRNA levels, demonstrating the superiority of the folate-PEG agent with the bivalent attachment for delivery of the nanoparticles into the tumor.

Systemic circulation of siRNA polyplexes might also cause potential side effects when they reach non-target tissues. Therefore, blood biochemistry examinations were carried out helping to realize the biocompatibility of the carriers (**Fig. 67B**).

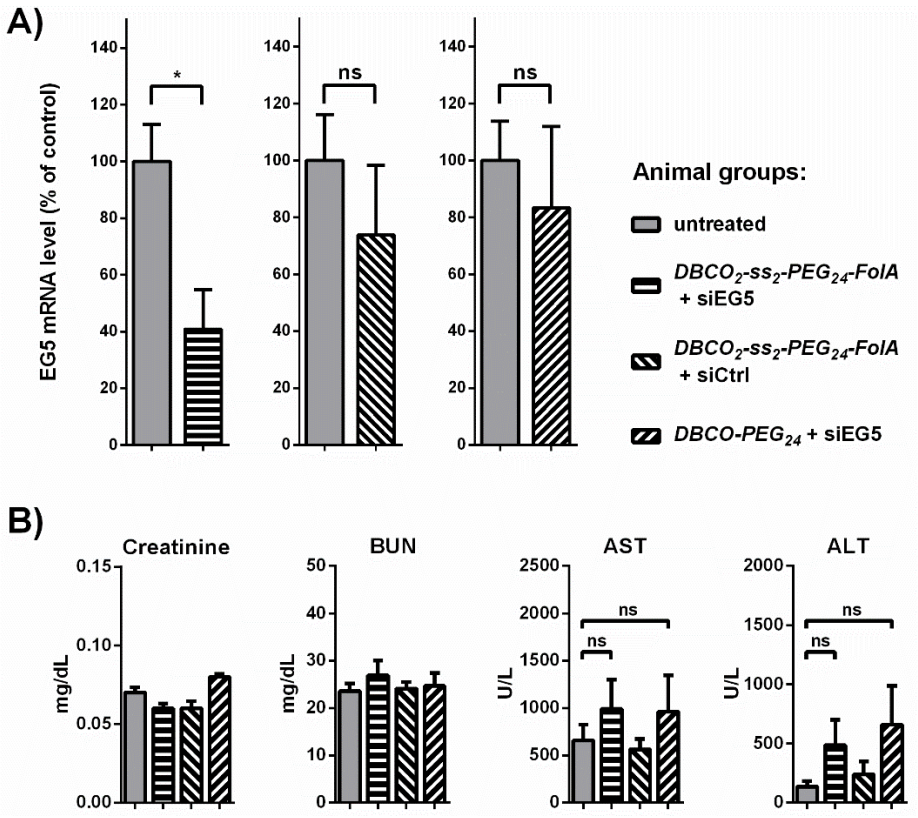

Fig. 67 Tumor-targeted gene silencing efficiency of ***1106*** *DBCO$_2$-ss$_2$-PEG$_{24}$-FolA* in L1210 tumor-bearing mice. **A)** mRNA level of EG5 gene after twofold i.v. injection of ***1106*** siRNA polyplexes with ***DBCO$_2$-ss$_2$-PEG$_{24}$-FolA*** with 50 µg of siEG5 or siCtrl, and ***DBCO-PEG$_{24}$*** with 50 µg of siEG5 at N/P 10. **B)** Clinical biochemistry parameters (ALT, AST, BUN and creatinine). Plasma was obtained from the treated animals 24 h after the second injection compared to untreated tumor-bearing mice. The *in vivo* gene silencing assay was performed by Dr. Dian-Jang Lee (Pharmaceutical Biotechnology, LMU). The blood biochemistry was measured in Small Animal Clinic (Faculty of Veterinary Medicine, LMU).

Blood samples were collected 24 h after the treatments with siRNA formulations to determine four relevant clinical biochemistry parameters (creatinine, BUN, AST and ALT). The liver enzymes (ALT and AST) were slightly, but not significantly increased for the two formulations prepared with siEG5. High values for those parameters indicate liver damage or acute hepatitis. The parameters BUN and creatinine, which are related to renal function, did not show any difference as compared to untreated controls. The unobtrusive body weight of animals, presented in **Fig. 66**, indicated that the formulations were well-tolerated compared to untreated controls.

In sum, the systemic delivery of a siRNA formulation functionalized with a targeted, bis-reactive DBCO agent into tumor tissue induced specific RNAi-mediated

degradation of EG5 mRNA of tumors. No significant side effects were recognized based on the body weight analysis and clinical chemistry of blood samples.

4 Discussion

4.1 Twin disulfides as opportunity for improving stability and transfection efficiency

The stability of a carrier system is one important requirement for efficient delivery of nucleic acids *in vivo*. Especially cationic carrier systems that complex nucleic acid via interelectrolytic forces often require additional moieties for stabilization [127, 146, 148]. For small nucleic acids like siRNA, that consist of only 21 bp, stability is a bigger issue than for large nucleic acids like pDNA with about 6000 bp. This can be explained by a smaller gain in entropy due to the exchange of less counter ions during polyplex formation [13, 161, 162]. Therefore stability is more critical for siRNA polyplexes than for polyplexes formed with pDNA. Fatty acids and tyrosine trimers for hydrophobic interactions and terminal cysteine residues for disulfide bridge formation have previously been used to stabilize polyplexes [82, 87, 119]. In this work, the CRC motif was integrated into sequence defined oligomers and examined for its ability to stabilize siRNA polyplexes. As CRC offers faster disulfide formation kinetics, higher stability of formed twin disulfides and orthogonal pairing in the presents of single cysteines [43], this motif offers the opportunities to serve as a new stability motif.

The comparison of the CRC motif with single cysteines did indeed show improved stability of the resulting polyplexes. This was observed at different N/P ratios, in the presence of serum and under reducing conditions. Especially for PEGylated CRC-polyplexes, a better siRNA binding ability was observed. PEG is known to reduce the binding ability of ethylenimine motifs in polyplexes [113, 114, 163]. An increase of stability does not necessarily result in better transfection efficiency. For pDNA polyplexes, the inclusion of twin disulfides triggers only minor overall differences. The influence of the motif on siRNA transfection efficiency ranges from total abolishment to significant increase. While T-shape lipo-oligomer and 3-arm structures lose efficiency for siRNA, PEGylated structures profit from the addition of twin disulfide motifs. Both findings can be explained by the stability profile of the corresponding polyplexes. T-shape and 3-arm structures already offer a suitable stability. Further increase of stability decreases transfection efficiency, most probably because the accessibility of the nucleic acid inside the cell is hindered. For PEGylated structures, the stability is

lower and seems to be a limiting factor. In this case, the increase of stability by the incorporation of the CRC motif increased the transfection efficiency. The lack of endosomal escape that was observed for PEGylated oligomers could be solved with INF7-modification in case of siRNA or chloroquine in case of pDNA. Since chloroquine is not suitable for *in vivo* applications, the incorporation of motifs increasing buffer capacity would be a valuable addition for pDNA delivery vehicles. This has been shown before. [62, 164]. The targeting effect of PEGylated polyplexes could be demonstrated by fluorescence microscopy. Particles could only be found in FR overexpressing KB cells when structures were equipped with folic acid. This result could be confirmed by flow cytometry. In addition to stability, the most important impact on biophysical properties can be observed in the size of the complexes. In general, cationic oligomers with cysteine residues and tyrosine trimers decreased in size by incorporation of CRC motifs. The influence of the decrease in size could nicely be observed in microscopy, where big particles were found for 3-arm oligomers. With the insertion of three CRC motifs small and equal distributed particles were found. In contrast, CRC incorporation into oleic acids-containing T-shape oligomers does not change the size of polyplexes. T-shape structures with hydrophobic stabilization are known to form uniform particles of small sizes even without cysteines [119, 137]. PEGylated structures with CRC form polyplexes with nucleic acid that are slightly bigger in size. For the polyplexes that decreased in size due to the incorporation of CRC, the zeta potential of particles increased. The influence on size and zeta potential of the particles might also be related to the protonated amino acid arginine that comes with the CRC motif. Twin disulfides might be a valuable tool to improve the stability and tune the size of cationic delivery systems to make them more suitable for different requirements. Improved serum stability and medium sizes (20 - 200 nm), big enough to minimize renal clearance and small enough to prevent capillary clogging, are important for *in vivo* studies. For oligoaminoethane-based oligomers, the most promising use for twin disulfides seems to be the enhancement of stability and transfection efficiency of PEG shielded, targeted structures.

4.2 Precise redox-sensitive cleavage sites for improved bioactivity of siRNA lipopolyplexes

In the first chapter, some oligomers were found to form polyplexes that are highly stable but showed decreased transfection efficiency. The carrier systems presented in this chapter are based on lipo-oligomers that already form stable polyplexes with siRNA. Beside high stabilization, the hydrophobic domains in these formulations offer endosomal membrane destabilization. Although high stability of siRNA polyplexes is desirable in the extracellular space and for cellular uptake, intracellular disassembly is important for the cytosolic release of siRNA and RNA-induced silencing complex formation. To improve the release, bioreducible sequence-defined lipo-oligomers were synthesized by solid-phase assisted synthesis using the disulfide building block Fmoc-succinoyl-cystamine for precise positioning of a disulfide unit between a lipophilic diacyl (bis-myristyl, bis-stearyl or bis-cholestanyl) domain and an ionizable oligocationic siRNA binding unit. The redox-triggered disassembly of lipopolyplexes could be demonstrated with gel shifts under reducing conditions. Whereas bioreducible structures showed a release of siRNA at intracellular concentrations of glutathione, the stable analogs did not respond. Major differences in membrane lytic activity could be observed for the different hydrophobic diacyl units used. Cholanic acid and stearic acid showed only moderate lytic activity. In contract, myristic acid revealed high lytic activity, especially at endosomal pH. Higher rates of membrane fusion events for dimyristyl lipids were reported in literature [136]. The pH sensitivity of the structures can be explained by the ionizable cationic backbone that is used for nucleic acid binding. With further protonation the interaction of structures with cell membrane increases. Only for bioreducible structures, the lytic activity could be abolished after incubation with glutathione at intracellular concentrations (10 mM). Consistent with glutathione-triggered siRNA release and reduced lytic activity, the reducible siRNA polyplexes show lower cytotoxicity and higher gene silencing efficacy in Neuro2A and DU145 cells than their stable analogs. In case of HeLa cell - derived KB cells, these properties decreased gene silencing efficiency. High extracellular disulfide cleavage was actually previously reported for HeLa cells [108]. Disulfide cleavage occurring at the extracellular cell surface might be an explanation for this finding. Reduction of the lipo-oligomer results in a short cationic strand and an uncharged lipid. The separated units

do not have amphiphilic character anymore, which can be responsible for endosomolytic activity but also enhanced cytotoxicity.

In sum, those siRNA carriers offer increased gene silencing efficacy in certain cell lines by combining extracellular polyplex stability, siRNA release under cytosolic conditions, and a high lytic activity under endosomal conditions with low cytotoxicity. Nevertheless, for cell lines with exceptional redox environments, the redox-sensitivity of carriers can also be a disadvantage.

4.3 Functionalized poly(sarcosine) as shielding agent for lipopolyplexes

In the previous chapter, a new class of redox-sensitive lipo-oligomers was successfully established for siRNA delivery. Beside beneficial effects of lipid-based delivery systems such as enhanced nanoparticle stability and endosomal escape capability, the distribution *in vivo* is often limited to certain tissues such as liver, lung and spleen [146, 165, 166]. In previous studies, it has been shown that T-shape oligomers similar to the ones that were synthesized in this approach show the strongest retention in liver tissue [119, 146]. Those effects might be related to a high stickiness of unshielded particles, but it is also possible that particular serum proteins incorporate on nanoparticle surfaces and impair tissue specificity [166-169]. An efficient shielding should reduce both interactions and enables a better distribution in the body. For this reason, one of the best performing candidates from redox-sensitive lipo-oligomers was chosen and extended by a click-reactive azido-function, resulting in carrier ***1073***. After the formation of siRNA lipopolyplexes, the particle surface was further modified with the shielding agent poly(sarcosine). The shielding ability was demonstrated in several assays. Poly(sarcosine) shielded particles were able to migrate in agarose gels under electric field, whereas unshielded polyplexes were immobile. The property of particles to migrate in gel structures is beneficial. Particles which are well migrating through the extracellular matrix, for instance, can reach cells more easily. The surface charge of polyplexes was strongly decreased when particles were shielded. As a result, the unspecific interaction with cells and thereby also the uptake was decreased. The biodistribution in mice revealed that 8 kDa poly(sarcosine) can strongly expand the circulation of the siRNA lipopolyplexes. Signals in paws of animals could be observed even after 24 h. The circulation was similar with 5 kDa PEG. Unshielded polyplexes

showed a strong retention in the liver. This shows that a sufficient shielding prevents the delivery of particles to certain tissues and changes distribution.

Besides the reduction of interactions with non-target tissue, a delivery system needs to be equipped with a ligand to target specific cells. In this approach folic acid was used. An interesting finding was the change in size of nanoparticles when folic acid was involved. For small degrees of particle modification with PSarFolA, the size of polyplexes did not significantly change compared to unshielded polyplexes (~170 nm). For higher amounts, aggregates were measured in DLS. Similar findings were observed for folic acid targeted lipo-polyplexes before in our lab by Katharina Müller et al. [148]. In this work, aggregation could be avoided by incorporation of tetra-glutamylated folic acid into the shielding agent. For further increase of PSarFolA to equimolar amounts, small defined particles of ~25 nm could be measured. The "reassembly process" towards small siRNA polyplexes is hard to explain. The influence of folic acid plays a major role in this process, since it was not observed for untargeted poly(sarcosine) shielded particles.

The specific binding of poly(sarcosine) folic acid functionalized polyplexes to FR-positive KB cell membranes could be demonstrated. Despite, the uptake into the cell did not work properly. The reasons for this clear effect are not fully understood. For both assays, ***1073*** polyplexes were functionalized with equimolar amounts of PSarFolA to form defined ~25 nm particles. One possible explanation for insufficient uptake is the choice of a bioreducible carrier (***1073***) which was found to be unsuitable for gene silencing in KB cells, most likely due to premature lipopolyplex disassembly. Cell biology aspects might be the basis for other explanations. In contrast to nonclathrin, noncaveolar endocytosis pathways reported for the vitamin folic acid [150, 151], for folate-targeted nanoparticles, caveolae- and clathrin-mediated endocytosis pathways were found via folate receptors [152-154]. The size of the nanoparticle and the ligand density on their surface were reported to influence the cellular uptake pathway. The well shielding ~8 kDa poly(sarcosine) seems to prevent the internalization despite the presence of a folate ligand. The strong shielding might prevent any further interaction of the lipo-cationic core with the cell membrane. The lack of gene silencing activity is a consequence of insufficient uptake. It should also be considered that ***1073*** contains the bioreducible disulfide building block (ssbb), which previously was found to delete gene silencing ability in KB cells by premature disulfide cleavage (see section 3.2, **Fig.**

43, compare ***991*** with ***992***). In conclusion, further work for example removal of the ssbb unit or fine-tuning of the shielding agent (see chapter 4.4) needs to be performed to combine *in vivo* shielding with functional receptor-targeted gene silencing.

4.4 Folate receptor-directed orthogonal click-functionalization of siRNA lipopolyplexes for tumor-targeted gene silencing *in vivo*

The previous chapter indicated that strong shielding might also prevent the uptake via certain receptor-mediated pathways. Therefore, the focus of this chapter aims at the optimization of a DBCO functionalized PEG shielding agent with folic acid as a ligand. Solid phase synthesis was used to obtain sequence defined shielding and targeting agents where every unit can precisely be adapted. Mono- and bis-DBCO agents, varying in PEG length were analyzed to serve as surface modifying compounds for siRNA lipopolyplexes. The lipo-oligomer ***991*** was chosen for forming core polyplexes that are active in folic receptor-positive KB cells (see chapter 3.2) and extended by a click-reactive azido-function to yield oligomer ***1106***. The shielding ability of agents increased with increasing equivalents, but the polyplex stability in serum decreased. 0.5 equivalents of an agent were found to be a suitable compromise. Structural details of the agents had a stronger impact on the polyplex properties than the degree of modification. Zeta potential strongly decreased with increasing PEG length. A notable disadvantage of long PEG chains was the formation of aggregates as detectable with DLS. Although those aggregates could not be observed in TEM images, it makes those formulations less reliable. Similar findings were observed for folic acid targeted lipo-polyplexes before [148]. The issues described for DLS size measurements with folic acid modified polyplexes have some things in common. Polyplexes with a surface charge higher than ~15 mV do not aggregate with folic acid. The hydrophobic character of folic acid might explain the clustering of polyplexes by PEG agents. After the reaction with the surface of polyplexes, this might result in polyplex accumulation. In case of weaker shielding, the positive residual charge of polyplexes might repulse and separate particles. When the surface charge is reduced, due to high equivalents of agents, or longer PEG chains, the particles might remain clustered together. In other work, the aggregation could be prevented by the incorporation of tetra-glutamylated folic acid into the shielding agent [148]. Due to the glutamates, an inversion towards

negative surface charge could be observed. However, *in vivo* stability was found to limit the formulations biodistribution.

For mono-DBCO structures, the binding to folic acid receptor (FR) positive KB cells was not influenced by the length of PEG. For bis-DBCO structures, the binding ability decreased with increasing PEG length. It cannot be excluded that bioreducible spacer blocks incorporated into the bivalent DBCO structures might be responsible for the weak binding, due to premature cleavage on the cell surface. More critically, only polyplexes with short PEG chains were internalized into cells, irrespective of the presence/absence of bioreducible linkages. In the previous chapter, we could also observe that well shielding poly(sarcosine) folic acid targeted polyplexes bind to KB cells, but cannot get internalized (see chapter 4.3). The reasons for insufficient internalization into cells are not yet understood. The trafficking of the vitamin folate via folate receptors is thought to occur by a non nonclathrin, noncaveolar pathway also known as CLIC/GEEC endocytosis pathway [150, 151]. Previously caveolae were thought to be involved in the uptake pathway [157]. It could be demonstrated that the uptake pathway indeed changes to caveolae-mediated endocytosis when glycosyl-phosphatidylinositol-anchored proteins (GPI-AP), like the folate-receptor, were cross-linked on cell surfaces [150, 158]. For folate targeted nanoparticles, uptake pathways like caveolae- and clathrin-mediated endocytosis were found [152-154]. The size of the nanoparticle and the ligand-density on their surface were reported to influence the cellular uptake pathway. Bigger size and higher density of folate on the particle surface was reported to shift the internalization pathway from caveolae- to clathrin-mediated endocytosis. [152-154]. Both parameters did also change for longer PEG_{48} and PEG_{72} chains in targeted ***1106*** siRNA polyplexes. Due to more spacious PEG agents, the density of the ligands on the surface decreases. The stability of the system decreases and the sizes are not reliable (aggregates could be measured in DLS) with longer PEG chains. The resulting particle properties seem to be unfavorable for the polyplex internalization. Furthermore, shorter PEG agents decrease the distance of the particle surface to the lipo-cationic core, resulting in a higher zeta potential. Although cationic charges might facilitate additional contacts with the negatively charged cell surface (often sugar polymers in membrane proteins like HSPG [170] or syndecan [171]), the remaining positive surface charge alone cannot be the explanation for better

internalization. Neutral and negatively charged folate-targeted systems are also known to be internalized via folate receptors [148, 172].

Consistent with the uptake data, the targeted polyplexes with short PEG_{24} revealed much higher gene silencing in KB cells then their long PEG analogs. For L1210 FR-positive murine leukemic cells, targeted siEG5 formulations with short PEG_{24} sequence were also superior in inducing cell cycle arrest in G2 stage. The folic acid ligand plays a crucial role for an efficient gene delivery. Compared to unshielded and partly shielded polyplexes without ligand, folic acid targeted polyplexes showed much higher silencing efficiency. This influence became even more obvious in biodistribution studies in mice. Targeted structures with short PEG_{24} chain showed strong retention at the tumor site, whereas the untargeted analog quickly accumulates in the liver. The advantage of two DBCO functions in one shielding agent became clear in biodistribution studies as well. Due to crosslinking ability, the stability of polyplexes might be increased, resulting in longer circulation and tumor retention. An interesting observation was the longer systemic retention of folate-targeted formulations in various tissues different from the tumor. In other experiments, we observed L1210 tumor metastases in spleen and liver two weeks after subcutaneous injection of leukemia cells into mice. Metastases might be a reasonable explanation for the retention of targeted polyplexes at different tumor cell-containing parts of the body. For longer PEG chains, instability and quick renal clearance of siRNA were observed. With bis-DBCO, this disadvantageous phenomena could also be reduced.

Comparing all experiments, the siRNA polyplex formation with 0.5 equivalents of bis-DBCO with short PEG_{24} and folic acid was overall best-performing. This formulation has a suitable size of <200 nm by DLS and TEM, high polyplex stability in serum, sufficient binding, uptake and transfection efficiency and the best biodistribution and tumor retention of all tested formulations. This formulation was then tested for gene silencing *in vivo* and showed ~60 % mRNA knock-down in subcutaneous FR-positive leukemic tumors of mice. No significant side effects were recognized based on the body weight analysis and clinical chemistry of blood samples.

5 Summary

The therapy with nucleic acids like pDNA or siRNA is a field of major importance and continually growing interest. Live threatening, severe diseases including cancer obtain a new chance for treatment by the use of gene therapy. Efficient delivery of nucleic acids is still a major challenge. There are a lot of requirements for a carrier to work as a gene delivery system: A suitable size, big enough to prevent rapid renal elimination but not too big to block fine capillaries; low unspecific interactions with blood components and non-target cells but high affinity to target cells; high stability outside the cell, efficient uptake, an escape mechanism from the endosome and facilitated disassembly inside the cytoplasm. The recent development of a solid-phase synthesis platform for the assembly of sequence-defined oligo(ethanamino)amides enables quick and easy synthesis of cationic oligomers for complexing nucleic acids. Beside specialized cationic building blocks, all natural amino acids, and further units can be incorporated to customize those delivery systems. The modular synthesis of gene delivery vehicles is an effective way to precisely optimize the function of carriers. In this thesis, two strategies were tested to enrich the library of oligocationic carriers by new redox-sensitive structures. Further, delivery systems were equipped with shielding and targeting domains and tested in animal studies.

The first part reveals that the incorporation of a twin disulfide forming CRC motif into various types of sequence-defined oligoamino acid based pDNA and siRNA carriers improves the stability of the resulting polyplexes. This was observed in the presence of serum and under reducing conditions. This increase of stability does not necessarily result in better transfection efficiency. For pDNA polyplexes, the inclusion of twin disulfides triggers only minor overall differences. The influence of the motif on siRNA transfection efficiency ranges from total abolishment to significant increase. While T-shape lipo-oligomer and 3-arm structures lose efficiency for siRNA, PEGylated structures profit from the addition of twin disulfide motifs. In addition to stability, the most important impact on biophysical properties can be observed in the size of the complexes. In general, cationic oligomers with cysteine residues and tyrosine trimers decreased in size by incorporation of CRC motifs. In contrast, CRC incorporation into oleic acids- or PEG-containing oligomers leads to an increase in size. Twin disulfides

might be a valuable tool to improve the stability and tune the size of cationic delivery systems to make them more suitable for different requirements.

In the second part, we presented bioreducible lipo-oligomers as siRNA carriers. In certain cell lines, the redox-sensitivity of those carriers strongly increased gene silencing efficacy by combining extracellular polyplex stability with siRNA release under cytosolic conditions, and a high lytic activity under endosomal conditions with low cytotoxicity. These apparently contradictory functional characteristics were programmed into the carriers by the introduction of a bioreducible disulfide bond between the cationic backbone and the hydrophobic domain. Precise positioning was enabled by a Fmoc-protected cystamine building block compatible with solid phase-assisted synthesis. The use of redox-sensitive carriers should be evaluated separately for each cell line, since reductive cleavage conditions may differ in cells with exceptional redox environment.

In the third part, the redox-sensitive lipo-oligomer ***992*** was extended by a click-reactive azido-function, resulting in carrier ***1073***. After the formation of siRNA lipopolyplexes, the particle surface was further modified with the shielding agent poly(sarcosine). Poly(sarcosine) shielded particles were able to migrate in agarose gels under electric field, whereas unshielded polyplexes were immobile. The surface charge of polyplexes was strongly decreased when particles were shielded. As a result, the unspecific interaction with cells and thereby also the uptake was decreased. The biodistribution in mice revealed that 8 kDa poly(sarcosine) can strongly expand the circulation of the siRNA lipopolyplexes. Signals in paws of animals could be observed even after 24 h. The circulation was similar with 5 kDa PEG. Unshielded polyplexes showed a strong retention in the liver. Folic acid modified poly(sarcosine) (PSarFolA) was then used for targeting the folate receptor (FR) positive cells. An interesting finding was the change in size of nanoparticles. For small degrees of particle modification with PSarFolA, the size of polyplexes did not significantly change compared to unshielded polyplexes (~170 nm). Increasing amounts resulted in aggregates (determined by DLS) and further increase to equimolar amounts of PSarFolA and ***1073*** led to small defined particles of ~25 nm. The specific binding of PSarFolA functionalized polyplexes to FR-positive KB cells could be demonstrated, but no uptake into cells was observed. As a consequence and probably because of the redox-sensitive carrier ***1073***, which is unfavorable for KB cells, the targeted system did not mediate any gene silencing.

In the fourth part, the lipo-oligomer ***991*** was extended by a click-reactive azido-function to yield oligomer ***1106***. siRNA polyplexes with non-reducible oligomers showed favorable gene silencing activity in folic receptor-positive KB cells. Polyplexes formed with 1106 were then modified with a DBCO functionalized PEG shielding agent with folic acid as a ligand. For precise optimization of the agents, solid phase synthesis was used. Different defined shielding and targeting agents with mono- and bis-DBCO and varying PEG length were synthesized and tested. We could show that the bivalent DBCO structure with short PEG_{24} sequence was superior in terms of particle formation, serum stability, receptor targeting, cellular uptake and gene silencing ability. Biodistribution assays with subcutaneous FR-positive L1210 tumor-bearing mice revealed the longest retention at the tumor site. The formulation was then tested for gene silencing *in vivo* and showed ~60 % mRNA knockdown. No significant side effects were recognized based on the body weight analysis and clinical chemistry of blood samples.

6 Appendix

6.1 Abbreviations

AB_5	Proteinic toxin complex containing 1 subunit A and 5 subunits B
Ac_2O	Acetic anhydride
bp	Base pair
bPEIS	Branched bioreducible polyethylenimine sulfide
Boc	*tert*-Butoxycarbonyl protecting group
BODIPY	Boron-dipyrromethene
CholA	5β-Cholanic acid
DBCO	Dibenzocyclooctyne group
DCM	Dichloromethane
DCVC	Dry column vacuum chromatography
DETA	Diethylene triamine
DIPEA	*N,N*-Diisopropylethylamine
DLS	Dynamic light scattering
DMEM	Dulbecco's modified Eagle's medium
DMF	*N,N*-Dimethylformamide
DNA	Desoxyribonucleic acid
DSP	Dithiodipropionic acid di(N-succinimidyl ester)
dsRNA	Double-stranded RNA
EDA	Ethylene diamine
EDTA	Ethylendiaminetetraacetic acid
EGFP	Enhanced green fluorescent protein
EHCO	N-(1-aminoethyl) iminobis[N-(oleoyl- cysteinyl-histidinyl-1-aminoethyl) Propionamide]
ER	Endoplasmatic reticulum
ERAD	Endoplasmatic reticulum-associated degradation
EtBr	Ethidium bromide
FBS	Fetal bovine serum
FCS	Fluorescence correlation spectroscopy
Fmoc	Fluorenylmethoxycarbonyl protecting group

FolA	Folic acid
FR	Folate receptor
GFP	Green fluorescent protein
GSH	Glutathione
Gtt	Glutaroyl triethylene tetramine
HBG	Hepes-buffered glucose
HBTU	2-(1H-benzotriazole-1-yl)-1,1,3,3-tetramethyluronium hexafluorophosphate
HDO	Oligoethylenimine with 1,6-hexandiol diacrylate
HEPES	*N*-(2-hydroxethyl) piperazine-N‘-(2-ethansulfonic acid)
HIV-1	Human immunodeficiency virus 1
HMW	High molecular weight
HOBt	1-Hydroxybenzotriazole
INF7	An endosomolytic influenza virus derived peptide
ivDde	1-(4,4-dimethyl-2,6-dioxocyclohex-1-ylidene)-3-methylbutyl protecting group
kDa	Kilodalton
LMW	Low molecular weight
LPEI	Linear polyethylenimine
MeCN	Acetonitrile
mM	Millimolar
mRNA	Messenger RNA
MTBE	Methyl *tert*-butyl ether
MTT	3-(4,5-dimethylthiazol-2-yl)-2,5-diphenyltetrazolium bromide
mV	Millivolt
MWCO	Molecular weight cut-off
MyrA	Myristic acid
N/P	Nitrogen to phosphates ratio
NEM	N-ethylmaleimide
NHS	*N*-Hydroxysuccinimide
nm	Nanometer
NMP	*N*-Methyl-2-pyrrolidone
NMR	Nuclear magnetic resonance
OEI	Oligoethylenimine

OleA	Oleic acid
PAA	Polyamino acid
PAEI	Poly(amido ethylenimine)
pCMVLuc	Plasmid encoding for firefly luciferase under the control of the cytomegalie virus (CMV) promoter
PDI	Polydispersity index
pDNA	Plasmid DNA
PEG	Polyethylene glycol
PEI	Polyethylenimine
PEIS	Bioreducible polyethylenimine sulfide
PIC	Polyion complex
pKa	$-\log_{10} K_a$ (acid dissociation constant)
PyBOP	Benzotriazol-1-yloxy-tripyrrolidinophosphonium hexafluorophosphate
RISC	RNA-induced silencing complex
RLU	Relative light units
RNA	Ribonucleic acid
RP-HPLC	Reversed-phase high-performance liquid chromatography
RPC	Reducible polycation
RT	Room temperature
SEC	Size-exclusion chromatography
siRNA	Small interfering RNA
SPAAC	Strain-promoted alkyne-azide cycloaddition
Sph	Succinoyl-pentaethylene hexamine
SPS	Solid-phase synthesis
SteA	Stearic acid
Stp	Succinoyl-tetraethylene pentamine
SV40	Simian virus 40
TAT	Trans-Activator of Transcription
TBE	Tris-boric acid-EDTA buffer
TEPA	Tetraethylene pentamine
TETA	Triethylene tetramine
TFA	Trifluoroacetic acid
THF	Tetrahydrofuran
TIS	Triisopropylsilane

6.2 Summary of SPS derived oligomers

Table 18 Summary of SPS derived oligomers

Oligomer ID	Topology	Sequence (C→N)	Proton. Amines	Chapter
49	T-Shape	C-Stp_2-K-ε[K-α,ε($OleA)_2$]αStp_2-C	13	3.1
386	3-arm	C-Stp_3-K-ε[-Stp_3-C]αStp_3-C	29	3.1
413	T-Shape	C-Stp_2-K-ε[K-α,ε($NH_2)_2$]αStp_2-C	13	3.1
454	T-Shape	C-Y_3-Stp_2-K-ε[K-α,ε($OleA)_2$]αStp_2-Y_3-C	13	3.1
464	T-Shape	C-Y_3-Stp_2-K-ε[K-α,ε($Y_3)_2$]αStp_2-Y_3-C	13	3.1
465	T-Shape	C-Y_3-Stp_2-K-ε[K-α,ε($NH_2)_2$]αStp_2-Y_3-C	13	3.1
468	T-Shape	C-Stp_2-K-ε[K-α,ε($Y_3)_2$]αStp_2-C	13	3.1
591	T-Shape	CRC-Stp_2-K-ε[K-α,ε($NH_2)_2$]αStp_2-CRC	15	3.1
592	T-Shape	CRC-Stp_2-K-ε[K-α,ε($OleA)_2$]αStp_2-CRC	15	3.1
593	T-Shape	CRC-Stp_2-K-ε[K-α,ε($Y_3)_2$]αStp_2-CRC	15	3.1
594	T-Shape	CRC-Y_3-Stp_2-K-ε[K-α,ε($NH_2)_2$]αStp_2-Y_3-CRC	15	3.1
595	T-Shape	CRC-Y_3-Stp_2-K-ε[K-α,ε($OleA)_2$]αStp_2-Y_3-CRC	15	3.1
596	T-Shape	CRC-Y_3-Stp_2-K-ε[K-α,ε($Y_3)_2$]αStp_2-Y_3-CRC	15	3.1
652	3-arm	CRC-Stp_3-K-ε[-Stp_3-C]αStp_3-C	30	3.1
653	3-arm	C-Stp_3-K-ε[-Stp_3-CRC]αStp_3-CRC	31	3.1
654	3-arm	CRC-Stp_3-K-ε[-Stp_3-CRC]αStp_3-CRC	32	3.1
736	PEG 2-arm	K-ε[-PEG_{24}-SucA]α K-ε[-Stp_4-C]αStp_4-C	26	3.1
737	PEG 2-arm	K-ε[-PEG_{24}-FolA]α K-ε[-Stp_4-C]αStp_4-C	26	3.1
738	PEG 2-arm	K-ε[-PEG_{24}-SucA]α K-ε[-Stp_4-CRC]αStp_4-CRC	28	3.1
739	PEG 2-arm	K-ε[-PEG_{24}- FolA]α K-ε[-Stp_4-CRC]αStp_4-CRC	28	3.1
740	-	W-Stp_2-ssbb-L_3-W	7	3.2
782	U-shape	K-αK-α,ε[Stp3-ssbb-($CholA)_2]_2$	19	3.2
783	U-shape	K-αK-α,ε[Stp3-($CholA)_2]_2$	19	3.2
871	i-Shape	Stp_4-H_6-K-α,ε(CholA)	12	3.2
969	i-Shape	Stp_4-H_6-ssbb-K-α,ε($CholA)_2$	12	3.2
989	T-Shape	Y_3-Stp_2-K-ε[G-K-α,ε($SteA)_2$]αStp_2-Y_3	13	3.2
990	T-Shape	Y_3-Stp_2-K-ε[G-ssbb-K-α,ε($SteA)_2$]αStp_2-Y_3	13	3.2
991	T-Shape	Y_3-Stp_2-K-ε[G-K-α,ε($CholA)_2$]αStp_2-Y_3	13	3.2
992	T-Shape	Y_3-Stp_2-K-ε[G-ssbb-K-α,ε($CholA)_2$]αStp_2-Y_3	13	3.2, 3.3
1073	T-Shape	Y_3-Stp_2-K-ε[G-ssbb-K-α,ε($CholA)_2$]αStp_2-Y_3-K-ε(N_3)	13	3.3
1081	T-Shape	Y_3-Stp_2-K-ε[G-K-α,ε($MyrA)_2$]αStp_2-Y_3	13	3.2
1082	T-Shape	Y_3-Stp_2-K-ε[G-ssbb-K-α,ε($MyrA)_2$]αStp_2-Y_3	13	3.2
1086	T-Shape	K-ε(N_3)-Y_3-Stp_2-K-ε[G-ssbb-K-α,ε($CholA)_2$]αStp_2-Y_3-K-ε(N_3)	13	3.3
1106	T-Shape	Y_3-Stp_2-K-ε[G-K-α,ε($CholA)_2$]αStp_2-Y_3-K-ε(N_3)	13	3.4
1107	T-Shape	Y_3-Stp_2-K-ε[G-K-α,ε($OleA)_2$]αStp_2-Y_3	13	3.2
1108	T-Shape	Y_3-Stp_2-K-ε[G-ssbb-K-α,ε($OleA)_2$]αStp_2-Y_3	13	3.2

6.3 Summary of SPS derived shielding agents

Table 19 Summary of SPS derived shielding agents

ID	Name	Sequence (C→N)	Chapter
1138	***DBCO-PEG_{24}***	PEG_{24}-DBCO	3.4
1139	***DBCO-PEG_{24}-FolA***	K-ε(PEG_{24}-DBCO)-FolA	3.4
1140	***DBCO-PEG_{48}-FolA***	K-ε[($PEG_{24})_2$-DBCO]-FolA	3.4
1141	***DBCO-PEG_{72}-FolA***	K-ε[($PEG_{24})_3$-DBCO]-FolA	3.4
1145	***$DBCO_2$-SS_2-PEG_{24}-FolA***	K-ε[PEG_{24}-K-α,ε(ssbb-$DBCO)_2$]-FolA	3.4
1146	***$DBCO_2$-SS_2-PEG_{48}-FolA***	K-ε[($PEG_{24})_2$-K-α,ε(ssbb-$DBCO)_2$]-FolA	3.4
1147	***$DBCO_2$-SS_2-PEG_{72}-FolA***	K-ε[($PEG_{24})_3$-K-α,ε(ssbb-$DBCO)_2$]-FolA	3.4

6.4 Analytical Data

6.4.1 ^{1}H NMR spectrum of disulfide-linker building block(ssbb)

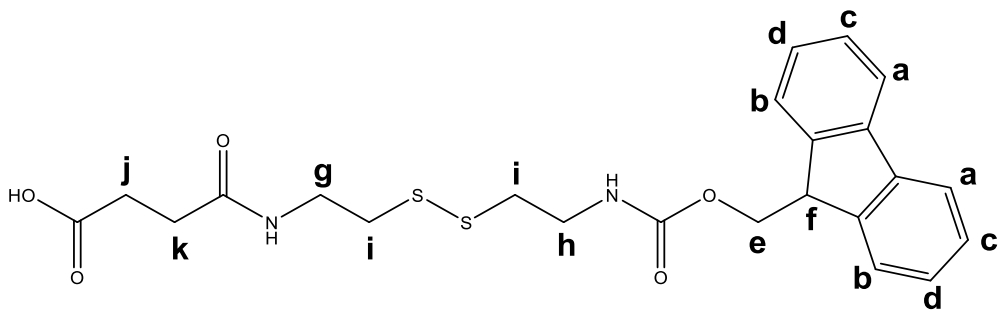

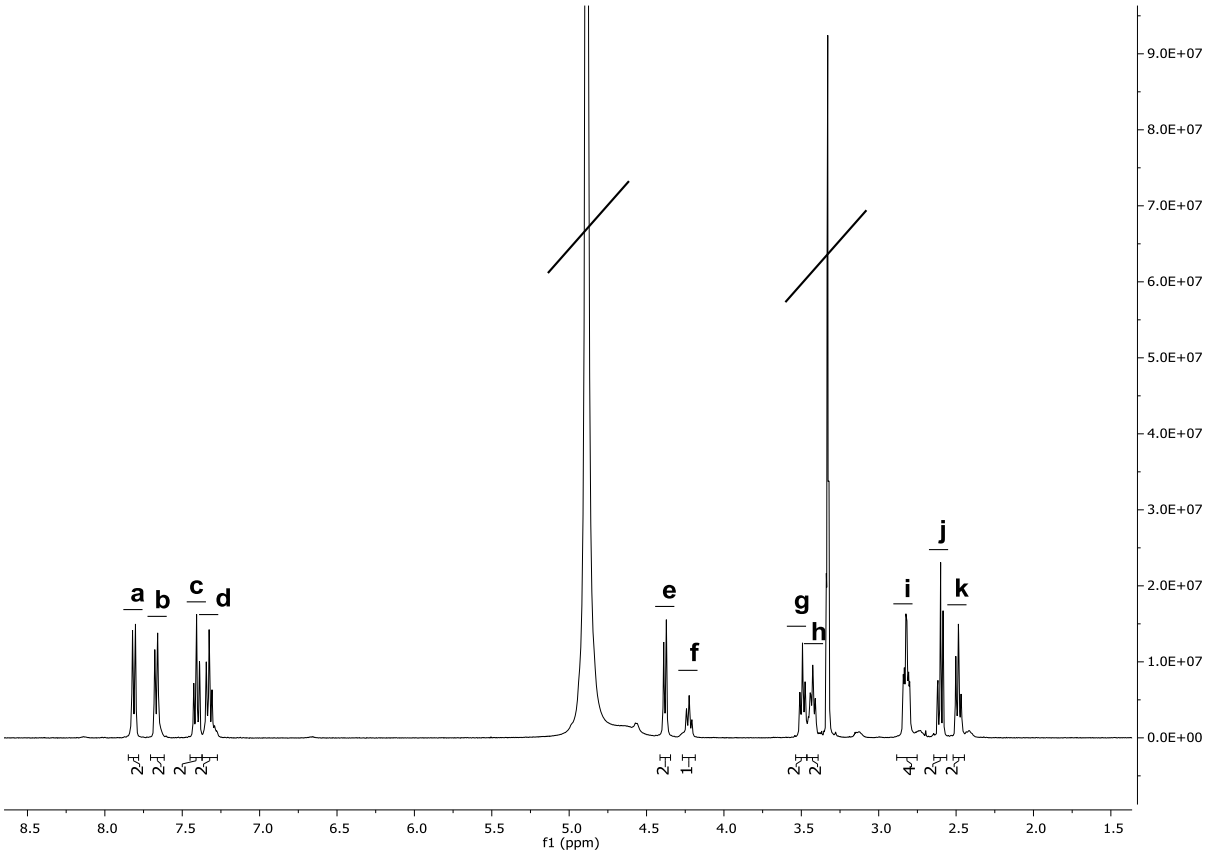

1-(9H-fluoren-9-yl)-3,12-dioxo-2-oxa-7,8-dithia-4,11-diazapentadecan-15-oic acid (ssbb) ^{1}H NMR (500 MHz, Methanol-d4) δ (ppm) 7.81 (d, J = 7.5 Hz, H*a*, 2H), 7.67 (d, J = 7.4 Hz, H*b*, 2H), 7.41 (t, J = 7.4 Hz, H*c*, 2H), 7.33 (t, J = 7.4 Hz, H*d*, 2H), 4.38 (d, J = 6.9 Hz, H*e*, 2H), 4.22 (t, J = 6.8 Hz, H*f*, 1H), 3.49 (t, J = 6.7 Hz, H*g*, 2H), 3.43 (t, J = 6.7 Hz, H*h*, 2H), 2.76-2.87 (m, H*i*, 4H), 2.60 (t, J = 6.6 Hz, H*j*, 2H), 2.48 (t, J = 6.8 Hz, H*k*, 2H).

6.4.2 ^{1}H NMR spectra of oligomers

49: **^{1}H NMR (400 MHz, Deuterium oxide)** δ (ppm) = 0.7-0.8 (s, 6 H, -CH3 oleic acid), 1.0-2.25 (m, 68 H, βγδH lysine, -CH2- oleic acid), 2.4-2.6 (m, 16 H, -CO-CH2-CH2-CO-), 2.8-3.1 (m, 8 H, εH lysine and cysteine), 3.15-3.6 (m, 64 H, -CH2- Tp), 4.0-4.5 (m, 4 H, αH amino acids), 5.15-5.3 (m, 4 H, -CH- oleic acid).

386: **^{1}H NMR (400 MHz, Deuterium oxide)** δ (ppm) = 1.15-2.0 (m, 6 H, βγδH lysine), 2.35-2.65 (m, 36 H, -CO-CH2-CH2-CO-), 2.8-3.1 (m, 8 H, εH lysine and cysteine), 3.11-3.3 (m, 36 H, -CH2- Tp), 3.32-3.67 (m, 108 H, -CH2- Tp), 4.09-4.4 (m, 4 H, αH amino acids).

413: **^{1}H NMR (400 MHz, Deuterium oxide)** δ (ppm) = 1.1-1.9 (m, 12 H, βγδH lysine), 2.4-2.7 (m, 16 H, -CO-CH2-CH2-CO-), 2.8-3.1 (m, 8 H, εH lysine and cysteine), 3.1-3.6 (m, 64 H, -CH2- Tp), 3.8-4.4 (m, 4 H, αH amino acids).

454: **^{1}H NMR (400 MHz, Deuterium oxide)** δ (ppm) = 0.7-0.8 (s, 6 H, -CH3 oleic acid), 0.8-2.0 (m, 68 H, βγδH lysine, -CH2- oleic acid), 2.3-2.6 (m, 16 H, -CO-CH2-CH2-CO-), 2.6-3.1 (m, 20 H, εH lysine, tyrosine and cysteine), 3.1-3.6 (m, 64 H, -CH2- Tp), 4.0-4.6 (m, 10 H, αH amino acids), 5.15-5.3 (m, 4 H, -CH- oleic acid), 6.65-7.35 (m, 24 H, -CH- tyrosine).

464: **^{1}H NMR (400 MHz, Deuterium oxide)** δ (ppm) = 1.1-1.9 (m, 12 H, βγδH lysine), 2.3-2.6 (m, 16 H, -CO-CH2-CH2-CO-), 2.6-3.1 (m, 32 H, εH lysine, cysteine and tyrosine), 3.1-3.6 (m, 64 H, -CH2- Tp), 3.8-4.5 (m, 16 H, αH amino acids), 6.65-7.15 (m, 48 H, -CH- tyrosine).

465: **^{1}H NMR (400 MHz, Deuterium oxide)** δ (ppm) = 1.1-1.8 (m, 12 H, βγδH lysine), 2.3-2.6 (m, 16 H, -CO-CH2-CH2-CO-), 2.6-3.1 (m, 20 H, εH lysine, cysteine and tyrosine), 3.1-3.6 (m, 64 H, -CH2- Tp), 3.7-4.5 (m, 10 H, αH amino acids), 6.65-7.15 (m, 24 H, -CH- tyrosine).

468: **^{1}H NMR (400 MHz, Deuterium oxide)** δ (ppm) = 0.9-1.9 (m, 12 H, βγδH lysine), 2.3-2.6 (m, 16 H, -CO-CH2-CH2-CO-), 2.6-3.1 (m, 20 H, εH lysine, cysteine and tyrosine), 3.1-3.6 (m, 64 H, -CH2- Tp), 3.75-4.5 (m, 10 H, αH amino acids), 6.65-7.15 (m, 24 H, -CH- tyrosine).

591: **^{1}H NMR (400 MHz, Deuterium oxide)** δ (ppm) = 1.2-2.0 (m, 20 H, βγδH lysine and βγH arginine), 2.4-2.6 (m, 16 H, -CO-CH2-CH2-CO-), 2.8-3.2 (m, 16 H, εH lysine, δH arginine and cysteine), 3.2-3.7 (m, 64 H, -CH2- Tp), 3.8-4.4 (m, 8 H, αH amino acids).

592: **^{1}H NMR (400 MHz, Deuterium oxide)** δ (ppm) = 0.7-0.9 (s, 6 H, -CH3 oleic acid), 1.0-2.3 (m, 76 H, βγδH lysine and βγH arginine, -CH2- oleic acid), 2.4-2.6 (m, 16 H, -CO-CH2-CH2-CO-), 2.8-3.2 (m, 16 H, εH lysine, δH arginine and cysteine), 3.2-3.7 (m, 64 H, -CH2- Tp), 4.0-4.5 (m, 8 H, αH amino acids), 5.15-5.3 (m, 4 H, -CH- oleic acid).

593: **^{1}H NMR (400 MHz, Deuterium oxide)** δ (ppm) = 0.9-1.9 (m, 20 H, βγδH lysine and βγH arginine), 2.4-2.6 (m, 16 H, -CO-CH2-CH2-CO-), 2.6-3.2 (m, 28 H, εH lysine, δH arginine, cysteine and tyrosine), 3.2-3.7 (m, 64 H, -CH2- Tp), 3.8-4.6 (m, 14 H, αH amino acids), 6.6-7.1 (m, 24 H, -CH- tyrosine).

594: **^{1}H NMR (400 MHz, Deuterium oxide)** δ (ppm) = 1.1-1.8 (m, 20 H, βγδH lysine and βγH arginine), 2.3-2.6 (m, 16 H, -CO-CH2-CH2-CO-), 2.6-3.1 (m, 28 H, εH lysine, δH arginine, cysteine and tyrosine), 3.1-3.6 (m, 64 H, -CH2- Tp), 3.8-4.6 (m, 14 H, αH amino acids), 6.65-7.15 (m, 24 H, -CH- tyrosine).

595: **^{1}H NMR (400 MHz, Deuterium oxide)** δ (ppm) = 0.5-0.7 (s, 6 H, -CH3 oleic acid), 0.8-1.9 (m, 76 H, βγδH lysine and βγH arginine, -CH2- oleic acid), 2.3-2.6 (m, 16 H, -CO-CH2-CH2-CO-), 2.6-3.1 (m, 28 H, εH lysine, δH arginine, tyrosine and cysteine), 3.1-3.6 (m, 64 H, -CH2- Tp), 4.0-4.6 (m, 14 H, αH amino acids), 5.15-5.3 (m, 4 H, -CH- oleic acid), 6.65-7.35 (m, 24 H, -CH- tyrosine).

596: **^{1}H NMR (400 MHz, Deuterium oxide)** δ (ppm) = 0.9-1.9 (m, 20 H, βγδH lysine and βγH arginine), 2.3-2.55 (m, 16 H, -CO-CH2-CH2-CO-), 2.6-3.1 (m, 40 H, εH lysine, δH arginine, cysteine and tyrosine), 3.1-3.6 (m, 64 H, -CH2- Tp), 3.8-4.6 (m, 20 H, αH amino acids), 6.65-7.15 (m, 48 H, -CH- tyrosine).

652: **^{1}H NMR (400 MHz, Deuterium oxide)** δ (ppm) = 1.15-2.0 (m, 10 H, βγδH lysine and βγH arginine), 2.35-2.65 (m, 36 H, -CO-CH2-CH2-CO-), 2.8-3.1 (m, 12 H, εH lysine, δH arginine and cysteine), 3.11-3.3 (m, 36 H, -CH2- Tp), 3.32-3.67 (m, 108 H, -CH2- Tp), 4.09-4.4 (m, 6 H, αH amino acids).

653: **^{1}H NMR (400 MHz, Deuterium oxide)** δ (ppm) = 1.15-2.0 (m, 14 H, βγδH lysine and βγH arginine), 2.35-2.65 (m, 36 H, -CO-CH2-CH2-CO-), 2.8-3.1 (m, 16 H, εH lysine, δH arginine and cysteine), 3.11-3.3 (m, 36 H, -CH2- Tp), 3.32-3.67 (m, 108 H, -CH2- Tp), 4.09-4.4 (m, 8 H, αH amino acids).

654: **^{1}H NMR (400 MHz, Deuterium oxide)** δ (ppm) = 1.15-2.0 (m, 18 H, βγδH lysine and βγH arginine), 2.35-2.65 (m, 36 H, -CO-CH2-CH2-CO-), 2.8-3.1 (m, 20 H, εH lysine, δH arginine and cysteine), 3.11-3.3 (m, 36 H, -CH2- Tp), 3.32-3.67 (m, 108 H, -CH2- Tp), 4.09-4.4 (m, 10 H, αH amino acids).

736: **^{1}H NMR (400 MHz, Deuterium oxide)** δ (ppm) = 1.2-1.9 (m, 12 H, βγδH lysine), 2.3-2.6 (m, 38 H, -CO-CH2-CH2-CO-, -CO-CH2- dPEG24), 2.6-3.1 (m, 8 H, εH lysine and cysteine), 3.1-3.6 (m, 128 H, -CH2- Tp), 3.5-3.7 (m, 98 H, -CH2-O- dPEG24, -CH2-N- dPEG24), 4.0-4.3 (m, 4 H, αH amino acids).

737: **^{1}H NMR (400 MHz, Deuterium oxide)** δ (ppm) = 1.2-1.9 (m, 12 H, βγδH lysine), 2.1-2.4 (m, 4 H, βγH glutamic acid) 2.3-2.6 (m, 34 H, -CO-CH2-CH2-CO-, -CO-CH2-dPEG24), 2.6-3.1 (m, 8 H, εH lysine and cysteine), 3.1-3.6 (m, 128 H, -CH2- Tp), 3.5-3.7 (m, 98 H, -CH2-O- dPEG24, -CH2-N- dPEG24), 4.0-4.3 (m, 4 H, αH amino acids), 4.3-4.7 (m, 3H, -CH2-N- pteroic acid, αH glutamic acid), 6.7 (d, 2H, aromatic ring H pteroic acid), 7.6 (d, 2H, aromatic ring H pteroic acid), 8.7 (s, 1H, aromatic ring H pteroic acid).

738: **^{1}H NMR (400 MHz, Deuterium oxide)** δ (ppm) = 1.2-1.9 (m, 20 H, βγδH lysine and βγH arginine), 2.3-2.6 (m, 38 H, -CO-CH2-CH2-CO-, -CO-CH2- dPEG24), 2.6-3.1 (m, 16 H, εH lysine, δH arginine and cysteine), 3.1-3.6 (m, 128 H, -CH2- Tp), 3.5-3.7 (m, 98 H, -CH2-O- dPEG24, -CH2-N- dPEG24), 4.0-4.3 (m, 4 H, αH amino acids).

739: **^{1}H NMR (400 MHz, Deuterium oxide)** δ (ppm) = 1.2-1.9 (m, 20 H, βγδH lysine and βγH arginine), 2.1-2.4 (m, 4 H, βγH glutamic acid) 2.3-2.6 (m, 34 H, -CO-CH2-CH2-CO-, -CO-CH2- dPEG24), 2.6-3.1 (m, 16 H, εH lysine, δH arginine and cysteine), 3.1-3.6 (m, 128 H, -CH2- Tp), 3.5-3.7 (m, 98 H, -CH2-O- dPEG24, -CH2-N- dPEG24), 4.0-4.3 (m, 4 H, αH amino acids), 4.3-4.7 (m, 3H, -CH2-N- pteroic acid, αH glutamic acid), 6.7 (d, 2H, aromatic ring H pteroic acid), 7.6 (d, 2H, aromatic ring H pteroic acid), 8.7 (s, 1H, aromatic ring H pteroic acid).

***740* (test structure):** Sequence (C→N): W-Stp$_2$-ssbb-L$_3$-W

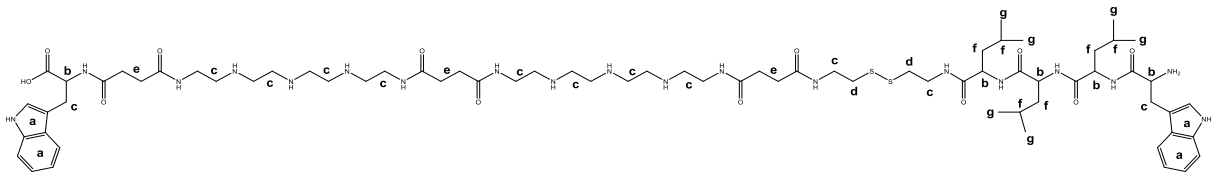

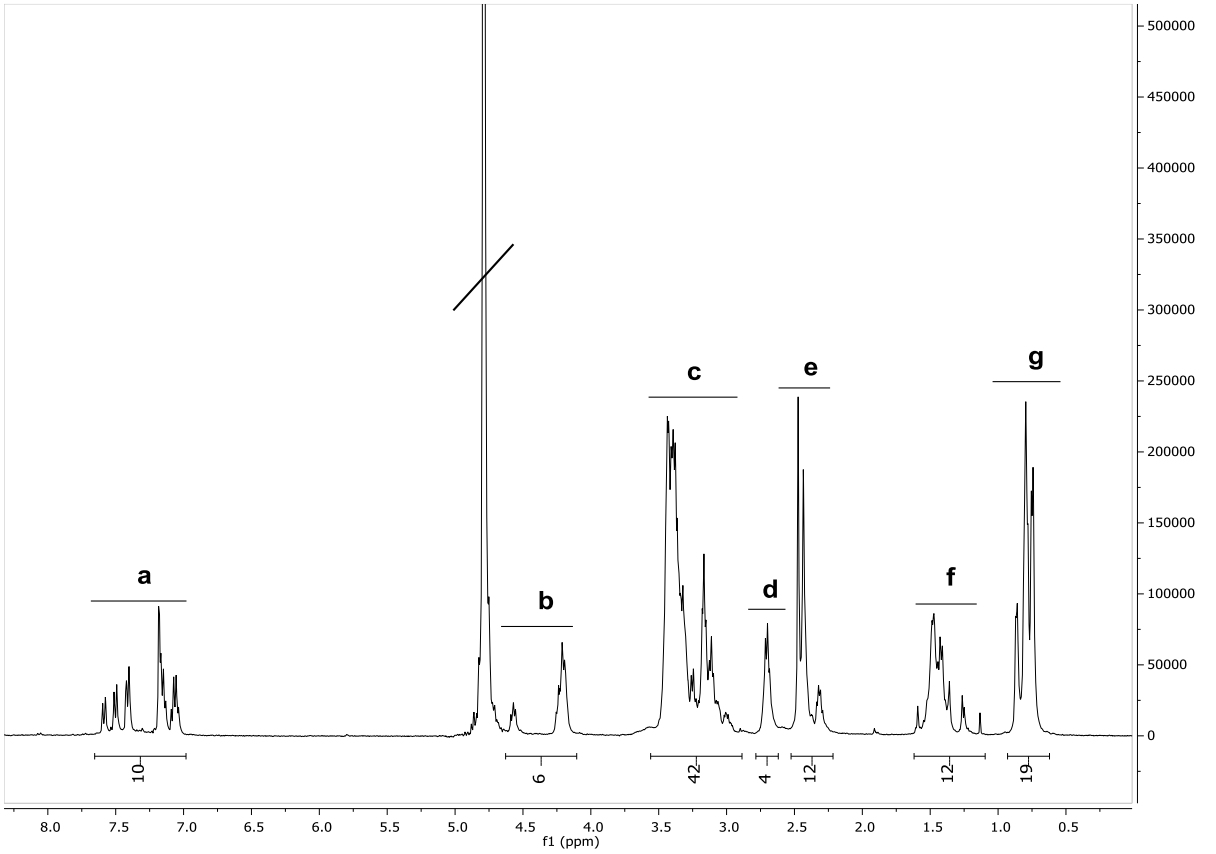

^{1}H NMR (500 MHz, Deuterium oxide) δ (ppm) = 0.60-0.95 (m, 18 H, δH leucine), 1.10-1.60 (m, 12 H, βγH leucine), 2.20-2.50 (m, 12 H, -CO-CH2-CH2-CO- Stp and ssbb), 2.60-2.80 (m, 4 H, -CH2-SS-CH2-), 2.90-3.55 (m, 40 H, -CH2- Tp and ssbb, εH tryptophane), 4.10-4.60 (m, 5 H, αH tryptophanes and leucines), 7.00-7.65 (m, 10 H, aromatic H tryptophane).

***782*:** Sequence (C→N): K-αK-α,ε[Stp3-ssbb-(CholA)$_2$]$_2$

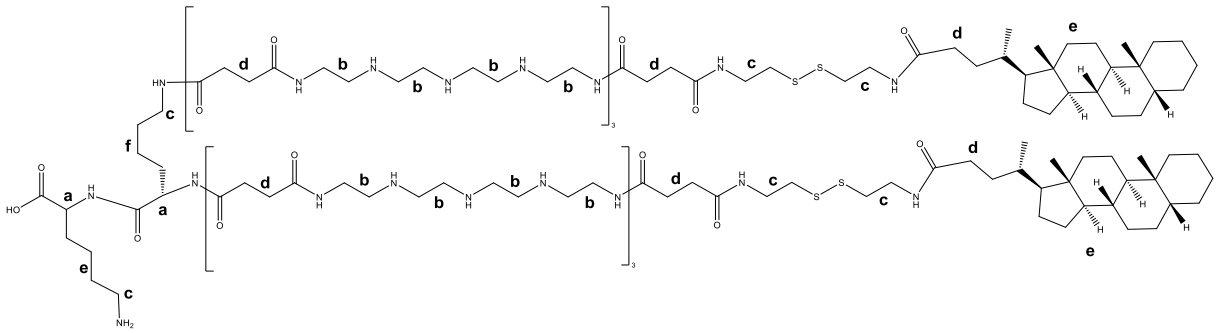

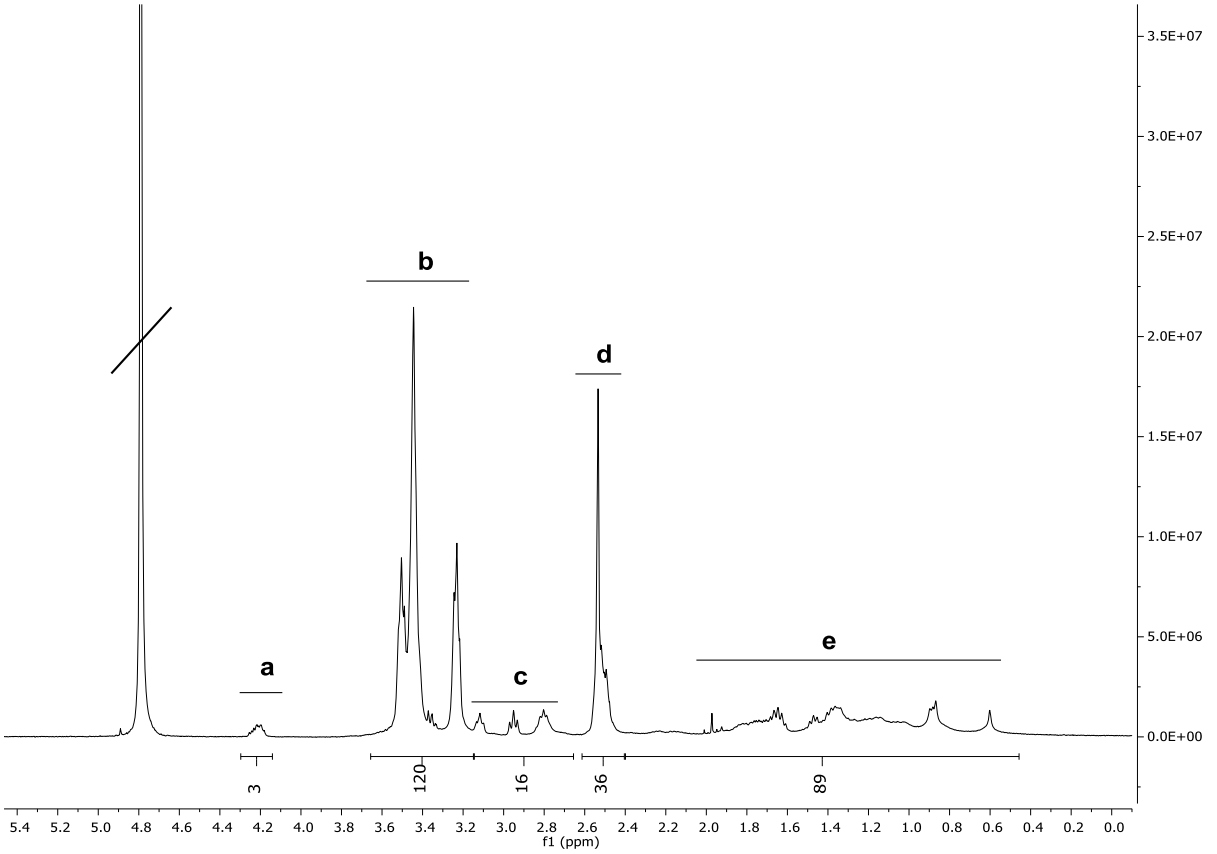

^{1}H NMR (500 MHz, Deuterium oxide) δ (ppm) = 0.45-2.40 m, 88 H, βγδH lysine, cholanic acid), 2.40-2.60 (m, 36 H, -CO-CH2-CH2-CO- Stp and ssbb, -CO-CH2-cholanic acid), 2.65-3.15 (m, 12 H, εH lysine, -CH2- ssbb), 3.15-3.65 (m, 96 H, -CH2-Tp), 4.15-4.30 (m, 2 H, αH lysines).

783: Sequence (C→N): K-αK-α,ε[Stp3-(CholA)$_2$]$_2$

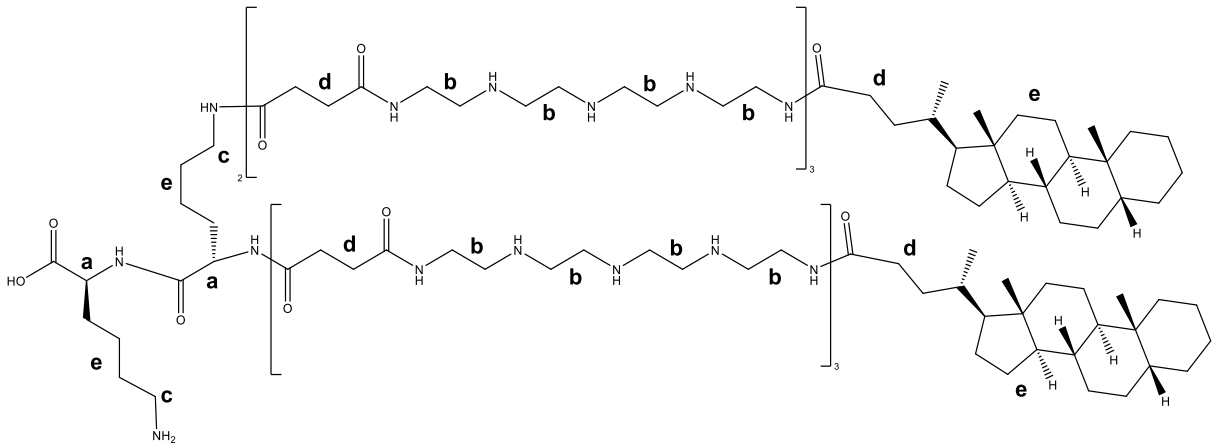

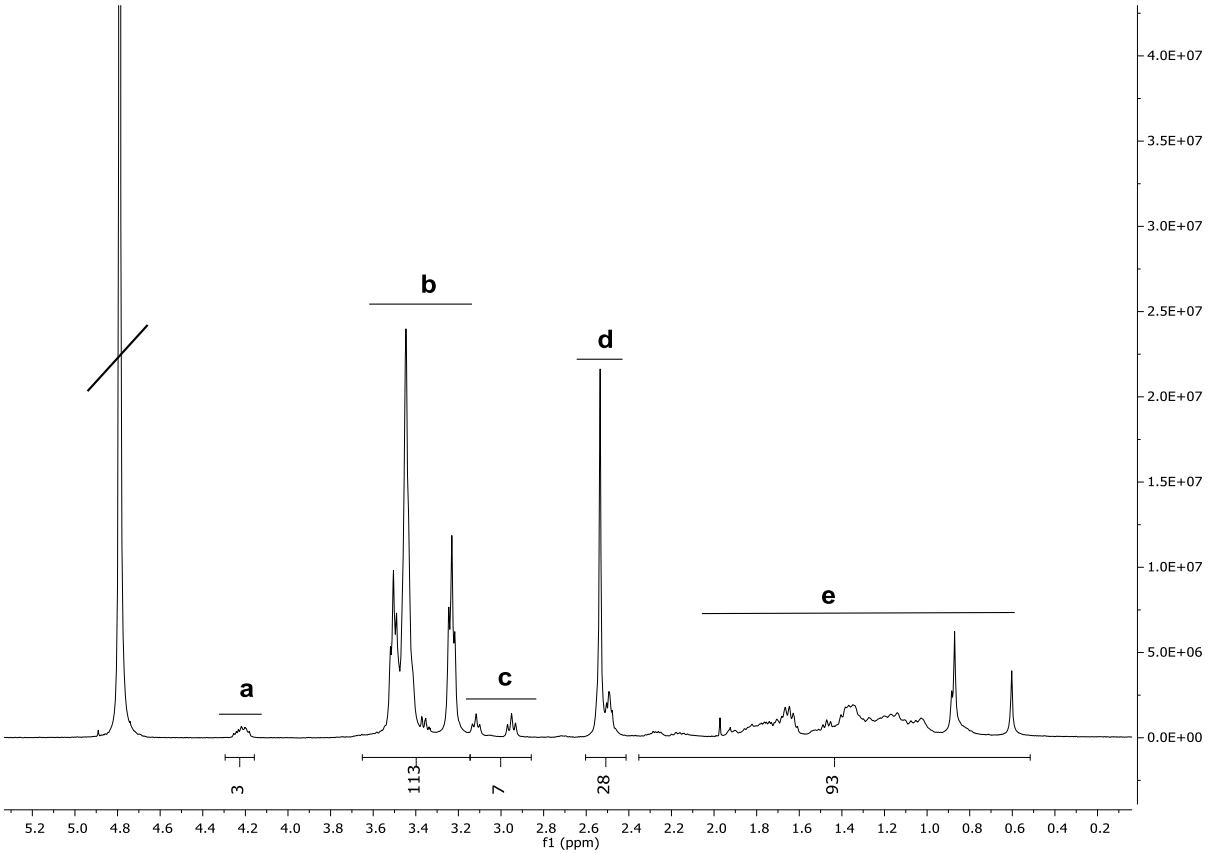

^{1}H NMR (500 MHz, Deuterium oxide) δ (ppm) = 0.50-2.35 m, 88 H, βγδH lysine, cholanic acid), 2.40-2.60 (m, 28 H, -CO-CH2-CH2-CO- Stp, -CO-CH2- cholanic acid), 2.85-3.15 (m, 4 H, εH lysine), 3.15-3.65 (m, 96 H, -CH2- Tp), 4.15-4.30 (m, 2 H, αH lysines).

***871*:** Sequence (C→N): Stp_4-H_6-K-α,ε$(CholA)_2$

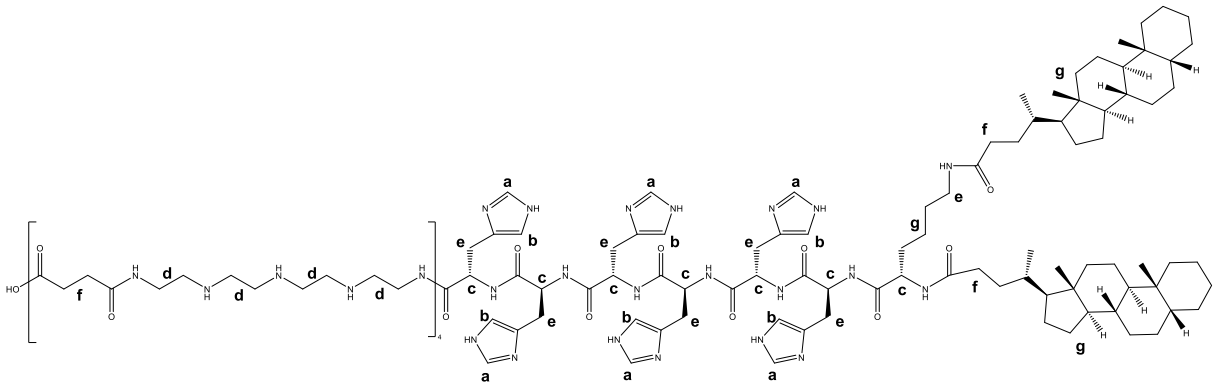

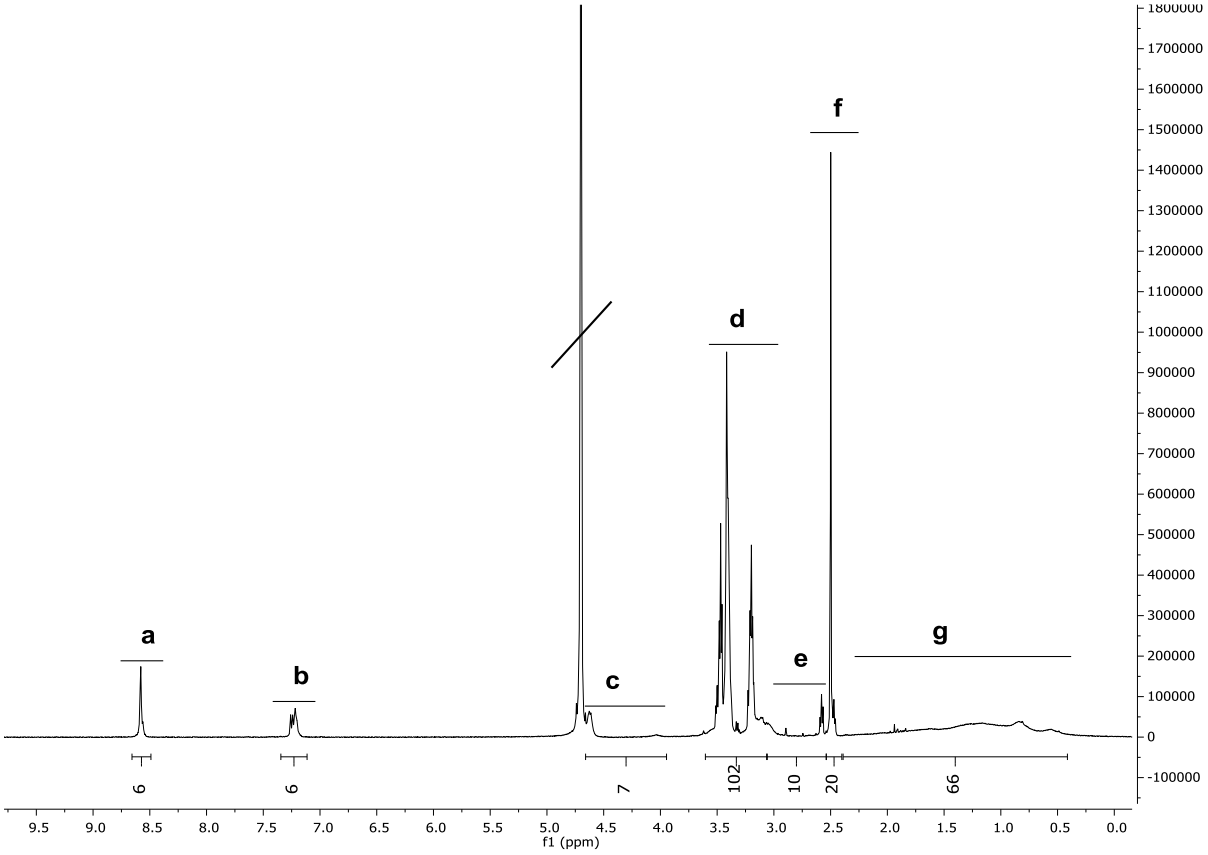

^{1}H NMR (500 MHz, Deuterium oxide) δ (ppm) = 0.40-2.30 m, 82 H, βγδH lysine, cholanic acid), 2.40-2.55 (m, 20 H, -CO-CH2-CH2-CO- Stp, -CO-CH2- cholanic acid), 2.55-3.05 (m, 14 H, εH lysine and histidine), 3.05-3.60 (m, 64 H, -CH2- Tp), 3.95-4.65 (m, 7 H, αH lysines and histidines), 7.10-7.35 (d, 6 H, aromatic H histidine), 8.5-8.65 (m, 6 H, aromatic H histidine).

***969*:** Sequence (C→N): Stp_4-H_6-ssbb-K-α,ε$(CholA)_2$

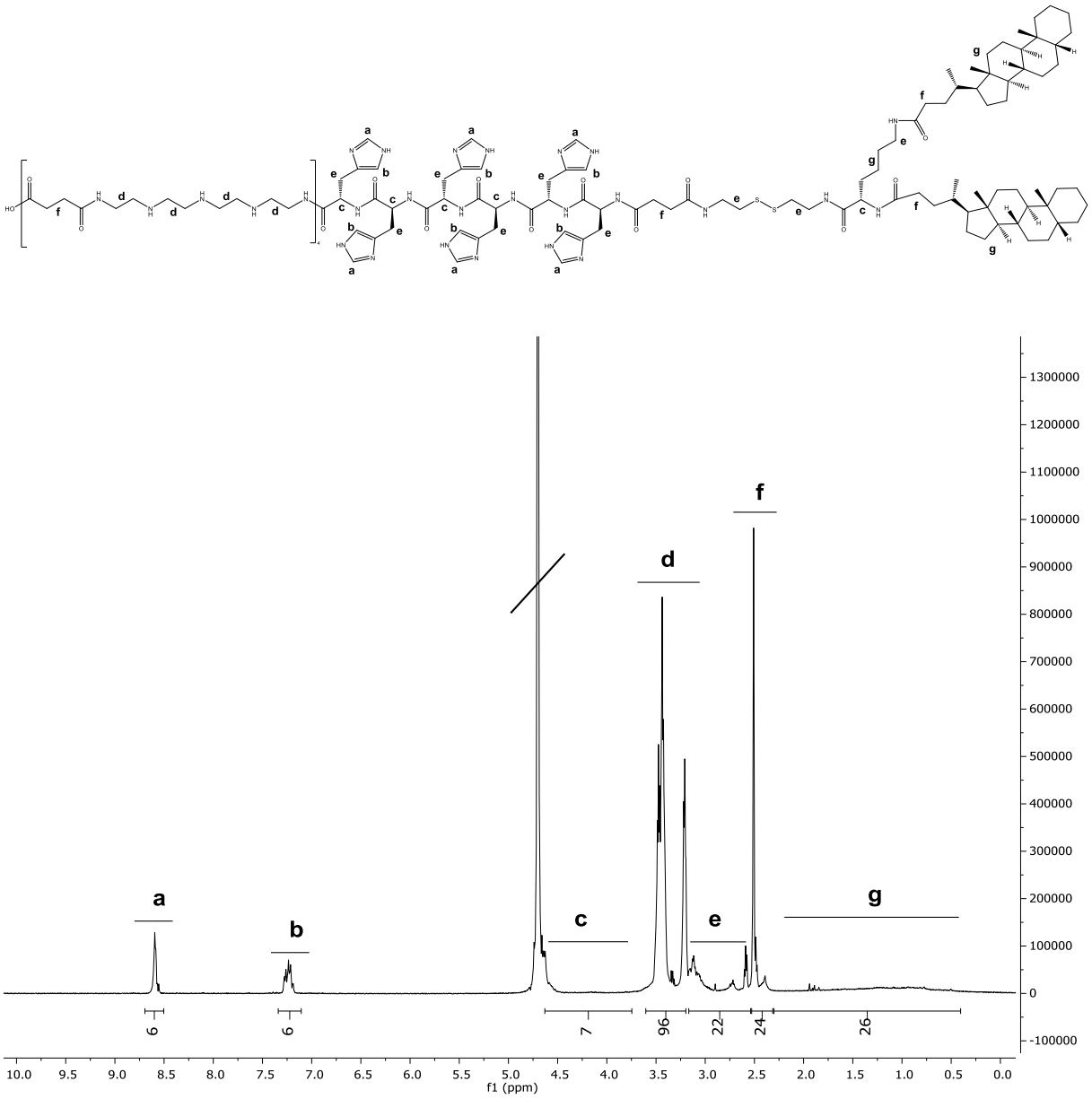

^{1}H NMR (500 MHz, Deuterium oxide) δ (ppm) = 0.40-2.30 m, 82 H, βγδH lysine, cholanic acid), 2.30-2.55 (m, 24 H, -CO-CH2-CH2-CO- Stp and ssbb, -CO-CH2- cholanic acid), 2.55-3.15 (m, 22 H, εH lysine and histidine, -CH2- ssbb), 3.15-3.65 (m, 64 H, -CH2- Tp), 3.75-4.65 (m, 7 H, αH lysines and histidines), 7.10-7.35 (d, 6 H, aromatic H histidine), 8.50-8.70 (m, 6 H, aromatic H histidine).

***989*:** Sequence (C→N): Y_3-Stp_2-K-ε[G-K-α,ε$(SteA)_2$]αStp_2-Y_3

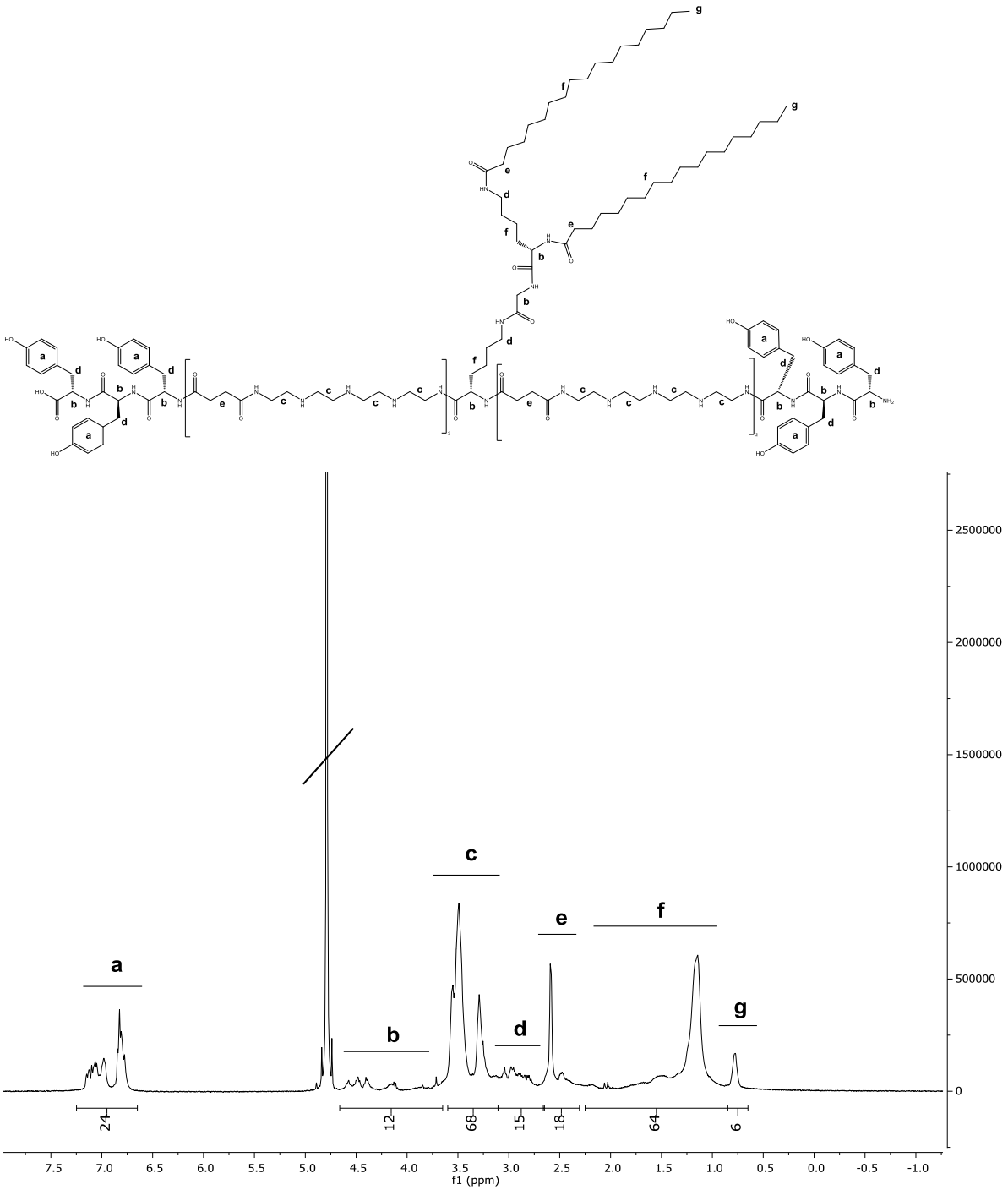

^{1}H NMR (500 MHz, Deuterium oxide) δ (ppm) = 0.65-0.85 (s, 6 H, -CH3 stearic acid), 0.85-2.25 (m, 76 H, βγδH lysine, -CH2- stearic acid), 2.3-2.65 (m, 20 H, -CO-CH2-CH2-CO- Stp, -CO-CH2- stearic acid), 2.65-3.1 (m, 16 H, εH lysine and tyrosine), 3.1-3.6 (m, 64 H, -CH2- Tp), 3.65-4.65 (m, 10 H, αH amino acids), 6.65-7.25 (m, 24 H, -CH- tyrosine).

***990*:** Sequence (C→N): Y_3-Stp_2-K-ε[G-ssbb-K-α,ε$(SteA)_2$]αStp_2-Y_3

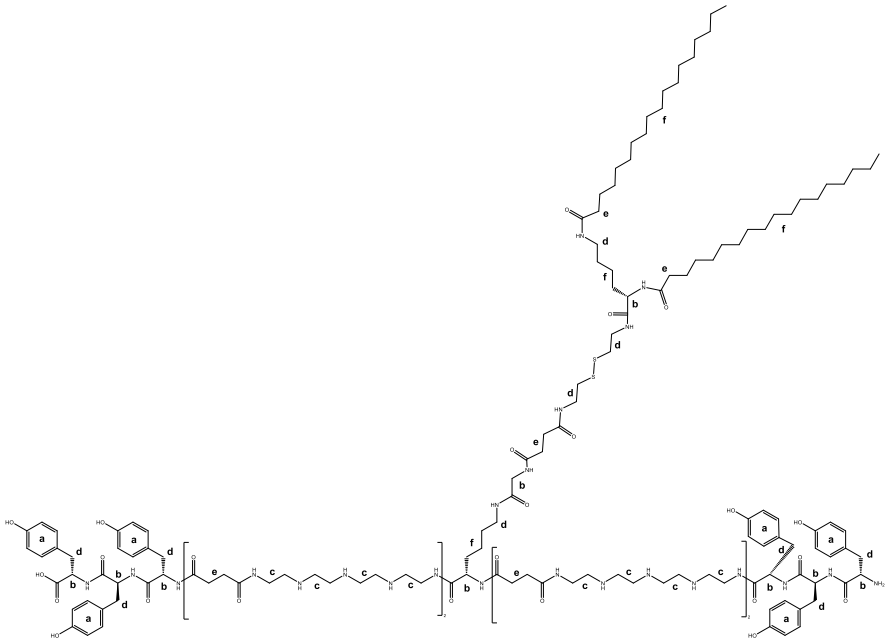

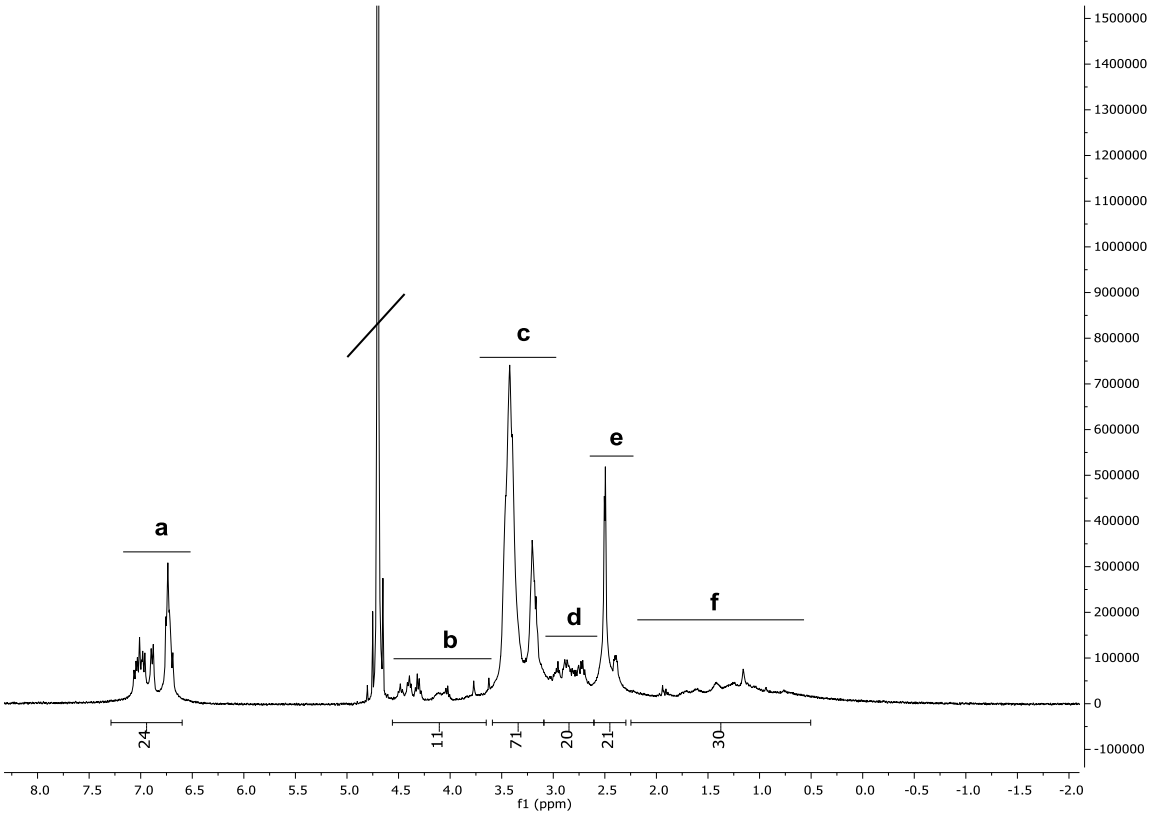

^{1}H NMR (500 MHz, Deuterium oxide) δ (ppm) = 0.50-2.25 (m, 82 H, βγδH lysine, -CH2- and -CH3 stearic acid), 2.3-2.6 (m, 24 H, -CO-CH2-CH2-CO- Stp and ssbb, -CO-CH2- stearic acid), 2.6-3.1 (m, 24 H, εH lysine and tyrosine, -CH2- ssbb), 3.1-3.6 (m, 64 H, -CH2- Tp), 3.65-4.55 (m, 10 H, αH amino acids), 6.6-7.3 (m, 24 H, -CH- tyrosine).

991: Sequence (C→N): Y_3-Stp_2-K-ε[G-K-α,ε$(CholA)_2$]αStp_2-Y_3

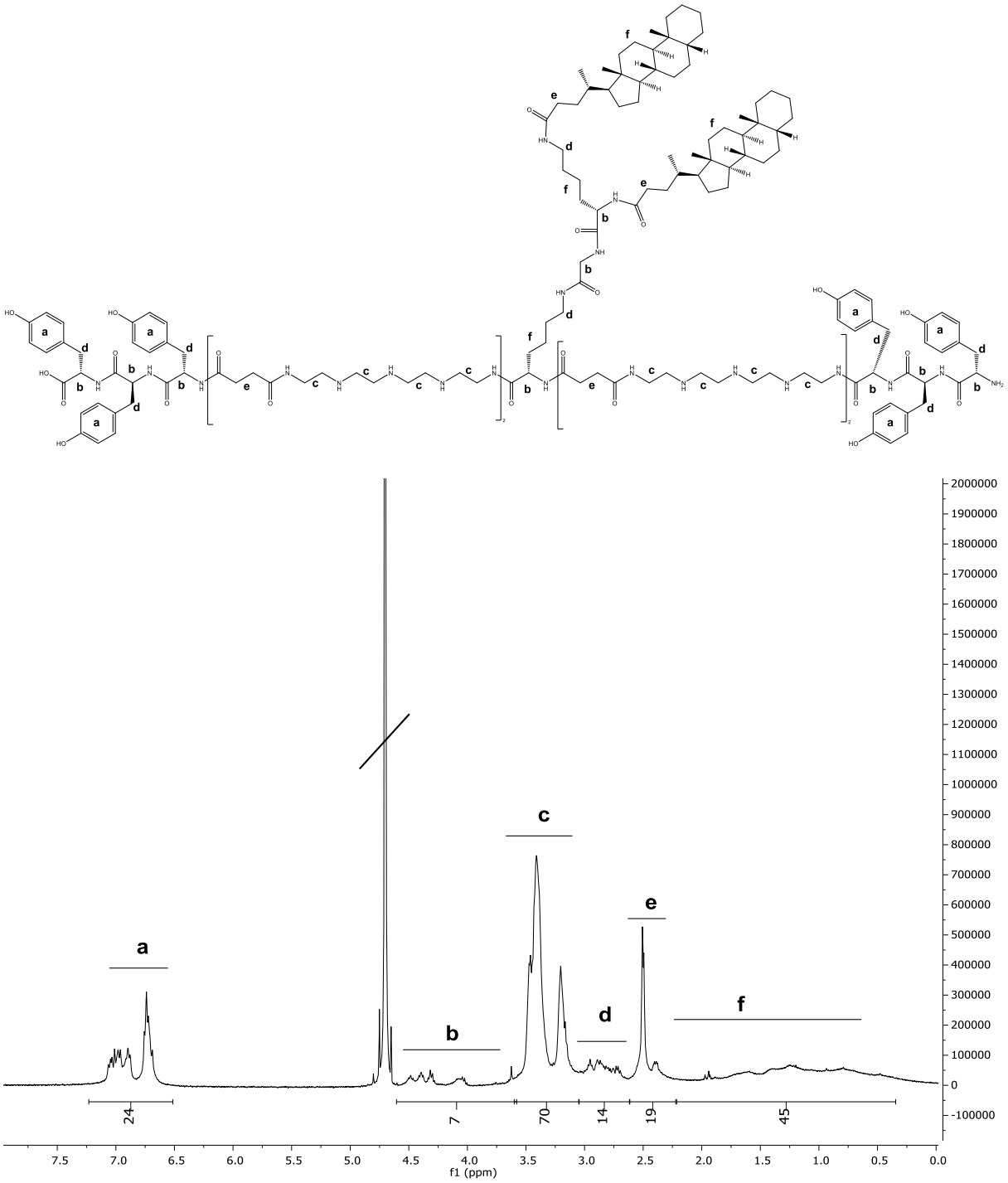

^{1}H NMR (500 MHz, Deuterium oxide) δ (ppm) = 0.35-2.20 (m, 88 H, βγδH lysine, cholanic acid), 2.2-2.6 (m, 20 H, -CO-CH2-CH2-CO- Stp, -CO-CH2- cholanic acid), 2.6-3.05 (m, 16 H, εH lysine and tyrosine), 3.05-3.60 (m, 64 H, -CH2- Tp), 3.60-4.60 (m, 10 H, αH amino acids), 6.50-7.25 (m, 24 H, -CH- tyrosine).

***992*:** Sequence (C→N): Y_3-Stp_2-K-ε[G-ssbb-K-α,ε$(CholA)_2$]αStp_2-Y_3

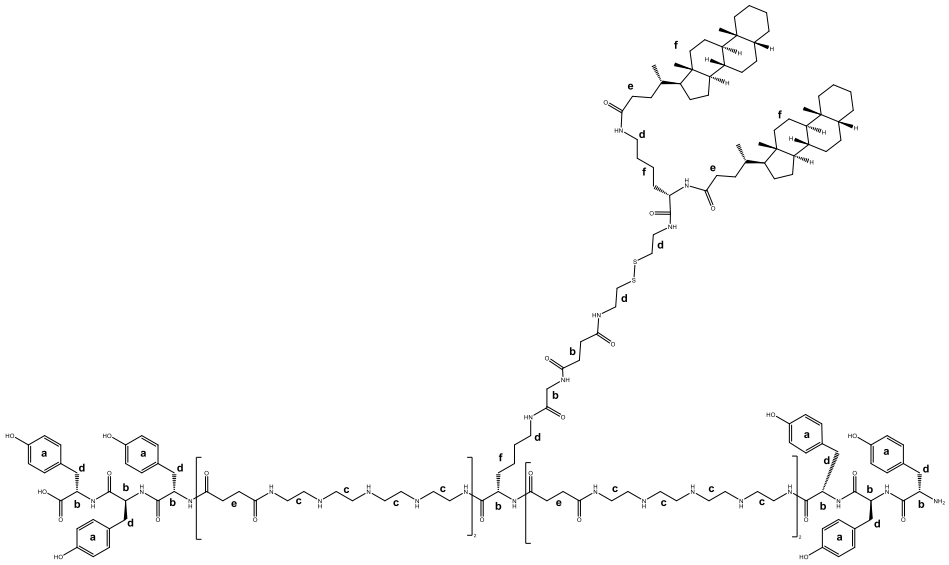

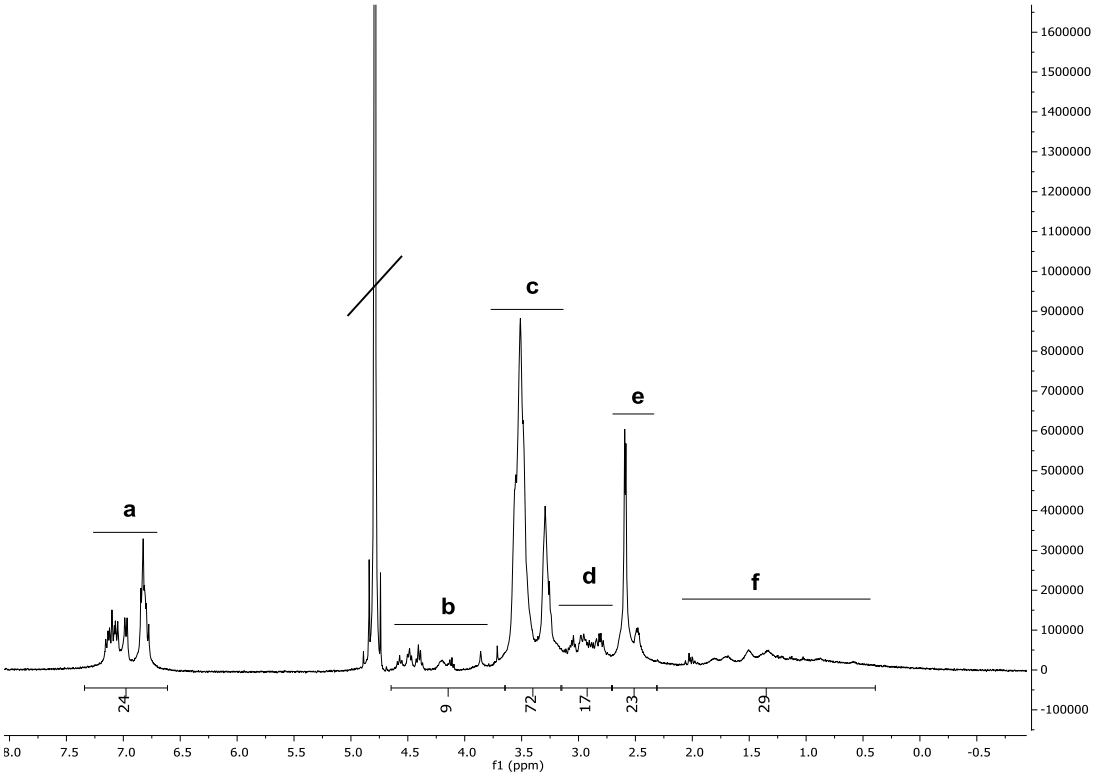

^{1}H NMR (500 MHz, Deuterium oxide) δ (ppm) = 0.40-2.30 (m, 88 H, βγδH lysine, cholanic acid), 2.3-2.7 (m, 24 H, -CO-CH2-CH2-CO- Stp and ssbb, -CO-CH2- cholanic acid), 2.70-3.15 (m, 24 H, εH lysine and tyrosine, -CH2- ssbb), 3.15-3.80 (m, 64 H, -CH2- Tp), 3.65-4.65 (m, 10 H, αH amino acids), 6.60-7.35 (m, 24 H, -CH- tyrosine).

1073: Sequence (C→N): Y_3-Stp_2-K-ε[G-ssbb-K-α,ε$(CholA)_2$]αStp_2-Y_3-K-ε(N_3)

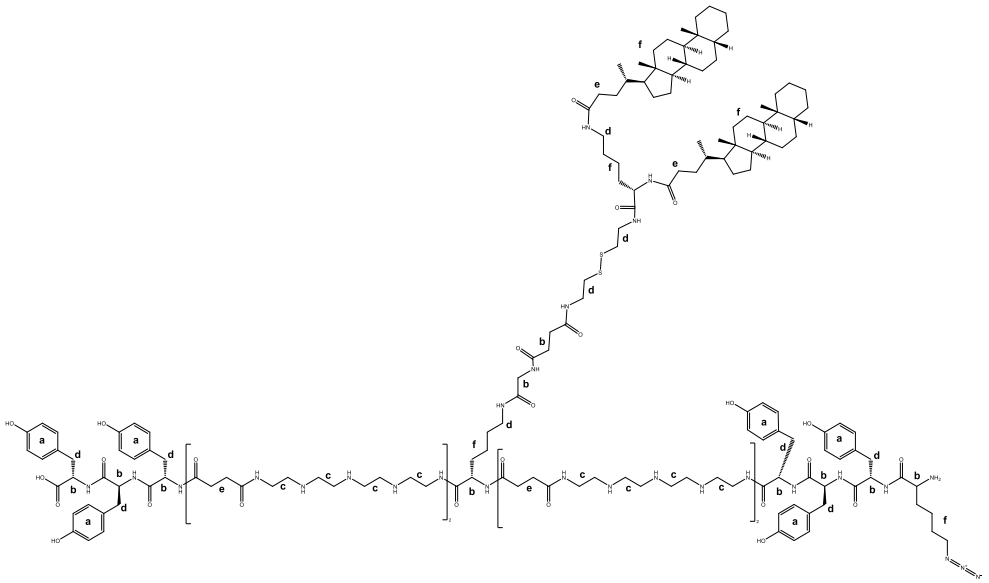

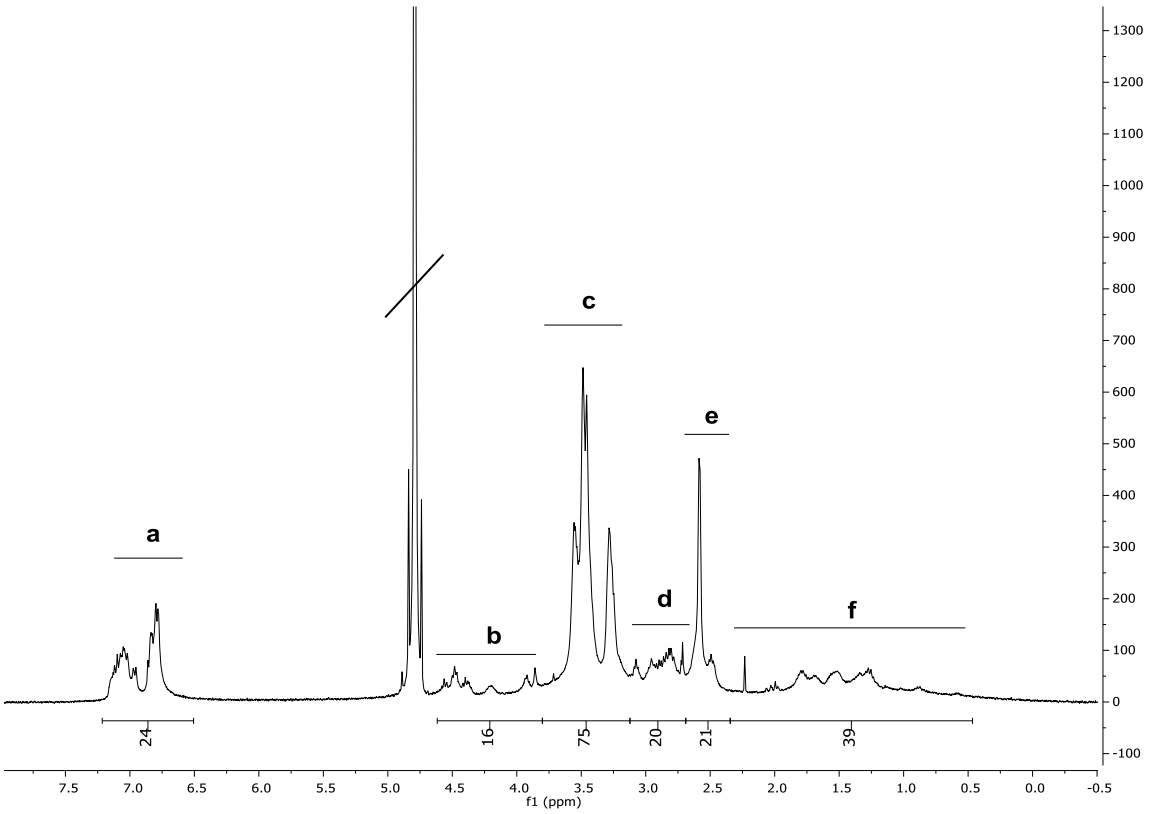

^{1}H NMR (500 MHz, Deuterium oxide) δ (ppm) = 0.40-2.30 (m, 96 H, βγδH lysine, βγδεH azidolysine, cholanic acid), 2.3-2.7 (m, 24 H, -CO-CH2-CH2-CO- Stp and ssbb, -CO-CH2- cholanic acid), 2.70-3.15 (m, 24 H, εH lysine and tyrosine, -CH2- ssbb), 3.15-3.80 (m, 64 H, -CH2- Tp), 3.65-4.65 (m, 11 H, αH amino acids), 6.60-7.35 (m, 24 H, -CH- tyrosine).

1081: Sequence (C→N): Y3-Stp2-K-ε[G-K-α,ε(MyrA)2]αStp2-Y3

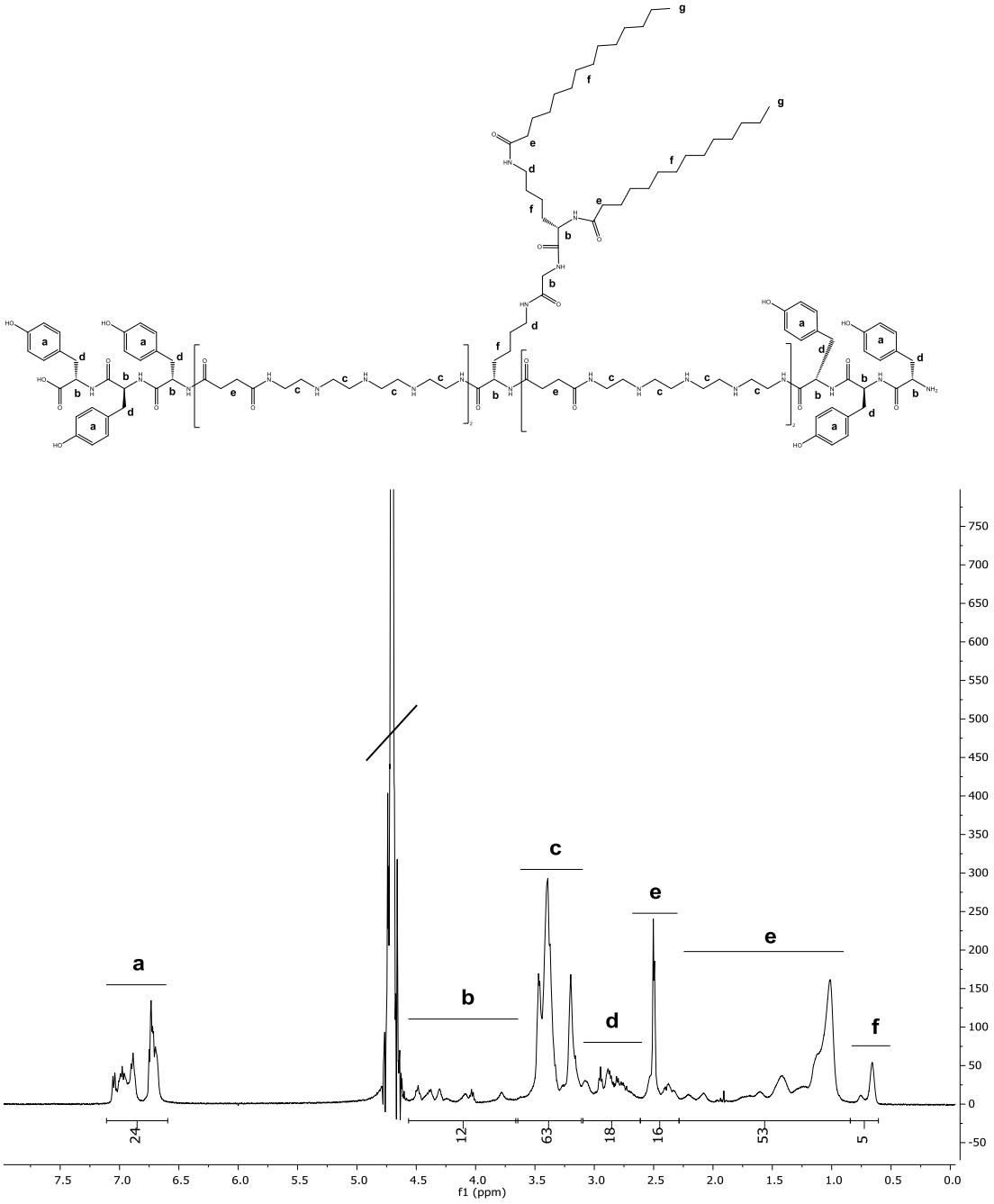

^{1}H NMR (500 MHz, Deuterium oxide) δ (ppm) = 0.60-0.85 (s, 6 H, -CH3 myristic acid), 0.85-2.30 (m, 56 H, βγδH lysine, myristic acid), 2.3-2.6 (m, 20 H, -CO-CH2-CH2-CO-Stp, -CO-CH2- myristic acid), 2.6-3.10 (m, 16 H, εH lysine and tyrosine), 3.10-3.65 (m, 64 H, -CH2- Tp), 3.65-4.55 (m, 10 H, αH amino acids), 6.60-7.10 (m, 24 H, -CH- tyrosine).

1082: Sequence (C→N): Y_3-Stp_2-K-ε[G-ssbb-K-α,ε$(MyrA)_2$]αStp_2-Y_3

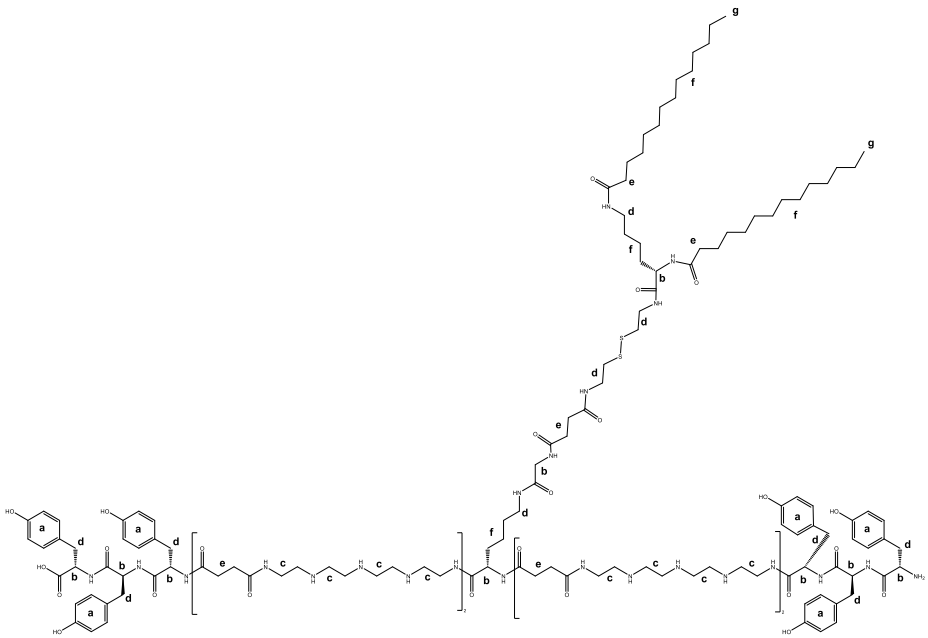

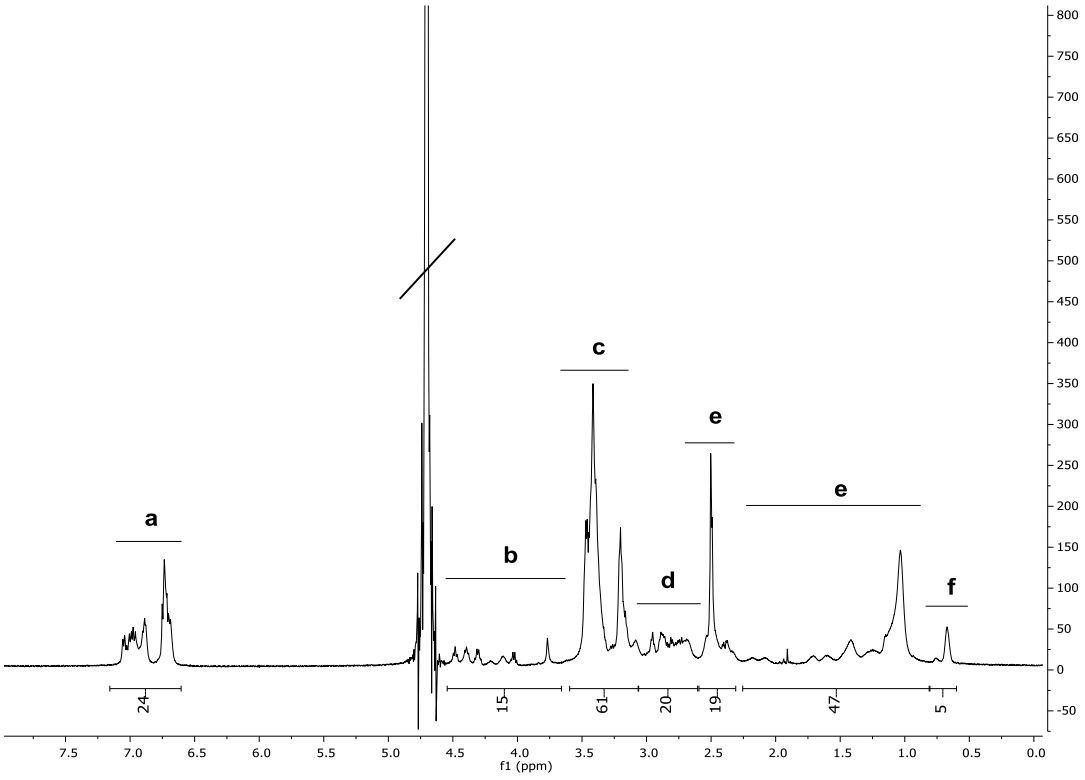

^{1}H NMR (500 MHz, Deuterium oxide) δ (ppm) = 0.60-0.80 (s, 6 H, -CH3 myristic acid), 0.80-2.25 (m, 56 H, βγδH lysine, myristic acid), 2.3-2.6 (m, 24 H, -CO-CH2-CH2-CO- Stp and ssbb, -CO-CH2- myristic acid), 2.60-3.05 (m, 24 H, εH lysine and tyrosine, -CH2- ssbb), 3.05-3.60 (m, 64 H, -CH2- Tp), 3.65-4.55 (m, 10 H, αH amino acids), 6.60-7.15 (m, 24 H, -CH- tyrosine).

1086: Sequence (C→N): K-ε(N_3)-Y_3-Stp_2-K-ε[G-ssbb-K-α,ε($CholA)_2$]αStp_2-Y_3-K-ε(N_3)

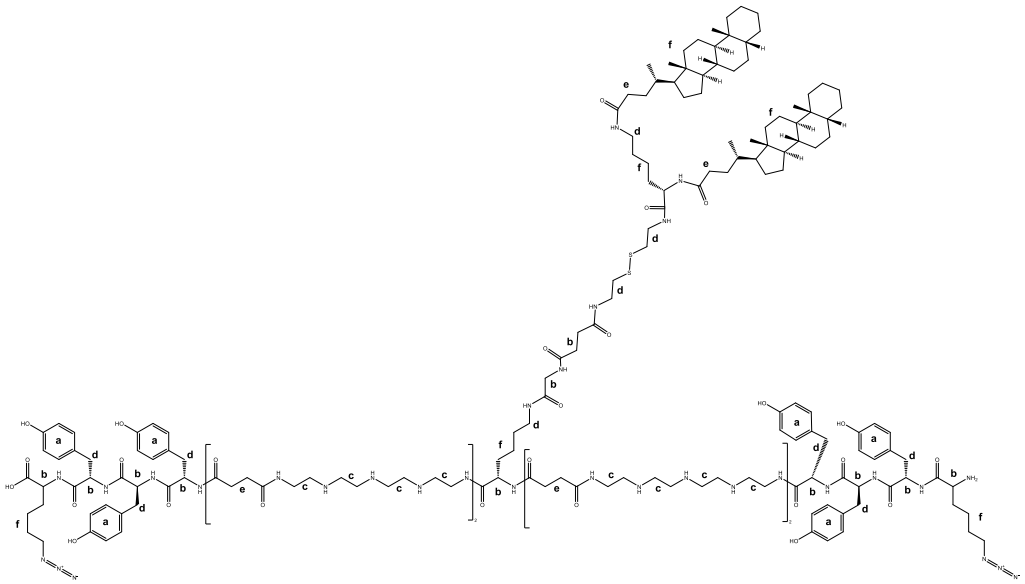

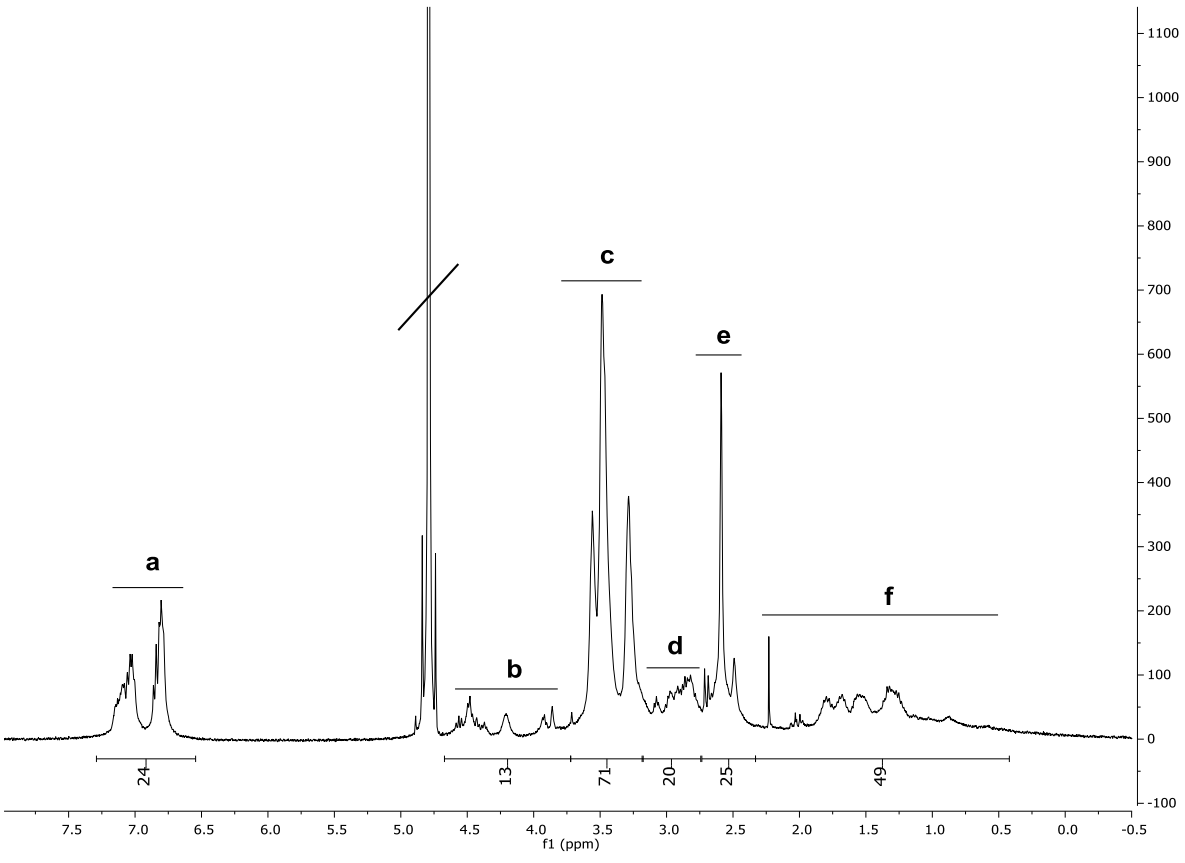

^{1}H NMR (500 MHz, Deuterium oxide) δ (ppm) = 0.40-2.30 (m, 104 H, βγδH lysine, βγδεH azidolysine, cholanic acid), 2.3-2.7 (m, 24 H, -CO-CH2-CH2-CO- Stp and ssbb, -CO-CH2- cholanic acid), 2.70-3.15 (m, 24 H, εH lysine and tyrosine, -CH2- ssbb), 3.15-3.80 (m, 64 H, -CH2- Tp), 3.65-4.65 (m, 12 H, αH amino acids), 6.60-7.35 (m, 24 H, -CH- tyrosine).

1106: Sequence (C→N): Y_3-Stp_2-K-ε[G-K-α,ε$(CholA)_2$]αStp_2-Y_3-K-ε(N_3)

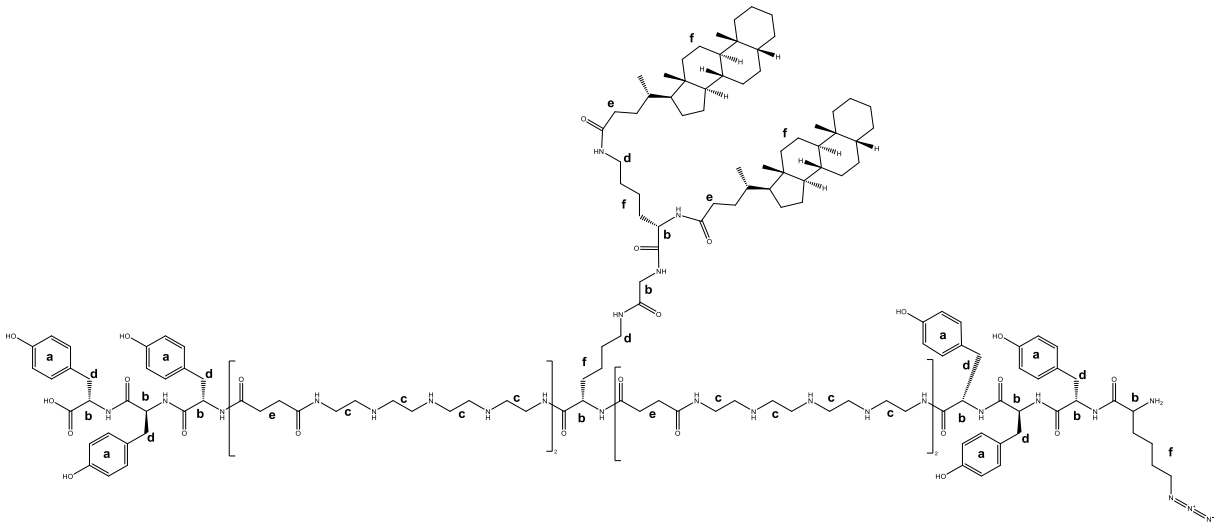

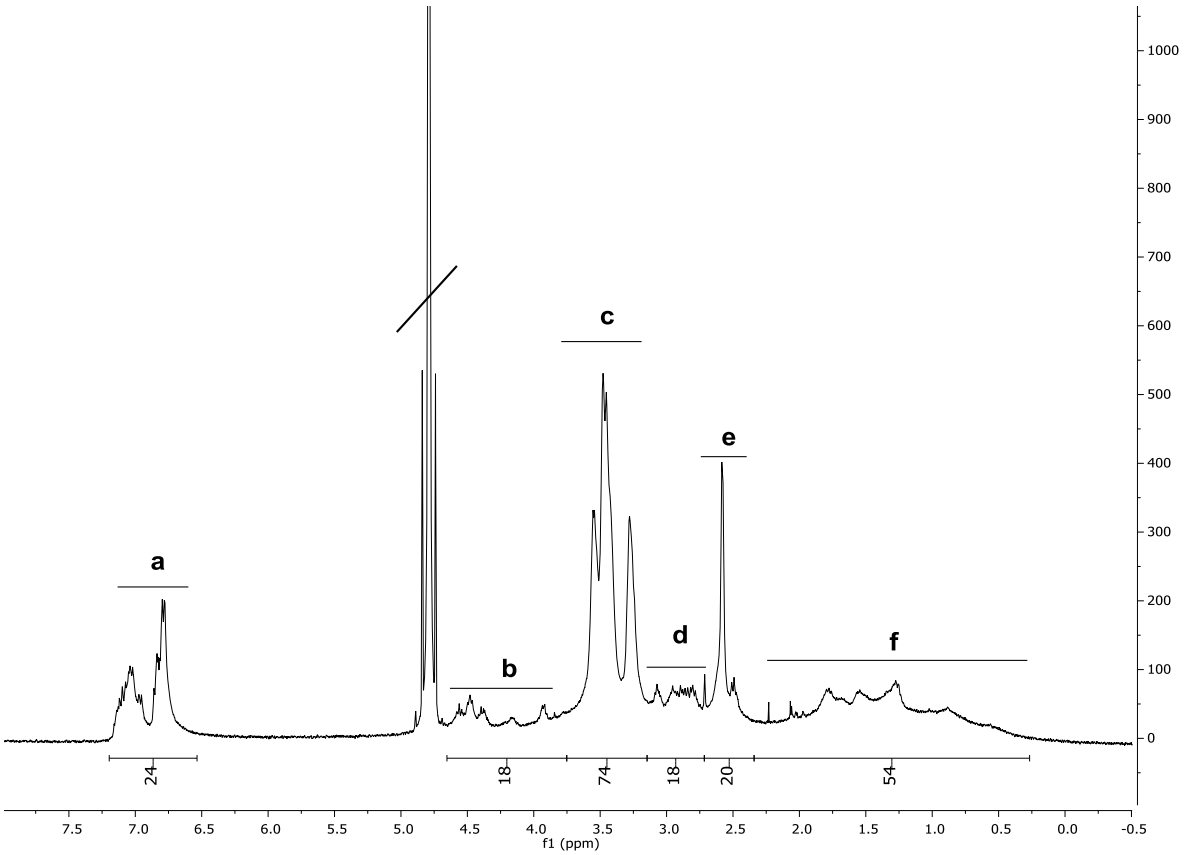

^{1}H NMR (500 MHz, Deuterium oxide) δ (ppm) = 0.35-2.20 (m, 96 H, βγδH lysine, βγδεH azidolysine, cholanic acid), 2.2-2.6 (m, 20 H, -CO-CH2-CH2-CO- Stp, -CO-CH2- cholanic acid), 2.6-3.05 (m, 16 H, εH lysine and tyrosine), 3.05-3.60 (m, 64 H, -CH2- Tp), 3.60-4.60 (m, 11 H, αH amino acids), 6.50-7.25 (m, 24 H, -CH- tyrosine).

***1107*:** Sequence (C→N): Y_3-Stp_2-K-ε[G-K-α,ε$(OleA)_2$]αStp_2-Y_3

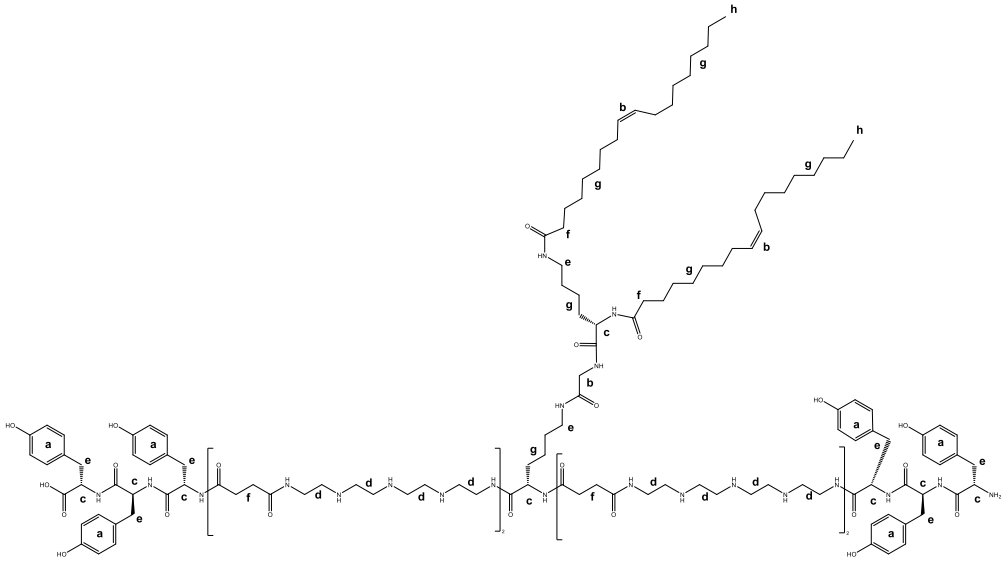

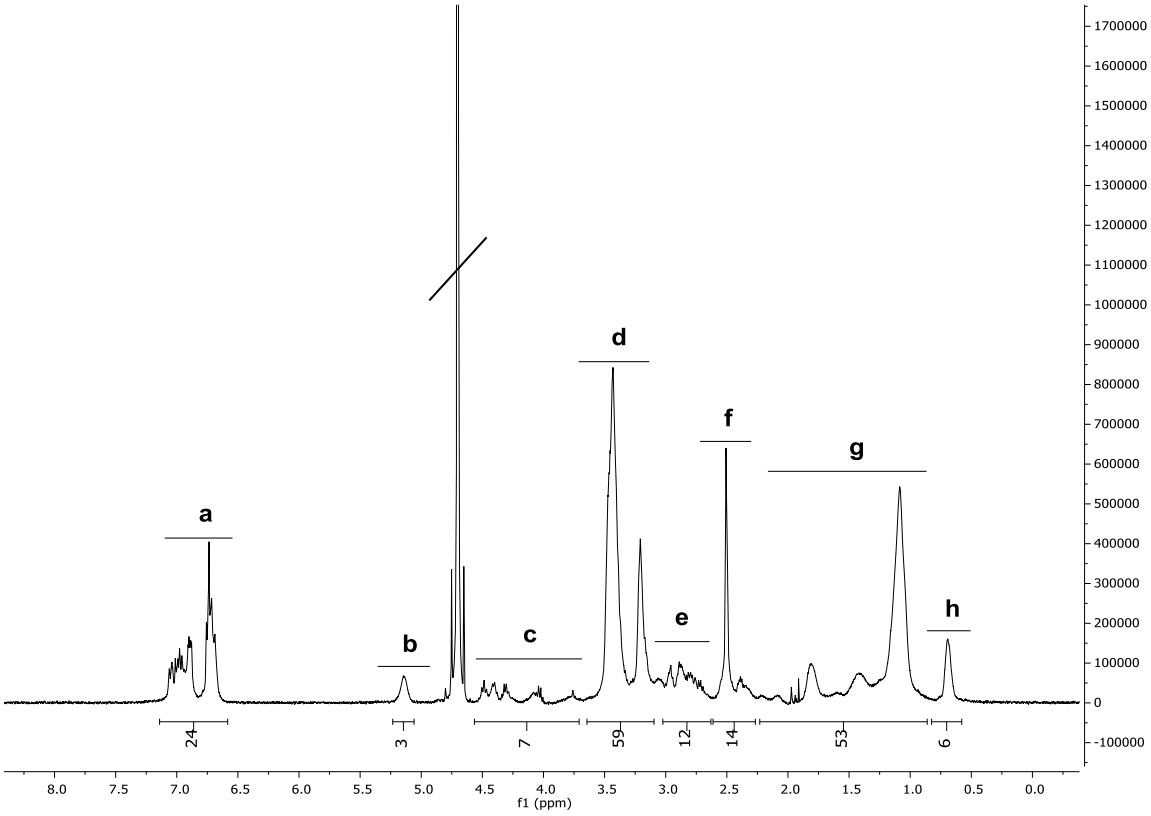

^{1}H NMR (500 MHz, Deuterium oxide) δ (ppm) = 0.60-0.85 (s, 6 H, -CH3 oleic acid), 0.85-2.25 (m, 72 H, βγδH lysine, -CH2- oleic acid), 2.25-2.60 (m, 20 H, -CO-CH2-CH2-CO- Stp, -CO-CH2- oleic acid), 2.65-3.1 (m, 16 H, εH lysine and tyrosine), 3.1-3.65 (m, 64 H, -CH2- Tp), 3.70-4.55 (m, 10 H, αH amino acids), 5.05 – 5.25 (s, 4 H,

-CH=CH- oleic acid), 6.60 -7.15 (m, 24 H, -CH- tyrosine).

***1108*:** Sequence (C→N): Y_3-Stp_2-K-ε[G-ssbb-K-α,ε$(OleA)_2$]αStp_2-Y_3

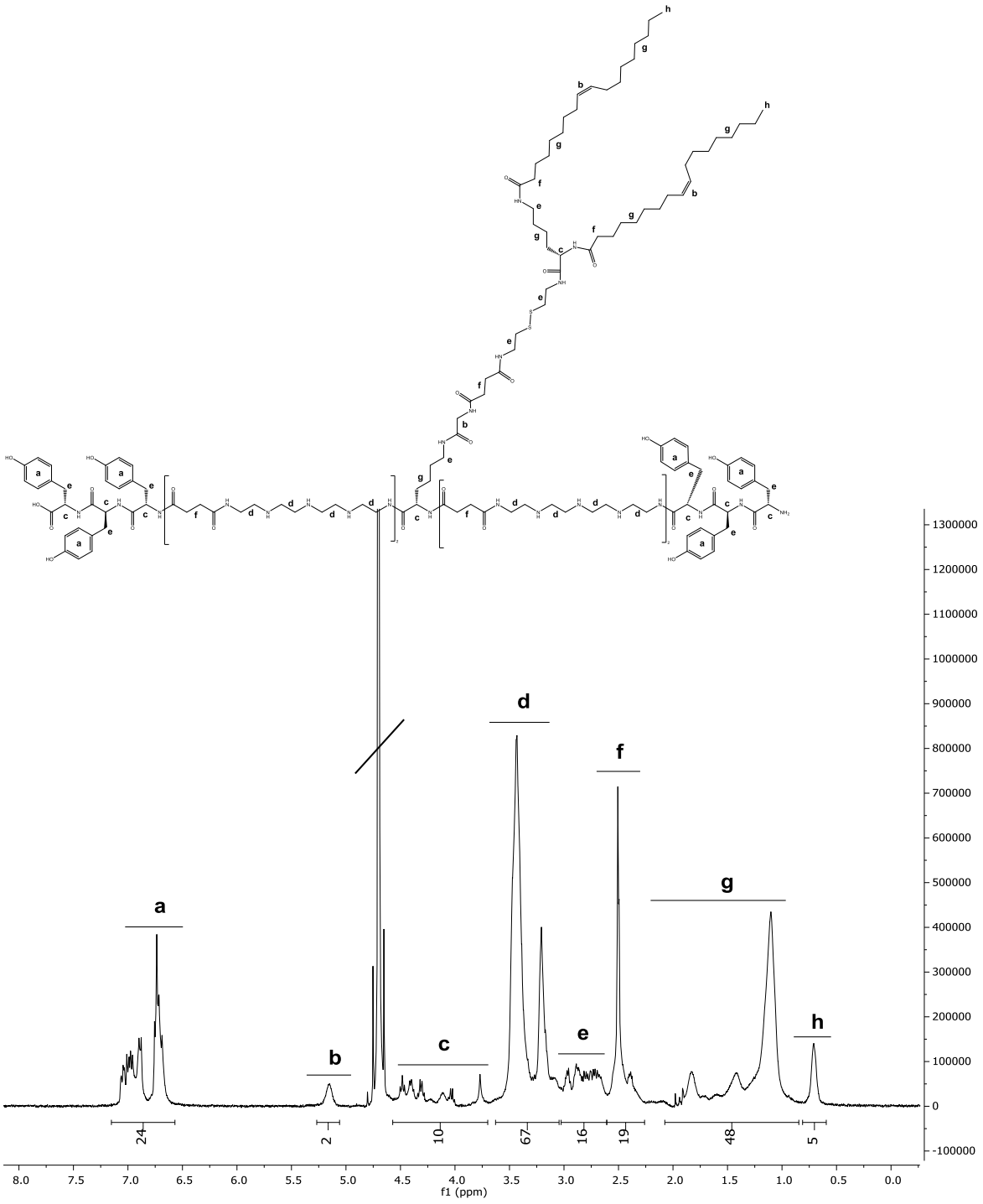

^{1}H NMR (500 MHz, Deuterium oxide) δ (ppm) = 0.60-0.80 (s, 6 H, -CH3 oleic acid), 0.85-2.10 (m, 72 H, βγδH lysine, -CH2- oleic acid), 2.25-2.60 (m, 22 H, -CO-CH2-CH2-CO- Stp, -CO-CH2- oleic acid), 2.60-3.0 (m, 22 H, εH lysine and tyrosine), 3.05-3.65 (m, 64 H, -CH2- Tp), 3.70-4.60 (m, 10 H, αH amino acids), 5.00 – 5.25 (s, 4 H, -CH=CH- oleic acid), 6.55 -7.15 (m, 24 H, -CH- tyrosine).

6.4.3 Mass spectra of oligomers

Table 20 Summarizing table oligomers. Mass data recorded with a Bruker MALDI-TOF instrument

Oligomer	Molecular formula	$[M+H]^+$ calc.	$[M+H]^+$ found
740 **(Test structure)**	$C_{72}H_{119}N_{19}O_{12}S_2$	1506.9	1506.1
782 **(CholA-ss-u)**	$C_{148}H_{280}N_{38}O_{21}S_4$	3055.0	3056.1
783 **(CholA-u)**	$C_{132}H_{252}N_{34}O_{17}$	2587.0	2587.2
871 **(CholA-i)**	$C_{138}H_{232}N_{40}O_{18}$	2738.9	2739.2
969 **(CholA-ss-i)**	$C_{146}H_{246}N_{42}O_{20}S_2$	2972.9	2973.2
989 **(SteA-t)**	$C_{152}H_{251}N_{31}O_{26}$	2927.9	2929.3
990 **(SteA-ss-t)**	$C_{160}H_{265}N_{33}O_{28}S_2$	3162.0	3163.6
991 **(CholA-t)**	$C_{164}H_{259}N_{31}O_{26}$	3080.0	3079.0
992 **(CholA-ss-t)**	$C_{172}H_{273}N_{33}O_{28}S_2$	3314.0	3314.2
1073 (CholA-ss-t-N_3)	$C_{178}H_{283}N_{37}O_{29}S_2$	3468.1	3466.2
1081 **(MyrA-t)**	$C_{144}H_{235}N_{31}O_{26}$	2815.8	2813.6
1082 **(MyrA-ss-t)**	$C_{152}H_{249}N_{33}O_{28}S_2$	3049.9	3048.2
1086 **(CholA-ss-t-2N_3)**	$C_{184}H_{293}N_{41}O_{30}S_2$	3622.2	3621.3
1106 **(CholA-t-N_3)**	$C_{170}H_{269}N_{35}O_{27}$	3234.1	3233.0
1107 **(OleA-t)**	$C_{152}H_{247}N_{31}O_{26}$	2923.9	2922.9
1108 **(OleA-ss-t)**	$C_{160}H_{261}N_{33}O_{28}S_2$	3158.0	3156.3

6.4.3.1 Full mass spectra of oligomers

740 (Test structure)

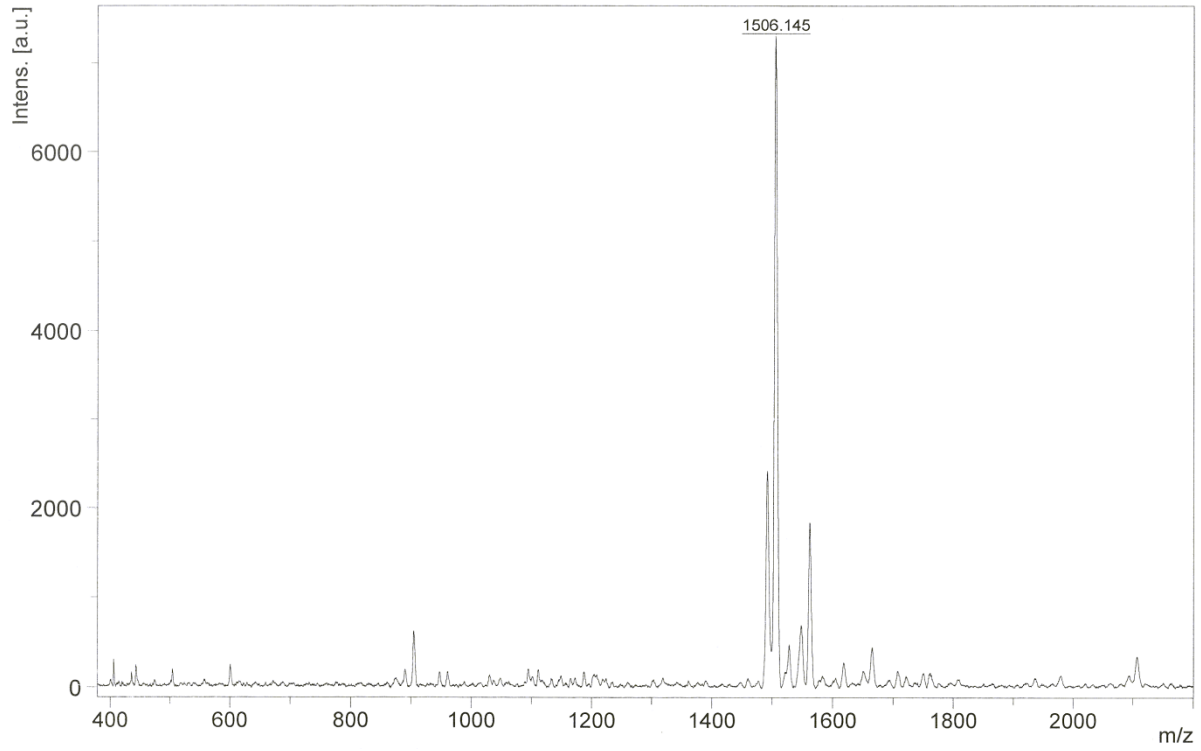

782 (CholA-ss-u)

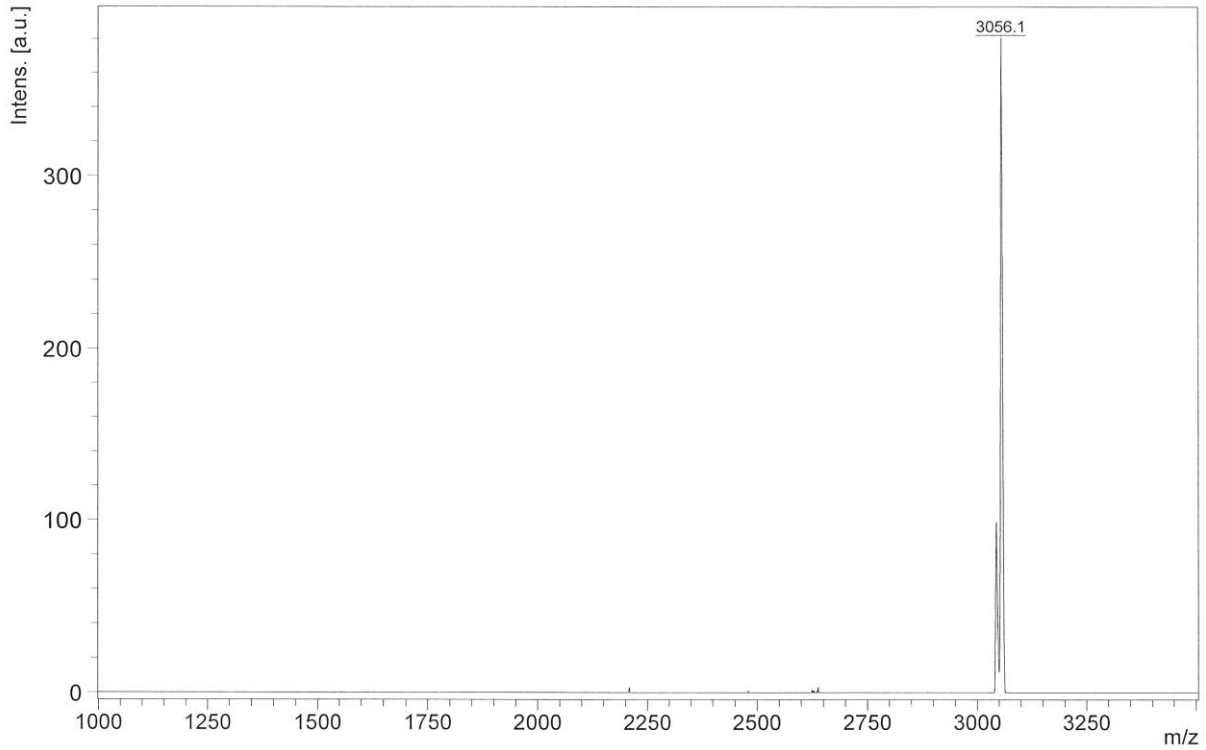

783 (CholA-u)

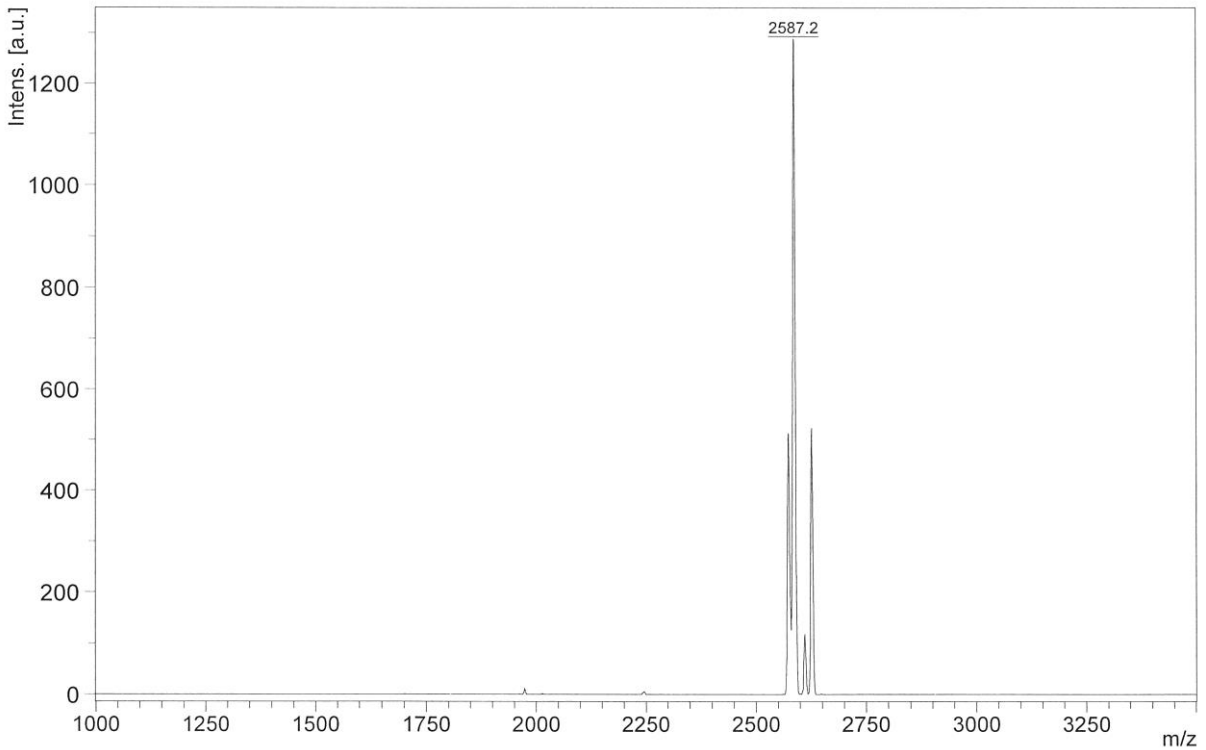

871 (CholA-i)

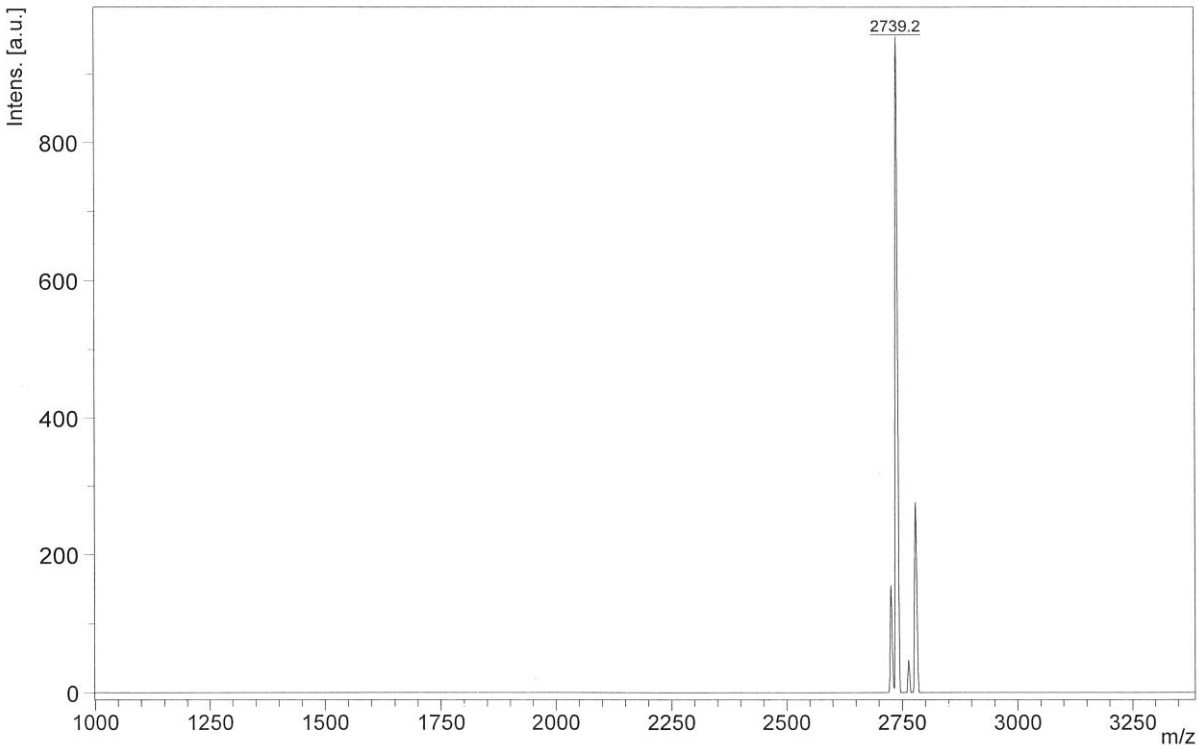

969 (CholA-ss-i)

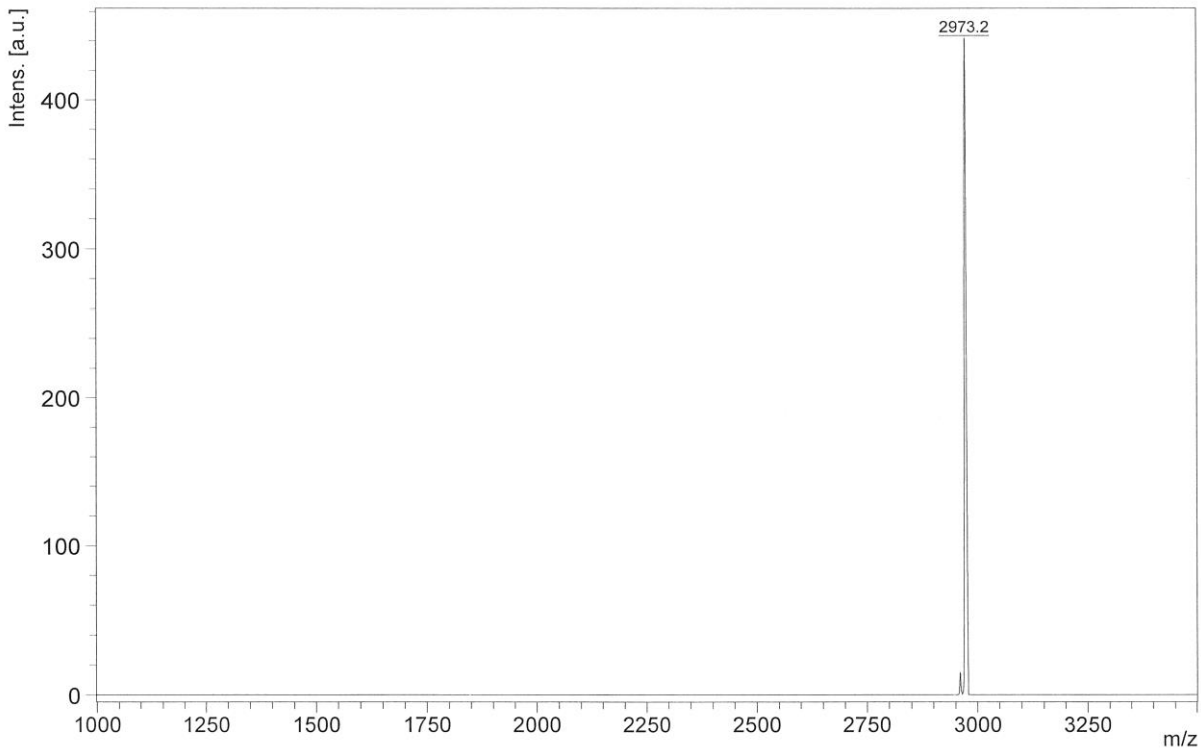

989 (SteA-t)

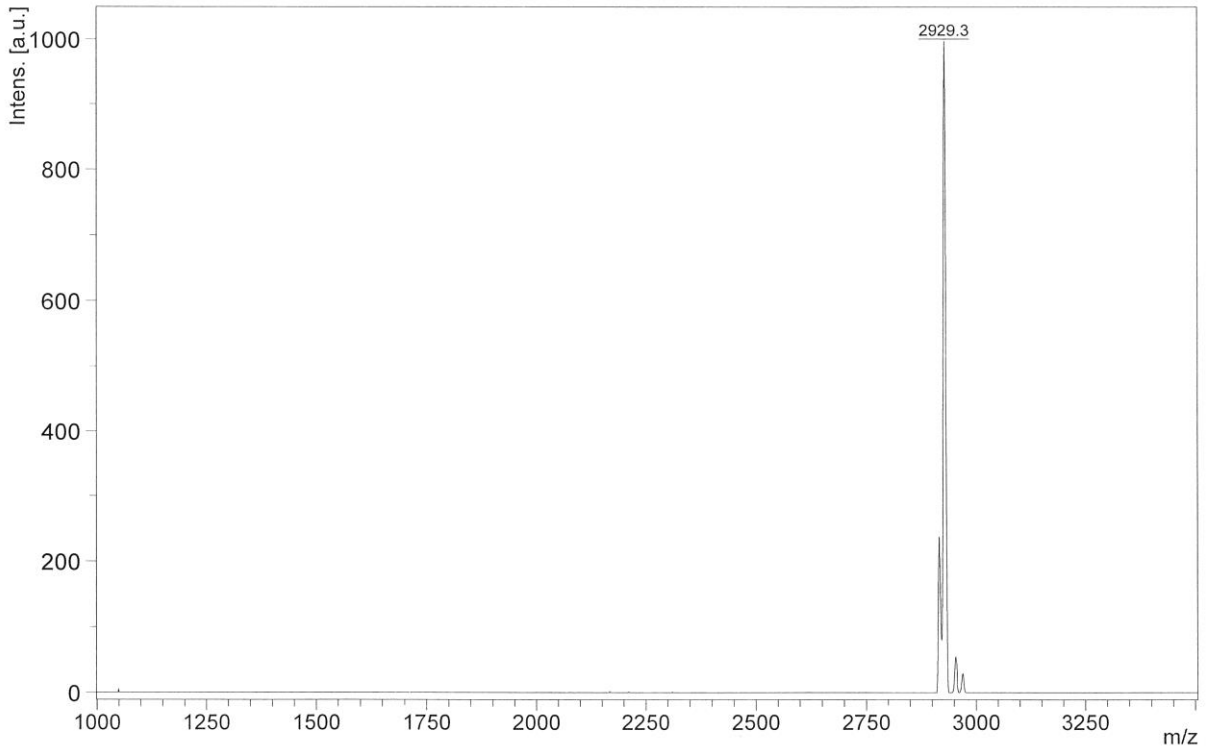

990 (SteA-ss-t)

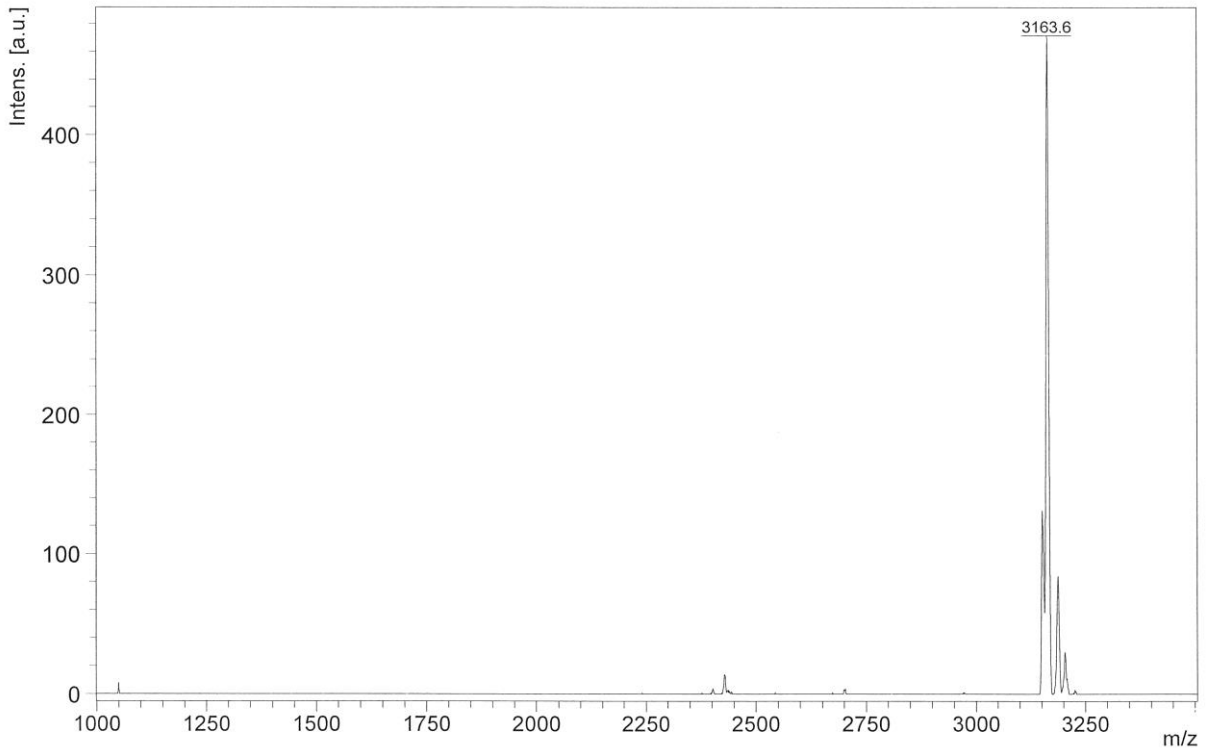

991 (CholA-t)

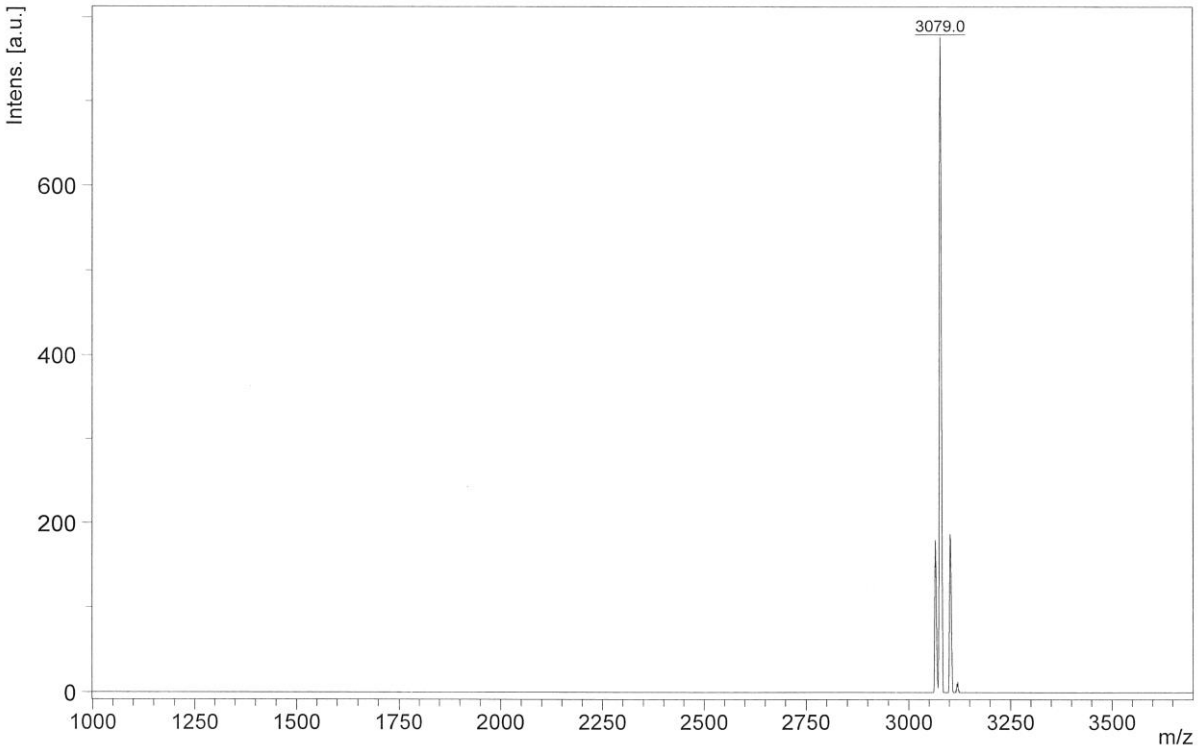

992 (CholA-ss-t)

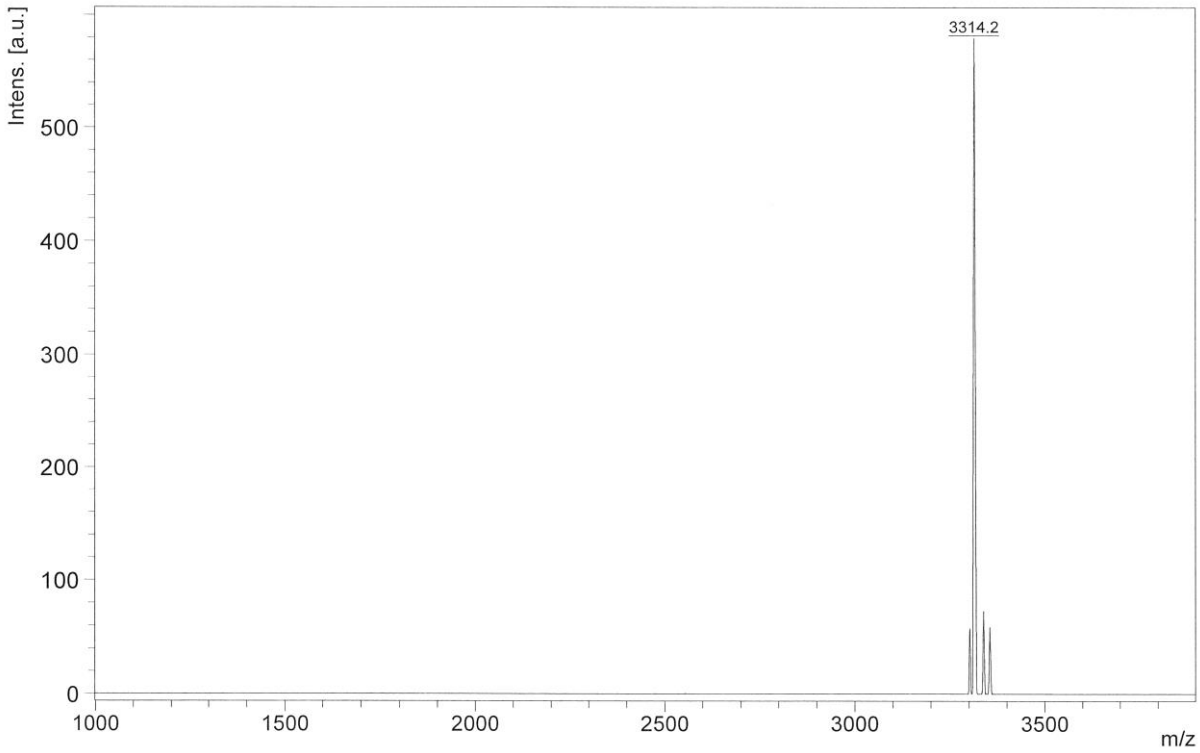

1073 (CholA-ss-t-N_3)

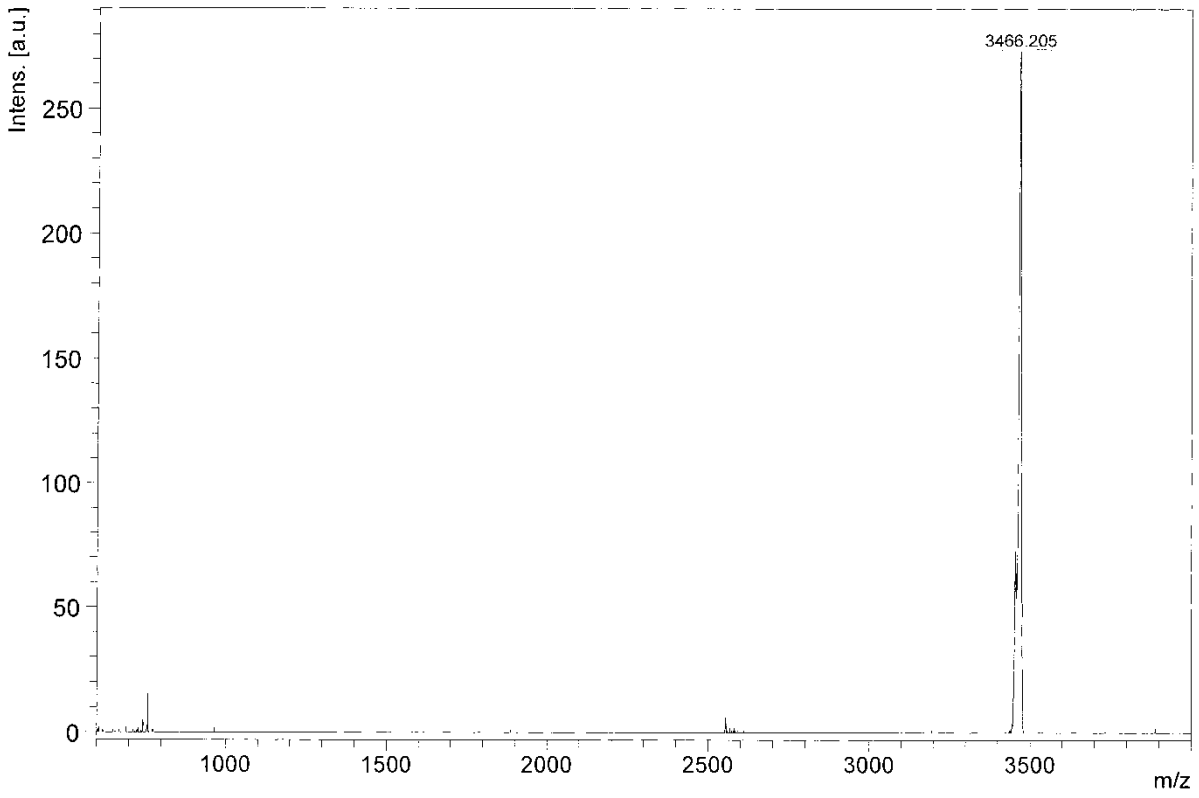

1081 (MyrA-t)

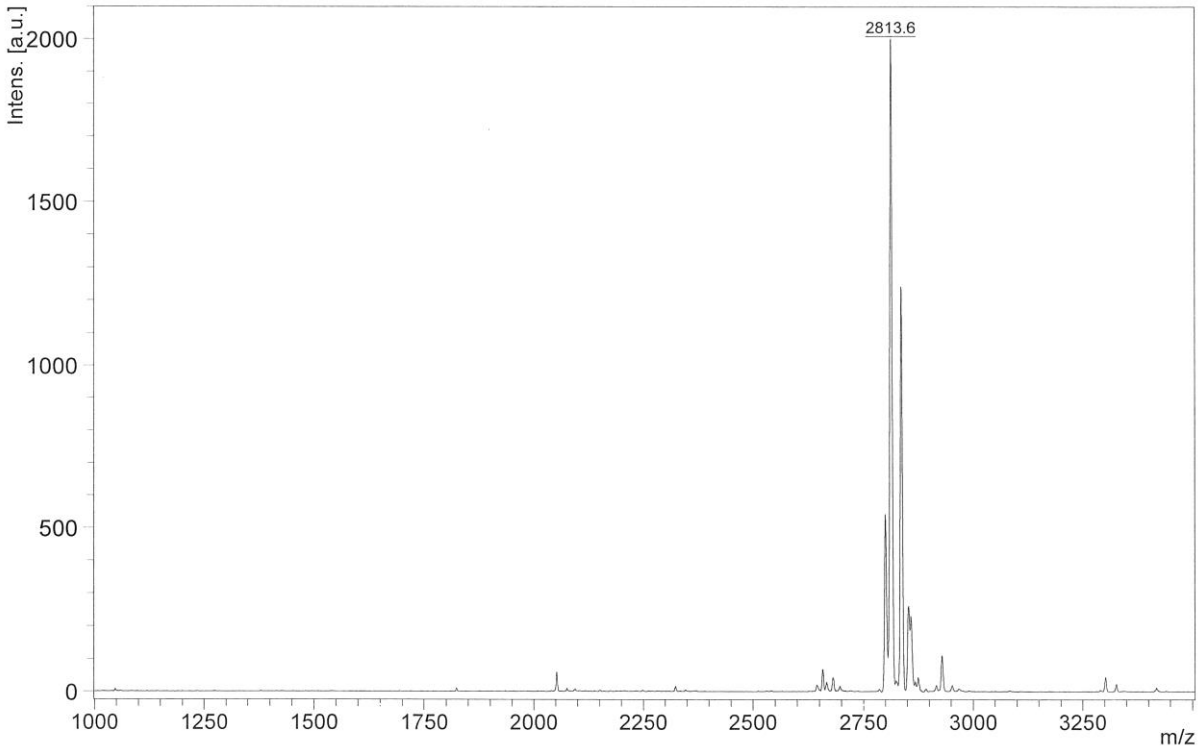

1082 (MyrA-ss-t)

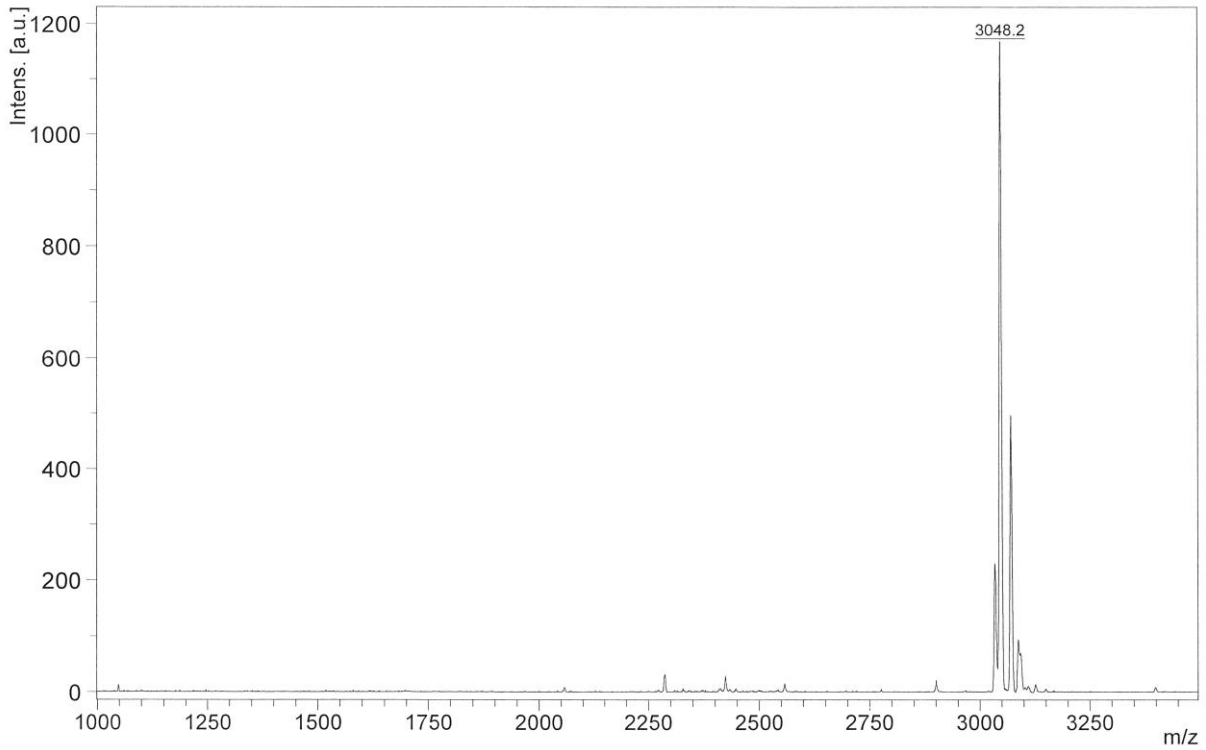

1086 (CholA-ss-t-2N_3)

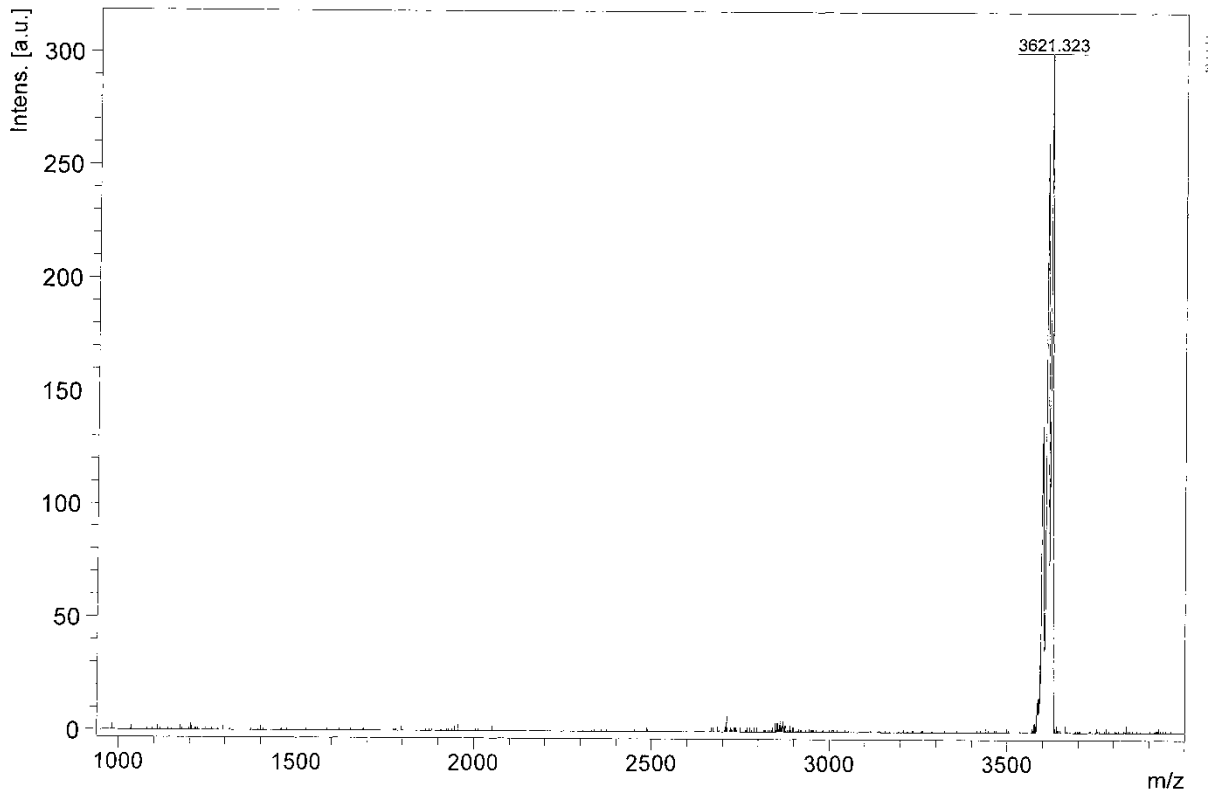

1106 (CholA-t-N_3)

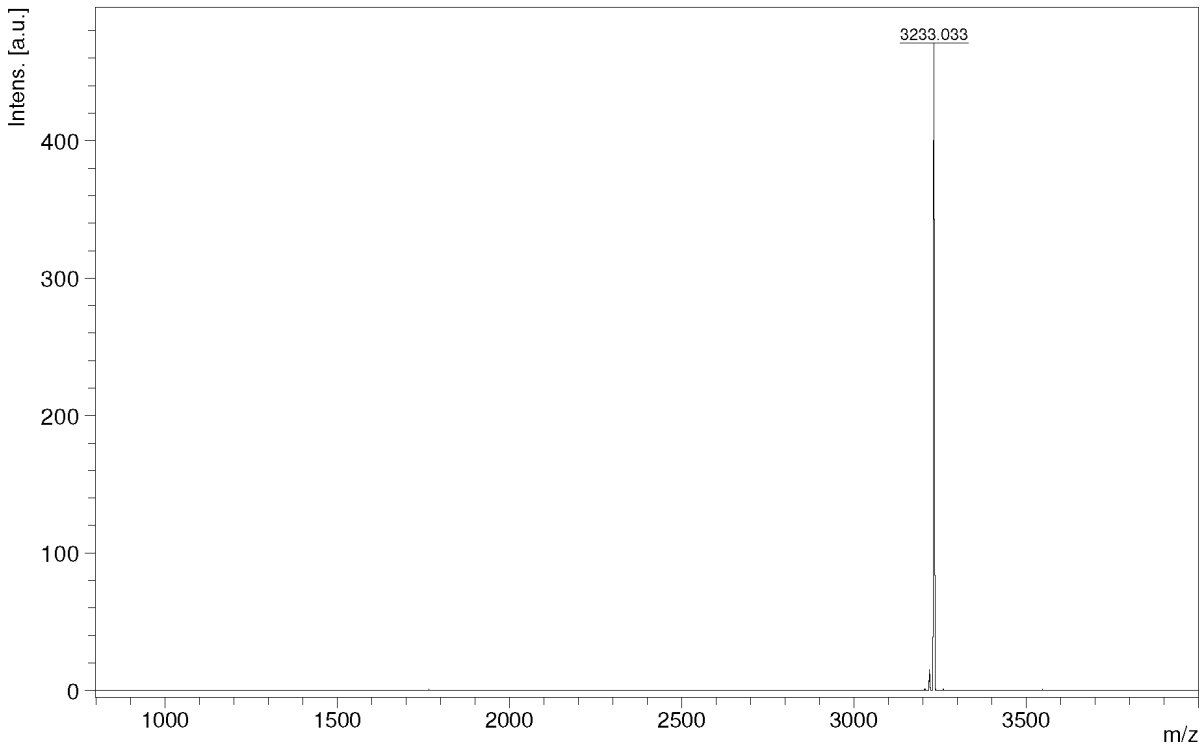

1107 (OleA-t)

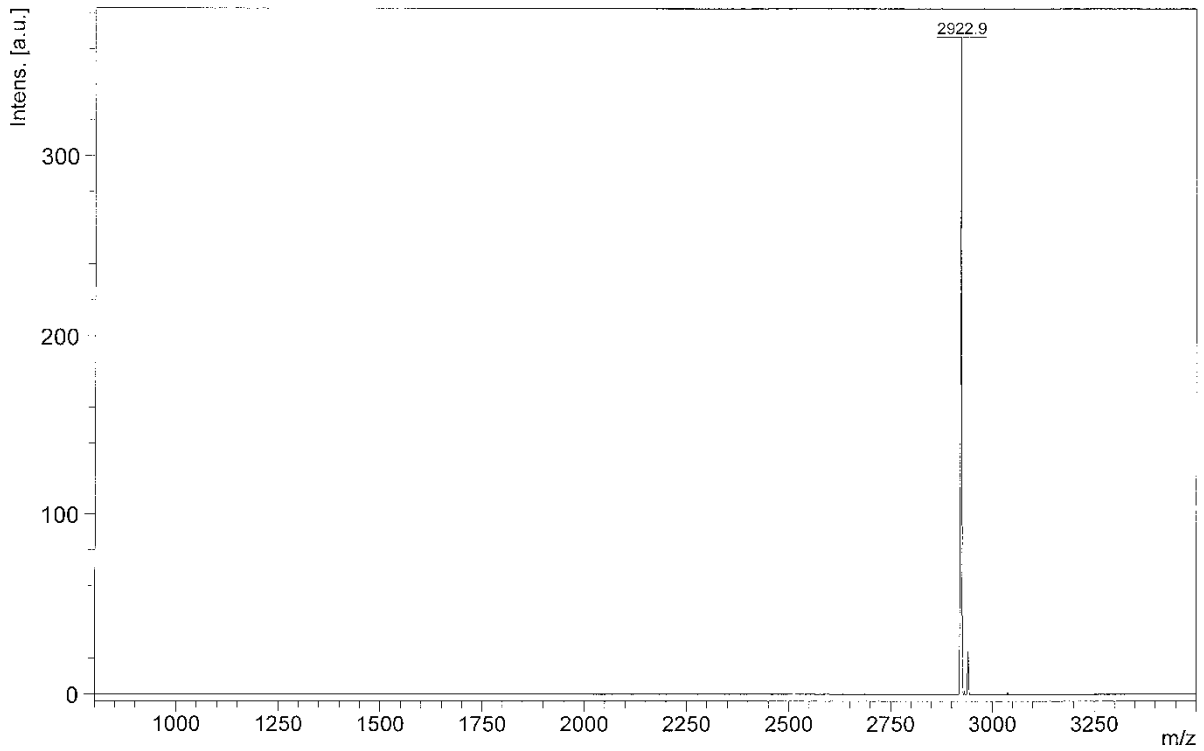

1108 (OleA-ss-t)

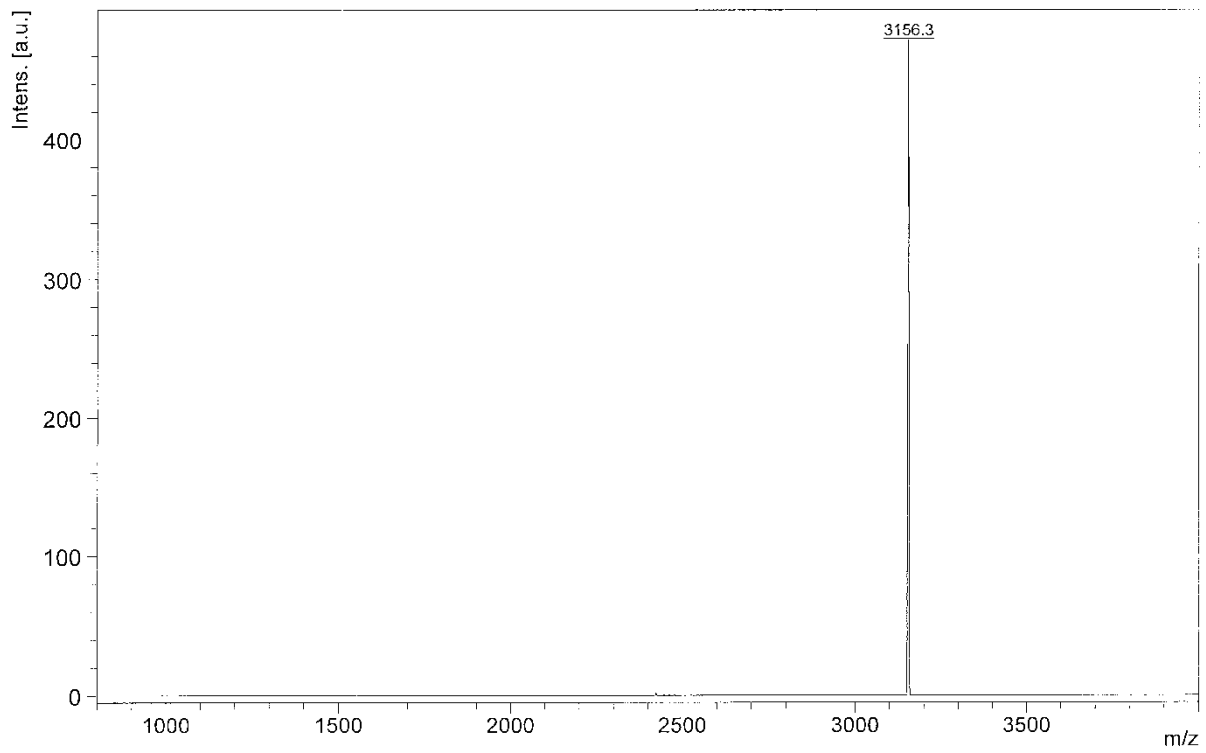

6.4.4 Mass spectra of shielding agents

Table 21 Summarizing table shielding agents. Mass data recorded with a Bruker MALDI-TOF instrument

Shielding agent	ID	Molecular formula	$[M+X]^+$ calc.	$[M+X]^+$ found
DBCO-PEG$_{24}$	***1138***	$C_{72}H_{120}N_2O_{28}$	1482.8 [Na]	1481.3 [Na]
DBCO-PEG$_{24}$-FolA	***1139***	$C_{97}H_{149}N_{11}O_{34}$	2033.0 [Na]	2035.5 [Na]
DBCO-PEG$_{48}$-FolA	***1140***	$C_{148}H_{250}N_{12}O_{59}$	3161.7 [Na]	3158.1 [Na]
DBCO-PEG$_{72}$-FolA	***1141***	$C_{199}H_{351}N_{13}O_{84}$	4289.4 [Na]	4284.2 [Na]
DBCO$_2$-ss$_2$-PEG$_{24}$-FolA	***1145***	$C_{140}H_{206}N_{18}O_{41}S_4$	2923.4 [H]	2922.9 [H]
DBCO$_2$-ss$_2$-PEG$_{48}$-FolA	***1146***	$C_{191}H_{307}N_{19}O_{66}S_4$	4073. [Na]	4073.1 [Na]
DBCO$_2$-ss$_2$-PEG$_{72}$-FolA	***1147***	$C_{242}H_{408}N_{20}O_{91}S_4$	5200. [Na]	5196.2 [Na]

6.4.4.1 Full mass spectra of shielding agents

1138 (DBCO-PEG$_{24}$)

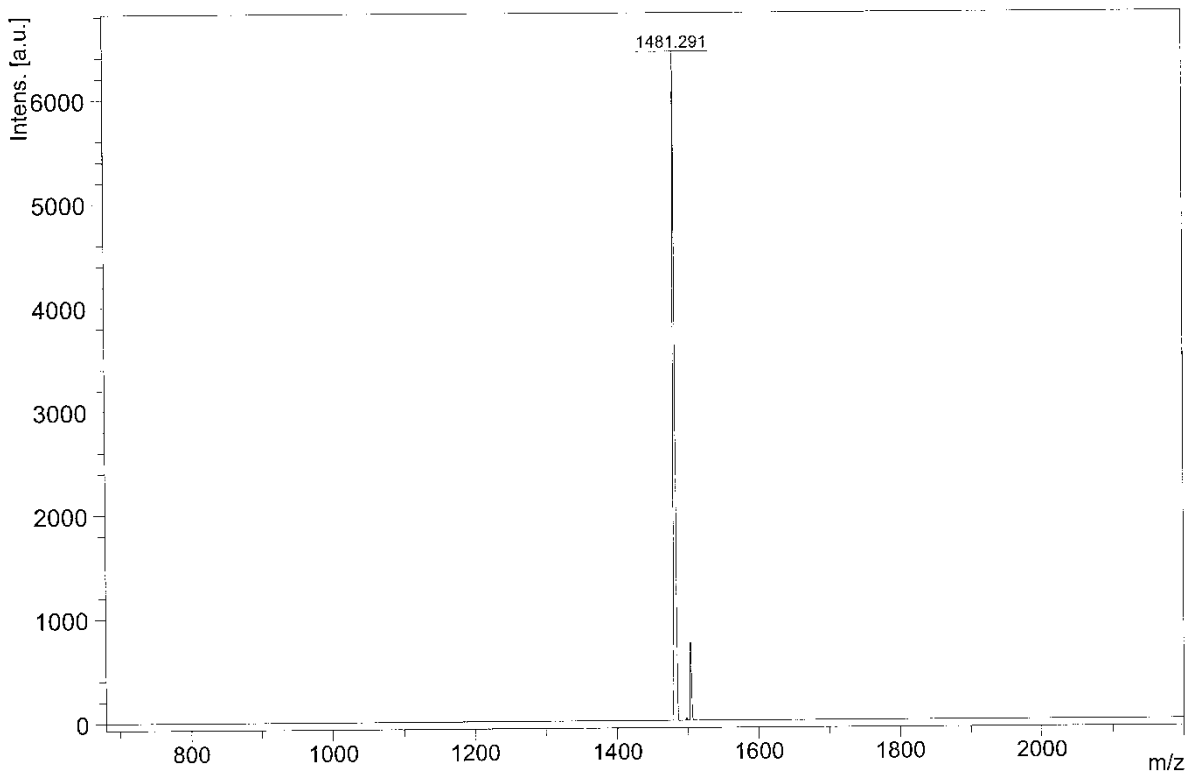

1139 (DBCO-PEG$_{24}$-FolA)

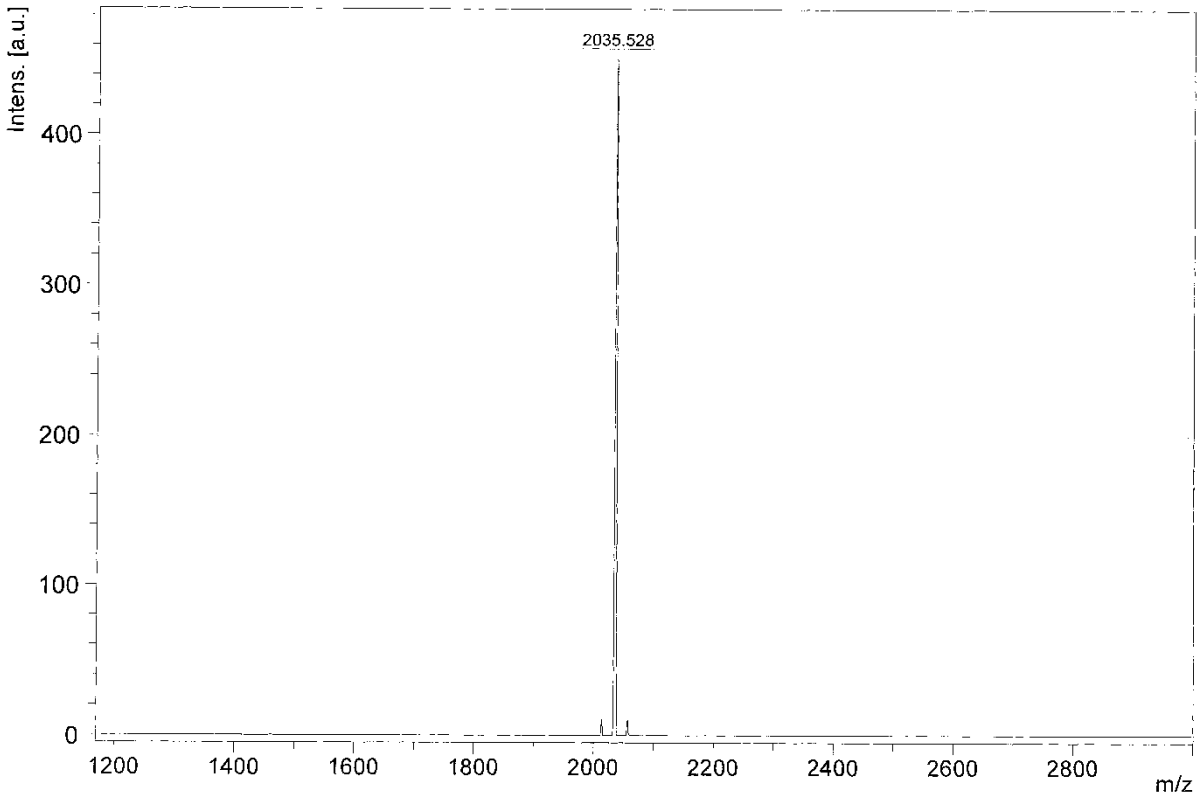

1140 (DBCO-PEG$_{48}$-FolA)

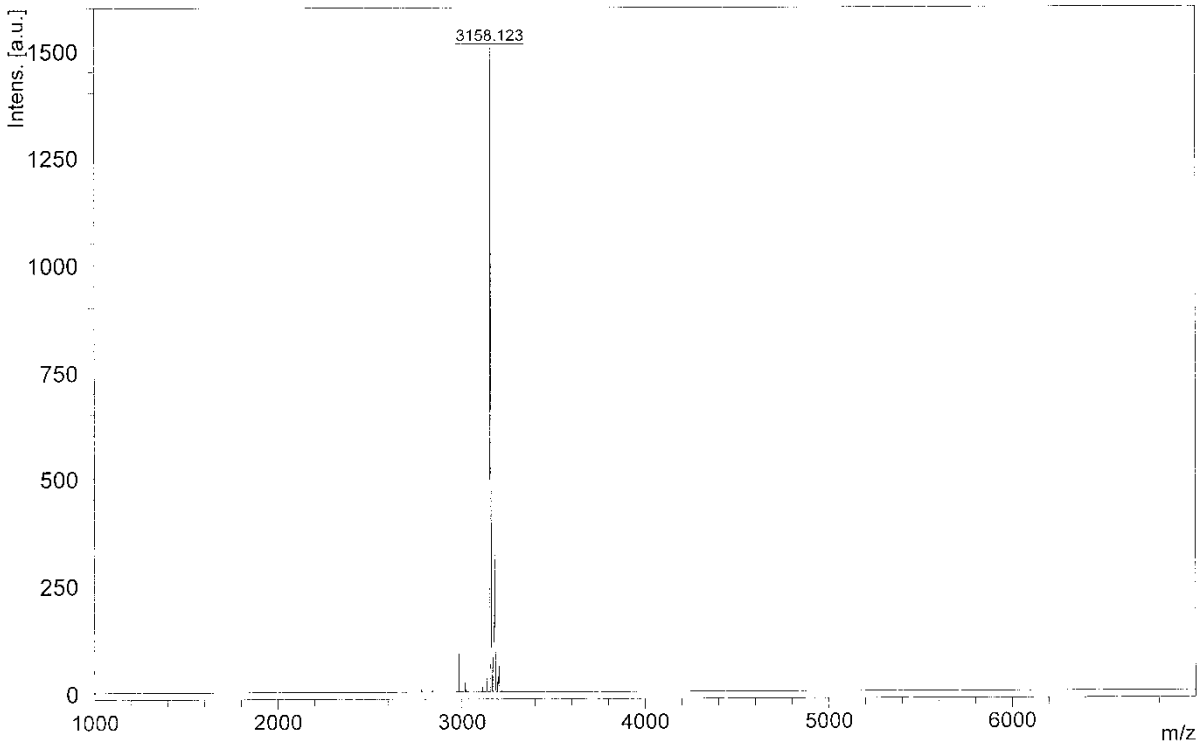

1141 (DBCO-PEG$_{72}$-FolA)

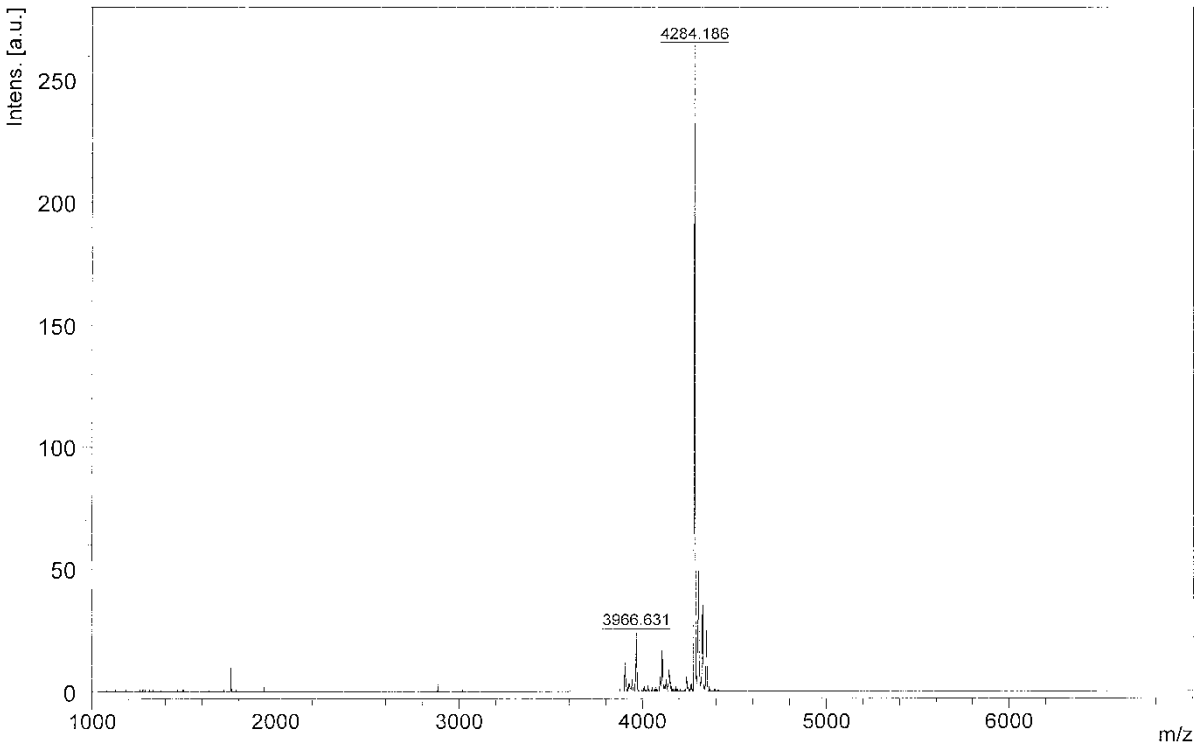

1145 (DBCO$_2$-ss$_2$-PEG$_{24}$-FolA)

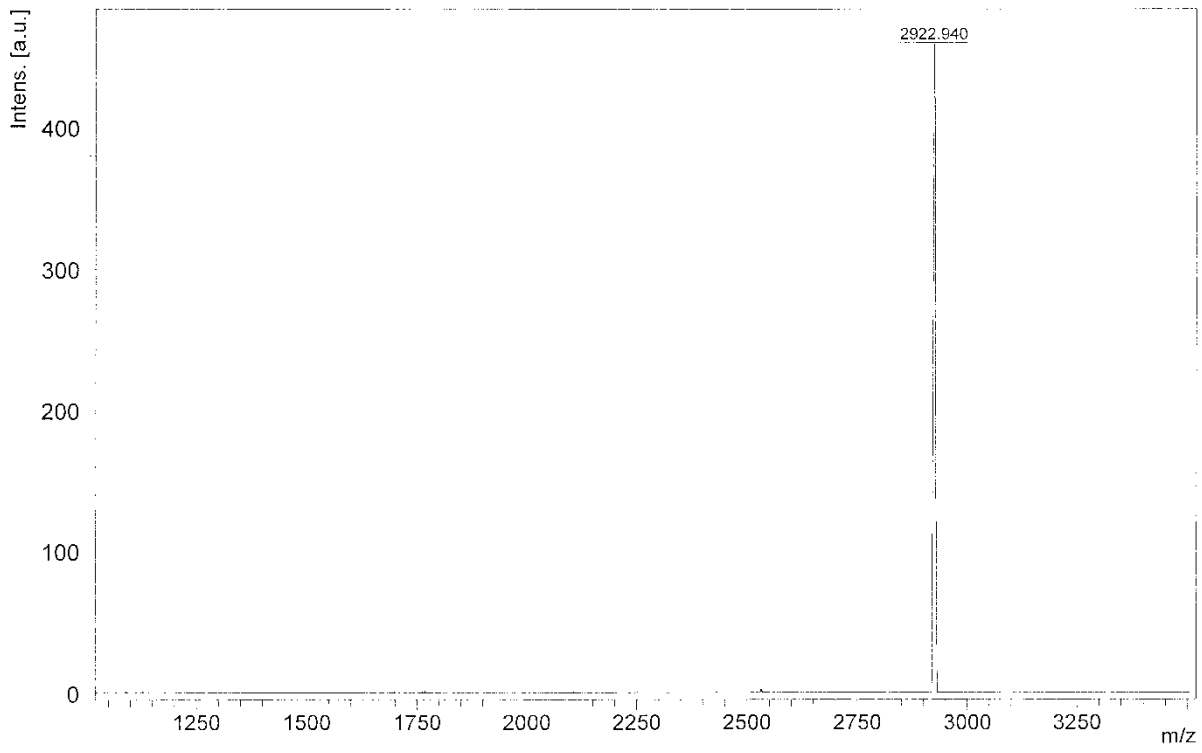

1146 ($DBCO_2$-ss_2-PEG_{24}-FolA)

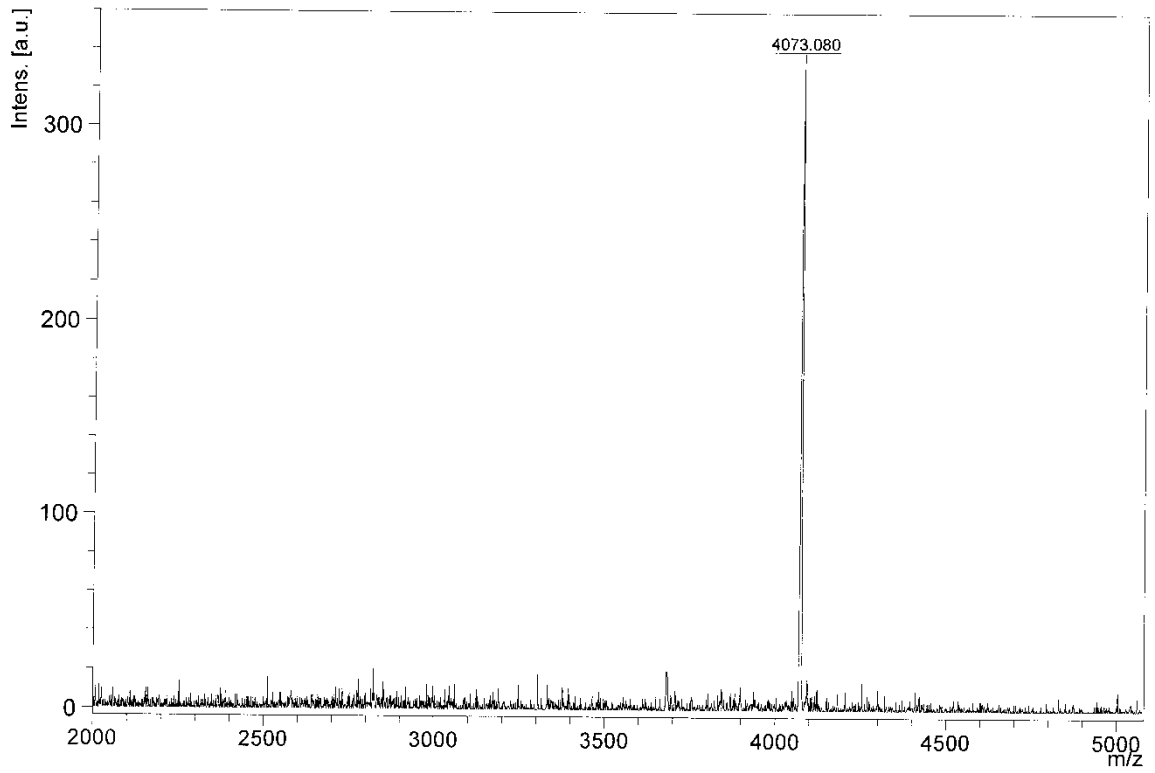

1147 ($DBCO_2$-ss_2-PEG_{24}-FolA)

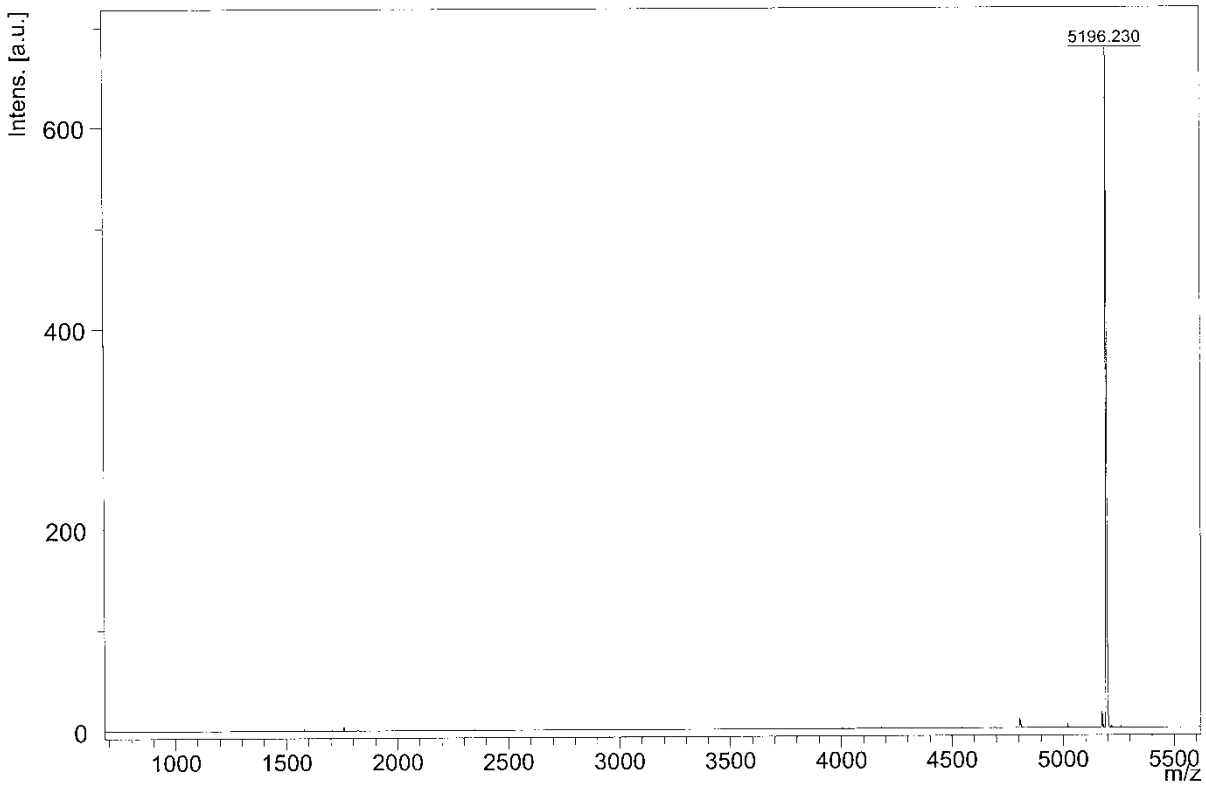

6.5 Copyright and licenses

The permissions for the reuse of published articles in this theses were requested from the respective journals.

Klein PM, Wagner E. *Bioreducible Polycations as Shuttles for Therapeutic Nucleic Acid and Protein Transfection.* ***Antioxid Redox Signal.*** 2014 Aug 10;21(5):804-17

Mary Ann Liebert, Inc. publishers does not require authors of the content being used to obtain a license for their personal reuse of full article, charts/graphs/tables or text excerpt.

Klein PM, Müller K, Gutmann C, Kos P, Krhac Levacic A, Edinger D, Höhn M, Leroux JC, Gauthier MA, Wagner E. *Twin disulfides as opportunity for improving stability and transfection efficiency of oligoaminoethane polyplexes.* ***J Control Release.*** 2015 May 10;205:109-19

The license for the reuse of the article in this thesis was obtained from Elsevier via RightsLink (License Number: 4155360203185)

Klein PM*, Reinhard S*, Lee DJ, Müller K, Ponader D, Hartmann L, Wagner E. *Precise redox-sensitive cleavage sites for improved bioactivity of siRNA lipopolyplexes.* ***Nanoscale***, 2016,8, 18098-18104 - Published by The Royal Society of Chemistry.

This article is licensed under a Creative Commons Attribution-NonCommercial 3.0 Unported Licence.

7 References

[1] D. Lew, S.E. Parker, T. Latimer, A.M. Abai, A. Kuwahararundell, S.G. Doh, Z.Y. Yang, D. Laface, S.H. Gromkowski, G.J. Nabel, M. Manthorpe, J. Norman, Cancer Gene-Therapy Using Plasmid DNA - Pharmacokinetic Study of DNA Following Injection in Mice, Human Gene Therapy 6(5) (1995) 553-564.
[2] S.M. Elbashir, J. Harborth, W. Lendeckel, A. Yalcin, K. Weber, T. Tuschl, Duplexes of 21-nucleotide RNAs mediate RNA interference in cultured mammalian cells, Nature 411(6836) (2001) 494-8.
[3] T. Tuschl, RNA interference and small interfering RNAs, Chembiochem 2(4) (2001) 239-45.
[4] A.F. Ibrahim, U. Weirauch, M. Thomas, A. Grunweller, R.K. Hartmann, A. Aigner, MicroRNA Replacement Therapy for miR-145 and miR-33a Is Efficacious in a Model of Colon Carcinoma, Cancer Research 71(15) (2011) 5214-5224.
[5] J. Kota, R.R. Chivukula, K.A. O'Donnell, E.A. Wentzel, C.L. Montgomery, H.W. Hwang, T.C. Chang, P. Vivekanandan, M. Torbenson, K.R. Clark, J.R. Mendell, J.T. Mendell, Therapeutic microRNA delivery suppresses tumorigenesis in a murine liver cancer model, Cell 137(6) (2009) 1005-17.
[6] D. Bumcrot, M. Manoharan, V. Koteliansky, D.W. Sah, RNAi therapeutics: a potential new class of pharmaceutical drugs, Nat Chem Biol 2(12) (2006) 711-9.
[7] X. Chen, N. Dudgeon, L. Shen, J.H. Wang, Chemical modification of gene silencing oligonucleotides for drug discovery and development, Drug Discov Today 10(8) (2005) 587-93.
[8] E. Wagner, Programmed drug delivery: nanosystems for tumor targeting, Expert Opin Biol Ther 7(5) (2007) 587-93.
[9] T.I. Kim, S.W. Kim, Bioreducible polymers for gene delivery, Reactive Funct Polym 71 (2011) 344.
[10] G. Saito, J.A. Swanson, K.D. Lee, Drug delivery strategy utilizing conjugation via reversible disulfide linkages: role and site of cellular reducing activities, Adv Drug Deliv Rev 55(2) (2003) 199-215.
[11] S. Son, R. Namgung, J. Kim, K. Singha, W.J. Kim, Bioreducible polymers for gene silencing and delivery, Acc Chem Res 45(7) (2012) 1100-12.
[12] P.L. Felgner, Y. Barenholz, J.P. Behr, S.H. Cheng, P. Cullis, L. Huang, J.A. Jessee, L. Seymour, F. Szoka, A.R. Thierry, E. Wagner, G. Wu, Nomenclature for synthetic gene delivery systems, Hum Gene Ther 8(5) (1997) 511-2.
[13] C. Scholz, E. Wagner, Therapeutic plasmid DNA versus siRNA delivery: common and different tasks for synthetic carriers, J Control Release 161(2) (2012) 554-65.
[14] J.F. Kukowska-Latallo, A.U. Bielinska, J. Johnson, R. Spindler, D.A. Tomalia, J.R. Baker, Efficient transfer of genetic material into mammalian cells using Starburst polyamidoamine dendrimers, Proc Natl Acad Sci USA 93 (1996) 4897.
[15] A. Schlossbauer, C. Dohmen, D. Schaffert, E. Wagner, T. Bein, pH-responsive release of acetal-linked melittin from SBA-15 mesoporous silica, Angew Chem Int Ed Engl 50(30) (2011) 6828-30.
[16] E. Wagner, J. Kloeckner, Gene delivery using polymer therapeutics, Polymer Therapeutics I: Polymers as Drugs, Conjugates and Gene Delivery Systems 192 (2006) 135-173.
[17] A.G. Ziady, T. Ferkol, D.V. Dawson, D.H. Perlmutter, P.B. Davis, Chain length of the polylysine in receptor-targeted gene transfer complexes affects duration of reporter

gene expression both in vitro and in vivo, Journal of Biological Chemistry 274(8) (1999) 4908-4916.
[18] B.H. Zinselmeyer, S.P. Mackay, A.G. Schatzlein, I.F. Uchegbu, The lower-generation polypropylenimine dendrimers are effective gene-transfer agents, Pharm Res 19(7) (2002) 960-7.
[19] M.A. Wolfert, L.W. Seymour, Atomic force microscopic analysis of the influence of the molecular weight of poly(L)lysine on the size of polyelectrolyte complexes formed with DNA 723, Gene Ther 3 (1996) 269.
[20] C. Plank, K. Mechtler, F.C. Szoka, Jr., E. Wagner, Activation of the complement system by synthetic DNA complexes: a potential barrier for intravenous gene delivery, Hum Gene Ther 7(12) (1996) 1437-46.
[21] K. Itaka, A. Harada, Y. Yamasaki, K. Nakamura, H. Kawaguchi, K. Kataoka, In situ single cell observation by fluorescence resonance energy transfer reveals fast intra-cytoplasmic delivery and easy release of plasmid DNA complexed with linear polyethylenimine, J Gene Med 6(1) (2004) 76-84.
[22] D.V. Schaffer, N.A. Fidelman, N. Dan, D.A. Lauffenburger, Vector unpacking as a potential barrier for receptor-mediated polyplex gene delivery, Biotechnology and Bioengineering 67(5) (2000) 598-606.
[23] L. Joshua-Tor, siRNAs at RISC, Structure 12(7) (2004) 1120-1122.
[24] R.S. Burke, S.H. Pun, Extracellular barriers to in Vivo PEI and PEGylated PEI polyplex-mediated gene delivery to the liver, Bioconjug Chem 19(3) (2008) 693-704.
[25] M. Breunig, U. Lungwitz, R. Liebl, A. Goepferich, Breaking up the correlation between efficacy and toxicity for nonviral gene delivery, Proc Natl Acad Sci U S A 104(36) (2007) 14454-9.
[26] M.L. Forrest, J.T. Koerber, D.W. Pack, A degradable polyethylenimine derivative with low toxicity for highly efficient gene delivery, Bioconjug Chem 14(5) (2003) 934-40.
[27] M.A. Gosselin, W.J. Guo, R.J. Lee, Efficient gene transfer using reversibly cross-linked low molecular weight polyethylenimine, Bioconjugate Chemistry 12(6) (2001) 989-994.
[28] S. Han, R.I. Mahato, Y.K. Sung, S.W. Kim, Development of biomaterials for gene therapy, Mol Ther 2(4) (2000) 302-17.
[29] J. Kloeckner, S. Bruzzano, M. Ogris, E. Wagner, Gene carriers based on hexanediol diacrylate linked oligoethylenimine: effect of chemical structure of polymer on biological properties, Bioconjug Chem 17(5) (2006) 1339-45.
[30] V. Knorr, M. Ogris, E. Wagner, An Acid Sensitive Ketal-Based Polyethylene Glycol-Oligoethylenimine Copolymer Mediates Improved Transfection Efficiency at Reduced Toxicity, Pharmaceutical Research 25(12) (2008) 2937-2945.
[31] D.W. Pack, A.S. Hoffman, S. Pun, P.S. Stayton, Design and development of polymers for gene delivery, Nat Rev Drug Discov 4(7) (2005) 581-93.
[32] M. Thomas, Q. Ge, J.J. Lu, J.Z. Chen, A.M. Klibanov, Cross-linked small polyethylenimines: While still nontoxic, deliver DNA efficiently to mammalian cells in vitro and in vivo, Pharmaceutical Research 22(3) (2005) 373-380.
[33] D. Fass, Disulfide bonding in protein biophysics, Annu Rev Biophys 41 (2012) 63-79.
[34] A. Holmgren, M. Bjornstedt, Thioredoxin and thioredoxin reductase, Methods Enzymol 252 (1995) 199-208.
[35] F.Q. Schafer, G.R. Buettner, Redox environment of the cell as viewed through the redox state of the glutathione disulfide/glutathione couple, Free Radical Biology and Medicine 30(11) (2001) 1191-1212.

[36] X. Chen, Y. Bai, J.L. Zaro, W.C. Shen, Design of an in vivo cleavable disulfide linker in recombinant fusion proteins, Biotechniques 49(1) (2010) 513-8.
[37] N.L. Letvin, V.S. Goldmacher, J. Ritz, J.M. Yetz, S.F. Schlossman, J.M. Lambert, In vivo administration of lymphocyte-specific monoclonal antibodies in nonhuman primates. In vivo stability of disulfide-linked immunotoxin conjugates, J Clin Invest 77(3) (1986) 977-84.
[38] P.E. Thorpe, P.M. Wallace, P.P. Knowles, M.G. Relf, A.N. Brown, G.J. Watson, R.E. Knyba, E.J. Wawrzynczak, D.C. Blakey, New coupling agents for the synthesis of immunotoxins containing a hindered disulfide bond with improved stability in vivo, Cancer Res 47(22) (1987) 5924-31.
[39] L.D. DeLeve, N. Kaplowitz, Glutathione metabolism and its role in hepatotoxicity, Pharmacol Ther 52(3) (1991) 287-305.
[40] C.Q. Xia, J. Wang, W.C. Shen, Hypoglycemic effect of insulin-transferrin conjugate in streptozotocin-induced diabetic rats, J Pharmacol Exp Ther 295(2) (2000) 594-600.
[41] R. Noiva, Protein disulfide isomerase: the multifunctional redox chaperone of the endoplasmic reticulum, Semin Cell Dev Biol 10(5) (1999) 481-93.
[42] D.P. Jones, J.L. Carlson, P.S. Samiec, P. Sternberg, Jr., V.C. Mody, Jr., R.L. Reed, L.A. Brown, Glutathione measurement in human plasma. Evaluation of sample collection, storage and derivatization conditions for analysis of dansyl derivatives by HPLC, Clin Chim Acta 275(2) (1998) 175-84.
[43] C. Wu, J.C. Leroux, M.A. Gauthier, Twin disulfides for orthogonal disulfide pairing and the directed folding of multicyclic peptides, Nat Chem 4(12) (2012) 1044-9.
[44] D.L. McKenzie, K.Y. Kwok, K.G. Rice, A potent new class of reductively activated peptide gene delivery agents, J Biol Chem 275(14) (2000) 9970-7.
[45] M.L. Read, K.H. Bremner, D. Oupicky, N.K. Green, P.F. Searle, L.W. Seymour, Vectors based on reducible polycations facilitate intracellular release of nucleic acids, J Gene Med 5(3) (2003) 232-45.
[46] M.L. Read, S. Singh, Z. Ahmed, M. Stevenson, S.S. Briggs, D. Oupicky, L.B. Barrett, R. Spice, M. Kendall, M. Berry, J.A. Preece, A. Logan, L.W. Seymour, A versatile reducible polycation-based system for efficient delivery of a broad range of nucleic acids, Nucleic Acids Res 33(9) (2005) e86.
[47] O. Boussif, F. Lezoualch, M.A. Zanta, M.D. Mergny, D. Scherman, B. Demeneix, J.P. Behr, A Versatile Vector for Gene and Oligonucleotide Transfer into Cells in Culture and in-Vivo - Polyethylenimine, P Natl Acad Sci USA 92(16) (1995) 7297-7301.
[48] S.M. Zou, P. Erbacher, J.S. Remy, J.P. Behr, Systemic linear polyethylenimine (L-PEI)-mediated gene delivery in the mouse, J Gene Med 2(2) (2000) 128-34.
[49] A.P. Tanna, D.L. Budenz, J. Bandi, W.J. Feuer, R.M. Feldman, L.W. Herndon, D.J. Rhee, J. Whiteside-de Vos, J. Huang, D.R. Anderson, Glaucoma Progression Analysis software compared with expert consensus opinion in the detection of visual field progression in glaucoma, Ophthalmology 119(3) (2012) 468-73.
[50] J.P. Behr, The proton sponge: a trick to enter cells the viruses did not exploit, Chimia 51 (1997) 34.
[51] R.V. Benjaminsen, M.A. Mattebjerg, J.R. Henriksen, S.M. Moghimi, T.L. Andresen, The possible “proton sponge” effect of polyethylenimine (PEI) does not include change in lysosomal pH, Mol Ther 21 (2013) 149.
[52] N.D. Sonawane, F.C. Szoka, Jr., A.S. Verkman, Chloride accumulation and swelling in endosomes enhances DNA transfer by polyamine-DNA polyplexes, J Biol Chem 278(45) (2003) 44826-31.
[53] A. von Harpe, H. Petersen, Y. Li, T. Kissel, Characterization of commercially available and synthesized polyethylenimines for gene delivery, J Control Release 69(2) (2000) 309-22.

[54] G. Grandinetti, N.P. Ingle, T.M. Reineke, Interaction of poly(ethylenimine)-DNA polyplexes with mitochondria: implications for a mechanism of cytotoxicity, Mol Pharm 8(5) (2011) 1709-19.
[55] S.M. Moghimi, P. Symonds, J.C. Murray, A.C. Hunter, G. Debska, A. Szewczyk, A two-stage poly(ethylenimine)-mediated cytotoxicity: implications for gene transfer/therapy, Mol Ther 11(6) (2005) 990-5.
[56] H. Koo, G.W. Jin, H. Kang, Y. Lee, K. Nam, C. Zhe Bai, J.S. Park, Biodegradable branched poly(ethylenimine sulfide) for gene delivery, Biomaterials 31(5) (2010) 988-97.
[57] L.V. Christensen, C.W. Chang, W.J. Kim, S.W. Kim, Z. Zhong, C. Lin, J.F. Engbersen, J. Feijen, Reducible poly(amido ethylenimine)s designed for triggered intracellular gene delivery, Bioconjug Chem 17(5) (2006) 1233-40.
[58] C. Lin, C.J. Blaauboer, M.M. Timoneda, M.C. Lok, M. van Steenbergen, W.E. Hennink, Z. Zhong, J. Feijen, J.F. Engbersen, Bioreducible poly(amido amine)s with oligoamine side chains: synthesis, characterization, and structural effects on gene delivery, J Control Release 126(2) (2008) 166-74.
[59] C. Lin, Z. Zhong, M.C. Lok, X. Jiang, W.E. Hennink, J. Feijen, J.F. Engbersen, Novel bioreducible poly(amido amine)s for highly efficient gene delivery, Bioconjug Chem 18(1) (2007) 138-45.
[60] P. Midoux, M. Monsigny, Efficient gene transfer by histidylated polylysine/pDNA complexes, Bioconjug Chem 10(3) (1999) 406-11.
[61] C. Pichon, M.B. Roufai, M. Monsigny, P. Midoux, Histidylated oligolysines increase the transmembrane passage and the biological activity of antisense oligonucleotides, Nucleic Acids Res 28(2) (2000) 504-12.
[62] U. Lachelt, P. Kos, F.M. Mickler, A. Herrmann, E.E. Salcher, W. Rodl, N. Badgujar, C. Brauchle, E. Wagner, Fine-tuning of proton sponges by precise diaminoethanes and histidines in pDNA polyplexes, Nanomedicine 10(1) (2014) 35-44.
[63] L. Hartmann, S. Haefele, R. Peschka-Suess, M. Antonietti, H.G. Boerner, Sequence positioning of disulfide linkages to program the degradation of monodisperse poly(amidoamines), Macromolecules 40(22) (2007) 7771-7776.
[64] L. Hartmann, S. Hafele, R. Peschka-Suss, M. Antonietti, H.G. Borner, Tailor-made poly(amidoamine)s for controlled complexation and condensation of DNA, Chemistry 14(7) (2008) 2025-33.
[65] L. Hartmann, E. Krause, M. Antonietti, H.G. Borner, Solid-phase supported polymer synthesis of sequence-defined, multifunctional poly(amidoamines), Biomacromolecules 7(4) (2006) 1239-44.
[66] D. Schaffert, N. Badgujar, E. Wagner, Novel Fmoc-polyamino acids for solid-phase synthesis of defined polyamidoamines, Org Lett 13(7) (2011) 1586-9.
[67] D. Schaffert, C. Troiber, E. Wagner, New sequence-defined polyaminoamides with tailored endosomolytic properties for plasmid DNA delivery, Bioconjug Chem 23(6) (2012) 1157-65.
[68] E.E. Salcher, P. Kos, T. Frohlich, N. Badgujar, M. Scheible, E. Wagner, Sequence-defined four-arm oligo(ethanamino)amides for pDNA and siRNA delivery: Impact of building blocks on efficacy, J Control Release 164(3) (2012) 380-6.
[69] A. Kwok, S.L. Hart, Comparative structural and functional studies of nanoparticle formulations for DNA and siRNA delivery, Nanomedicine 7(2) (2011) 210-9.
[70] E. Wagner, Biomaterials in RNAi therapeutics: quo vadis?, Biomater Sci 1 (2013) 804.
[71] J. DeRouchey, C. Schmidt, G.F. Walker, C. Koch, C. Plank, E. Wagner, J.O. Radler, Monomolecular assembly of siRNA and poly(ethylene glycol)-peptide copolymers, Biomacromolecules 9(2) (2008) 724-32.

[72] E. Wagner, Polymers for siRNA Delivery: Inspired by Viruses to be Targeted, Dynamic, and Precise, Accounts of Chemical Research 45(7) (2012) 1005-1013.
[73] M. Meyer, A. Philipp, R. Oskuee, C. Schmidt, E. Wagner, Breathing life into polycations: Functionalization with pH-responsive endosomolytic peptides and polyethylene glycol enables siRNA delivery, Journal of the American Chemical Society 130(11) (2008) 3272-+.
[74] S.Y. Lee, M.S. Huh, S. Lee, S.J. Lee, H. Chung, J.H. Park, Y.K. Oh, K. Choi, K. Kim, I.C. Kwon, Stability and cellular uptake of polymerized siRNA (poly-siRNA)/polyethylenimine (PEI) complexes for efficient gene silencing, Journal of Controlled Release 141(3) (2010) 339-346.
[75] H. Mok, S.H. Lee, J.W. Park, T.G. Park, Multimeric small interfering ribonucleic acid for highly efficient sequence-specific gene silencing, Nat Mater 9(3) (2010) 272-8.
[76] P. Heissig, P.M. Klein, P. Hadwiger, E. Wagner, DNA as Tunable Adaptor for siRNA Polyplex Stabilization and Functionalization, Mol Ther Nucleic Acids 5 (2016) e288.
[77] C. Dohmen, T. Frohlich, U. Lachelt, I. Rohl, H.P. Vornlocher, P. Hadwiger, E. Wagner, Defined Folate-PEG-siRNA Conjugates for Receptor-specific Gene Silencing, Mol Ther Nucleic Acids 1 (2012) e7.
[78] M. Meyer, C. Dohmen, A. Philipp, D. Kiener, G. Maiwald, C. Scheu, M. Ogris, E. Wagner, Synthesis and biological evaluation of a bioresponsive and endosomolytic siRNA-polymer conjugate, Mol Pharm 6(3) (2009) 752-62.
[79] R.G. Parmar, M. Busuek, E.S. Walsh, K.R. Leander, B.J. Howell, L. Sepp-Lorenzino, E. Kemp, L.S. Crocker, A. Leone, C.J. Kochansky, B.A. Carr, R.M. Garbaccio, S.L. Colletti, W. Wang, Endosomolytic bioreducible poly(amido amine disulfide) polymer conjugates for the in vivo systemic delivery of siRNA therapeutics, Bioconjug Chem 24(4) (2013) 640-7.
[80] T. Frohlich, D. Edinger, V. Russ, E. Wagner, Stabilization of polyplexes via polymer crosslinking for efficient siRNA delivery, Eur J Pharm Sci 47(5) (2012) 914-20.
[81] V. Russ, H. Elfberg, C. Thoma, J. Kloeckner, M. Ogris, E. Wagner, Novel degradable oligoethylenimine acrylate ester-based pseudodendrimers for in vitro and in vivo gene transfer, Gene Ther 15(1) (2008) 18-29.
[82] T. Frohlich, D. Edinger, R. Klager, C. Troiber, E. Salcher, N. Badgujar, I. Martin, D. Schaffert, A. Cengizeroglu, P. Hadwiger, H.P. Vornlocher, E. Wagner, Structure-activity relationships of siRNA carriers based on sequence-defined oligo (ethane amino) amides, J Control Release 160(3) (2012) 532-41.
[83] D. Schaffert, C. Troiber, E.E. Salcher, T. Frohlich, I. Martin, N. Badgujar, C. Dohmen, D. Edinger, R. Klager, G. Maiwald, K. Farkasova, S. Seeber, K. Jahn-Hofmann, P. Hadwiger, E. Wagner, Solid-Phase Synthesis of Sequence-Defined T-, i-, and U-Shape Polymers for pDNA and siRNA Delivery, Angewandte Chemie-International Edition 50(38) (2011) 8986-8989.
[84] C. Troiber, J.C. Kasper, S. Milani, M. Scheible, I. Martin, F. Schaubhut, S. Kuchler, J. Radler, F.C. Simmel, W. Friess, E. Wagner, Comparison of four different particle sizing methods for siRNA polyplex characterization, Eur J Pharm Biopharm 84(2) (2013) 255-64.
[85] X.L. Wang, R. Xu, Z.R. Lu, A peptide-targeted delivery system with pH-sensitive amphiphilic cell membrane disruption for efficient receptor-mediated siRNA delivery, J Control Release 134(3) (2009) 207-13.
[86] S. Matsumoto, R.J. Christie, N. Nishiyama, K. Miyata, A. Ishii, M. Oba, H. Koyama, Y. Yamasaki, K. Kataoka, Environment-responsive block copolymer micelles with a

disulfide cross-linked core for enhanced siRNA delivery, Biomacromolecules 10(1) (2009) 119-27.
[87] C. Dohmen, D. Edinger, T. Frohlich, L. Schreiner, U. Lachelt, C. Troiber, J. Radler, P. Hadwiger, H.P. Vornlocher, E. Wagner, Nanosized multifunctional polyplexes for receptor-mediated siRNA delivery, ACS Nano 6(6) (2012) 5198-208.
[88] E.P. Feener, W.C. Shen, H.J.P. Ryser, Cleavage of Disulfide Bonds in Endocytosed Macromolecules - a Processing Not Associated with Lysosomes or Endosomes, Journal of Biological Chemistry 265(31) (1990) 18780-18785.
[89] A.A. Kale, V.P. Torchilin, "Smart" drug carriers: PEGylated TATp-modified pH-sensitive liposomes, J Liposome Res 17(3-4) (2007) 197-203.
[90] V. Knorr, L. Allmendinger, G.F. Walker, F.F. Paintner, E. Wagner, An acetal-based PEGylation reagent for pH-sensitive shielding of DNA polyplexes, Bioconjug Chem 18(4) (2007) 1218-25.
[91] M. Meyer, E. Wagner, pH-responsive shielding of non-viral gene vectors, Expert Opin Drug Deliv 3(5) (2006) 563-71.
[92] Y. Nie, M. Gunther, Z. Gu, E. Wagner, Pyridylhydrazone-based PEGylation for pH-reversible lipopolyplex shielding, Biomaterials 32(3) (2011) 858-69.
[93] G.F. Walker, C. Fella, J. Pelisek, J. Fahrmeir, S. Boeckle, M. Ogris, E. Wagner, Toward synthetic viruses: endosomal pH-triggered deshielding of targeted polyplexes greatly enhances gene transfer in vitro and in vivo, Mol Ther 11(3) (2005) 418-25.
[94] S. Cerritelli, D. Velluto, J.A. Hubbell, PEG-SS-PPS: reduction-sensitive disulfide block copolymer vesicles for intracellular drug delivery, Biomacromolecules 8(6) (2007) 1966-72.
[95] R. Kuai, W.M. Yuan, Y. Qin, H.L. Chen, J. Tang, M.Q. Yuan, Z.R. Zhang, Q. He, Efficient Delivery of Payload into Tumor Cells in a Controlled Manner by TAT and Thiolytic Cleavable PEG Co-Modified Liposomes, Molecular Pharmaceutics 7(5) (2010) 1816-1826.
[96] Y. Ping, Q.D. Hu, G.P. Tang, J. Li, FGFR-targeted gene delivery mediated by supramolecular assembly between beta-cyclodextrin-crosslinked PEI and redox-sensitive PEG, Biomaterials 34(27) (2013) 6482-6494.
[97] H. Sun, B. Guo, R. Cheng, F. Meng, H. Liu, Z. Zhong, Biodegradable micelles with sheddable poly(ethylene glycol) shells for triggered intracellular release of doxorubicin, Biomaterials 30(31) (2009) 6358-66.
[98] M. Kursa, G.F. Walker, V. Roessler, M. Ogris, W. Roedl, R. Kircheis, E. Wagner, Novel shielded transferrin-polyethylene glycol-polyethylenimine/DNA complexes for systemic tumor-targeted gene transfer, Bioconjug Chem 14(1) (2003) 222-31.
[99] G. Saito, G.L. Amidon, K.D. Lee, Enhanced cytosolic delivery of plasmid DNA by a sulfhydryl-activatable listeriolysin O/protamine conjugate utilizing cellular reducing potential, Gene Ther 10(1) (2003) 72-83.
[100] J. Mercer, M. Schelhaas, A. Helenius, Virus entry by endocytosis, Annu Rev Biochem 79 (2010) 803-33.
[101] K.J. Oh, L. Senzel, R.J. Collier, A. Finkelstein, Translocation of the catalytic domain of diphtheria toxin across planar phospholipid bilayers by its own T domain, Proc Natl Acad Sci U S A 96(15) (1999) 8467-70.
[102] M. Pirazzini, F. Bordin, O. Rossetto, C.C. Shone, T. Binz, C. Montecucco, The thioredoxin reductase-thioredoxin system is involved in the entry of tetanus and botulinum neurotoxins in the cytosol of nerve terminals, Febs Letters 587(2) (2013) 150-155.
[103] R. Ratts, H. Zeng, E.A. Berg, C. Blue, M.E. McComb, C.E. Costello, J.C. vanderSpek, J.R. Murphy, The cytosolic entry of diphtheria toxin catalytic domain

requires a host cell cytosolic translocation factor complex, J Cell Biol 160(7) (2003) 1139-50.
[104] M. Schelhaas, J. Malmstrom, L. Pelkmans, J. Haugstetter, L. Ellgaard, K. Grunewald, A. Helenius, Simian virus 40 depends on ER protein folding and quality control factors for entry into host cells, Cell 131(3) (2007) 516-529.
[105] B. Tsai, C. Rodighiero, W.I. Lencer, T.A. Rapoport, Protein disulfide isomerase acts as a redox-dependent chaperone to unfold cholera toxin, Cell 104 (2001) 937.
[106] C.P. Walczak, K.M. Bernardi, B. Tsai, Endoplasmic reticulum-dependent redox reactions control endoplasmic reticulum-associated degradation and pathogen entry, Antioxidants & redox signaling 16(8) (2012) 809-18.
[107] N.L.B. Wernick, D.J.F. Chinnapen, J.A. Cho, W.I. Lencer, Cholera Toxin: An Intracellular Journey into the Cytosol by Way of the Endoplasmic Reticulum, Toxins 2(3) (2010) 310-325.
[108] L. Brulisauer, N. Kathriner, M. Prenrecaj, M.A. Gauthier, J.C. Leroux, Tracking the bioreduction of disulfide-containing cationic dendrimers, Angew Chem Int Ed Engl 51(50) (2012) 12454-8.
[109] B.A. Kellogg, L. Garrett, Y. Kovtun, K.C. Lai, B. Leece, M. Miller, G. Payne, R. Steeves, K.R. Whiteman, W. Widdison, H.S. Xie, R. Singh, R.V.J. Chari, J.M. Lambert, R.J. Lutz, Disulfide-Linked Antibody-Maytansinoid Conjugates: Optimization of In Vivo Activity by Varying the Steric Hindrance at Carbon Atoms Adjacent to the Disulfide Linkage, Bioconjugate Chemistry 22(4) (2011) 717-727.
[110] C. Wu, C. Belenda, J.C. Leroux, M.A. Gauthier, Interplay of chemical microenvironment and redox environment on thiol-disulfide exchange kinetics, Chemistry 17(36) (2011) 10064-70.
[111] D. Schaffert, M. Kiss, W. Rodl, A. Shir, A. Levitzki, M. Ogris, E. Wagner, Poly(I:C)-mediated tumor growth suppression in EGF-receptor overexpressing tumors using EGF-polyethylene glycol-linear polyethylenimine as carrier, Pharm Res 28(4) (2011) 731-41.
[112] A. Zintchenko, A. Philipp, A. Dehshahri, E. Wagner, Simple modifications of branched PEI lead to highly efficient siRNA carriers with low toxicity, Bioconjug Chem 19(7) (2008) 1448-55.
[113] I. Martin, C. Dohmen, C. Mas-Moruno, C. Troiber, P. Kos, D. Schaffert, U. Lachelt, M. Teixido, M. Gunther, H. Kessler, E. Giralt, E. Wagner, Solid-phase-assisted synthesis of targeting peptide-PEG-oligo(ethane amino)amides for receptor-mediated gene delivery, Org Biomol Chem 10(16) (2012) 3258-68.
[114] C.Y. Zhang, P. Kos, K. Muller, W. Schrimpf, C. Troiber, U. Lachelt, C. Scholz, D.C. Lamb, E. Wagner, Native chemical ligation for conversion of sequence-defined oligomers into targeted pDNA and siRNA carriers, J Control Release 180 (2014) 42-50.
[115] H. Wei, L.R. Volpatti, D.L. Sellers, D.O. Maris, I.W. Andrews, A.S. Hemphill, L.W. Chan, D.S. Chu, P.J. Horner, S.H. Pun, Dual responsive, stabilized nanoparticles for efficient in vivo plasmid delivery, Angew Chem Int Ed Engl 52(20) (2013) 5377-81.
[116] Q. Leng, P. Scaria, J. Zhu, N. Ambulos, P. Campbell, A.J. Mixson, Highly branched HK peptides are effective carriers of siRNA, J Gene Med 7(7) (2005) 977-86.
[117] M. Neu, O. Germershaus, S. Mao, K.H. Voigt, M. Behe, T. Kissel, Crosslinked nanocarriers based upon poly(ethylene imine) for systemic plasmid delivery: in vitro characterization and in vivo studies in mice, J Control Release 118(3) (2007) 370-80.
[118] M. Zheng, Y. Zhong, F. Meng, R. Peng, Z. Zhong, Lipoic acid modified low molecular weight polyethylenimine mediates nontoxic and highly potent in vitro gene transfection, Mol Pharm 8(6) (2011) 2434-43.

[119] C. Troiber, D. Edinger, P. Kos, L. Schreiner, R. Klager, A. Herrmann, E. Wagner, Stabilizing effect of tyrosine trimers on pDNA and siRNA polyplexes, Biomaterials 34(5) (2013) 1624-33.
[120] G. Creusat, A.S. Rinaldi, E. Weiss, R. Elbaghdadi, J.S. Remy, R. Mulherkar, G. Zuber, Proton sponge trick for pH-sensitive disassembly of polyethylenimine-based siRNA delivery systems, Bioconjug Chem 21(5) (2010) 994-1002.
[121] M. Ogris, P. Steinlein, M. Kursa, K. Mechtler, R. Kircheis, E. Wagner, The size of DNA/transferrin-PEI complexes is an important factor for gene expression in cultured cells, Gene Ther 5(10) (1998) 1425-33.
[122] H. Luthman, G. Magnusson, High efficiency polyoma DNA transfection of chloroquine treated cells, Nucleic Acids Res 11(5) (1983) 1295-308.
[123] M. Cotten, F. Langle-Rouault, H. Kirlappos, E. Wagner, K. Mechtler, M. Zenke, H. Beug, M.L. Birnstiel, Transferrin-polycation-mediated introduction of DNA into human leukemic cells: stimulation by agents that affect the survival of transfected DNA or modulate transferrin receptor levels, Proc Natl Acad Sci U S A 87(11) (1990) 4033-7.
[124] J. Cheng, R. Zeidan, S. Mishra, A. Liu, S.H. Pun, R.P. Kulkarni, G.S. Jensen, N.C. Bellocq, M.E. Davis, Structure-function correlation of chloroquine and analogues as transgene expression enhancers in nonviral gene delivery, J Med Chem 49(22) (2006) 6522-31.
[125] P. Erbacher, A.C. Roche, M. Monsigny, P. Midoux, Putative role of chloroquine in gene transfer into a human hepatoma cell line by DNA/lactosylated polylysine complexes, Exp Cell Res 225(1) (1996) 186-94.
[126] M. Neu, O. Germershaus, M. Behe, T. Kissel, Bioreversibly crosslinked polyplexes of PEI and high molecular weight PEG show extended circulation times in vivo, J Control Release 124(1-2) (2007) 69-80.
[127] O.M. Merkel, D. Librizzi, A. Pfestroff, T. Schurrat, K. Buyens, N.N. Sanders, S.C. De Smedt, M. Behe, T. Kissel, Stability of siRNA polyplexes from poly(ethylenimine) and poly(ethylenimine)-g-poly(ethylene glycol) under in vivo conditions: effects on pharmacokinetics and biodistribution measured by Fluorescence Fluctuation Spectroscopy and Single Photon Emission Computed Tomography (SPECT) imaging, J Control Release 138(2) (2009) 148-59.
[128] C.P. Leamon, R.B. DePrince, R.W. Hendren, Folate-mediated drug delivery: effect of alternative conjugation chemistry, J Drug Target 7(3) (1999) 157-69.
[129] C.P. Leamon, P.S. Low, Folate-mediated targeting: from diagnostics to drug and gene delivery, Drug Discov Today 6(1) (2001) 44-51.
[130] X.L. Wang, R. Xu, X. Wu, D. Gillespie, R. Jensen, Z.R. Lu, Targeted systemic delivery of a therapeutic siRNA with a multifunctional carrier controls tumor proliferation in mice, Mol Pharm 6(3) (2009) 738-46.
[131] K.L. Kozielski, S.Y. Tzeng, J.J. Green, A bioreducible linear poly(beta-amino ester) for siRNA delivery, Chem Commun (Camb) 49(46) (2013) 5319-21.
[132] J. Hoon Jeong, L.V. Christensen, J.W. Yockman, Z. Zhong, J.F. Engbersen, W. Jong Kim, J. Feijen, S. Wan Kim, Reducible poly(amido ethylenimine) directed to enhance RNA interference, Biomaterials 28(10) (2007) 1912-7.
[133] P.M. Klein, E. Wagner, Bioreducible polycations as shuttles for therapeutic nucleic acid and protein transfection, Antioxidants & redox signaling 21(5) (2014) 804-17.
[134] S. Wieczorek, S. Vigne, T. Masini, D. Ponader, L. Hartmann, A.K. Hirsch, H.G. Borner, Combinatorial screening for specific drug solubilizers with switchable release profiles, Macromol Biosci 15(1) (2015) 82-9.

[135] U. Lachelt, E. Wagner, Nucleic Acid Therapeutics Using Polyplexes: A Journey of 50 Years (and Beyond), Chem Rev 115(19) (2015) 11043-78.
[136] R. Koynova, B. Tenchov, L. Wang, R.C. Macdonald, Hydrophobic moiety of cationic lipids strongly modulates their transfection activity, Mol Pharm 6(3) (2009) 951-8.
[137] P.M. Klein, S. Reinhard, D.J. Lee, K. Muller, D. Ponader, L. Hartmann, E. Wagner, Precise redox-sensitive cleavage sites for improved bioactivity of siRNA lipopolyplexes, Nanoscale 8(42) (2016) 18098-18104.
[138] J.M. Baskin, J.A. Prescher, S.T. Laughlin, N.J. Agard, P.V. Chang, I.A. Miller, A. Lo, J.A. Codelli, C.R. Bertozzi, Copper-free click chemistry for dynamic in vivo imaging, Proc Natl Acad Sci U S A 104(43) (2007) 16793-7.
[139] P.V. Chang, J.A. Prescher, E.M. Sletten, J.M. Baskin, I.A. Miller, N.J. Agard, A. Lo, C.R. Bertozzi, Copper-free click chemistry in living animals, Proc Natl Acad Sci U S A 107(5) (2010) 1821-6.
[140] V.V. Rostovtsev, L.G. Green, V.V. Fokin, K.B. Sharpless, A stepwise huisgen cycloaddition process: copper(I)-catalyzed regioselective "ligation" of azides and terminal alkynes, Angew Chem Int Ed Engl 41(14) (2002) 2596-9.
[141] Q. Wei, T. Becherer, S. Angioletti-Uberti, J. Dzubiella, C. Wischke, A.T. Neffe, A. Lendlein, M. Ballauff, R. Haag, Protein interactions with polymer coatings and biomaterials, Angew Chem Int Ed Engl 53(31) (2014) 8004-31.
[142] C. Hörtz, A. Birke, L. Kaps, S. Decker, E. Wächtersbach, K. Fischer, D. Schuppan, M. Barz, M. Schmidt, Cylindrical Brush Polymers with Polysarcosine Side Chains: A Novel Biocompatible Carrier for Biomedical Applications, Macromolecules 48(7) (2015) 2074-2086.
[143] M. Sela, Immunological studies with synthetic polypeptides, Adv Immunol 5 (1966) 29-129.
[144] E. Hara, M. Ueda, C.J. Kim, A. Makino, I. Hara, E. Ozeki, S. Kimura, Suppressive immune response of poly-(sarcosine) chains in peptide-nanosheets in contrast to polymeric micelles, J Pept Sci 20(7) (2014) 570-7.
[145] K. Klinker, R. Holm, P. Heller, M. Barz, Evaluating chemical ligation techniques for the synthesis of block copolypeptides, polypeptoids and block copolypept(o)ides: a comparative study, Polymer Chemistry 6(25) (2015) 4612-4623.
[146] W. Zhang, K. Muller, E. Kessel, S. Reinhard, D. He, P.M. Klein, M. Hohn, W. Rodl, S. Kempter, E. Wagner, Targeted siRNA Delivery Using a Lipo-Oligoaminoamide Nanocore with an Influenza Peptide and Transferrin Shell, Adv Healthc Mater 5(12) (2016) 1493-504.
[147] E. Gullotti, Y. Yeo, Extracellularly activated nanocarriers: a new paradigm of tumor targeted drug delivery, Mol Pharm 6(4) (2009) 1041-51.
[148] K. Muller, E. Kessel, P.M. Klein, M. Hohn, E. Wagner, Post-PEGylation of siRNA Lipo-oligoamino Amide Polyplexes Using Tetra-glutamylated Folic Acid as Ligand for Receptor-Targeted Delivery, Mol Pharm 13(7) (2016) 2332-45.
[149] L. Liu, M. Zheng, D. Librizzi, T. Renette, O.M. Merkel, T. Kissel, Efficient and Tumor Targeted siRNA Delivery by Polyethylenimine-graft-polycaprolactone-block-poly(ethylene glycol)-folate (PEI-PCL-PEG-Fol), Mol Pharm 13(1) (2016) 134-43.
[150] S. Sabharanjak, P. Sharma, R.G. Parton, S. Mayor, GPI-anchored proteins are delivered to recycling endosomes via a distinct cdc42-regulated, clathrin-independent pinocytic pathway, Dev Cell 2(4) (2002) 411-23.
[151] L. Maldonado-Baez, C. Williamson, J.G. Donaldson, Clathrin-independent endocytosis: a cargo-centric view, Exp Cell Res 319(18) (2013) 2759-69.

[152] Y.-L. Li, N. Van Cuong, M.-F. Hsieh, Endocytosis Pathways of the Folate Tethered Star-Shaped PEG-PCL Micelles in Cancer Cell Lines, Polymers 6(3) (2014) 634.
[153] W.L. Langston Suen, Y. Chau, Size-dependent internalisation of folate-decorated nanoparticles via the pathways of clathrin and caveolae-mediated endocytosis in ARPE-19 cells, J Pharm Pharmacol 66(4) (2014) 564-73.
[154] C. Dalal, A. Saha, N.R. Jana, Nanoparticle Multivalency Directed Shifting of Cellular Uptake Mechanism, The Journal of Physical Chemistry C 120(12) (2016) 6778-6786.
[155] K. Muller, P.M. Klein, P. Heissig, A. Roidl, E. Wagner, EGF receptor targeted lipo-oligocation polyplexes for antitumoral siRNA and miRNA delivery, Nanotechnology 27(46) (2016) 464001.
[156] X. Wang, P. Gobbo, M. Suchy, M.S. Workentin, R.H.E. Hudson, Peptide-decorated gold nanoparticles via strain-promoted azide-alkyne cycloaddition and post assembly deprotection, RSC Advances 4(81) (2014) 43087-43091.
[157] T.E. Ritter, O. Fajardo, H. Matsue, R.G. Anderson, S.W. Lacey, Folate receptors targeted to clathrin-coated pits cannot regulate vitamin uptake, Proc Natl Acad Sci U S A 92(9) (1995) 3824-8.
[158] S. Mayor, K.G. Rothberg, F.R. Maxfield, Sequestration of GPI-anchored proteins in caveolae triggered by cross-linking, Science 264(5167) (1994) 1948-51.
[159] F.M. van de Water, O.C. Boerman, A.C. Wouterse, J.G. Peters, F.G. Russel, R. Masereeuw, Intravenously administered short interfering RNA accumulates in the kidney and selectively suppresses gene function in renal proximal tubules, Drug Metab Dispos 34(8) (2006) 1393-7.
[160] Y.H. Bae, K. Park, Targeted drug delivery to tumors: myths, reality and possibility, J Control Release 153(3) (2011) 198-205.
[161] V.A. Bloomfield, DNA condensation by multivalent cations, Biopolymers 44(3) (1997) 269-82.
[162] L. Wan, Y. You, Y. Zou, D. Oupicky, G. Mao, DNA release dynamics from bioreducible poly(amido amine) polyplexes, J Phys Chem B 113(42) (2009) 13735-41.
[163] D. He, K. Muller, A. Krhac Levacic, P. Kos, U. Lachelt, E. Wagner, Combinatorial Optimization of Sequence-Defined Oligo(ethanamino)amides for Folate Receptor-Targeted pDNA and siRNA Delivery, Bioconjug Chem 27(3) (2016) 647-59.
[164] P. Kos, U. Lachelt, A. Herrmann, F.M. Mickler, M. Doblinger, D. He, A. Krhac Levacic, S. Morys, C. Brauchle, E. Wagner, Histidine-rich stabilized polyplexes for cMet-directed tumor-targeted gene transfer, Nanoscale 7(12) (2015) 5350-62.
[165] B. Shi, E. Keough, A. Matter, K. Leander, S. Young, E. Carlini, A.B. Sachs, W. Tao, M. Abrams, B. Howell, L. Sepp-Lorenzino, Biodistribution of small interfering RNA at the organ and cellular levels after lipid nanoparticle-mediated delivery, J Histochem Cytochem 59(8) (2011) 727-40.
[166] A. Akinc, W. Querbes, S. De, J. Qin, M. Frank-Kamenetsky, K.N. Jayaprakash, M. Jayaraman, K.G. Rajeev, W.L. Cantley, J.R. Dorkin, J.S. Butler, L. Qin, T. Racie, A. Sprague, E. Fava, A. Zeigerer, M.J. Hope, M. Zerial, D.W. Sah, K. Fitzgerald, M.A. Tracy, M. Manoharan, V. Koteliansky, A. Fougerolles, M.A. Maier, Targeted Delivery of RNAi Therapeutics With Endogenous and Exogenous Ligand-Based Mechanisms, Mol Ther 18(7) (2010) 1357-1364.
[167] S. Schottler, G. Becker, S. Winzen, T. Steinbach, K. Mohr, K. Landfester, V. Mailander, F.R. Wurm, Protein adsorption is required for stealth effect of poly(ethylene glycol)- and poly(phosphoester)-coated nanocarriers, Nat Nanotechnol 11(4) (2016) 372-7.

[168] D. Pozzi, G. Caracciolo, C. Marchini, M. Montani, A. Amici, L. Callipo, A.L. Capriotti, C. Cavaliere, A. Lagana, Surface adsorption of protein corona controls the cell uptake mechanism in efficient cationic liposome/DNA complexes in serum, J Control Release 148(1) (2010) e94-5.
[169] M. Lundqvist, J. Stigler, G. Elia, I. Lynch, T. Cedervall, K.A. Dawson, Nanoparticle size and surface properties determine the protein corona with possible implications for biological impacts, Proc Natl Acad Sci U S A 105(38) (2008) 14265-70.
[170] H.C. Christianson, M. Belting, Heparan sulfate proteoglycan as a cell-surface endocytosis receptor, Matrix Biol 35 (2014) 51-5.
[171] G. Orr, D.J. Panther, K.J. Cassens, J.L. Phillips, B.J. Tarasevich, J.G. Pounds, Syndecan-1 mediates the coupling of positively charged submicrometer amorphous silica particles with actin filaments across the alveolar epithelial cell membrane, Toxicol Appl Pharmacol 236(2) (2009) 210-20.
[172] R.J. Lee, P.S. Low, Folate-mediated tumor cell targeting of liposome-entrapped doxorubicin in vitro, Biochim Biophys Acta 1233(2) (1995) 134-44.

8 Publications

Original articles (*indicates equal contributions)

Müller K, **Klein PM**, Heissig P, Roidl A, Wagner E. *EGF receptor targeted lipo-oligocation polyplexes for antitumoral siRNA and miRNA delivery.* Nanotechnology. 2016 Nov 18;27(46):464001

Klein PM*, Reinhard S*, Lee DJ, Müller K, Ponader D, Hartmann L, Wagner E. *Precise redox-sensitive cleavage sites for improved bioactivity of siRNA lipopolyplexes*. Nanoscale. 2016 Oct 27;8(42):18098-18104

Müller K, Kessel E*, **Klein PM***, Höhn M, Wagner E. *Post-PEGylation of siRNA lipo-oligoamino amide polyplexes using tetra-glutamylated folic acid as ligand for receptor-targeted delivery.* Mol Pharm. 2016 Jul 5;13(7):2332-45

Zhang W, Müller K, Kessel E, Reinhard S, He D, **Klein PM**, Höhn M, Rödl W, Kempter S, Wagner E. *Targeted siRNA Delivery Using a Lipo-Oligoaminoamide Nano-Core with an Influenza Peptide and Transferrin Shell.* Adv Healthc Mater. 2016 Jun;5(12):1493-504

Heissig P, **Klein PM**, Hadwiger P, Wagner E. *DNA as tunable adaptor for siRNA polyplex stabilization and functionalization.* Mol Ther Nucleic Acids. 2016 Mar 1;5:e288

Lee DJ, Kessel E, Edinger D, He D, **Klein PM**, Voith von Voithenberg L, Lamb DC, Lächelt U, Lehto T, Wagner E. *Dual antitumoral potency of EG5 siRNA nanoplexes armed with cytotoxic bifunctional glutamyl-methotrexate targeting ligand.* Biomaterials. 2016 Jan;77:98-110

Zhang P, He D, **Klein PM**, Liu X, Röder R, Döblinger M, Wagner E. *Enhanced Intracellular Protein Transduction by Sequence Defined Tetra-Oleoyl Oligoaminoamides Targeted for Cancer Therapy.* Adv. Funct. Materials. 2015 Nov 11; 25:6627–6636

Klein PM, Müller K, Gutmann C, Kos P, Krhac Levacic A, Edinger D, Höhn M, Leroux JC, Gauthier MA, Wagner E. *Twin disulfides as opportunity for improving stability and transfection efficiency of oligoaminoethane polyplexes.* J Control Release. 2015 May 10;205:109-19

Reviews

Klein PM, Wagner E. *Bioreducible Polycations as Shuttles for Therapeutic Nucleic Acid and Protein Transfection*. Antioxid Redox Signal. 2014 Aug 10;21(5):804-17

Manuscripts in preparation

Klein PM, Klinker K, Zhang W, Kern S, Kessel E, Barz M, Wagner E. *Functionalized poly(sarcosine) as shielding agent for lipopolyplexes.* Manuscript in preparation

Klein PM, Zhang W*, Lee DJ*, Kern S, *Wagner E. Folate receptor-directed orthogonal click-functionalization of siRNA lipopolyplexes for tumor-targeted gene silencing in vivo.* Manuscript in preparation

Meeting abstracts and poster presentations

Klein PM, Reinhard S, Zhang W, Klinker K, Kern S, Kessel E, Barz M, Wagner E. *Novel Poly(Sarcosine) Click Shielding Agents Improve Circulation of Redox-Sensitive siRNA Lipo-Polyplexes In Vivo.* 20th Annual Meeting of the American Society of Gene & Cell Therapy, Washington, USA (May 2017) - *selected for oral presentation and honored with the Meritorious Abstract Travel Award*

Klein PM, Müller K, Lee DJ, Zhang W, Kopp F, Roidl A, Wagner E. *miR-200c: function and delivery.* SFB 1032 meeting, Tutzing, Germany (Mar 2017)

Lee DJ, Kessel E, He D, **Klein PM**, Lächelt U, Wagner E. *Oligoaminoamide-based siRNA carriers for in vivo tumor targeting and gene silencing.* 126th German Pharmaceutical Society (DPhG) Annual Meeting, Munich, Germany (Oct 2016)

Klein PM, Reinhard S, Lee DJ, Müller K, Ponader D, Hartmann L, Wagner E. *Precise integration of redox-sensitive cleavage sites for enhanced gene silencing and reduced toxicity of siRNA lipo-polyplexes.* 22th German Society for Gene Therapy (DG-GT) Annual Meeting, Heidelberg, Germany (Sep 2016)

Müller K, **Klein PM**, Kopp F, Roidl A, Wagner E. *miR-200c: function and delivery*. SFB 1032 meeting, München, Germany (Jan 2016)

Lee DJ, Kessel E, He D, **Klein PM**, Lächelt U, Lehto T, Wagner E. *Synergistic antitumoral potency mediated by EG5 siRNA nanoplexes with bifunctional glutamyl-MTX targeting ligand.* 29th American Association of Pharmaceutical Scientists (AAPS) Annual Meeting, Orlando, USA (Oct 2015)

Lee DJ, Kessel E, He D, **Klein PM**, Lächelt U, Lehto T, Wagner E. *Targeted Co-delivery of bifunctional glutamyl-methotrexate and EG5 siRNA using nanoplexes for combined antitumoral potency.* 125th German Pharmaceutical Society (DPhG) Annual Meeting, Düsseldorf, Germany (Sep 2015)

9 Acknowledgements

After an intensive period of more than four years, my PhD study finally comes to an end. It has been a period of intense learning for me, not only in the scientific area, but also on a personal level. Writing this dissertation has had a big impact on me. I would like to reflect on the people who have supported and helped me so much throughout this whole period.

First of all, I thank my supervisor Professor Dr. Ernst Wagner for giving me the opportunity to work in his research group. I am very grateful for his wise counsel and sympathetic ear during the whole time. I especially enjoyed that I was given the freedom of being creative and that I could start projects based on my own ideas. I learned a lot under his supervision.

I want to thank our collaboration partners Prof. Dr. Laura Hartmann and Dr. Daniela Ponader for synthesizing and providing the solid phase compatible bioreducible building block. I also want to thank PD Dr. Matthias Barz and his PhD student Kristina Klinker for synthesizing and providing DBCO functionalized poly(sarcosine) shielding agents.

Special thanks to Katharina, Wei, DJ and Ana who spent a lot of time in the cell culture testing my latest compounds. All synthetic work would be irrelevant without your contribution. As a team we are strong.

Many thanks to DJ, Sarah and Eva for carrying out *in vivo* animal experiments. Especially the latest projects profit a lot from your highly significant work.

I would like to thank Sören for the great collaboration on our project about bioreducible lipo-oligomers and for measuring mass spectrometry together with Stephan in our working group.

I thank Christina, Claudia and Uli for teaching me solid phase synthesis during my very first weeks in the lab.

Many thanks to Wolfgang for the support with our technical equipment, for repairing almost any broken instrument or computer and for ensuring the technical maintenance, to Miriam for helping with the microscopy experiments and to the remaining team of

technicians: Anna, Ursula and Melinda for keeping the everyday life in the lab running. I thank Markus for taking care of the animals and Olga for her organizational skills.

I greatly appreciate the efforts of Dr. Martina Rüffer for the organization of hiking events, the Christmas party and the traditional Weißwurst Frühstück.

I want to thank all other members of the Wagner research group for the great atmosphere in the lab. We were not only able to support each other by deliberating over our problems and findings, but also happily by talking about things other than just our papers. We had a lot of great events and we spent time together not only as colleagues but also as friends: Ski trips in Kühtai, hiking events, several BBQs, lab dinners, PhD celebrations, Fasching and Christmas parties, football games, Oktoberfest, celebrations for new publications and more…

I would also like to thank my parents and my brother Christoph for my carefree childhood and for supporting me in all areas of my life.

Thank you, Elena, for enriching so many years of my life and for your dedicated support. Finally, I want to thank you, Konrad, for being the greatest enrichment of my life. It is a miracle to see you grow up.